Author/s:
Wichmann, Johannes

Title:
The role of the MYST lysine acetyltransferase TIP60 in human cells and mice

Date:
2020

Persistent Link:
https://hdl.handle.net/11343/261677

The role of the MYST lysine acetyltransferase TIP60 in human cells and mice

Johannes Werner Wichmann

ORCID iD: 0000-0002-0663-5109

Doctor of Philosophy

October 2020

The Walter and Eliza Hall Institute of Medical Research

Department of Medical Biology

Faculty of Medicine, Health and Dentistry

The University of Melbourne

Submitted in total fulfilment of the degree of Doctor of Philosophy

Abstract

Histone acetylation affects the way DNA and associated proteins are packaged in the cell nucleus and regulate chromatin organisation and gene expression. Acetylation of core histones has been broadly correlated with initiating and maintaining open chromatin, poised or active gene transcription, DNA damage repair, as well as chromosome decondensation during mitosis and meiosis. The acetylation of lysine residues is catalysed by histone lysine acetyltransferases (KATs) and deacetylases (HDACs), which are tightly regulated. Dysregulation of KATs and aberrant lysine acetylation has been associated with tumorigenesis and negative prognoses in a wide range of cancer, presenting a new area of potential therapeutic targets. Potential acetylation targets of KATs catalysing the acetylation of histones have predominantly been studied in cell-free assays, where the enzymes show little substrate specificity. In contrast, histone acetyltransferases appear to acetylate surprisingly specific residues in whole cells.

In this thesis I investigate the effects of acute deletion of the MYST lysine acetyltransferase TIP60 (KAT5) using inducible cre-recombinase and CRISPR/Cas9-mediated deletion in human cells and mouse cells, as well as mouse embryos and its potential role in cancer cells. I found that loss of TIP60 caused complete cell growth arrest in human and mouse cells. In the absence of TIP60 cells displayed cell cycle arrest in G1 and G2/M phase with increased endoreplication, accompanied by chromosomal segregation defects. Remarkably, the proliferation arrest caused by loss of TIP60 also occurred in the absence of the tumour suppressors p53, INK4A and ARF and therefore was independent of these. In contrast, cell survival was not affected. Growth arrest independent of major tumour suppressors flags TIP60 a potential target for novel cancer therapeutics.

TIP60 was found to be essential for of H2AZ acetylation, particularly, lysine 7 acetylation. In contrast, global chromatin bound H2AZ levels were not reduced. H2A and H4 acetylation was reduced slightly in TIP60 depleted cells. Identifying H2AZ lysine 7 acetylation as a biomarker for TIP60 activity is a major step in developing TIP60 as a drug target. The mRNA levels of 6236 human and 8238 mouse genes, including many metabolic genes, were dependent on TIP60, supporting a role for TIP60 as a key transcriptional co-activator.

Characterization of key mechanisms causing chromosomal aberrations and identifying approaches that can be used to reduce likelihood of genome instability due histone acetylation defects will pave the way for better detection of early changes in cancer and development of therapeutic applications in the future. This work represents important steps towards the development of histone lysine acetyltransferases as drug targets. A comprehensive analysis of histone acetylation activity of TIP60 shines light on the potential of its many proposed roles.

Declaration

This is to certify that:

I. This thesis presents my original work only, except where indicated below.

II. Acknowledgement has been made in the text to all other material presented.

III. This thesis is fewer than 100 000 words in length, exclusive of figures, tables, and bibliographies.

Others have contributed to work presented in this thesis as follows:

Ms Catherine Pitt, Ms Samantha Eccles, and Ms Rose May collected and performed IHC staining of *Tip60*^{gt} blastocysts. Ms Catherine Pitt performed genotyping, *in uteri* histology, and ES cell outgrowth assay of *Tip60*^{gt} blastocysts. Ms Elizabeth Allan performed a single replicate of the *in vitro* Tip60 and H2AZ acetylation assay. Dr Alexandra Garnham and Prof Gordon Smyth performed the bioinformatics analysis of my RNA-sequencing data, while planning, samples collection and library preparation was done by me and HT-sequencing was conducted by Dr Stephen Wilcox.

I estimate that my own contribution to this work is 90%.

_____

Johannes W. Wichmann

Publications

Jonathan B Baell, David J Leaver, Stefan J Hermans, Gemma L Kelly, Margs S Brennan, Natalie L Downer, Nghi Nguyen, **Johannes Wichmann**, Helen M McRae , Yuqing Yang , Ben Cleary, H Rachel Lagiakos, Stephen Mieruszynski, Guido Pacini, Hannah K Vanyai, Maria I Bergamasco, Rose E May, Bethany K Davey, Kimberly J Morgan, Andrew J Sealey, Beinan Wang , Natasha Zamudio, Stephen Wilcox, Alexandra L Garnham, Bilal N Sheikh, Brandon J Aubrey, Karen Doggett, Matthew C Chung, Melanie de Silva, John Bentley, Pat Pilling, Meghan Hattarki, Olan Dolezal, Matthew L Dennis, Hendrik Falk , Bin Ren, Susan A Charman, Karen L White, Jai Rautela, Andrea Newbold, Edwin D Hawkins, Ricky W Johnstone, Nicholas D Huntington, Thomas S Peat, Joan K Heath, Andreas Strasser, Michael W Parker, Gordon K Smyth, Ian P Street , Brendon J Monahan , Anne K Voss, Tim Thomas (2018). **Inhibitors of histone acetyltransferases KAT6A/B induce senescence and arrest tumour growth.** *Nature*. 2018;560(7717):253-257. doi:10.1038/s41586-018-0387-5

Publications under revision

Johannes Wichmann, Catherine Pitt, Samantha Eccles, Alexandra Garnham, Rose May, Elizabeth Allan, Stephen Wilcox, Marco J. Herold, Gordon K Smyth, Brendon Monahan, Tim Thomas, Anne K Voss (*revised version invited for resubmission to iScience*). **Loss of TIP60 abolishes H2AZ lysine 7 acetylation and causes p53, INK4A and ARF-independent cell cycle arrest.**

Acknowledgements

I am very grateful to my joint supervisors Prof. Anne K. Voss, Head of the Epigenetics and Development Division at WEHI, and A/Prof. Tim Thomas, who enabled me to come to Australia as an international PhD student and supported my professional and personally development. They made it possible to stem the task of a PhD, while visiting my family in Germany regularly and starting my own family here in Australia. All members of my PhD committee, Prof Joan Heath, Prof Marco Herold, and Dr Brendon Monahan, have provided professional and personal guidance. They taught me all necessary skills to become a successful scientist.

I thank Prof Günther Schütz, Prof Frieder Schwenk, Prof Manuel Serrano, Dr Tyler Jacks for making mutant and transgenic mice available to the scientific community, Prof Steven Henikoff for the gift of pAG-Tn5 and adapters for the CUT&Tag experiments and Associate Prof Marco Herold for the gift of *FgH1tUTG*. I gratefully acknowledge the expert assistance provided by WEHI Research Services Centres: WEHI Bioservices, WEHI FACS Facility, WEHI Histology Services, WEHI Imaging Facility, WEHI Genomics Laboratory, the Melbourne Advanced Genome Editing Centre (MAGEC) at WEHI, and the WEHI Single Cell Sequencing.

This time would not have been as enjoyable without the ongoing help and friendship of all my colleagues, who were never too busy to help each other, whether it was asking for a pen or the correct statistical tool to analyse complicated data. My fellow PhD candidates, Sophia, Helen, Maria, Zoe, Kimberly, and Melody, all the knowledgeable postdocs, Natasha, Stephen, Yuqing, Karen, and Ming, as well as the very skilled research assistants, Evelyn, Rose, Sam, Havva, Shezlie, Lauren, and Aileen. I am very grateful to

the animal technicians, Melissa, Jacky, Faye, Leanne, Emily, and Lauren for teaching me all the basics about animal handling and looking after my mice. Special thanks to our divisional coordinator Tanya, who brightens up even the worst day in the lab with her joyful character and helped with every little need. In fact, everyone at WEHI, whom I had the pleasure to work with, has been nothing but friendly and helpful.

Finally, I want to thank my parents and brothers, who supported me from across the globe, my loving and supporting wife Evelyn and my wonderful little son Blue.

List of abbreviations

-	Null allele
%	Percentage
+	Wild-type allele
°C	Degrees Celsius
ac	Acetylation
AGRF	Australian Genome Research Facility
ANOVA	Analysis of variance
AR	Androgen receptor
bFGF	Basic fibroblast growth factor
bp	Base pair
BrdU	5-bromo-2'-deoxyuridine
BSA	Bovine serum albumin
C. elegans	*Caenorhabditis elegans*
CCDC8	Coiled-coil domain-containing protein 8
cDNA	Complementary DNA
ciTIP60	catalytically inactive TIP60 mutants
CNS	Central nervous system
CO_2	Carbon dioxide
CUT&Tag	Cleavage under targets and tagmentation
D. melanogaster	*Drosophila melanogaster*
DAPI	4',6-diamidino-2-phenylindole
DMEM	Dulbecco's modified Eagle's medium
DMSO	Dimethyl sulfoxide
DNA	Deoxyribonucleic acid
dNTP	Deoxynucleotide triphosphate
Dox	Doxycycline
DSB	Double-strand breaks in the DNA
E	Embryonic day
E. coli	*Escherichia coli*
EGF	Epidermal growth factor
ER	Estrogen receptor
ERT2	*RosaCreERT2*

FBS	Foetal bovine serum
fl	Femtolitre
fl	Allele with *loxP* sites
g	Gram
GI tract	Gastro-intestinal
gt	Genetrap allele
Gy	Gray
h	hour
H&E	Haematoxylin and eosin
H2A	Histone 2A
H2AK5	Histone 2A lysine 5
H2AX	Histone 2A histone family member X
H2AZ	Histone 2A histone family member Z
H2AZK4	Histone 2A histone family member Z lysine 4
H2AZK7	Histone 2A histone family member Z lysine 7
H2B	Histone 2B
H_2O	Water
H3	Histone 3
H3K122suc	Succinylated histone H3 lysine 122
H3K14	Histone 3 lysine 14
H3K27	Histone 3 lysine 27
H3K36	Histone 3 lysine 36
H3K4	Histone 3 lysine 4
H3K79	Histone 3 lysine 79
H3K9	Histone 3 lysine 9
H4	Histone 4
H4K12	Histone 4 lysine 12
H4K16	Histone 4 lysine 16
H4K5	Histone 4 lysine 5
H4K8	Histone 4 lysine 8
HAT	Histone acetyltransferase
HBO1	Histone acetyltransferase bound to ORC1
HDAC	Histone deacetylase
HEPES	N-2-hydroxyethyl piperazine-N-2-ethane sulfonic acid

HI-FBS	Heat-inactivated foetal bovine serum
HTATIP	HIV tat interacting protein
Ig	Immunoglobulin
iKO	Induced Knock-out allele
K	lysine
KAT	Lysine acetyltransferase
KAT5	Lysine acetyltransferase 5 (also TIP60 or HTATIP)
kb	Kilo-base pair
kDa	Kilo Dalton
KO	Knock-out
l	Litre
M	Molar
me	Methylation
me2	Dimethylation
me3	Trimethylation
MEF	Murine embryonic fibroblast
mg	Milligram
min	Minute
ml	Millilitre
mM	Millimolar
MQ-H_2O	Milli-Q purified water
mRNA	Messenger RNA
MT-PBS	Mouse tonicity phosphate-buffered saline
MTT	1-(4,5-Dimethylthiazol-2-yl)-3,5-diphenylformazan
n	Sample size
NSC	Neuronal stem cell
N-terminal	Amino terminal
P	Postnatal day
p	p-value
PBS	Phosphate buffered saline
PCR	Polymerase chain reaction
PI	Propidium iodide
PR	Progesterone receptor
PTM	Post-transcriptional modification

qPCR	Quantitative polymerase chain reaction
R	Arginine
RNA	Ribonucleic acid
RT	Room temperature
RT-qPCR	Reverse transcriptase reaction followed by quantitative polymerase chain reaction
s	Seconds
S	Serine
SDS-PAGE	SDS-polyacrylamide gel electrophoresis
SEM	Standard error of the mean
SN	Supernatant
TIP60	Tat-interactive protein 60 kDa (also KAT5 or HTATIP)
TMRE	Tetramethylrhodamine, ethyl ester
TP73	Tumour protein p73
TSS	Transcription start site
TUNEL	Terminal deoxynucleotide transferase-mediated dUTP nick-end labelling
WEHI	The Walter and Eliza Hall Institute of Medical Research
x *g*	Gravity
β	Beta
γ	Gamma

Table of Contents

List of Figures

List of Tables

Chapter 1 Literature Review

1.1 Introduction to epigenetics

The blueprint for an organism's development is found in the genetic information, the DNA sequence. In 1865, Mendel laid the foundation for genetic inheritance in his work with pea plants, describing how progeny acquires one allele from each of their parents to make up their individual genetic information (Mendel, 1865). In 1956, Waddington showed that the response to an environmental cue can lead to a stable heritable trait (Waddington, 1956) and introduced the concept of the epigenetic landscape, laying the foundation for the field of 'epigenetics' (Waddington, 2014). Epigenetics describes how cells with the same genetic information are able to differentiate into the diverse cell types of an individual with specific phenotypes. Waddington is considered the father of epigenetics, although scientific discoveries over the last decades demanded us to rethink about how we define epigenetics. A variety of definitions are in use and the need to define the word before using it has been advocated (Greally, 2018). The term epigenetic is derived from the Greek words ἐπί (*epí*, "on top of") and γένος (*genos*, "race, stock, kin", a group of common descent). Epigenetics was defined by Morris and Wu as follows (Wu, 2001): "*Epigenetics is the study of changes in gene function that are mitotically and/or meiotically heritable and that do not entail a change in DNA sequence"*

Mechanistically, different epigenetic states are thought to be generated through covalent modifications of DNA or associated proteins, that is, different epigenetic states are the result of covalent modifications of chromatin.

1.2 Chromatin

1.2.1 Chromatin structure

Epigenetic mechanisms unfold in the cell nucleus at the level of chromatin. The term *chromatin* describes the organization of genomic DNA and proteins, including histones and non-histone proteins, in the cell nucleus (Mirsky and Pollister, 1946). Human diploid cells harbour approximately 6.2 billion base pair (bp) of DNA (human genome, GRCh38.p13). Each bp stretches 3.4 Å along the DNA strand, totalling to approximately 2.1 m of DNA per nucleus (Wilkins et al., 1953).

In eukaryotes, 145 – 147 bp of DNA is wrapped around a core of histone proteins forming a nucleosome unit (Figure 1.1A) (Finch et al., 1977; Oudet et al., 1975). The histone core consists of two H3-H4 and two H2A-H2B dimers interacting with their core protein domain, while their N-termini are stretched outwards from the histone core (Figure 1.1B) (Luger et al., 1997). Nucleosomes are connected by 10 – 80 bp of linker DNA (Van Holde, 1988), creating the characteristic beads on a string euchromatin structure (Figure 1.1A) (Luger et al., 1997; Olins and Olins, 1974).

Specific histones, such as histone H1 and H5 can attach to nucleosomes at the entry and exit point of the DNA, forming various levels of denser chromatin structures (Fyodorov et al., 2018; Hergeth and Schneider, 2015; Loden and van Steensel, 2005). *In vitro* studies suggest a structured 30 nm chromatin fibre leading to the formation of heterochromatin (Figure 1.1A) (Finch and Klug, 1976; Tremethick, 2007), however, the existence of the 30 nm chromatin fibre has not yet been proven *in vivo* (Maeshima et al., 2016). Euchromatin is correlated to more active transcription, while heterochromatin regions are correlated with lower or absent gene transcription (Hsu, 1962; Huisinga et al., 2006; Littau et al., 1964).

At the highest level, the human DNA is organised into 23 pairs of chromosomes. During mitosis, the incredible feat of condensing an average of 45.7 cm of DNA into 1.8 μm^3 per chromosome (Chen et al., 2017), is mediated through the organisation of chromatin.

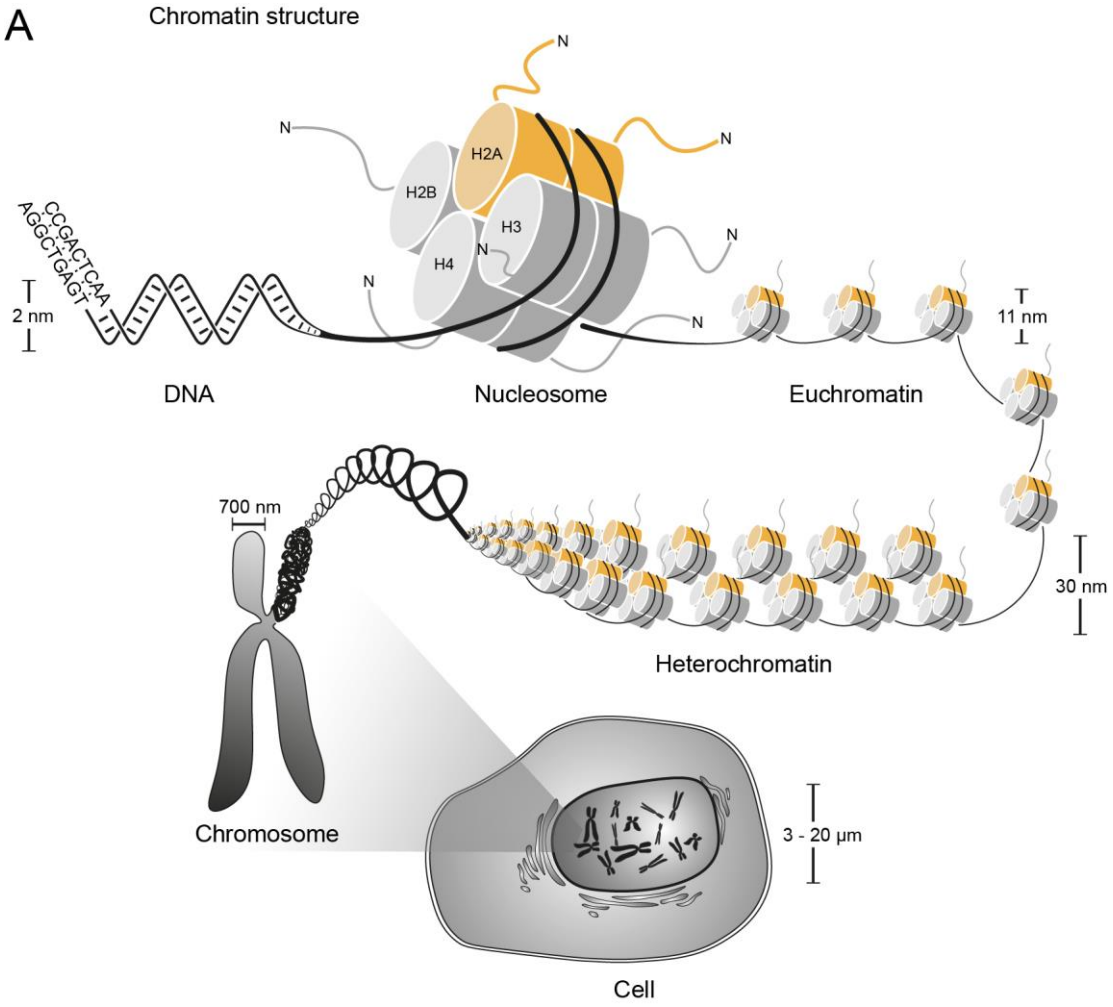

Figure 1.1: Chromatin organization. (A) Schematic showing 2 nm DNA double helix, the characteristic 'beads on a string' 11 nm euchromatin fibre including nucleosomes consisting of 146 bp of DNA wrapped around a core of 8 histone proteins, and the more densely packed 30 nm heterochromatin fibre. In humans, DNA is organised in 23 pairs of chromosomes, which during mitosis are condensed to an average volume of 1.8 μm^3 per chromosome. Based on (Pierce, 2005).

The chromosome positions within the interphase nucleus are surprisingly stationary (Abney et al., 1997; Marshall et al., 1997). During chromosome decondensation after cell

division, centromeres disperse uniformly and display reduced movement during interphase (Shelby et al., 1996), suggesting that final positions of chromosome are dictated by the localization of centromeres during cell division and restricted to chromosome territories (CTs). Chromatin interacts with the nuclear envelope to position chromosomes within the nucleus (Marshall et al., 1996) while distant DNA sequences interact in topologically associating domains (TADs) (Jin et al., 2013).

Chromatin organisation fulfils at least two critical roles. Firstly, compacting DNA by a factor of approximately 10,000 into the mitotic nucleus, and secondly, regulating access to DNA necessary for a spectrum of functions, including DNA replication, DNA repair, and gene transcription. Cells have various ways of regulating chromatin structure, such as architectural proteins, DNA methylation, RNA binding, histone variant exchange, and histone modifications, influencing the accessibility of the underlying DNA to regulatory proteins and transcription machinery.

1.2.2 Histone dynamics

Histones are not static in the nucleosome core particle (NCP). The sequence of histones along nucleosomal DNA is H2A, H2B, H4, H3, H3, H4, H2B, H2A (Figure 1.2A, B) (Richmond et al., 1984). While the H3-H4 tetramer binds tightly to the central part of the 146 bp of DNA, the H2A-H2B dimer is located peripherally at the entry and exit site of DNA onto the histone octamer. The DNA-histone interaction is weaker at the H2A-H2B side of the nucleosome and allows for transient destabilization of nucleosomes (Gansen et al., 2009; Li et al., 2005) and exchange of H2A-H2B dimers (Figure 1.2C) (Kimura and Cook, 2001; Louters and Chalkley, 1985). In fact, it was shown that histone destabilization is often initiated by reduced interaction between H3-H4 tetramers and H2A-H2B dimers (Bohm et al., 2011).

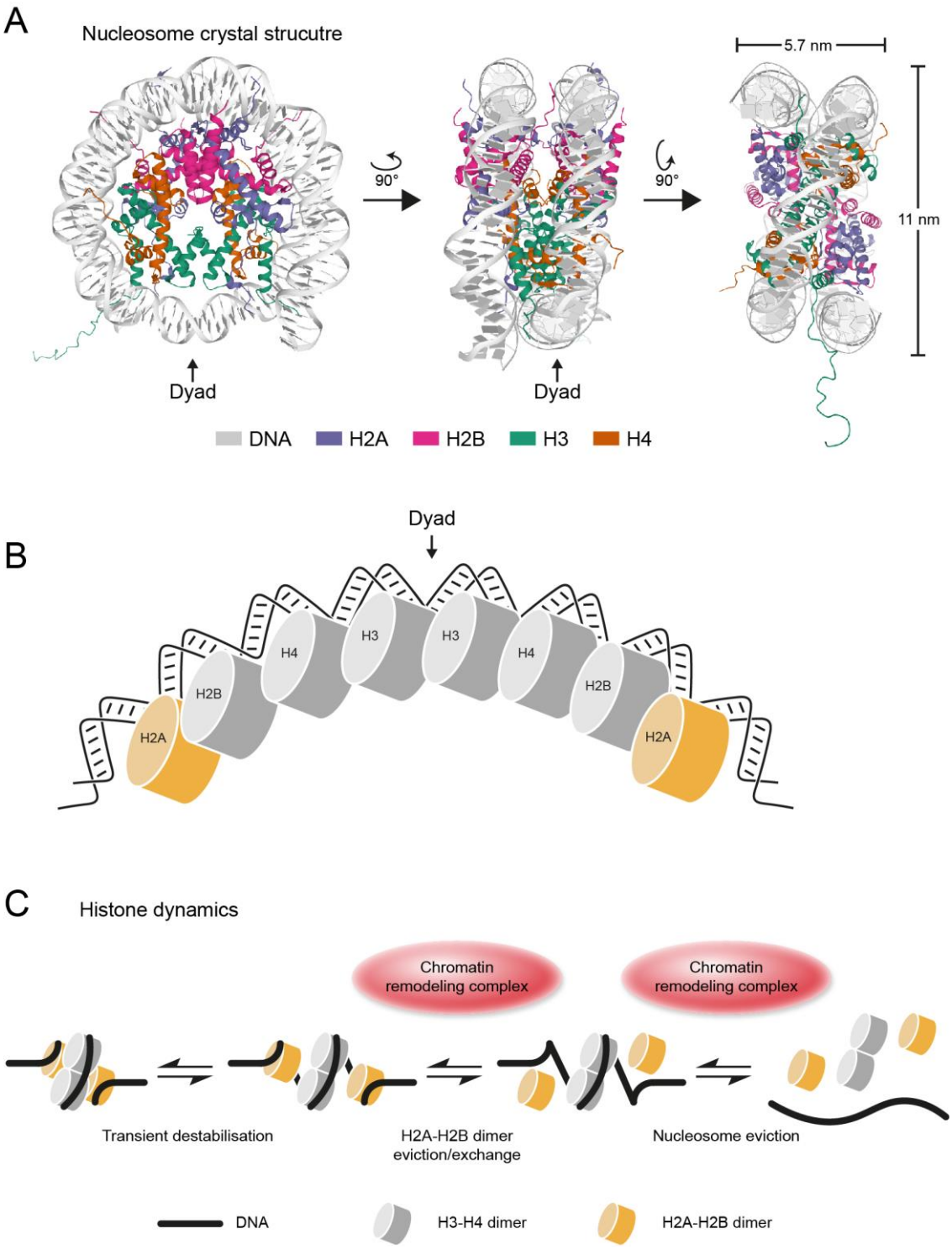

Figure 1.2: Nucleosome structure. (A) Crystal structure of human nucleosome with 146 bp of DNA (PDB, 1AOI) (Berman et al., 2000; Luger et al., 1997). **(B)** Sequence of histone binding along the 146 bp of DNA in a nucleosome. **(C)** Transient relaxation of histone octamer and DNA interaction at the H2A-H2B dimer often initiates eviction of H2A-H2B dimer and H3-H4 dimer by chromatin remodelling complexes. The diagrams

displayed were redrawn based on (Ransom et al., 2010) in (B) and (Petesch and Lis, 2012) in (C).

Histones are a natural obstacle to the access of DNA and, unsurprisingly, histone positions are very dynamic during DNA replication and transcription. During DNA replication, approximately 300 bp of DNA up- and downstream of the replication fork are nucleosome free (Gasser et al., 1996; Sogo et al., 1986). Parental histones are tethered by histone chaperones, while the replication fork moves over the underlying DNA sequence (Figure 1.3A) (Ransom et al., 2010). Histones are deposited step-wise into newly synthesized DNA by histone chaperone complexes such as the chromatin assembly factor-1 (CAF-1) complex (Kaufman et al., 1995; Smith and Stillman, 1989), which was shown to be essential for S-phase DNA replication (Hoek and Stillman, 2003; Takami et al., 2007). In a first step, H3-H4 tetramers are deposited onto newly synthesized DNA in association with the replication fork. In a second step, two H2A-H2B dimers complete the nucleosomes independently of the replication fork (Smith and Stillman, 1991). The facilitates chromatin transcription (FACT) complex is a likely candidate for H2A-H2B dimer deposition and eviction in DNA replication as well as RNA transcription (Belotserkovskaya, 2003; Tsunaka et al., 2016; VanDemark et al., 2006).

During RNA polymerase II (RNAPII) mediated transcription similar H3-H4 tetramers and H2A-H2B dimer dynamics are seen, with rapid exchange of H2A-H2B dimers and lower levels of exchange of H3-H4 tetramers (Thiriet, 2005). Highly transcribed RNAPI ribosomal RNA coding DNA loci correlate with higher exchange of H3-H4 dimers (Thiriet, 2005).

In yeast, and also in vertebrates, a robust nucleosome positioning was observed around the nucleosome depleted region (NDR) of the transcription start site (TSS), with the -1 nucleosome upstream of the TSS and +1 to +5 nucleosomes downstream of the TSS

(Barski et al., 2007; Yuan, 2005). The +1 nucleosome, downstream of RNAPII complexes, poses a strong barrier to transcription (Weber et al., 2014). Cells utilize not only large protein complexes to facilitate and regulate key events in transcription, but also histone modifications and non-canonical histone variants.

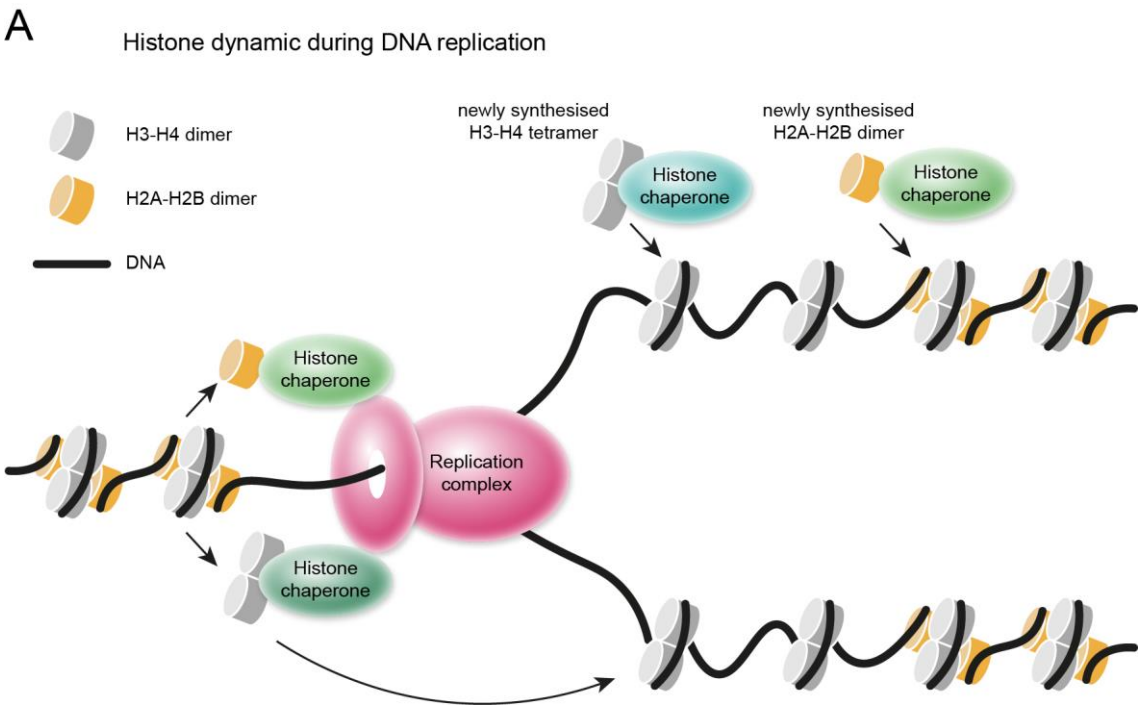

Figure 1.3: Histone dynamic during DNA replication. (A) During DNA replication, histones are evicted from the DNA, tethered by histone chaperones and then re-deposited into both newly synthesized and parental DNA strand. Newly synthesized H3-H4 tetramers are deposited in concert with the replication process, while H2A-H2B dimers are integrated later. Diagram redrawn base on (Ransom et al., 2010).

1.2.3 Histone modifications

Histone modification are covalent post translational modification (PTM) of histones, including methylation, phosphorylation, acetylation, ubiquitylation, and SUMOylation (Zhao and Garcia, 2015). The majority of PTMs are found on the accessible histone tails,

but modifications in the globular histone core domain have also been observed (Kebede et al., 2015; Tropberger and Schneider, 2010).

Specific enzymes catalyse the chemical reaction of adding or removing PTMs. For example, methyltransferases mediate the transfer of methyl-groups from an S-adenosyl methionine (SAM) donor to a lysine or arginine residue and demethylases remove the methyl-groups. The addition of a phosphate-group to various amino acids, such as tyrosine, serine, threonine, histidine, and aspartic and glutamic acid, is catalysed by kinases and phosphate groups are removed by phosphatases. The addition of an acetyl-group to histone lysine residues is catalysed by histone lysine acetyltransferases (HAT) utilizing acetyl-CoA as a donor (Figure 1.4A, B). Acetylation is reversed by histone deacetylases (HDAC). Ubiquitylation and SUMOylation is the addition of a ubiquitin or SUMO protein to lysine mediated by a cascade of enzymes. Histone PTMs have specific effects depending on the type of modification, the amino acid residue that is modified as well as the surrounding PTMs found on the same and neighbouring histones. Not only does the modification alter the chemical properties of the amino acid, but it also serves as a recognition site for histone binding proteins (Yun et al., 2011).

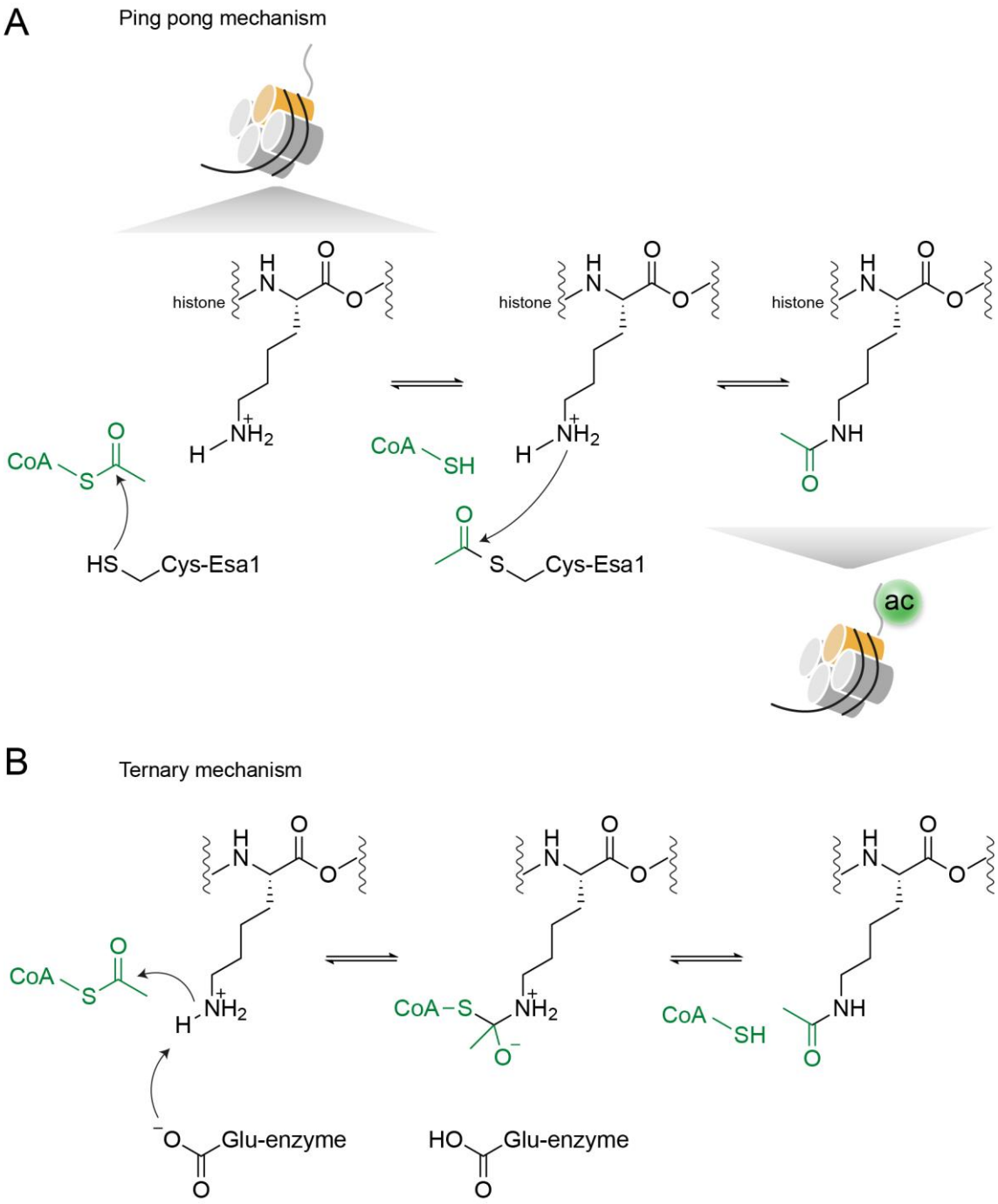

Figure 1.4: Chemical mechanism of lysine acetylation. (A) Chemical mechanism of acetyltransferases utilizing acetyl-CoA as a donor to transfer an acetyl-group onto a ε-lysine residue of histones. Shown is the Esa1 typical ping-pong mechanism, involving an acetyl-cysteine intermediate. **(B)** Other HATs, such as GCN5 or PCAF, utilize a different mechanism with a ternary complex and direct nucleophilic attack of the ε-lysine to the acetyl CoA. The diagrams displayed are based on (Berndsen et al., 2007; Yan et al., 2002) in **(A)** and (Hodawadekar and Marmorstein, 2007; Tanner et al., 1999) in **(B)**.

1.2.3.1 Histone methylation

Histones can be mono-, bi-, or tri-methylated at lysine and arginine residues, although, most methylation is observed on N-terminal H3 lysine residues (Paik and Kim, 1980). The effect of methylation depends greatly on which residue is methylated and to what degree. H3K4, H3K36, H3K48, and H3K79 methylation is associated with gene activation and H3K9 and H3K27 with gene repression (Barski et al., 2007; Bernstein et al., 2002; Bernstein et al., 2005; Bernstein et al., 2006; Mikkelsen et al., 2007). Bivalent promoters have both H3K4me3 and H3K27me3 and can be readily activated or repressed correlating with an increase in H3K4me3 or H3K27me3, respectively (Voigt et al., 2013). Specific methylation marks have been correlated with functional regions in the genome. For example, H3K4me3 marks promotor regions (Guenther et al., 2007; Santos-Rosa et al., 2002) and H3K36me3 active gene bodies (Bannister et al., 2005). H3K4me1 methylation is used as a marker for enhancer regions (Heintzman et al., 2007), while H3K27ac distinguishes between active and inactive enhancer (Creyghton et al., 2010). In contrast, H3K27me3 marks repressed genes and H3K9me3 is distinctive of heterochromatin (Boyer et al., 2006; Peters et al., 2003; Rea et al., 2000). Hypermethylation was observed in constitutive heterochromatin regions, such as centromeric, peri-centric and telomeric heterochromatin (Suka et al., 2002; Sullivan and Karpen, 2004) reviewed in (Maison and Almouzni, 2004; Richards and Elgin, 2002). Although these marks still hold true for their distinctive regions, it has become clear that histone marks are widely distributed through different regions in the genome and not all regions harbour distinctive histone marks, suggesting redundancies between marks.

1.2.3.2 Histone acetylation

The focus of this work is on histone lysine acetylation, which was discovered by Allfrey in 1964 (Allfrey et al., 1964). Advances in mass spectrometry analysis of the acetylome revealed more than 3600 acetylation sites in human cells (Choudhary et al., 2009). All core histones are found to be mono-acetylated on lysine residues, specifically on their N-terminus. Major core histone acetylation sites include H4 lysine 5, 8, 12, 16, and 20, H3 lysine 4, 9, 14, 18, 23, 27, 36, and 56, H2A lysine 5, 9, 12, and 15, and H2B lysine 5, 11/12, 15/16, and 20 (Sabari et al., 2016; Thorne et al., 1990). Electrochemically, histones are positively charged and well suited for tightly binding negatively charged DNA. The addition of acetyl-groups to histone lysine residues reduces their positive charge and weaken the bond between histones and DNA (Bradbury, 1993; Lee et al., 1993). Congruently, histone acetylation has often been correlated with more open chromatin organisation (Garcia-Ramirez et al., 1995) and higher accessibility of underlying DNA (Hebbes et al., 1994). Unsurprisingly, histone acetylation was shown to be essential for activation of gene expression (Allfrey et al., 1964; Hassig et al., 1998; Hebbes et al., 1988; Kadosh and Struhl, 1998; Kuo et al., 1998; Wang et al., 1998) and is generally associated with actively transcribed gene loci (Stasevich et al., 2014; Wang et al., 2009b; Wang et al., 2008). Conversely, constitutive heterochromatin was shown to be hypoacetylated (Casas-Delucchi et al., 2012; Csankovszki et al., 2001; Richards and Elgin, 2002; Suka et al., 2002; Sullivan and Karpen, 2004).

1.2.3.3 Histone code hypothesis

During embryonic development, histone PTMs regulate the timely expression of developmental genes. In adult cells, PTMs play an important role in translating inside and outside cues into gene transcription responses, regulating cell proliferation or

differentiation. The 'histone code' theory, proposed by (Strahl and Allis, 2000), that a combination of histone PTMs give rise to a local and temporal ‘histone code’ on top of the DNA sequence that is written, read and erased by proteins and thus facilitate the regulation of genes associated with the PTM histone code (Strahl and Allis, 2000).

1.2.4 Histone variants

The four canonical core histones (H2A, H2B, H3, and H4) can be replaced by less abundant histone variants or non-canonical histones such as H2AZ, H2AX, macroH2A, H3.3, cenH3 (CENPA). The assembly and rearrangement of histone variants within nucleosomes is an energy-dependent and dynamic process depending on dedicated enzymatic complexes (Hota and Bruneau, 2016), suggesting distinct roles for histone variants. Indeed, histone variants display distribution patterns in certain tissues, developmental stages, and genomic localizations, e.g. at the centromeres of chromosomes, transcription start sites, certain promoter elements, across gene bodies of active or inactive genes, silenced genes, and in higher level chromatin structured areas of the DNA (Henikoff and Smith, 2015). PTMs are not only found on the canonical core histones, but also on histone variants or non-canonical histones (Martire and Banaszynski, 2020). A key difference between canonical histones and histone variants is that the latter are expressed throughout all phases of the cell cycle (Nekrasov et al., 2012; Wu and Bonner, 1981), whereas canonical histones are expressed during DNA replicative S-phase (Ma, 2000; Robbins and Borun, 1967).

1.2.4.1 Histone variant H2AZ

This work focuses on the histone H2 variant Z (H2AZ), originally identified by West and Bonner (West and Bonner, 2002). H2AZ makes up around 10% of H2A in mammalian cells (Santisteban et al., 2011) and is constitutively expressed throughout the cell cycle (Wu and Bonner, 1981). Two isoforms of H2AZ, namely H2AZ.1 and H2AZ.2 have been identified (Eirin-Lopez et al., 2009). By deleting either isoform, non-redundant effects on gene expression and increased apoptosis were found in H2AZ.2, but not H2AZ.1 deleted cells (Matsuda et al., 2010). A later study showed increased exchange of H2AZ.2 at sites of DSBs, but not H2AZ.1 (Nishibuchi et al., 2014).

H2AZ shares only a 60% homology with canonical H2A (Thatcher and Gorovsky, 1994). Although, the globular core domain is highly homologous between H2A and H2AZ, key differences in the C- and N-terminal tails alter the chemical properties of H2AZ. The C-terminus of H2AZ functions in the extension of an acidic patch on the surface of H2AZ-H2B dimers compared to H2A-H2B dimers, which interacts with the H4 N-terminal tail of neighbouring nucleosomes (Suto et al., 2000). H2AZ mediated extension of the acidic patch results in increased formation and stability of heterochromatin, but decreased interaction between chromatin fibres (Fan et al., 2002; Fan et al., 2004). Interestingly, the acetylation of H4 N-terminal residues leads to failure to form higher order chromatin organisation (Allahverdi et al., 2011). The incorporation of H2AZ into nucleosomes was shown to destabilise nucleosomes (Rudnizky et al., 2016). Further, the histone composition of a nucleosome was shown to modulate the effect of H2AZ on nucleosome stability. In example, H3.3 containing nucleosomes were destabilised by H2AZ incorporation compared to nucleosomes containing H3 and H2AZ (Jin and Felsenfeld, 2007).

Secondly, H2AZ differs in its N-terminal sequence containing additional lysine residues, which are frequently acetylated and were shown to be essential for survival in the ciliate *Tetrahymena* (Ren and Gorovsky, 2001). H2AZ is mainly acetylated at K4 and K7, and to a lesser extent K11, K13 and K15 (Figure 1.5A) (Giaimo et al., 2019; Ishibashi et al., 2009). In yeast, Esa1 (yeast orthologue of the mammalian TIP60) and Gcn5 were shown to acetylate Htz1 (yeast orthologue of the mammalian H2AZ) on lysine 14 (Keogh et al., 2006; Millar et al., 2006), while Hda1 (related to mammalian HDAC4, -5, -6, -7, -9, and -10), a class II HDAC (Yang and Gregoire, 2005), was shown to deacetylate Htz1 lysine 14 (Lin et al., 2008). Many studies have been conducted on yeast histone variants. Although H2AZ is conserved from yeast to humans, homologies between yeast Htz1/H2AZ (CAA99011.1 and GAX67964.1, respectively) and human H2AZ (NP_002097.1) are exclusively based on the globular domain of H2AZ, not the highly acetylated N-terminal tail. When considering only the N-terminal tail, human H2AZ is more similar to human H2A (AAN59974.1) than to yeast Htz1 (CAA99011.1**)** (Figure 1.5B).

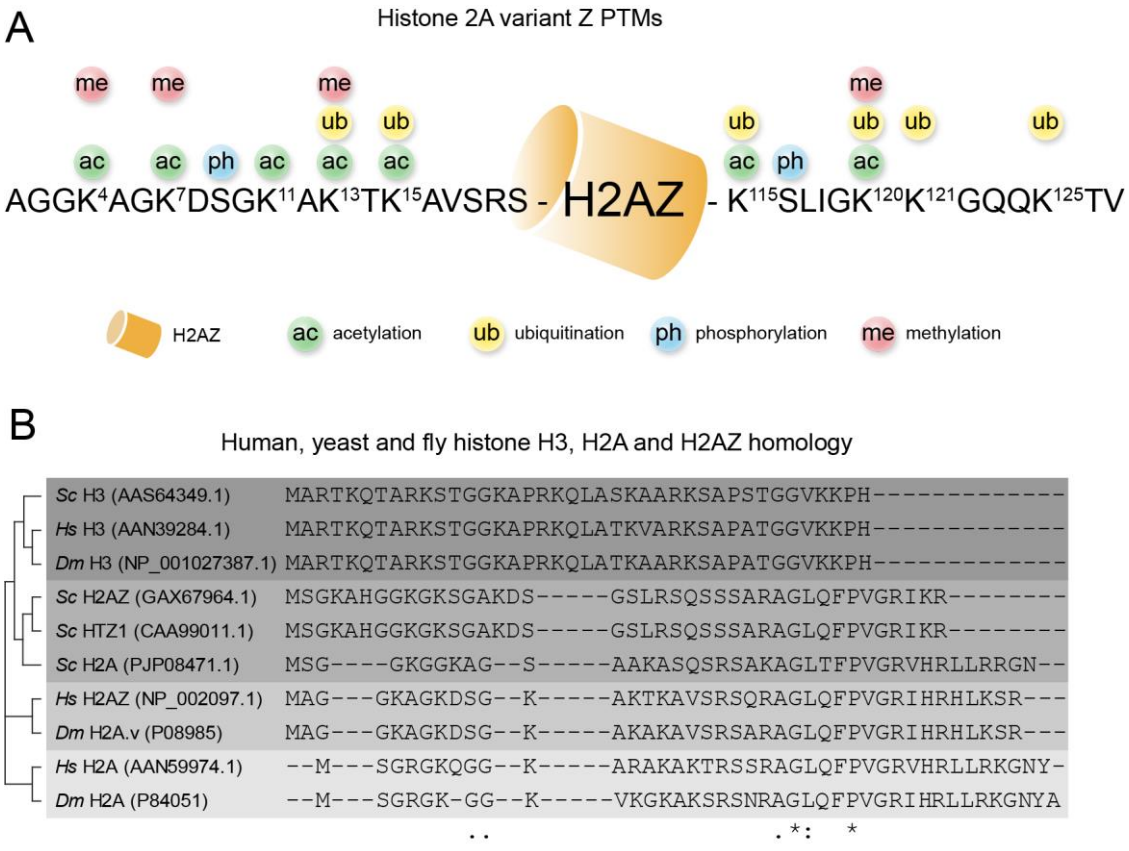

Figure 1.5: Histone 2A variant Z characteristics. (A) N- and C-terminal PTMs of H2AZ commonly found in mammalians. **(B)** Homology of N-terminal domains of *H. sapiens* (*hs*), *D. melanogaster* (*dm*), and *S. cerevisiae* (*sc*) H3, H2A, and H2AZ aligned by EMBL-EBI Clustal Omega, using clustalo (v1.2.4) (Madeira et al., 2019). Interestingly, *sc* H2AZ and HTZ1 are closer correlated to *sc* H2A, while *hs* and *dm* H2A correlate closer to each other as well as *hs* and *dm* H2AZ. Note, the N-terminal methionine of histones is cleaved off and amino acid counting conventionally starts with "1" at what is actually the second amino acid of the original protein product. The diagram displayed in **(A)** is based on (Binda et al., 2013; Giaimo et al., 2019).

1.2.4.2 H2AZ deposition

In yeast, the Htz1-H2B dimer is deposited into nucleosomes by the Swi2/Snf2-related ATPase (SWR1) chromatin remodelling complex by an ATP-dependent mechanism (Luk et al., 2010; Mizuguchi et al., 2004). Luk and colleagues showed that SWR1 first loads one Htz1-H2B dimer onto an existing nucleosome, creating a heterotypic nucleosome with one canonical H2A-H2B dimer and one Htz1-H2B dimer. Subsequent loading of a

second Htz1-H2B dimer leads to homotypic Htz1-H2B containing nucleosomes (Luk et al., 2010).

Two human SWR1 homolog complexes were identified, namely the SNF-2-related CREB-binding protein activator protein (SRCAP) (Ruhl et al., 2006) and the EP400 (p400)/TIP60 complex (Cai et al., 2005; Cai et al., 2003; Doyon et al., 2004) and shown to deposit H2AZ-H2B dimer into nucleosomes in vertebrae (Gevry et al., 2007; Ruhl et al., 2006). Eviction of H2AZ has been attributed to acidic leucine-rich nuclear phosphoprotein 32 family member E (ANP32A) (Obri et al., 2014) and the inositol-requiring protein 80 (INO80) chromatin remodelling complex in yeast (Papamichos-Chronakis et al., 2011). The localization of H2AZ to specific regions in the genome are often linked to the function of H2AZ and will be discussed in detail in the next section.

1.2.5 The cellular functions of H2AZ

In vivo, H2AZ is essential in early embryonic development in flies and mice (Faast et al., 2001; van Daal et al., 1988), but is not essential in yeast (Jackson and Gorovsky, 2000). Further, H2AZ is essential in embryonic stem cells (ESCs), maintaining stem cell identity by regulating poised developmental genes (Creyghton et al., 2008; Hu et al., 2013; Li et al., 2012b; Pandey and Dou, 2013). H2AZ has been shown to be important in a plethora of cellular processes, including DNA damage repair (Xu et al., 2012), cell cycle regulation (Dhillon et al., 2006; Long et al., 2020), pericentric heterochromatin organisation (Rangasamy et al., 2003), heterochromatin to euchromatin borders (Meneghini et al., 2003), and transcriptional regulation (Santisteban et al., 2000), reviewed in (Giaimo et al., 2019).

1.2.5.1 H2AZ in transcription

The invention of methods analysing genome-wide localization of DNA binding proteins, combining chromatin immunoprecipitation and high-throughput sequencing co-precipitated DNA (ChIP-chip, ChIP-seq), revealed that approximately 75% of yeast H2AZ is found in promotor regions (Guillemette et al., 2005), which was later confirmed in humans (Barski et al., 2007). While H2AZ is found widely at the TSS of active and inactive genes, acetylated H2AZ (H2AZac) exclusively accumulates at the TSS of active genes in human cell lines (Millar et al., 2006; Valdes-Mora et al., 2012). Further, deposition of H2AZ poises genes for transcriptional activation, and its presence at inactive promoters allows rapid activation in response to cues (Zhang et al., 2005). In ESCs, H2AZ is localized to promotors of active and poised developmental genes and is redistributed upon differentiation (Creyghton et al., 2008) and in TGF-β mediated epithelial to mesenchymal transition (EMT), H2AZ is depleted from epithelial specific genes and accumulates at mesenchymal differentiation genes to repress or activate genes, respectively (Domaschenz et al., 2017). Globally, H2AZ was shown to be essential for efficient formation and initiation of RNAPII complex (Adam et al., 2001) and the RNAPII subunit RPB1 was found as one of the top hits in a H2AZ reader screen (Draker et al., 2012). Later studies showed that H2AZ accumulated at the -1 and +1 nucleosome surrounding the TSS (Albert et al., 2007; Barski et al., 2007), resulting in a decreased barrier for RNAPII transcription (Weber et al., 2014).

H2AZ is not only found at promotor regions but also at other regulatory elements, such as enhancer regions (Barski et al., 2007; Brunelle et al., 2015; Gevry et al., 2007). Nucleosome depletion from regulatory elements has been correlated with promotor activity (Lee et al., 2004). H2AZ correlates with higher turnover of nucleosomes (Dion et al., 2007), destabilizes nucleosomes (Henikoff et al., 2009), and induces nucleosome

eviction (Du et al., 2017; Li et al., 2012b), suggesting a role of H2AZ in gene activation by favouring nucleosome depleted regions at both promoter and enhancer regions. The effects of H2AZ acetylation on binding RPB1, lowering the +1 nucleosome barrier for transcription, and histone turnover are unknown.

A good example of how H2AZ regulates gene transcription is its role in androgen receptor (AR) regulated gene activity. Initially AR target genes are inactive and promoter regions contain ubiquitinylated H2AZ (Draker et al., 2011; Slupianek et al., 2010). Upon AR binding to target genes, H2AZ is deubiquitinated and acetylated leading to gene activity (Ito et al., 2018). H2AZ occupancy relative to nucleosome occupancy has been shown to decrease after AR binding at AR target genes (Draker et al., 2011), while ER target gene activation lead to increased H2AZ occupancy (Gevry et al., 2009). Both studies, however, showed that H2AZ was essential for hormone receptor target gene activation. H2AZ dynamics during gene activation are not yet well understood. Bromodomain protein 2 (BRD2) was shown to bind H2AZ containing nucleosomes at AR-regulated genes, leading to transcriptional activation (Draker et al., 2012). While it was shown that BRD8 binds acetylated H4 (Draker et al., 2012), the acetylation status of H2AZ is unknown.

H2AZ function has been implicated in a wide range of cellular processes, such as cell cycle progression through activation of cyclin D1 through H2AZ acetylation (Dalvai et al., 2013), the activation of target genes of the oncoprotein MYC by decreasing H2AZ occupancy (Farris et al., 2005), as well as cell cycle inhibition by activating the cyclin dependent kinase inhibitor 1A (CDKN1A; $p21^{WAF1/CIP1}$) through eviction of H2AZ from *CDKN1A* (Gevry et al., 2007). A growing body of research displays the importance of H2AZ in neuronal development and neuron differentiation (Shen et al., 2018), as well as in certain brain functions, such as memory consolidation (Zovkic et al., 2014) and conditioning (Narkaj et al., 2018).

These numerous functions suggest a broad role of H2AZ in transcriptional activation. It is widely accepted that H2AZ plays an essential role in gene transcription regulation. However, activation of gene transcription has been correlated with both an increase and decrease in H2AZ occupancy at gene promoter regions. These discrepancies may be due to specific PTMs decorating H2AZ histones in these various settings. Further, the dynamic of H2AZ accumulation, H2AZ eviction and gene transcription are not clear.

1.2.5.2 H2AZ in chromatin organisation

Superficially contradictory functions of H2AZ are the induction and inhibition of heterochromatin formation. In yeast, Htz1 has been shown to protect euchromatin by antagonizing heterochromatin spreading from telomeric regions (Meneghini et al., 2003). Similarly, H2AZ is known to flank nucleosome depleted regions (NDR) in yeast (Raisner et al., 2005). In contrast, pericentric heterochromatin has been shown to be enriched in H2AZ (Rangasamy et al., 2003) and newly synthesised H2AZ was shown to be deposited into peri-centric heterochromatin during G1 phase (Boyarchuk et al., 2014). Furthermore, H2AZ is localised to centromeres during M-phase (Nekrasov et al., 2012), where it was shown to promote HP1 association to chromatin fibres (Fan et al., 2004; Rangasamy et al., 2004) and to play an integral part in heterochromatin organisation (Greaves et al., 2007).

Some insight into these contradicting functions comes from the investigation of PTMs. Acetylation of H2AZ appears essential in preserving telomeric heterochromatin boundaries (Babiarz et al., 2006) and was shown to exclusively accumulate at the TSS of active genes, supporting a role of H2AZ acetylation in providing permissive chromatin organisation (Millar et al., 2006; Valdes-Mora et al., 2012). In contrast, ubiquitination of

H2AZ is associated with its localization to the inactive X chromosome (Sarcinella et al., 2007).

1.2.5.3 H2AZ in DNA methylation

DNA methylation is a modification of the canonical DNA molecule by adding a methyl group to cysteines in the DNA mediated by DNA methyltransferases (Zemach et al., 2010). DNA methylation is frequently found in the CpG dinucleotide context (Zemach et al., 2010). DNA methylation is an important developmental mechanism for processes, such as genomic imprinting (Li et al., 1993) and X-chromosome inactivation (Mohandas et al., 1981), and has been correlated with decreased gene transcription (Ben-Hattar and Jiricny, 1988; Weber et al., 2007). DNA methylation is inherited from parents to their offspring, however, parental DNA methylation patterns are erased during germline development and re-established in the sperm and egg, as well as drastically reduced during early embryonic development in a more targeted manner and quickly re-establishment (Sanford et al., 1987), reviewed in (Greenberg and Bourc'his, 2019; Messerschmidt et al., 2014).

H2AZ correlates with hypomethylated DNA (Conerly et al., 2010) and is excluded from hypermethylated DNA loci (Zilberman et al., 2008), instead, macroH2A correlates with hypermethylated DNA (Barzily-Rokni et al., 2011). Artificial reduction of H2AZ occupancy leads to increased DNA methylation (Murphy et al., 2018). H2AZ and H3K4me1 are highly enriched in so called placeholder nucleosomes in zebrafish sperm and early embryonic development (Murphy et al., 2018). During genome activation in the early embryo, genes that show increased placeholder nucleosome occupancy are hypomethylated and become active or poised, representing genes that are important for early embryonic development (Murphy et al., 2018).

1.2.5.4 Other functions of H2AZ

H2AZ is transiently exchanged onto chromatin at sites of double-strand breaks in the DNA (DSB) together with H2AX and has been shown to play an important role in the DNA damage response by inducing a more open chromatin organisation (Xu et al., 2012). Interestingly, H2AZ.2, but not H2AZ.1 accumulates at DSBs (Nishibuchi et al., 2014). Furthermore, changes in H2AZ regulation are associated with a wide range of events in cancer. Increased H2AZ expression was shown in cancers of the breast (Hua et al., 2008) and skin, leading to aberrant gene expression (Vardabasso et al., 2015). Deletion of H2AZ.2 in skin cancer was shown to desensitize cancer cells to chemotherapies (Vardabasso et al., 2015). Enhanced H2AZ deposition into chromatin has been reported in lung cancer (Hsu et al., 2018a) and increased H2AZ occupancy at TSS of cell cycle regulatory genes was observed in bladder cancer (Kim et al., 2013). Valdés-Mora and colleagues investigated the role of H2AZ acetylation in prostate cancer cell lines, suggesting a global upregulation of H2AZ acetylation, resulting in aberrant gene transcription through activation of new enhancers (Valdes-Mora et al., 2017; Valdes-Mora et al., 2012).

Acetylation of histone residues has clearly been shown to extend the function of histones and histone variants and is essential in promoting an open chromatin conformation and DNA accessibility (Garcia-Ramirez et al., 1995; Hebbes et al., 1994). Histone lysine acetylation is catalysed by lysine acetyltransferases. In the next section, I will briefly mention the currently known nuclear histone acetyltransferases and then introduce the largest family of nuclear histone lysine acetyltransferases, the MYST family.

1.3 MYST lysine acetyltransferases

Histone acetylation is facilitated by nuclear acetyltransferase. Well characterized histone acetyltransferases can be catalogued in three families, the GNAT family (GCN5-related N-acetyltransferases) (Dyda et al., 2000), the pair of p300 and CBP (Kalkhoven, 2004), and the MYST (MOZ, Ybf2/Sas3, Sas2, TIP60) family of acetyltransferases (MOF (KAT8), MOZ (KAT6A), QKF (KAT6B), HBO1 (KAT7)) (reviewed in (Voss and Thomas, 2018)). All 5 MYST family members contain a highly conserved MYST domain, accommodating the acetyltransferase activity and acetyl-CoA binding (Figure 1.6A). Many HATs also include various histone and DNA binding domains, such as chromodomains and the PHD zinc fingers interacting with nucleosomal histones and C2H2-zink finger domains, interacting with nucleosomes (Deguchi et al., 2003; Holbert et al., 2007). The members of the MYST family HATs have been investigated with a focus on their histone acetylation activity. Males absent on the first (MOF) has been shown to be essential for H4K16 acetylation in fruit flies, mice, and humans (Akhtar and Becker, 2000; Taipale et al., 2005; Thomas et al., 2008) and histone acetyltransferase binding to ORC (HBO1) acetylates H3K14 (Kueh et al., 2011). Monocytic leukaemia zinc finger (MOZ) and querkopf (QKF) have been described to acetylate H3K9 (Voss et al., 2009; Voss et al., 2012), H3K14 (Doyon et al., 2006), and H3K23 (Lv et al., 2017; Simo-Riudalbas et al., 2015).

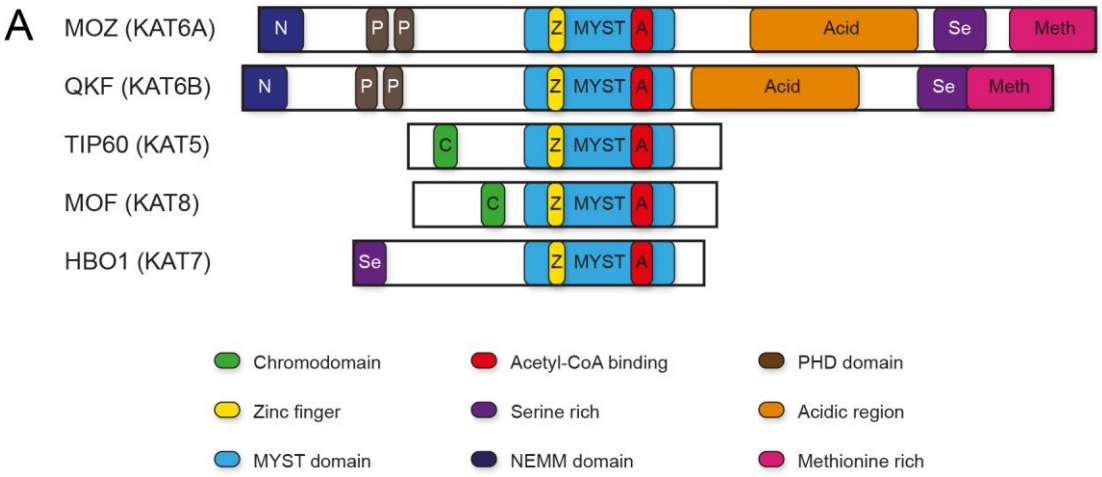

Figure 1.6: MYST family histone lysine acetyltransferase protein domains. (A) Schematic drawing of protein domains of the 5 members of MYST family acetyltransferases. The closely related pairs of MOZ and QKF as well as TIP60 and MOF share several domains additionally to the MYST domain, which is characteristic for all members of the family. N = NEMM domain, P = PHD domain, MYST = MYST domain, Z = zinc finger domain, A = acetyl-CoA binding site, Acid = acidic domain, Se = serine rich domain, Meth = methionine rich domain, C = chromodomain. Diagram redrawn based on (Voss and Thomas, 2018).

1.3.1 The lysine acetyltransferase TIP60 (KAT5)

In this study, I examine the cellular and biochemical activity of TIP60, the founding member of the MYST family of histone acetyltransferases. TIP60 was first identified as a protein interacting with HIV-1 TAT, a protein expressed by the human immunodeficiency virus (HIV) (Kamine et al., 1996). Later studies show that TAT binding to TIP60 facilitates TIP60 degradation resulting in impaired TIP60-mediated apoptosis (Col et al., 2005).

1.3.2 TIP60 protein structure and isoforms

TIP60 has been observed in 4 splice variants in humans. The predominant TIP60 isoforms are isoform 2 (TIP60α, NM_006388.4), encoded by 14 exons producing a 513-amino acid

protein, and isoform 3 (TIP60β, NM_182709.3), which excludes exon 5 (Figure 1.7A) (Ran and Pereira-Smith, 2000). Both isoforms, TIP60α and TIP60β, were shown to be expressed across a wide range of cell types, with TIP60β at slightly higher levels (Ran and Pereira-Smith, 2000). Interestingly, TIP60β was found to localise to both cytoplasm as well as nucleus, while TIP60α was constrained to the nucleus (Ran and Pereira-Smith, 2000). Other splice variants of TIP60 consist of the longer isoform 1 (NM_182710.3) retaining intron 1 and the shorter isoform 4 (NM_001206833.2) retaining intron 1 and skipping exon 5, both of which have not been investigated in depth. Interestingly, another shorter isoform of TIP60 was found in mice, called TIP55 (NM_001199249.1), retaining intron 11, which contains an early termination of the reading frame (Kim et al., 2006), resulting in a much shorter protein. TIP55 was found at levels between 25 – 50% compared to TIP60α/β levels during early embryonic development between E8.5 and E11.5 (Acharya et al., 2018). A recent study showed that murine embryos specifically lacking TIP55 die around E11.5 with proliferation defects in heart and neuronal tube cell populations, suggesting a role of TIP55 in proliferation during organogenesis, but not during implantation (Acharya et al., 2018).

The crystal structure of human TIP60 MYST domain shows the pocket for acetyl-CoA ligand binding (PDB, 2OU2) (Figure 1.7B) (Berman et al., 2000; Wu). Glycine 380 (amino acid sequence based on TIP60 isoform 2 (NP_006379.2)) is conserved in the family of MYST lysine acetyltransferases and its mutation has been shown to impair acetyl-CoA binding. Further, autoacetylation at lysine 327 and the highly conserved cysteine 369 and glutamic acid 403 in the catalytic centre of the MYST HAT domain have been correlated with TIP60 activity *in vitro* (Yang et al., 2012). Catalytically inactive Tip60 mutants have been described with double mutation of Q377E and G380E (Gavaravarapu and Kamine, 2000; Ikura et al., 2000; Wolf et al., 1998), as well as the

point mutation of E403Q (Yang et al., 2012). The chromodomain of TIP60 was shown to bind H3K4me3 (Kim et al., 2015) and H3K9me3 (Sun et al., 2009).

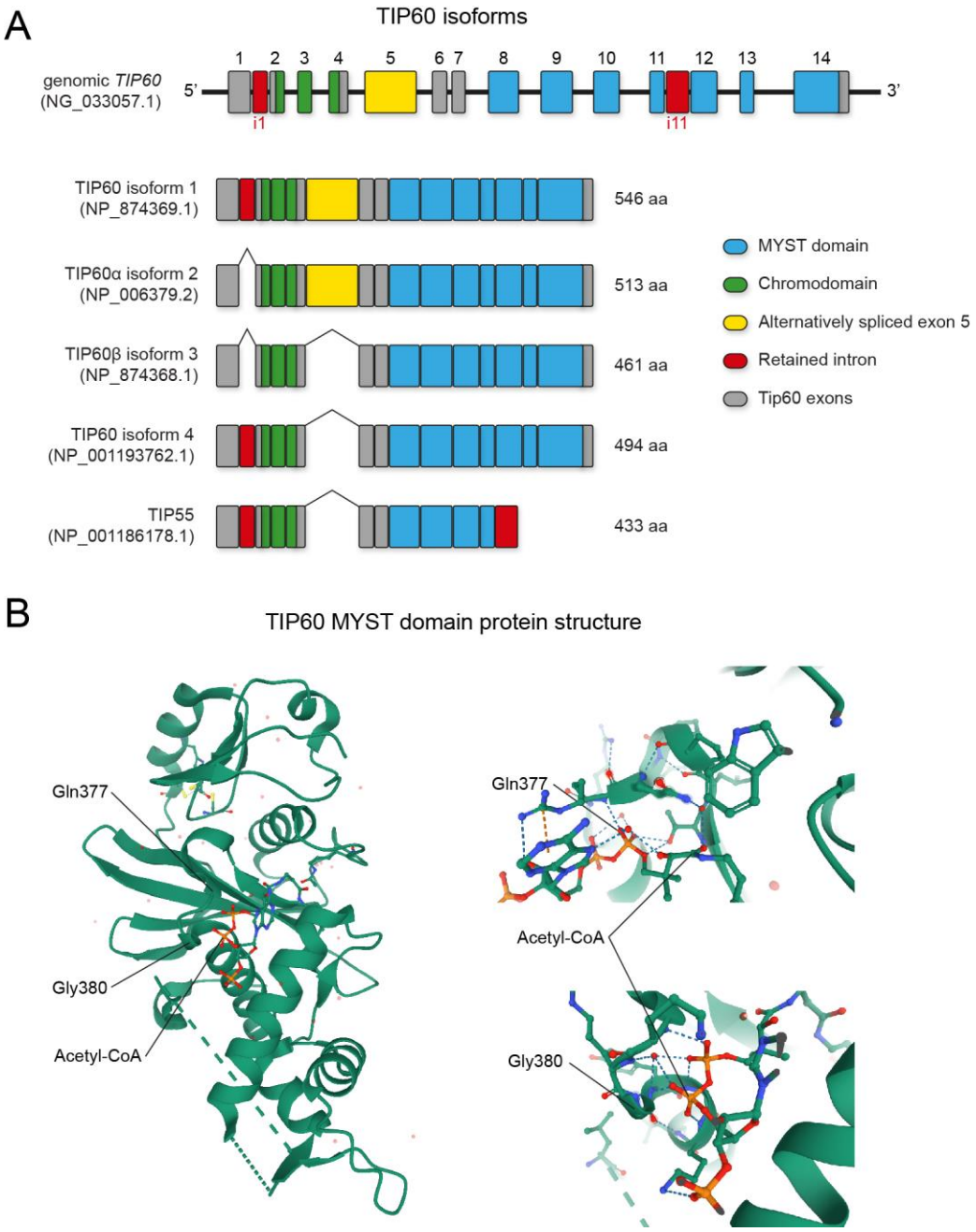

Figure 1.7: Human TIP60 isoforms. (A) Schematic drawing of human genomic *TIP60*, with exons numbered and common isoforms. Mouse specific TIP55 is displayed for completeness **(B)** Protein structure of MYST domain of TIP60 (2OU2, uniprot) and acetyl-CoA ligand. Marked are important amino acid Q377 and G380, which are essential to the HAT activity of TIP60. The diagram in (A) was drawn based on (Sheridan et al., 2001).

1.3.3 Regulation of TIP60 activity

Tip60 mRNA is expressed ubiquitously, although much more strongly during spermatocyte meiosis, suggesting a general role in all cell types as well as potential tissue-specific roles (Thomas et al., 2007). TIP60 localizes to the nucleus (McAllister et al., 2002). Free TIP60 is rapidly degraded by MDM2 (Legube et al., 2002). Besides degradation-dependent regulation of TIP60, its binding properties are regulated by ubiquitination by UHRF1 independently of degradation (Dai et al., 2013). TIP60 activation was shown to depend on autoacetylation of lysine 327 (Yang et al., 2012) and N-terminal lysine acetylation at multiple lysins, which can be removed by SIRT1 and HDAC3 (Wang et al., 2010; Yi et al., 2014). Further the acetylation activity of TIP60 is guided to substrates through various subunits of a large complex containing TIP60, namely nucleosome acetyltransferase of histone H4 (NuA4) complex.

1.3.4 The NuA4/TIP60 complex

In vivo, TIP60 occurs primarily in the NuA4 complex (Mitchell et al., 2008), which is localized in the nucleus and conserved from yeast to vertebrates (Cai et al., 2005; Cai et al., 2003; Doyon et al., 2004). NuA4 is a multi-subunit complex consisting of 13 subunits in yeast, including Tra1, Epl1, Eaf1, Eaf2, Eaf3, Eaf5, Eaf6, Eaf7, Arp4, Esa1, Act1, Yng2, Yaf9. Most of the subunits are conserved between yeasts and mammals (Doyon et al., 2004). In mammals, the NuA4 complex has at least 17 subunits, including TRRAP, EP400, BRD8, EPC1, TIP60, DMAP1, ING3, RUVBL1, RUVBL2, BAF53a, actin, MRG15, GAS41, EAF6, YL-1, MRGBP, ANP32E, and MBTD1 (Figure 1.8A) (Cai et al., 2005; Cai et al., 2003; Doyon et al., 2004; Jacquet et al., 2016; Obri et al., 2014).

Interestingly, the yeast SWR1 complex (Swr1[HAS/SWI2], Bdf1, Eaf2/swc4. Vps72, Rvb1/Tip49A, Rvb2/Tip49B, Arp4, Act1, and Yaf9) contains the yeast homologues of the human NuA4 complex subunits that are missing in the yeast NuA4 complex (Doyon et al., 2004), suggesting that yeast NuA4 and SWR1 may have merged their functions to form the mammalian NuA4 complex (Auger et al., 2008). Studies in yeast suggest a peripheral localization of TIP60 within the complex (Wang et al., 2018a). A smaller subcomplex of the NuA4 containing Esa1, Yng2 and Epl1 has been suggested to be able to act independently of NuA4 and was coined piccolo-NuA4 complex (Figure 1.8B) (Boudreault et al., 2003).

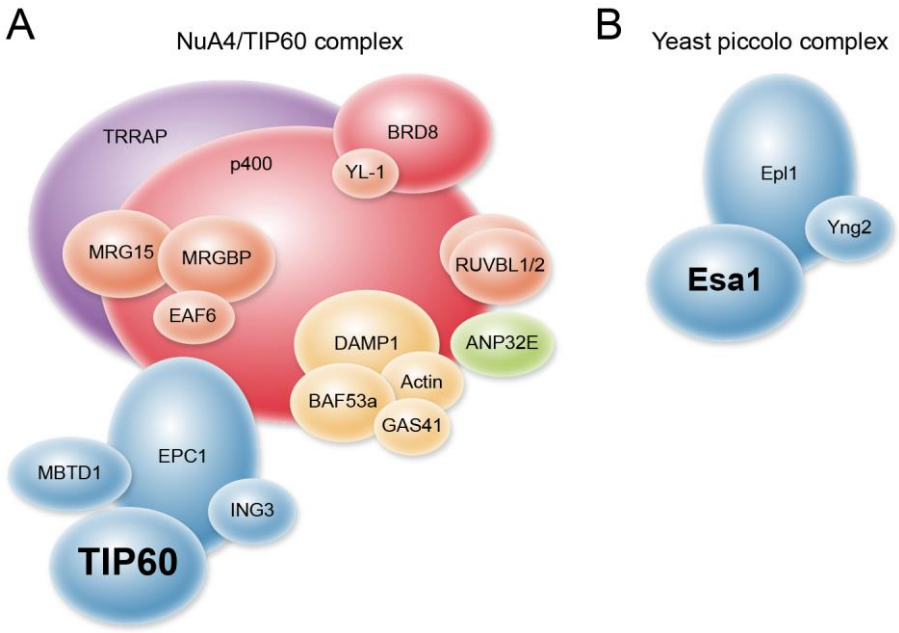

Figure 1.8: Schematic of TIP60 containing NuA4 complex. (A, B) Schematic displaying human NuA4 complex (A) and yeast piccolo complex (B). Schematic based on (Cai et al., 2005; Cai et al., 2003; Doyon et al., 2004; Jacquet et al., 2016; Obri et al., 2014).

An interactome study in yeast suggests that the NuA4 complex is a hub for subunits acting in a plethora of functions (Mitchell et al., 2008). Besides TIP60, the NuA4 complex

comprises other enzymatic activities and binding properties described further in the next section.

1.3.4.1 NuA4 subunits with protein reader domains

At least 9 NuA4 subunits possess protein-protein binding activity. BRD8 contains a bromodomain (Monden et al., 1997), mediating binding to acetylated histones (Filippakopoulos et al., 2012) and has been described to enhance thyroid hormone receptor mediated transactivation (Monden et al., 1999; Monden et al., 1997). DNA methyltransferase (DNMT)-1 associated protein 1 (DMAP1) contains a conserved SANT domain (Doyon et al., 2004), responsible for binding unacetylated H3 and H4 histone tails (Badri et al., 2008; Boyer et al., 2002; Boyer et al., 2004; Mo et al., 2005) and was found to bind preferably to H2AZ containing nucleosomes (Draker et al., 2012). Inhibitor of growth protein 3 (ING3) contains a PHD finger domain (Nagashima et al., 2003), shown to bind to H3K4me3 (Pena et al., 2006). Morf-related genes on chromosomes 15 (MRG15) contains a chromodomain, mediating binding to H3K36me2/3(Zhang et al., 2006). MRGBP is tightly bound to MRG15 (Bowman et al., 2006) and is thought to play a role in stability of MRG15 (Hayakawa et al., 2007). Glioma Amplified Sequence 41 (GAS41) contains a YEATS domain, which was shown to bind H3K14ac, H3K27ac, and H3K122suc (Cho et al., 2018; Hsu et al., 2018b; Klein et al., 2018; Wang et al., 2018b). Lastly, malignant brain tumour domain-containing protein 1 (MBTD1) was shown to bind H4K20me1/2, mediating targeting of the NuA4 complex to specific promotor regions (Jacquet et al., 2016). ANP32E was shown to act as a H2AZ chaperone essential for binding H2AZ-H2B dimers during eviction of H2AZ from existing nucleosomes (Obri et al., 2014). Similarly, the YL-1 homolog in yeast, namely swc2, was shown to interact with H2AZ during histone exchange mediated through the SWR1 complex (Wu

et al., 2005). β-actin is a cytoskeletal protein and BRG1-associated factor 53a (BAF53a) is a β-actin like protein, supporting ATPase activity of RUVBL1/2 in the BRG1 complex as well as its localization to chromatin (Zhao et al., 1998).

1.3.4.2 NuA4 subunits with scaffold characteristics

Transformation/transcription domain-associated protein (TRRAP) is thought to serve as a scaffold for the NuA4 complex and has been found in several other large complexes, such as the Spt-Ada-Gcn5 acetyltransferase (SAGA) complex (reviewed in (Murr et al., 2007)). Enhancer of polycomb homolog 1 (EPC1) functions as a smaller peripheral scaffolding protein facilitating the formation of the piccolo-NuA4 complex (Boudreault et al., 2003) and recruitment of MBTD1 (Zhang et al., 2020).

1.3.4.3 NuA4 subunits with enzymatic activities

Besides the acetyltransferase activity of TIP60, the NuA4 subunit EP400 is an ATPase activity containing protein related to the yeast SWR1 complex (Xu et al., 2010). Further, RUVBL1 (also TIP49, Pontin) and RUVBL2 (also TIP48, Reptin) form a hexamer and possess AAA+ ATPase and DNA helicase activity (Kanemaki et al., 1999). RUVBL1/2 are also subunits of the human INO8 (Shen et al., 2000) and SRCAP complex (Cai et al., 2005).

1.4 The cellular functions of TIP60

TIP60 has been implicated in a wide range of functions including embryonic development, gene transcription, chromatin remodelling, DNA damage response,

apoptosis and cell cycle regulation, brain functions and general metabolism via histone and non-histone protein acetylation as well as non-catalytic functions, such as histone PTM reader and scaffolding functions.

1.4.1 The role of TIP60 in embryonic development

Hu and colleagues showed that germline deletion of *Tip60* in mice leads to early embryonic lethality at the blastocyst stage (Hu et al., 2009). In embryonic stem cells (ESCs) TIP60 is essential for self-renewal, by repressing the transcription of developmental genes (Fazzio et al., 2008). However, acetylation of histones is a hallmark of gene activation and not repression, suggesting that TIP60 HAT activity is not directly involved in transcriptional repression. HDAC6 was found to be important for binding of the NuA4 complex to target gene promoters (Chen et al., 2013b). A later study implies that the lysine acetyltransferases activity of TIP60 is not essential for ESC proliferation and gene expression in culture (Acharya et al., 2017). *In vivo*, catalytically dead *Tip60* mutant mice display severe growth restrictions from at least E6.5 onward (Acharya et al., 2017), and so normal development is disrupted only two days later than in *Tip60* null embryos.

1.4.2 The proposed histone lysine acetylation targets of TIP60

A wide range of H4, H2A and some H3 lysine residues have been reported to be acetylated by TIP60. Studies utilizing cell free assays are prone to overestimating the substrate range, as the protein complex context of HATs and the cellular context provide layers of regulation (Voss and Thomas, 2018). Furthermore, siRNA knockdown experiments have suggested targets of HAT that have not been replicated by genetic loss

of function experiments (Kueh et al., 2020; Voss and Thomas, 2018). Studies utilizing supposedly TIP60 specific inhibitors must be considered with the caveat that most KAT inhibitors were found to be non-specific (Dahlin et al., 2017).

TIP60 has been reported to acetylate histone H2AK5, as well as H4K5, H4K8, H4K12, H4K16, and H3K14 in cell free assays (Kimura and Horikoshi, 1998) and H2AK15 in siRNA knockdown experiments in human cell lines (Jacquet et al., 2016). In yeast, Esa1 (yeast orthologue of TIP60) and Gcn5 were shown to acetylate Htz1 (yeast orthologue of H2AZ) on lysine 14, resulting in transcription initiation (Keogh et al., 2006; Millar et al., 2006). In *D. melanogaster*, dTIP60 has been shown to acetylate H4K5ac and H2Av (fly orthologue of H2AZ) (Kusch et al., 2014). TIP60 occupancy correlates with H2AK5ac in MCF-7 cells (Jeong et al., 2011) and H2AZac at NOTCH1 target loci in murine immune cell lines (Giaimo et al., 2018).

In contrast, other MYST histone acetyltransferases appear to have specific histone acetylation activity *in vivo.* In particular, MOF appears to acetylate specifically H4K16 (Akhtar and Becker, 2000; Gupta et al., 2008; Taipale et al., 2005; Thomas et al., 2008) and the major target of HBO1 seems to be H3K14 (Feng et al., 2016; Kueh et al., 2011; Kueh et al., 2020; Mishima et al., 2011) At the beginning of my project, the consequences of a genetic deletion of TIP60 in mammalian cells had not been assessed. Therefore, I conducted a comprehensive assessment of the effects of complete loss of TIP60 on all proposed histone lysine targets within primary cells and cell lines.

1.4.3 The role of TIP60 in the regulation of transcription

On a genome-wide level, TIP60 has been shown to accumulate at active RNA polymerase II (RNAPII) promoters (Ravens et al., 2015; Wang et al., 2009b), suggesting a general role of TIP60 in regulating transcription. TIP60 has been reported to acetylate

transcription factors and histones, acting as a co-factor for transcriptional activation (Table 1). MYC has been reported to bind directly to TIP60, followed by TIP60-mediated acetylation of MYC and stabilization (Patel et al., 2004). MYC was further shown to recruit TIP60 to MYC target gene loci (Frank et al., 2003). Furthermore, TIP60 has been shown to act as a co-activator for nuclear hormone receptors. The recruitment of TIP60 to a specific set of genes by estrogen receptor (ER) increases acetylation of the local histones through a cascade of protein binding and activity, resulting in enhanced gene transcription (Jeong et al., 2011). In addition, AR, ER and progesterone receptor (PR)-mediated transcription is enhanced by TIP60 in a ligand dependent manner (Brady et al., 1999). Interestingly, TIP60 was shown to directly acetylate the AR and is antagonized by HDAC1 (Gaughan et al., 2002). In another example, acetylation of the transcription factor FOXP3 by TIP60 was shown to increase the ability of FOXP3 to activate gene transcription (Xiao et al., 2014). The HAT activity of TIP60 was shown to be essential in co-activating C/EBPα target genes in a lymphocyte cell line (Bararia et al., 2008).

TIP60 was often found to interact with transcription factors. The interaction of TIP60 with SOX9 leads to increased transcriptional activity of SOX9 target genes (Hattori et al., 2008). Similarly, during myoblast differentiation, TIP60 was shown to directly interact with MYOD1 and to enhance transcriptional activation by MYOD1 (Kim et al., 2011). Direct interaction between TIP60 and the NF-κB signalling factor RELA (p65) was shown to enhance RELA (p65)-mediated transcriptional activation (Kim et al., 2012d). In *D. melanogaster*, heat shock factor (HSP) recruits dTIP60 to target gene promoters, resulting in TIP60-dependent chromatin remodelling and subsequent gene transcription (Kusch et al., 2014). dTIP60 is further required for transcription of HIF1α target genes, which was shown to be conserved in humans (Perez-Perri et al., 2016). Indirect binding of TIP60 to transcription factors via co-factors, such as Fe65-mediated binding of TIP60

to the cytoplasmic cleavage product of amyloid-beta precursor protein (APP) widens the potential roles of TIP60 in regulatory processes (Cao and Sudhof, 2001).

Incongruent with its other functions, TIP60 has also been described as a co-repressor. For example, TIP60 has been proposed to bind STAT3 and repress STAT3-mediated gene transcription (Xiao et al., 2003). The authors suggest a role of co-complexing of HDAC7 with the STAT3/TIP60, which increases the repressing effect of TIP60. Further, TIP60 has been suggested to CREB and inhibit PKA-mediated activation of CREB and subsequent CREB-dependent gene activation (Gavaravarapu and Kamine, 2000). Interestingly, CREB inhibition was shown to be independent of the HAT activity of TIP60. Lastly, TIP60 has been observed to inhibit Tumour protein p73 (TP73) target gene activation by binding TP73 and MDM2 leading to TP73 degradation (Kim et al., 2008). TP73 inhibition was found to be HDAC-independent.

In general, this body of research shows that TIP60 might act as a co-regulator of transcription factors through several different mechanisms, including scaffolding, KAT activity, and reader capabilities.

Table 1: Proposed roles of TIP60 as transcriptional co-regulator.

Factor	**Type of interaction**	**Effect**	**Reference**
MYC	Direct acetylation of MYC by TIP60	Stabilization of MYC	(Patel et al., 2004)
MYC	Recruitment of TIP60 by MYC to target loci	Increased histone acetylation	(Frank et al., 2003)
AR, ER, PR	Direct interaction with steroid receptors	Increased transcription	(Brady et al., 1999)
ERα	Acetylation of histones at target genes	Increased transcription	(Jeong et al., 2011)
AR	Direct acetylation of AR	Increased transcription	(Gaughan et al., 2002)
FOXP3	Direct acetylation of FOXP3	Increased transcription	(Xiao et al., 2014)
C/EBPα	Acetylation of H3 and H4 at target genes	Increased transcription	(Bararia et al., 2008)
SOX9	Direct interaction of SOX9	Increased transcription	(Hattori et al., 2008)

MYOD	Direct interaction with MYOD	Increased transcription	(Kim et al., 2011)
RELA (p65)	Direct interaction with RELA	Increased transcription	(Kim et al., 2012d)
PAX6	Direct interaction with PAX6	Increased transcription	(Kim et al., 2012a)
NRL	Direct interaction with NRL	Increased transcription	(Kim et al., 2012c)
HSP	Deposition of acetylated H2Av at target genes	Increased transcription	(Kusch et al., 2014)
E2F1	Recruitment by E2F1 to target genes	Increased transcription	(Taubert et al., 2004)
HIF1α	Direct interaction; recruitment of TIP60 by HIF1α to chromatin	Increased transcription	(Perez-Perri et al., 2016)
APP	Indirect binding via Fe65	Increased transcription	(Cao and Sudhof, 2001)
STAT3	Direct interaction and recruitment of HDAC7	Decreased transcription	(Xiao et al., 2003)
CREB	Inhibits PKA-mediated activation of CREB	Decreased transcription	(Gavaravarapu and Kamine, 2000)
TP73	Direct interaction and recruitment of MDM2	Decreased transcription	(Kim et al., 2008)

1.4.4 The role of TIP60 in nucleosomal histone dimer exchange

A global role of TIP60 in transcription might stem from its function in chromatin remodelling. EP400, a subunit of the TIP60 containing NuA4 complex (Doyon et al., 2004), was shown to mediate the exchange of H2A-H2B to H2AZ-H2B dimers through its ATPase activity (Chan et al., 2005; Gevry et al., 2007; Ikura et al., 2000). In *D. melanogaster*, the dTIP60 and EP400 complex has been shown to preferentially exchange phosphorylated H2Av, a *D. melanogaster* homologue of H2AZ, in *in vitro* nucleosome arrays and at sites of DNA damage (Kusch, 2004). TIP60 is highly expressed during spermatogenesis and essential for proper spermatid development, during which TIP60 leads to histone hyperacetylation and subsequent histone replacement by protamines resulting in genome compaction (Dong et al., 2017).

1.4.5 TIP60 in DNA damage response

A well-studied role of TIP60 is its role in the DNA damage response (DDR). The DDR is the ability of cells to sense DNA damage and activate a cascade of events resulting in DNA damage repair. The DDR requires a transient cell cycle arrest to allow time for the repair. Failure to repair DNA damage or excessive DNA damage steers the cell towards permanent cell cycle exit or apoptosis.

The catalytic activity of TIP60 has been shown to be important for effective DSB repair in human cells and potential induction of apoptosis (Ikura et al., 2000). Sun and colleagues found that TIP60-dependent acetylation of ataxia-telangiectasia mutated (ATM) upon DNA damage is essential for ATM kinase activity (Sun et al., 2005). ATM plays a key role in the DDR cascade activated by DNA damage. ATM is recruited to DSBs by the MRN complex (Uziel et al., 2003) and ATM kinase activity is upregulated rapidly after DNA damage (Bakkenist and Kastan, 2003), resulting in activation of key substrates through phosphorylation, such as H2AX (Burma et al., 2001; Rogakou et al., 1998), TP53 (p53) (Banin et al., 1998), MDM2 (Khosravi et al., 1999) and various cell cycle specific regulators (CHK2 in G1-phase, NBS1, BRCA1, FANCD2, and SMC1 in S-phase, and BRCA1 and RAD17 in G2/M-phase) (Bakkenist and Kastan, 2004). A subsequent study revealed, that TIP60 is localized to H3K9me3 at DSBs and deemed this interaction necessary for TIP60 acetylation activity (Sun et al., 2009). However, a different mode of TIP60 recruitment through the NuA4 complex scaffold protein TRRAP and subsequent H4 hyperacetylation at DSB sites have been shown (Murr et al., 2006). Binding of TIP60 to ATM has also been reported to depend on initial binding of FOXO3A to ATM (Adamowicz et al., 2016).

The repair of DSB requires remodelling of local chromatin organisation. Various subunits of the NuA4 complex play a role in chromatin remodelling at sites of DSBs, including

EPC1, MBTD1 and EP400. TIP60 has been shown to acetylate histones at sites of DSBs, such as H2AX, resulting in TIP60 dependent H2AX eviction (Ikura et al., 2007). Later studies revealed that H2AX eviction after DNA damage is impaired in EPC1, MBTD1 and TIP60 knockout cells (Jacquet et al., 2016). Specifically, TIP60 and the MBTD1 subunit of the NuA4 complex were shown to regulate TP53-binding protein 1 (TP53BP1) binding to sites of DNA damage (Jacquet et al., 2016). EP400 accumulates at sites of DSB and is needed to destabilize nucleosomes for further binding of DSB signalling factors (Xu et al., 2010). ANP32A is also recruited to sites of DSBs, most likely together with the NuA4 complex, and leads to H2AZ eviction from DSBs (Gursoy-Yuzugullu et al., 2015). In *Drosophila* the dTIP60 chromatin-remodelling complex acetylates H2Av, a *Drosophila* histone variant mediating functions of human H2AZ and H2AX combined (Baldi and Becker, 2013), and exchanges it with the unmodified form after induction of DSBs in *D. melanogaster* cells (Kusch, 2004) ensuring, optimal stress response and cell survival, rather than cell death (Kusch et al., 2014). Together, extensive research suggests a broad multi-functional role of TIP60 in the DNA damage response.

1.4.6 The role of TIP60 in regulating cell cycle arrest and apoptosis

1.4.6.1 Cell cycle regulation

During a human lifetime, cells undergo approximately 10 quadrillion (10^{16}) cell divisions and each can lead to a cancerous cell, if not regulated tightly (Weinberg, 2014). The regulation of the cell cycle is facilitated by a network of factors. The main actors are cyclins, cyclin-dependent kinases (CDK) and cyclin-dependent kinase inhibitors (CDKI) (reviewed in (Vermeulen et al., 2003)). Generally, cells divide in two consecutive stages: the replication of DNA (S-phase) and the division into two daughter cells with equal DNA

content (M-phase). In between the S- and M-phase are growth phases, namely the G1- and G2-phase, respectively. Cells can arrest in any phase of the cell cycle, for example, reversibly in a quiescent G0-phase, transiently in S-phase to undergo DNA-repair or during the G1 or G2-phase to allow time for further growth. Each phase is marked by the expression of certain cyclins, which are required for the activation of CDKs and progression through the respective phase of the cell cycle (Figure 1.9). In early G1-phase cyclins of type D (cyclin D1, D2, and D3) activate CDK4 and CDK6, facilitating entry into G1-phase and cyclin E activates CDK2 initiating the transition from G1- to S-phase. Cyclin A activates CDK2 in S-phase and CDK1 during transition from G2- to M-phase, while cyclin B activates CDK1 during mitosis in M-phase. Cyclin H activates CDK7 throughout the cell cycle and regulates other CDKs via phosphorylation. CDKs phosphorylate a complex network of target proteins facilitating a plethora of functions throughout the cell cycle.

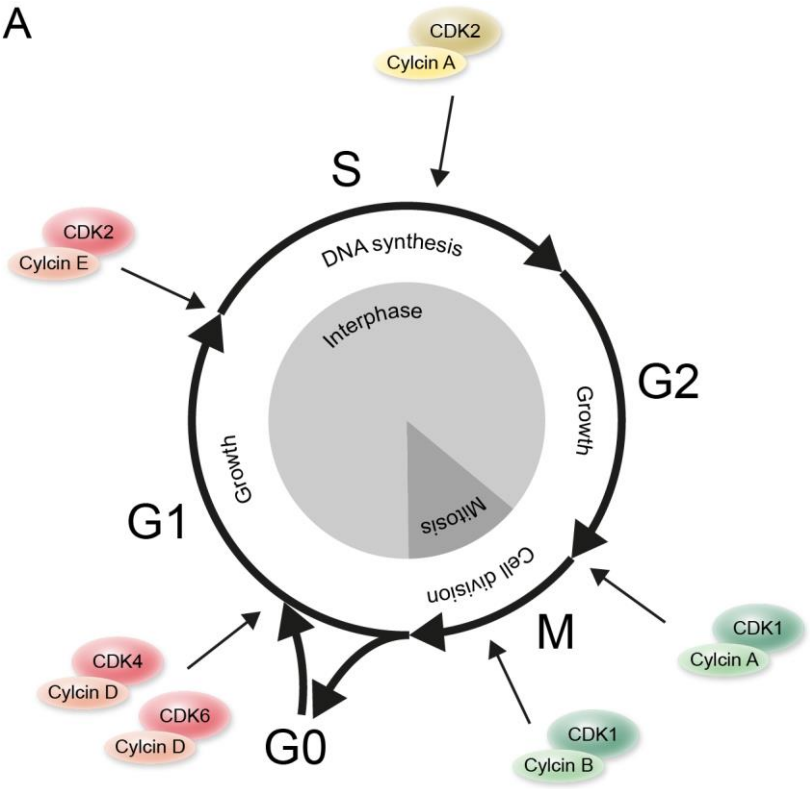

Figure 1.9: Cell cycle phases and their respective cyclins and CDKs. (A) The cell cycle generally divided into mitosis and interphase. Most cell reside in G1 phase, which marks growth and general cell activity. Cells transition into S-phase and start replicating their DNA. After DNA replication cells enter a second growth phase serving as a preparation to enter M-phase. In M-phase cells traverse several sub-phases, namely, pro-, meta-, ana-, and telophase, during which the DNA condenses and splits into two daughter cells. The cell cycle is tightly regulated by cyclins and CDKs, which are important for transitions between cell cycle phases. Drawn based on (Vermeulen et al., 2003).

DNA replication is prone to introduce DNA damage, which is controlled by certain cell cycle checkpoints, at which cell cycle progression can be inhibited by CDKIs. CDKIs repress the activity of CDKs and allow, for example, time for an appropriate response to DNA damage. Two major DNA damage checkpoints are the G1-S checkpoint before cells initiate DNA replication, and the G2-M checkpoint after DNA replication. The most prominent G1-S checkpoint downstream actor is TP53. Another checkpoint is the spindle

checkpoint controlling proper attachment of spindles to kinetochores of the sister-chromatid (reviewed in (Gorbsky, 2015).

The evasion of cell cycle checkpoints is a hallmark of cancer. Frequent mutations found in cancer are in genes important for cell cycle regulation. Apart from mutations in *TP53*, *MYC*, *RAS*, and *RB1*, the *CDKN2A* and *CDKN2B* loci are commonly mutated in cancer (Kandoth et al., 2013; Ma et al., 2018) and the *CDKN4C* locus is occasionally mutated. *CDKN2A CDKN2B CDKN4C* encode the CDKs of the INK4 family ($p15^{INK4B}$, $p16^{INK4A}$, $p18^{INK4C}$, and $p19^{ARF}$). These CDKIs inhibit CDK4 and CDK6 leading to cell cycle arrest in G1-phase upon cell cycle abnormalities, such as metabolic stress and DNA damage. The *CDKN2A* locus encodes for two proteins, namely $p16^{INK4A}$ and14^{ARF} ($p19^{ARF}$ in mice). Both $p16^{INK4A}$ and $p19^{ARF}$ have been shown to act as tumour suppressor *in vivo*, however, *in vitro* they display various effects on proliferation (Sharpless et al., 2004). Overexpression of $p16^{INK4A}$ and $p19^{ARF}$ leads to cellular senescence (Jacobs et al., 1999). Another family of CDKIs, the CIP/KIP family, include $p21^{Waf1/Cip1}$, $p27^{Cip2}$, and $p57^{Kip2}$. The CDKI $p21^{Waf1/ CIP1}$ is responsible for p53-mediated cell cycle arrest (El-Deiry, 1993; Harper et al., 1993). The role of CDKIs is to prevent cell cycle progression, creating the opportunity to repair DNA damage or manage cytotoxic stress. If the DNA damage cannot be repaired the cellular response shifts toward pro-apoptotic signalling to prevent the mitosis of damaged cells. These mechanisms are crucial for genetic integrity and the prevention of cancer. TP53 plays an important role in inducing either cell cycle arrest or apoptosis through transactivation of downstream target genes. In the case of low DNA damage TP53 can upregulate $p21^{Waf1}$ expression, leading to cell cycle arrest and in case of severe oncogenic DNA damage TP53 activates pro-apoptotic genes, such as *NOXA*, *PUMA* and *BAX* leading to programmed cell death (reviewed in (Chen, 2016)).

1.4.6.2 The role of TIP60 in TP53 function

TP53 has been termed "guardian of the genome" (Lane, 1992). It acquired this title due to its critical role in inducing cell cycle arrest and apoptosis upon cell stress, such as DNA damage and mitotic defects (reviewed in (Levine, 1997; Vousden, 2006; Vousden and Prives, 2009).

In healthy cells, TP53 levels are suppressed by MDM2 (Haupt et al., 1997) which also mediates degradation of free TIP60 (Legube et al., 2002), suggesting a shared regulation pathway for both TP53 and TIP60. In a negative feedback, *MDM2* gene expression is upregulated TP53 binding to its promoter (Tang et al., 2006). Acetylation of TP53 by TIP60 was not only one of the earliest examples that non-histone proteins are regulated by a histone acetyltransferase *in vivo* (Gu and Roeder, 1997), but was also shown to be crucial for its activity as a transcription factor (Figure 1.10A) (Tang et al., 2008).

TP53-dependent transcription of baseline levels of *MDM2* was shown to be independent of TP53K120 acetylation (Tang et al., 2006). However, other TP53 target genes have been shown to depend on TP53K120 acetylation (Gu and Roeder, 1997). TIP60 acetylates TP53 at K120, which is essential in TP53 dependent activation of pro-apoptotic genes, such as *PUMA* (Tang et al., 2006) and *BAX* (Kaya-Okur et al., 2019; Sykes et al., 2006). Notably, activation of TP53 target genes that favour cell cycle arrest, such as *CDKN1A*, also depend on TIP60 co-activation, but in a TP53K120 acetylation independent manner (Legube et al., 2004; Tang et al., 2006). TIP60-mediated TP53K120 acetylation is regulated by other proteins, such as Coiled-coil domain-containing protein 8 (CCDC8) (Dai et al., 2011). In mice TP53K117 acetylation is equivalent to human K120 acetylation and was shown to be important for apoptosis, but not cell cycle arrest or senescence (Li et al., 2012a). TP53 mediates cell cycle arrest through transcriptional activation of *CDKN1A* ($p21^{CIP1/Waf1}$), which is in part regulated by acetylation of TP53 lysine 164

(TP53K161 and K162 in mice). In mice the mutation of 3 TP53 lysines to arginines (K117, K161, and K162) lead to ablation of TP53-mediated cell cycle arrest, senescence, and apoptosis, indicating the importance of lysine 161 and 162 in TP53-mediated cell cycle arrest and senescence (Li et al., 2012a). Notably, TP53 mutant mice with arginine instead of lysine at position 117, 161, and 162, which are incompetent for p53-mediated cell cycle arrest, senescence, or apoptosis, did not display early-onset tumorigenesis as seen in TP53 null mice, indicating that TP53 possesses tumour suppressor functions that are independent of its acetylation (Li et al., 2012a). For example, the regulation of metabolism and production of reactive oxygen species was not impaired in these triple mutant $TP53^{K117R, K161R, K162R}$ mice (Li et al., 2012a). Tang and colleagues found that in human cells only the mutation of 8 TP53 lysines to arginines (K120, K164, K370, K372, K373, K381, K382, and K386) lead to complete loss of $p21^{CIP1/Waf1}$, which was not observed in $TP53^{K370R, K372R, K373R, K381R, K382R, K386R}$, $TP53^{K120R}$ or $TP53^{K164R}$ cells, while $TP53^{K120R, K164R}$ cells displayed reduced $p21^{CIP1/Waf1}$ levels (Tang et al., 2008). In addition, TP53 is acetylated at K320 by PCAF (Sakaguchi et al., 1998) leading to transcription of anti-apoptotic genes, such as *CDKN1A* (Knights et al., 2006). Other TP53 acetylation sites include 6 lysines in the C-terminal region of human TP53 (7 lysines in murine p53), which were shown to play a role in fine tuning the activity of TP53 (Krummel et al., 2005) (reviewed in (Kruse and Gu, 2009)), as well as TP53 lysine 164 (and K161 and K162 in mice), which is acetylated by EP300 (Tang et al., 2008).

TIP60 binding to TP53 is regulated by proteins, such as UHRF1, which binds TIP60 and interferes with TP53-TIP60 interaction along with TIP60 degradation independently of ubiquitination (Dai et al., 2013).

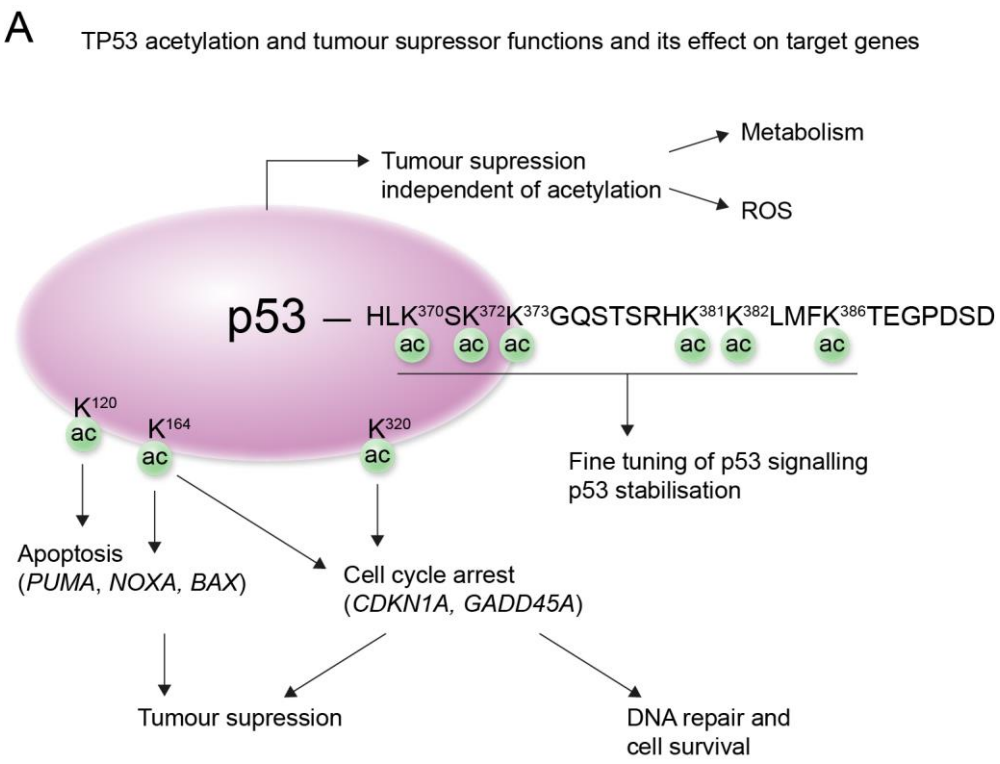

Figure 1.10: Role of acetylation in TP53-mediated tumour suppressor functions. (A) TP53 is acetylated at multiple sites, regulating TP53 stability as well as target specificity. Diagram based on (Gu and Roeder, 1997; Kaya-Okur et al., 2019; Knights et al., 2006; Kruse and Gu, 2009; Li et al., 2012a; Sakaguchi et al., 1998; Sykes et al., 2006; Tang et al., 2006; Tang et al., 2008)

1.4.6.3 TIP60 in apoptosis

TIP60 can promote cell death or cell survival depending on the specific context. TIP60 was first identified as a protein interacting with the HIV-1 tat protein (Kamine et al., 1996). In this context, TIP60 appears to promote cell death, as HIV-1 tat binding to TIP60 facilitates the degradation of TIP60 resulting in impaired TIP60-mediated apoptosis (Col et al., 2005). Overexpression of catalytically inactive TIP60 leads to defects in DNA damage repair and decreased apoptosis upon γ-irradiation (Ikura et al., 2000). Similarly, siRNA knockdown of TIP60 impairs the UV-induced DNA damage response and apoptosis (Kranz et al., 2008). Kim and colleagues found that TIP60 inhibited TP73-mediated apoptosis through inhibition of TP73 target genes, such as *CDKN1A*

($p21^{CIP1/Waf1}$) and *BAX* (Kim et al., 2008). In contrast, genetic loss of TIP60 in murine blastocysts causes apoptotic cell death (Hu et al., 2009), indicating that in this instance TIP60 is required for cell survival.

The apparent contradiction in pro-survival and pro-apoptotic roles of TIP60 has not been resolved and therefore I conducted experiments to test if genetic deletion of TIP60 influenced cell survival.

1.4.7 The role of TIP60 in cancer

The involvement of chromatin-mediated mechanisms in the development of tumours has long been deemed an important avenue to cancer therapy (reviewed in (Kaypee et al., 2016)). Many KATs have implications in tumorigenesis (Farria et al., 2015), The roles of TIP60 appear to be unclear, as it has been reported to promote or slow cancer progression. Heterozygous loss of *Tip60* accelerates tumour progression in mouse models of breast cancer (Bassi et al., 2016) and lymphoma (Gorrini et al., 2007). A later study found lowTip60 mRNA levels correlated with decreased survival and increased relapse rates (McGuire et al., 2019). Reduced levels of TIP60 are associated with poor outcome in melanoma patients (Chen et al., 2012), in metastatic colorectal cancer (Sakuraba et al., 2009) and in metastatic gastric cancer (Sakuraba et al., 2011). Furthermore, TIP60 is downregulated in acute myeloid leukaemia (AML) (Zhao et al., 2012) and acts as a tumour suppressor in colon cancer (Chevillard-Briet et al., 2014). In *C. elegans* the NuA4 complex was shown to reduce RAS signalling (Fisher et al., 2010). In contrast, in prostate cancer high levels of nuclear TIP60 correlate with hormone treatment refractory disease (Halkidou et al., 2003). TIP60 was further shown to acetylate the tumour suppressor retinoblastoma protein (RB1), leading to proteasomal degradation of RB1 (Leduc et al., 2006).

Amplification, deletion, and mutation of TIP60 may lead to chromatin anomalies, dysregulation of oncogenes and tumour suppressors and thus cause and accelerate cancer. TIP60-dependent up-regulation of HIF1A and NF-kB activity may strengthen tumour growth and angiogenesis (Kim et al., 2012b; Perez-Perri et al., 2016). Furthermore, cancer pathogenesis can be hastened by an impaired DNA damage response and evasion of apoptosis.

Histone hyperacetylation was found in the tumours of the K6/ODC transgenic skin cancer mouse model (Hobbs et al., 2002). A subsequent study found a basal increase of TIP60 protein levels in K6/ODC mouse skin, as well as substantial increase of TIP60 protein levels in spontaneous ODC/Ras skin tumours compared to neighbouring skin tissue (Hobbs et al., 2006). This study found increased interaction between TIP60 and several transcription factors (TF), including E2F1, MEF-1, NFATc, Pbx-1, Smad 3/4, and USF-1, and NF-1, when comparing normal skin with ornithine decarboxylase (ODC) overexpressing skin. This effect was further increased when comparing ODC-overexpressing skin with ODC/Ras skin tumours. In example, E2F1 occupancy increased at target genes and subsequent transcriptional activation was observed in K6/ODC skin. Interestingly, *Tip60* mRNA levels were not increased in K9/ODC melanomas and the authors suggest a posttranscriptional activation of *Tip60* mRNA translation.

The seemingly contradictory reports of TIP60 in various cancers may reflect context-specific functions, affected by parameters such as cancer type and stage, or they may result from changes in TIP60 levels/function that are a consequence rather than a cause of certain oncogenic processes.

1.4.8 The role of TIP60 in brain functions and neurodegenerative disease

HATs play an important role in neuronal development and function, as well as neurological diseases (Sheikh, 2014). Brain functions, such as learning and memory (Xu et al., 2014), and circadian rhythm and associated sleep patterns have been shown to depend on TIP60 activity (Pirooznia et al., 2012). Furthermore, TIP60 acts as a co-activator of PAX6, an important neuronal transcription factor (Kim et al., 2012a). TIP60 has been shown to bind and co-activate the APP-mediated gene transcription together with Fe65 (Cao and Sudhof, 2001). The extracellular cleavage product of APP is associated with Alzheimer's disease (Nunan and Small, 2000). In addition, TIP60 overexpression was shown to rescue axonal transport defects observed in *D. melanogaster* Alzheimer's disease model (Johnson et al., 2013). In contrast, heterozygous *Tip60* deletion correlated with slowed neurodegeneration in spinocerebellar ataxia type 1 (SCA1) mice (Venkatraman et al., 2014).

A recent publication studies three individuals with heterozygous missense mutations in the *TIP60* gene, resulting in amino acid point mutations in the chromodomain (p.R53H) and in the MYST domain near the acetyl-CoA binding site (p.C369S and p.S413A; amino acid sequence based on TIP60 isoform 2 (NP_006379.2)) (Humbert et al., 2020). All three mutations are conserved from yeast to humans and caused a dominant negative phenotype, including seizures, developmental delay, intellectual disability, and sleep disturbance. All three mutations decreased the ability of TIP60 to acetylate canonical oligonucleosome arrays *in vitro*. The two mutations in the MYST domain led to dysregulation of gene transcription, including downregulation of genes important in development, neuronal function, and circadian rhythm (*LHX9* and *KIRREL3*), and upregulation of genes correlated with intellectual disability (*GFPT2*), circadian rhythm (*PER1*). Another recent study screened parent-offspring trios for *de novo* missense

mutations associated with developmental disorders and found 3 mutations in *TIP60*, (p.R307C, p.S413A, and p.D454N; amino acid sequence based on TIP60 isoform 2 (NP_006379.2)) (Kaplanis et al., 2020).

These studies suggest that TIP60 plays an essential role in neurological functions and heterozygous loss of catalytically active TIP60 leads to dominant negative phenotypes.

1.4.9 The role of TIP60 in metabolism

Protein acetylation has been shown to represent an important regulatory mechanism in metabolic processes (Wang et al., 2010). In humans, PEPCK-C, a key metabolic enzyme in gluconeogenesis (reviewed in (Nye et al., 2008)) is acetylated by TIP60, leading to increased activity (Lin et al., 2009).

In conclusion TIP60 was shown to function in a wide range of cellular processes, including DNA damage response, cell cycle regulation, cell survival, transcriptional regulation, differentiation, brain functions, and metabolism. Further, TIP60 is implicated in a range of diseases, such as cancer formation and progression, neurodegenerative disease, and developmental disorders.

Chapter 2 Rationale and Aims

2.1 Rationale

Previous literature represents a large body of study displaying apparent contradicting functions of TIP60 in a wide range of areas, such as cell survival, cancer progression, and histone acetylation. Tip60 has been reported to have both pro-apoptotic and pro-survival functions. Further, TIP60-mediated coregulation of activation or repression of transcription in conjunction with transcription factors has been shown for many prominent examples. Lastly, Tip60 has been reported to both promote or oppose cancer progression.

Previously proposed TIP60 histone acetylation targets include a wide range of histones, including the canonical core histones H2A, H3, and H4, as well as the histone variant H2AZ, while other MYST family members have been shown to exhibit histone lysine specificity towards one or two histone lysines. Most previous studies utilized cell free assays, RNAi depletion, or overexpression models to investigate the role of TIP60. However, very little is known about the effect of genetic loss of TIP60.

2.2 Aims

In this body of work, I utilized a genetic deletion of *TIP60* to investigate the effect of loss of TIP60 in murine and human cells. My aims were to:

1. Characterize the effect of loss of TIP60 on cell survival and proliferation
2. Identify the histone acetylation targets of TIP60
3. Investigate the role of TIP60 in gene transcription
4. Identify gene targets of TIP60
5. Characterize the importance of TIP60 acetylation activity

Chapter 3 Material and Methods

3.1 Mouse strains

Experiments including mice were performed with the approval of the Walter and Eliza Hall Institute for Medical Research Animal Ethics Committee and according to the Australian code of practice for the care and use of animals for scientific purposes. Mice were bread on a *C57BL/6* genetic background unless stated otherwise. For all experiments, each mutant sample used was compared to separate wild-type litter mate controls within the same strain.

3.1.1 The *RosaCreERT2* allele

RosaCreERT2 (*ERT2*) transgenic mice were described earlier (Seibler et al., 2003). To facilitate cre-activation and induce recombination of *loxP* sites, mice were treated with 100 μg/g bodyweight tamoxifen (Sigma, T5648) in corn oil (Sigma, C8267) by oral gavage every 2nd day for 5 days. Cultured cells were treated *in vitro* with 250 nM 4-OHT (Sigma, H7904) in growth medium for a maximum of 5 days, if not indicated otherwise, and consequently grown in 4-OHT free growth medium for the residual time. 4-OHT stock was made up in 100% ethanol to a final concentration of 5 mM 4-OHT. Cells treated with equal amounts of ethanol were used for vehicle controls.

3.1.2 The *NestinCre* allele

NestinCre (*Nes*) transgenic mice were kindly supplied by Prof Günther Schütz's laboratory and described earlier (Tronche et al., 1999). *NestinCre* initiates *loxP* recombination in the forebrain neuroepithelium at E10.5 (Blaess et al., 2006; Graus-Porta et al., 2001)

3.1.3 Genetic knockout alleles

3.1.3.1 *Tip60* genetrap allele

The *Tip60*^{gt} allele was generated in a random gene trap mutagenesis screen in embryonic stem cells (ESCs) by the Texas Institute of Genomic Medicine. *Tip60*^{gt} ESCs were imported and generation of *Tip60*$^{gt/+}$ mice by blastocyst injection was commissioned at the Australian Phenomics facility. The *Tip60*^{gt} allele harbours an insertion with a 3' splice acceptor site between exon 4 and 5 of *Tip60*, introducing a premature stop codon. *Tip60*$^{gt/+}$ mice were bred on a C57BL/6 inbred and a mixed FVB/BALB/c background. Experimental blastocysts were harvested from the C57BL/6 strain.

3.1.3.2 The conditional *Tip60* allele

Tip60$^{fl/+}$ mice were generated by CRISPR/Cas9 on a C57BL/6 background by Dr Andrew Kueh, using techniques previously described (Kueh et al., 2017; Yang et al., 2013). Briefly, two sgRNAs of the sequence GTACGGAGATGATCCGGGCG and TGGAAGCTACGCCTGCAACT were used to insert *loxP* sites flanking exons 3 and 4 of the *Tip60* gene. The deletion of 602 bp of exons 3 and 4 is predicted to result in a frameshift and disruption of TIP60 protein synthesis. Successful targeting was confirmed by sequencing. Mice were maintained on a *C57BL/6* genetic background. *Tip60*$^{fl/+}$ mice were generated before I commenced this PhD.

3.1.3.3 *Trp53* and *Cdkn2a* knockout allele

Trp53$^{-/-}$ mice (Jacks et al., 1994) and *Cdkn2a*$^{-/-}$ mice (Serrano et al., 1996) were bred on *C57BL/6* background and used for generating MEFs.

3.2 Primary cell isolation and cell culture

All cell culture experiments were carried out using standard sterile procedures. All solutions used in tissue culture were sterilized by autoclaving or filtration.

3.2.1 Gelatine coating

Tissue culture plates were coated with 0.1% (w/v) gelatine solution (Sigma, G1890) in MQ-H_2O for MEF and ESC cultures. Gelatine solution was added to culture plates, incubated for 30 min (min) at 37°C, and aspirated. Plates were air dried in the tissue culture hood and used immediately for culturing cells or stored at 4°C for up to 3 days.

3.2.2 Cell culture conditions

Murine embryonic fibroblasts (MEFs) were cultured in MEF medium (DMEM (Gibco, 11885084), 10% HI-FBS (SAFC, 12003C), and 2 mM GlutaMAX (Gibco, 35050061)) at 37°C, in 5% CO_2, and 3% O_2 (near physiological tissue oxygen conditions). HEK293T, HEK293, and U2OS cells were cultured in MEF medium at 37°C in 5% CO_2 and normal O_2 levels. ESCs were grown in 2i medium (KO-DMEM (Gibco, 10829018), 2 mM GlutaMAX (Gibco, 35050061), 100 U/ml penicillin and 100 µg/ml streptomycin (Gibco, 15140163), 0.1 mM non-essential amino acids (Gibco, 11140076), 0.1 mM 2-mercaptoethanol (Gibco, 21985023), N-2 Supplement (Gibco, 17502001), B-27 Supplement (Gibco, 17504044), 1% (v/v) heat-inactivated, ESC-quality foetal bovine serum (HI-ESQ-FBS; Gibco, 16141079), 1 µM PD0325901 (Stemgent, 04-0006), 3 µM CHIR99021 (Stemgent,04-0004), and 1000 U/ml LIF (Millipore ESG1107)) at 37°C in

5% CO_2. *D. melanogaster* S2 cells were cultured in Schneider's *Drosophila* Medium (Gibco, 21720024) supplemented with 10% (v/v) HI-FBS (SAFC, 12003C) at room temperature (RT).

3.2.3 MEF isolation

For MEF isolation E13.5 embryos were dissected and washed in ice cold PBS (Gibco, 14200166). The head was collected for genotyping, extremities, the tail and internal organs were removed, the torso was collected in RT MEF medium, supplemented with 1% (v/v) penicillin and streptomycin (Gibco, 15140163), and minced by pipetting several times through a 18G and 21G needle. The cells were centrifuged with low speed (500 x *g*) for 5 min and resuspended in 37°C MEF medium, supplemented with 1% (v/v) penicillin and streptomycin. Individual embryos were plated on a gelatine-coated 15 cm petri dish in 30 ml pre-warmed MEF medium, supplemented with 1% (v/v) penicillin and streptomycin.

3.2.4 ESC isolation

For ESC isolation E3.5 blastocysts were flushed and washed in M2 medium, separated and washed in 2i medium by mouth pipetting, and cultured in gelatine coated 4-well plates (Nunc, NUN144444) for ESC derivation at 37°C in 5% CO_2 until inner cell mass outgrows where apparent (~7 days). Outgrowths were gently trypsinized to retain small cell clumps and plated on gelatine coated tissue culture plastic in 2i medium until colonies formed. At the following passage, an aliquot of cells was taken for genotyping.

3.2.5 E3.5 blastocyst culture

E3.5 blastocysts were cultured for up to 3 days. Briefly, E3.5 embryos were collected in M2 medium (Sigma, M7167), washed 3 times with M2 medium and twice with ESC medium (4.5 g/l DMEM (Gibco; 11965084), 2 mM L-glutamine (Gibco, 25030081), 100 U/ml penicillin and 100 µg/ml streptomycin (Gibco, 15140163), 0.1 mM non-essential amino acids (Gibco, 11140076), 0.1 mM 2-mercaptoethanol (Gibco, 21985023), 1 mM sodium pyruvate (Gibco, 11360070), 20% (v/v) HI-ESQ-FBS (Gibco, 16141079), 1000 U/ml LIF (Millipore ESG1107)) by mouth pipetting, and cultured in gelatine-coated chamber slides (Millicell E2 slide, PE2GS0816) in ESC medium at 37°C, 5% CO2 in air.

3.2.6 Inducible CRISPR/Cas9 *Tip60* mutant cells

Doxycycline (dox) inducible CRISPR/Cas9 mutant cell lines were generated as described earlier (Aubrey et al., 2015; Kueh and Herold, 2016). I used two single guide RNAs, sgRNA1 GCCGGCACCGCCTCAAGCCG and sgRNA2 CTGCCTCCCTACCAGCGCCG, to target exons 8 and 11, both target human the human *TIP60* gene, as well as the mouse *Tip60* gene. Cells were treated with 1 µg/ml dox for the indicated time to induce the transcription of the construct expressing the sgRNAs. Indels were analysed using sgRNA specific primers (Table 4). To calculate the indel frequency, I only considered sequences with at least 25 reads and divided the amount of reads for each specific indel by the total number of reads.

3.2.6.1 Virus production

Lentiviral particles were produced in HEK293T cells. Briefly, $2x10^6$ HEK293T cells were seeded per 10 cm plate and grown for 1 day. 3rd generation lentiviral packaging

plasmids, including 5 µg pMDL, 2.5 µg pRSV-REV, and 3 µg pVSV.G as well as 10 µg of lentiviral transfer vector were mixed in 250 µl H_2O and vortexed briefly. 250 µl 500 mM CaCl2 was added, vortexed briefly, 500 µl 2X HBS (280 mM NaCl, 50 mM HEPES, 1.5 mM Na_2HPO_4, pH = 7) was added, vortexed for 10 seconds (s) on the highest setting, incubated for 10 min at RT, added dropwise to the HEK293T cells, mixed by swirling the plate, and incubated for 1 day. Medium was exchanged to fresh target cell-specific medium and supernatant was collected every 24 h up to 3 times, filtered through a 0.45 µm filter and immediately used on target cells.

3.2.6.2 Lentivirus transduction

Lentiviral transduction was performed in a 6-well plate format. Briefly, 2 ml of lentiviral containing supernatant was supplemented with 5 µg/ml polybrene (Sigma, H9268-5G) and added to target cells, when cells were 30-50% confluent. Viral supernatant was replaced with a fresh aliquot of viral supernatant 2 to 3 times, depending on transduction efficiency, and cells were split when confluent. For simultaneous transduction of Cas9 and sgRNA expressing virus constructs, virus particles were produced in separate cultures and target cells were transduced with 1.5 ml of each supernatant. Three days after removing the last viral supernatant, cells were either selected by flow cytometry cell sorting for mCherry and/or GFP expression or in 1 mg/ml neomycin (Gibco, 10131035) selection medium for 8 days.

3.2.6.3 Overhang sequencing of indels

CRISPR/Cas9 indels were analysed by overhang high-throughput sequencing (HT-S). Genomic DNA was prepared using the QIAprep Spin Miniprep Kit (Quiagen, 27106)

according to the manufacturer's instructions and concentrations were measured using a spectrophotometer (DeNovix NanoDrop™, DS-11). Specific sequencing primers were designed to target the respective sgRNA binding site and the forward primer overhang 5'-GTGACCTATGAACTCAGGAGTC-specific sequence and reverse primer overhang 5'-CTGAGACTTGCACATCGCAGC-specific sequence. 100 ng DNA lysate in 10 µl MyTaq HS Red Mix (Bioline, BIO-25048), 500 nM of forward and reverse primer, and 8 µl MQ-H_2O were used in a first PCR reaction with sgRNA specific primers (Table 3) and 1st HT-S PCR program (Table 8) in a S1000 Thermal Cycler (Biorad). PCR reaction products were cleaned by adding 30 µl Ampure XP beads (Beckman, A63880), washing beads with 200 µl 80% EtOH and eluting in 30 µl nuclease free H_2O (Invitrogen, AM9906). A second PCR amplification was performed with 8 µl clean PCR amplicons, 10 µl MyTaq HS Red Mix (Bioline, BIO-25048) and 500 nM of a combination of unique barcoding primers utilizing the overhangs and an eight-base index sequence derived from the Illumina Nextera design (forward primer: 5'-CAAGCAGAAGACGGCATACGAGATCCGGTCTCGGCATTCCTGCTGAACCGCTCTTCCGATCTNNNNNNNNGTGACCTATGAACTCAGGAGTC-3' and reverse primer: 5'-AATGATACGGCGACCACCGAGATCTACACTCTTTCCCTACACGACGCTCTTCCGATCTNNNNNNNNCTGAGACTTGCACATCGCAGC-3', with NNNNNNNN representing individual indices) with the 2nd HT-S PCR program (Table 8). 10 µl of each PCR reaction product were pooled and cleaned with 1.2X Ampure XP beads (Beckman, A63880) as before. The indexed pool was diluted to 12 pM for sequencing with a 300-cycle kit with single reads (281 cycles) and a second 44-cycle index read on a MiSeq instrument (Illumina) according to the manufacturer's instructions.

3.2.7 HDAC inhibitor treatment

Cells were treated with concentration of sodium-butyrate (NaBu; Sigma, B5887) or trichostatin A (TSA; Sigma, T8552) for 4 days. Where indicated, dox was added simultaneously with HDAC inhibitor. Cells were analysed by MTS assay, western blot, and staining for SA-β-galactosidase activity.

3.2.8 MTS cell growth and viability assay

A colorimetric method, the ([3-(4,5-dimethylthiazol-2-yl)-5-(3-carboxymethoxyphenyl)-2-(4-sulfophenyl)-2H-tetrazolium, inner salt] MTS assay was used to determine cell growth and viability. Cells were grown in a 96-well plate format in 200 µl growth medium and 20 µl MTS reagent (Promega, G3581). The optimal cell seeding density was determined by an MTS assay applied to a cell dilution series. For experimental MTS assays, 2500 U2OS cells and 3000 MEF cells were seeded and incubated for 3 to 5 days. MTS reagents was incubated for 1.5 h under normal growth conditions and absorbance at 490 nm was measured using a plate reader (Hidex, 425-106).

3.3 Molecular biology

3.3.1 Genotyping PCR

Genomic DNA was obtained from cells, embryonic, foetal or adult mouse tissue by direct lysis using 100 µl DirectPCR Tail lysis buffer (Viagen, 102-T), supplemented with 0.3 mg/ml proteinase K (Sigma, 3115887001). Samples were digested for 2 – 16 h at 55°C and 900 rpm in a heat block. 1 µl crude DNA lysate in 9 µl MQ-H_2O and 10 µl MyTaq HS Red Mix (Bioline, BIO-25048) was used per genotyping PCR reaction with gene

specific primers (Table 3) and PCR programs (Table 8) in a S1000 Thermal Cycler (Biorad). 10 µl pf PCR products were separated on 2% (w/v) agarose gel (Bioline, BIO-41025) supplemented with 0.5 µg/ml ethidium bromide (Invitrogen, 15585011), run at 100 mV for 30 to 60 min, and imaged using Biorad ChemiDoc (Biorad, Gel Doc XR+, Universal Hood II)

3.3.2 RT-qPCR

RT-qPCRs were performed in triplicates. RNA was isolated using RNeasy Kit (Qiagen, 74106) with on-column DNase I digestion according to the manufacturer's instructions and quantified using a spectrophotometer (DeNovix NanoDrop™, DS-11). 10 µg of extracted RNA were used as a template for the generation of cDNA. Briefly, RNA was incubated with 5 µM oligo-(dT)15 (Promega, C110A), and 10 mM dNTPs (Promega, U1511) for 5 min at 65°C, left on ice for 10 min, added to 5X first-strand buffer (Invitrogen, y02321), containing 10 U/µl Superscript III (Invitrogen, G19046030), 2 U/µl RNasin (Promega, N2511), and 5 mM DTT (Invitrogen, y00147), incubated at 50°C for 1 h to facilitate reverse transcription of cDNA, and 85°C for 5 min to inactivate residual enzymatic activity and stored at -80°C until required. A 1:4 dilution of cDNA in 9 µl MQ-H_2O, and 10 µl of SYBR sensimix (Bioline, QT605) and 0.25 mM gene specific primers (Table 5) were used in qPCR experiments. Triplicates were measured in a 384 LightCycler plate (Roche, 04729749001), run with standard PCR settings (95°C for 10 min followed by 45 cycles of 95°C for 20 s, 60°C for 30 s and 72°C for 30 s, followed by a continuous ramp to 95°C at a rate of 1°C/min) in a LightCycler480 (Roche).

Each qPCR primer was analysed in a five-fold serial dilution to create a standard curve used to calculate relative concentrations in samples based on Cp values. The means of technical replicates were normalized to the housekeeping genes.

3.3.3 RNA sequencing

RNA sequencing was performed on *Tip60$^{fl/fl}$;ERT2* and *Tip60$^{+/+}$;ERT2* MEFs induced with 4-OHT for 3 days and 5 days, as well as *iC-TIP60* HEK293g1/C9, *iC-TIP60* HEK293g2/C9 and guide-only HEK293g1 and HEK293g2 controls induced with dox for 3 days. RNA was isolated using RNeasy Kit (Qiagen, 74106). The indexed libraries were pooled and diluted to 1.5 pM for paired end sequencing (2x 81 cycles) on a NextSeq 500 instrument using the v2 150 cycle High Output kit (Illumina) as per manufacturer's instructions, generating 80 bp paired-end reads. The base calling and quality scoring were determined using Real-Time Analysis on board software v2.4.6, while the FASTQ file generation and de-multiplexing utilized bcl2fastq conversion software v2.15.0.4.

For *Tip60$^{fl/fl}$;ERT2* and *Tip60$^{+/+}$;ERT2* MEF samples, all reads were mapped onto the mouse genome, build mm10, using the align function of Rsubread, version 1.30.5 (Liao et al., 2019). The total number of mapped reads per library are displayed in Methods Table 5. Reads overlapping each Entrez gene were summarized into counts using featureCounts from Rsubread with inbuilt RefSeq annotation. Differential expression analyses were then undertaken using the edgeR version 3.22.5 (McCarthy et al., 2012), and limma version 3.36.5 (Ritchie et al., 2015) software packages. Lowly expressed genes were filtered out using the filterByExpr function of edgeR with default settings. Additionally, genes without a gene symbol and ribosomal RNAs were removed. Sex-linked genes (Xist and all gene unique to the Y-chromosome) were removed to address an imbalance in the sexes between *Tip60$^{fl/fl}$;ERT2* and *Tip60$^{+/+}$;ERT2* MEF samples. Following filtering 14,188 genes remained. RNA composition was then normalized using the TMM method (Robinson and Oshlack, 2010). Multiple dimensional scaling (MDS) plots were used to determine if substantial variation existed within treatment groups. The

distance between each pair of samples is computed as the leading fold change, defined as the root-mean-square of the largest 500 log2 fold changes between that pair of samples. The correlation between samples from the same litter was estimated, the counts were then transformed to log2-counts per million (CPM) with associated precision weights using voom (Law et al., 2014). Differential expression between the *Tip60$^{fl/fl}$;ERT2* and *Tip60$^{+/+}$;ERT2* MEF samples was then assessed using linear models and robust empirical Bayes moderated t-statistics (Phipson et al., 2016). The linear models and voom both incorporated the correlation estimate.

For HEK293g1/C9, HEK293g2/C9 and guide-only HEK293g1 and HEK293g2 samples, all reads were mapped using the align function of Rsubread align function to the human genome, build hg38. The number of total mapped reads for each sample is given in Method Table 5. Like the MEF data, gene counts were generated using featureCounts and inbuilt RefSeq annotation, and expression-based filtering was performed using fitlerByExpr with default settings. Additionally, ribosomal RNAs and obsolete gene IDs with no corresponding gene symbol were also removed. TMM normalization was then applied. Similarly to the MEF data, the counts were transformed to log2-CPM with associated precision weights using voom. Differential expression was then assessed between the groups using linear models and empirical Bayes moderated t-statistics.

For each analysis, the p-values were adjusted using the Benjamini and Hochberg method to control the false discovery rate (FDR) below 5%. The multi-dimension scaling (MDS) plots, mean-difference (MD) plot and barcode plots were generated using the plotMDS, plotMD and barcodeplot functions of limma, respectively. The heatmap was created using the pheatmap software package version 1.0.12. All gene set tests were carried out using ROAST with 9,999 rotations (Wu et al., 2010). Gene ontology analyses were performed using the goanna function of limma.

3.3.4 CUT&Tag sequencing

CUT&Tag was performed on 100,000 cells per sample as described earlier (Kaya-Okur et al., 2019) with slight modifications. pAG-Tn5 with adapters were initially generously gifted by the Henikoff laboratory and were later ordered commercially (EpiCypher, 15-1017). All buffers were made up fresh and for antibodies targeting phosphorylated targets (RNAPII) fresh PhosSTOP (Roche, 04906837001) phosphatase inhibitor was added. Digitonin stock solution was made up fresh as 5% (w/v) in DMSO (CST, 12611P). 10 µl concanavalin-A beads (Bangs Laboratories, BP531) per sample were washed twice in 10 volumes of binding buffer (20 mM HEPES pH 7.5 (Sigma, 83264), 10 mM KCl (Sigma, 60142), 1 mM $CaCl_2$ (Sigma, 21115), and 1 mM $MnCl_2$ (Sigma, M1787)) and resuspended in 10 µl binding buffer per sample. Cells were washed twice with PBS, scraped in PBS, counted and mixed with spike-in S2 *D. melanogaster* cells in a ratio of 43:57 (Mammalian cells: S2 cells) for a combined cell number of 100,000 cells per sample. Cells were washed twice in 1 ml wash buffer (20 mM HEPES pH 7.5, 150 mM NaCl (Sigma, 71386), 0.5 mM spermidine (Sigma, S0266), and 1 protease inhibitor tablet per 50 ml buffer (Roche, 05056489001)), resuspended in 90 µl wash buffer per sample, and concanavalin-A beads were added dropwise while vortexing on a low setting and incubated for 10 min at RT on a roller. Cells were immobilised using a magnetic rack (ThermoFisher, MR02), and the supernatant was removed. The cells were resuspended in 100 µl ice-cold antibody buffer (wash buffer supplemented with 0.05 % (w/v) digitonin (Merck, 300410), 2 mM EDTA (Invitrogen, 15575020), and 0.1 % (w/v) BSA (Sigma, A8577)) per sample and split into 50 µl aliquots. Primary antibody was added to respective tubes as indicated in Table 9 and incubated for 2 h at RT on a roller. The supernatant was removed and 100 µl ice cold dig-wash buffer (wash buffer supplemented

with 0.05% (w/v) digitonin) containing secondary antibody as indicated in Table 9 were added to the cells. The cells were incubated for 60 min at RT on a roller, washed trice in 1 ml dig-wash buffer (wash buffer supplemented with 0.05% (w/v) digitonin) and resuspended in 100 µl ice-cold dig-300 buffer (20 mM HEPES pH 7.5, 300 mM NaCl, 0.5 mM spermidine, 0.01 % (w/v) digitonin and 1 protease inhibitor tablet per 50 ml buffer) supplemented with 1:250 pA-Tn5 adapter complex (provided by the Henikoff lab) or 2.5 µl pAG-Tn5 (EpiCypher, 15-1017). The cells were incubated for 60 min at RT on a roller. Cells were washed trice in 1 ml dig-300 buffer, resuspended in 100 µl tagmentation buffer (dig-300 buffer supplemented with 0.01 mM $MgCl_2$ (Sigma, 63069)) while gently vortexing and incubated at 37°C for 60 min. Tagmentation was stopped by adding 3.34 µl 0.5 M EDTA, 1 µl 10% (w/v) SDS (Sigma, 71736), and 0.83 µl 20 mg/ml thermolabile proteinase K (NEB, P8111S) to each sample, mixed by vortexing on full speed and incubated in a heat block at 37°C for 60 min and 800 rpm, followed by heat inactivation at 55°C for 10 min. DNA was extracted using Ampure XP beads (Beckman, A63880). Briefly, 122 µl Ampure XP beads were added to each sample and incubated for 5 min at RT, washed twice in 1 ml 80% ethanol without removing the samples from the magnetic rack. Residual ethanol was removed, Ampure XP beads were air-dried for 5 min at RT. DNA fragments were eluted in 25 µl TE buffer (10 mM Tris-HCl pH=8.0 (Invitrogen, 15568025), 1 mM EDTA, and 25 µg/ml RNAse A (ThermoFisher, EN0531) by vortexing and incubation at 37°C for 10 min. DNA eluates were transferred to new tubes. 10 µl sample DNA fragments were used to generate sequencing libraries using 400 nM sample specific nextera i5 and i7 primer combinations (Table 7) and 12.5 µl 2X NEBNext Ultra II Q5 Master Mix (NEB, M0541L) in a total of 25 µl and amplified with the following PCR settings: 72°C for 5 min followed by 13 cycles of 98°C for 30 s, 98°C for 10 s and 63°C for 10 s, and 72°C for 1 min. PCR products were cleaned up using 30

µl Ampure XP beads as described above, eluted in 25 µl 10 mM Tris-HCl pH 8.0 and stored at -20°C. The clean libraries were analysed by High Sensitivity D1000 gels (Agilent, 5067- 5584) on an Agilent 2200 tapestation using 2 µl sample and an electronic ladder. Large DNA bands >1200 bp were further investigated by PCR with Illumina p5 and p7 sequencing primers. Briefly, 0.1 µl of fragment library was used in PCR mixtures with 400 nM Illumina p5 and p7 primers (Table 7) and 12.5 µl 2X MyTaq HS Red Mix (Bioline, BIO-25048) in a total of 25 µl and amplified with the following PCR settings: 95°C for 3 min followed by 15 cycles of 95°C for 20 s, 64°C for 30 s and 72°C for 20 s. PCR products were analysed on a 2% agarose gel. Library concentrations were measured in a size range of 125 bp and 1200 bp. Libraries were pooled into a 2 nM library of 20 µl. Libraries with low concentrations are used completely in the pool and the pool is subsequently concentrated using Ampure XP beads (1.2X volume) as described above. The pooled indexed libraries were diluted to 1.5 pM for paired end sequencing (2x 36 cycles) on a NextSeq 500 instrument using the v2 150 cycle Mid Output kit (Illumina) as per manufacturer's instructions, generating 36 bp paired-end reads. The base calling and quality scoring were determined using Real-Time Analysis on board software v2.4.6, while the FASTQ file generation and de-multiplexing utilized bcl2fastq conversion software v2.15.0.4.

As the samples contain *H. sapiens*, *D. melanogaster*, and *E. coli* DNA, an index was first built containing all three genomes to allow for competitive alignment. This index was built via Rsubread (2.0.1) (Liao et al., 2019) using builds hg38, R6.35, and K12 substrain MG1655 for the *H. sapiens, D. melanogaster* and *E. coli* gnomes respectively. All libraries were aligned to this index using Rsubread's align function with minimum fragment length set to 30. In all cases approximately 90% of fragments (read pairs) mapped uniquely to the combined genomes. Read counts were obtained using Rsubread's

featureCounts function. For *D. melanogaster*, read counts were summarized by chromosome. For *H. sapiens*, read counts were obtained for the putative promoter regions (transcription start site ± 1000 bp) of protein-coding genes. Gene annotation was obtained from Gencode (hg38 version 35). For genes with multiple TSS, the most 5' start site was used.

Downstream analyses used the limma (3.44.3) (Ritchie et al., 2015) and edgeR (3.30.3) (Robinson et al., 2010) software packages. Genes with low counts across all samples were filtered using edgeR's filterByExpr function with default settings. Library sizes were normalized by *D. melanogaster* content. The raw library size for each sample was set as the combined total of the filtered *H. sapiens* promoter counts and the *D. melanogaster* count. The library sizes were then scaled so as to equalize the total *D. melanogaster* count-per-million across the samples. The resulting normalized library sizes were applied to the human differential analyses.

Biological variation between replicate samples was estimated using edgeR's estimateDisp function. Differential abundance between the *iC-TIP60* and control samples for each histone mark was assessed by generalized linear models and quasi-likelihood F-tests (Lun et al., 2016). Violin plots were created using ggplot2 (3.3.2).

Wiggle plots were created using Seqmonk (v1.45.1). Bam file reads were mapped to the human genome (GRCh38.p13) and probes were created in a 2 bp window with 2 bp steps, quantified, and smoothed with a 500 bp smoothing normalisation.

3.3.5 Cloning of lentiviral transfer plasmids

3.3.5.1 Chemically competent Dh5α *E. coli*

Chemically competent Dh5α *E. coli* were prepared by inoculating 10 ml of L broth (1% (w/v) tryptone (Merck, 1.07213.1000), 0.5% (w/v) yeast extract (Merck, 1.03753.9025), 1% (w/v) NaCl, pH=7.3 – 7.4 in Type II water (resistivity of >1 MΩ-cm, conductivity of <1 µS/cm and total organic compounds (TOCs) of <50 parts per billion (ppb))) with 5 µl of previous chemically competent Dh5α *E. coli* stock and incubated at 37°C and 200 rpm overnight in a shaking incubator (Infors HT, Multitron standard 2018). 1 ml of overnight culture was used to inoculate a 100 ml L broth culture and incubated at 37°C and 200 rpm until OD_{600} of 0.5 - 0.6 was reached. 40 ml of bacteria suspension was centrifuged at 4000x*g* for 10 min at 4°C, resuspended in 20 ml sterile 50 mM $CaCl_2$, incubated for 20 min on ice, centrifuged as before and resuspended in 4 ml sterile 50 mM $CaCl_2$ + 15% glycerol (Ajax Finechem, AJA242-500ML). 50 µl aliquots were snap frozen on dry ice and stored at -80°C. Each batch was tested by transforming an ampicillin-resistance plasmid by heat shock, plating on 50 µg/ml ampicillin (Gibco, 11593027) supplemented LG agar (1% (w/v) Tryptone (Merck, 1.07213.1000), 0.5% (w/v) yeast extract (Merck, 1.03753.9025), 0.5% (w/v) NaCl, 0.2% (w/v) D-Glucose (AJAX, A783), 10 mM Tris-HCl, 1 mM $MgCl_2$, 1.5% (w/v) agar (Merck, 1.01614.1000), pH=7.4 in Type II water (resistivity of >1 MΩ-cm, conductivity of <1 µS/cm and total organic compounds (TOCs) of <50 ppb)). Plates were incubated upside-down at 37°C for 2 days and colonies were counted. Around 100 colonies were expected for efficient transfection.

3.3.5.2 Heat-shock transformation of plasmids into chemically competent Dh5α *E. coli*

Plasmid preparation was performed in Dh5α *E. coli.* Plasmids were transformed into Dh5α *E. coli* by heat-shock. Briefly, chemically competent Dh5α *E. coli* were thawed on ice, 5 ng plasmid was added and flicked gently 20 times to mix. Bacteria and plasmid mixtures were incubated on ice for 30 min, heat shocked in a water filled heat block at 42°C for 30 s, incubated on ice for 5 min. 950 µl RT L broth (1% (w/v) tryptone (Merck, 1.07213.1000), 0.5% (w/v) yeast extract (Merck, 1.03753.9025), 1% (w/v) NaCl, pH=7.3 – 7.4 in Type II water (resistivity of >1 MΩ-cm, conductivity of <1 µS/cm and total organic compounds (TOCs) of <50 ppb)) was added and the samples were incubated for 20 min at 37°C and 300 rpm in a heat block, before being used to inoculate a 100 ml L broth culture supplemented with 50 µg/ml ampicillin (Gibco, 11593027) and incubated at 37°C and 200 rpm overnight.

3.3.5.3 Plasmid extraction

Plasmids were extracted from 50 – 100 ml cultures by Wizard® Plus Midipreps DNA Purification System (Promega, A7640) and from 5 – 10 ml cultures by Wizard® Plus SV Minipreps DNA Purification Systems (Promega, A1465) according to the manufacturer's instructions. Plasmid concentration and quality was measured by spectrophotometry (DeNovix NanoDrop^{TM}, DS-11).

3.3.5.4 Cloning lentiviral transfer vector with dox inducible sgRNA

CRISPR/Cas9 sgRNAs were cloned into the lentivirus transfer vector *FgH1tUTG* (*FgH1tUTG* was a gift from Associate Prof Marco Herold (Addgene plasmid # 70183;

http://n2t.net/addgene:70183; RRID:Addgene_70183) (Aubrey et al., 2015). *FgH1tUTG* plasmid was isolated from a 10 ml bacterial culture and linearized via BsmBI by combining 2 µl Buffer 3.1 (NEB, B7203S), 2 µg of plasmid, and 2 µl BsmBI enzyme (NEB, R0580) and 14 µl nuclease-free H_2O (Invitrogen, AM9906) and incubating the mixture at 55°C for 6 h, followed by heat inactivation at 80°C for 20 min. Linearization was checked on a 1% (w/v) agarose gel supplemented with 0.5 µg/ml ethidium bromide (Invitrogen, 15585011) by adding 1 µl linearized plasmid to 9 µl H_2O and 2 µl 6X loading dye (Thermo Scientific, R0611). Linearized plasmid displayed a sharp slower band compared to non-linearized plasmid. Linearized backbone DNA was phosphorylated by adding 2 µl phosphatase (Antarctic Phosphatase, NEB, M0289S) and 2 µl buffer (NEB, B0289S) to 19 µl linearized plasmid and incubating the mixture 1 h at 37°C followed by heat inactivation at 80°C for 20 min.

sgRNA sense and antisense oligonucleotides (Sigma, Table 6) were annealed by mixing 3 µl each of 100 mM sense- and anti-sense oligonucleotides in 14 µl duplex buffer (100 mM CH_3CO_2K, 30 mM HEPES, pH 7.5) and performing the following PCR protocol: 95°C for 5 min followed by a temperature gradient from 95°C to 50°C at -0.1°C per second, 50°C for 10 min followed by a temperature gradient from 50°C to 4°C at -1°C per second. Annealed oligonucleotides were phosphorylated by combining 5 µl annealed oligonucleotides, 12 µl water, 2 µl PNK buffer (NEB, B0201S), and 1 µl PNKinase (NEB, M0201S) and incubating the mixture at 37°C for 30 min followed by heat inactivation at 70°C for 10 min.

Annealed, phosphorylated oligonucleotide were ligated into the linearized backbone using a 1:300 backbone to insert ratio by combining 1 µl ligase (NEB, M0202S), 1 µl ligase reaction buffer (NEB, B0202S), 1.2 µl linearized backbone, 1.2 µl annealed oligonucleotide to 5.6 µl H_2O and incubating at 8°C for 18 h, followed by heat

inactivation at 70°C for 10 min. 2 µl of ligation mixture was directly transformed into chemically competent Dh5α *E. coli* via heat shock, incubated for 1 h at 37°C and 300 rpm in a heat block. 500 µl of the transformation culture were plated onto 50 µg/ml ampicillin (Gibco, 11593027) supplemented LG agar (1% Tryptone (Merck, 1.07213.1000), 0.5% yeast extract (Merck, 1.03753.9025), 0.5% NaCl, 0.2% D-Glucose (AJAX, A783), 10 mM Tris-HCl, 1 mM $MgCl_2$, 1.5% agar (Merck, 1.01614.1000), pH 7.4 in Type II water (resistivity of >1 MΩ-cm, conductivity of <1 µS/cm and total organic compounds (TOCs) of <50 ppb)). Plates were incubated upside-down at 37°C for 2 days. A no insert ligation mixture was used as a negative control and only ~5 colonies were expected to grow. Single colonies were picked, transferred into 5 ml L broth supplemented with 50 µg/ml ampicillin and incubated at 37°C and 200 rpm overnight. Plasmids were extracted from 5 ml cultures. 1000 ng plasmid was mixed with 1 µl sequencing primer (5' – CAGACATACAAACTAAAGAAT – 3') in a total volume of 12 µl in H_2O and Sanger sequenced at the Australian Genome Research Facility (AGRF) to check for the correct insertion of the sgRNA sequence into the *FgH1tUTG* vector. The correct plasmid was transformed into Dh5α *E. coli* and extracted from a 100 ml culture.

3.3.5.5 Catalytically inactive and wild-type TIP60 overexpression constructs

Lentiviral transfer plasmids containing coding sequenced for the human wild-type TIP60 ($TIP60^{WT}$) and two catalytically inactive forms of TIP60 [TIP60 double point mutation ($TIP60^{Q377E,G380E}$) or TIP60 single point mutation ($TIP60^{E403Q}$)] were ordered from VectorBuilder. The plasmids contained an IRES and co-translated GFP and TIP60, as well as expressing a neomycin resistance cassette under a separate promotor. The plasmid maps are displayed in Table 2.

3.3.5.6 Plasmid maps

Table 2: Maps of plasmids created during this study.

Plasmid	Map
TIP60-sgRNA	
hTIP60-WT	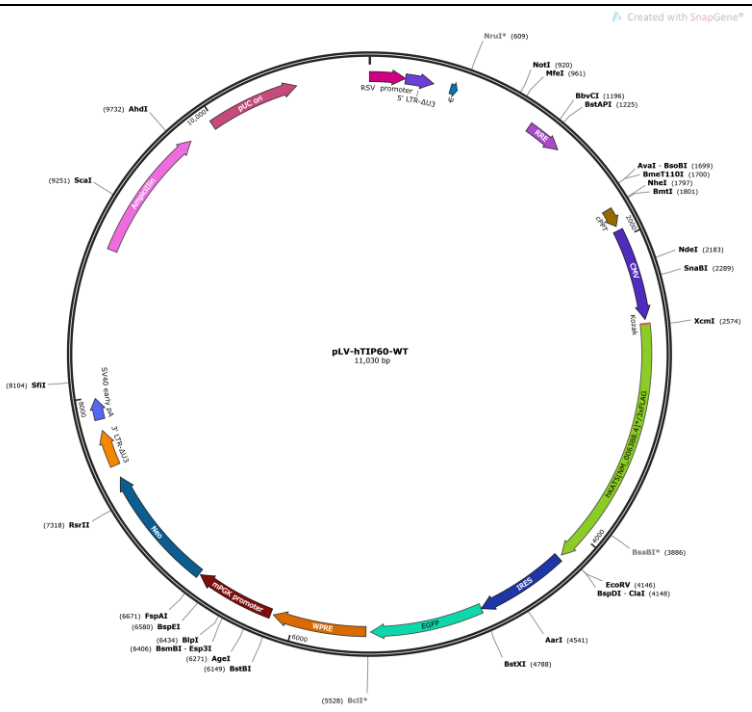

ci-hTIP60-Q377E-G380E	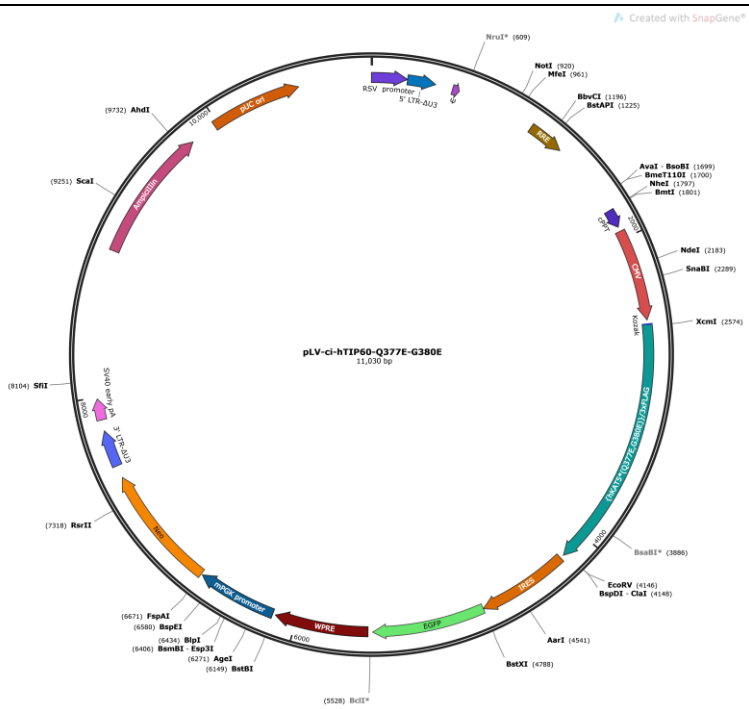
ci-hTIP60-E403Q	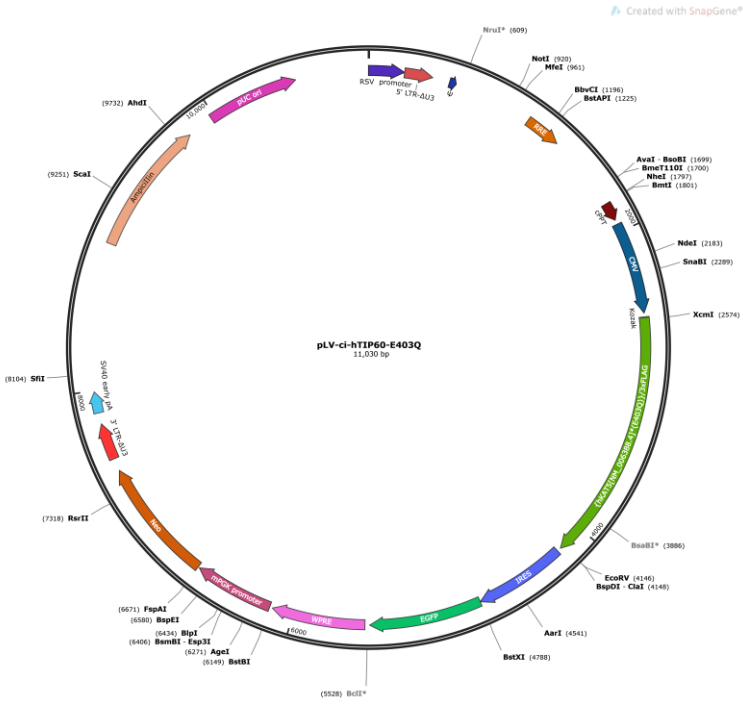

3.3.6 Primers and oligonucleotides

Table 3: Genotyping primer.

Gene	Primer sequence (5'-3')

Tip60 wild-type forward	GGTGAGTAGGTCCCCCATTTC
Tip60 wild-type reverse	ATCCCACCCTCTGCCTTCTCT
Tip60 KO specific forward	GCGGTCGCAGATACTCGG
Tip60 genetrap forward	GCAGTCAACAAACGTCTGGA
Tip60 genetrap reverse	AATTGCTGAGGGTACCGTTG
Rosa26CreERT2 / *NestinCre* forward	CGCGGTCTGGCAGTAAAAAC
Rosa26CreERT2 / *NestinCre* reverse	GCAGATGGCGCGGCAACACC
Trp53 wild-type forward	TTATGAGCCACCCGAGGT
Trp53 wild-type reverse	TATACTCAGAGCCGGCCT
Trp53 KO specific forward primer	TCCTCGTGCTTTACGGTATC
Cdkn2a wild-type forward	GTGATCCCTCTACTTTTTCTTCTGACTT
Cdkn2a wild-type reverse	CGGAACGCAAATATCGCAC
Cdkn2a KO specific forward primer	GAGACTAGTGAGACGTGCTACTTCCA
YRPT sex determination forward	TTGGAAGGCCATCATTCTAGG
YRPT sex determination reverse	CATCCCACTCCAGTTGTCCT

Table 4: High-throughput sequencing (HT-S) primer. Primer sequences without the 5'-HT-S specific overhangs. For forward primer the overhang 5'-GTGACCTATGAACTCAGGAGTC-primer specific sequence-3' and for reverse primer the overhang 5'-CTGAGACTTGCACATCGCAGC-primer specific sequence-3' was added. Specificity for human (h) or mouse (m) genome is indicated. OT = off-target.

Gene	**Primer sequence (5'-3')**	**Species**
TIP60 sgRNA1 hm forward	GATGGAATACCGTCAGCACCA	H/M
Tip60 sgRNA1 m reverse	CCCAAGACCCCTCATACCAAG	M
TIP60 sgRNA1 h reverse	CCCTGGACCCCTCATACCAA	H
Tip60 sgRNA2 m forward	GTGGGCTACTTCTCCAAGG	M
Tip60 sgRNA2 m reverse	GGCAAAGTAGATGCTGGAACCT	M
TIP60 sgRNA2 h forward	TTCCACATCGTGGGCTACTTC	H
TIP60 sgRNA2 h reverse	ATCACAGTAGCCTGGCCCAT	H
Tip60 sgRNA1 OT #1 forward	CGAGAGCTTTAAAGTGCGGGC	M
Tip60 sgRNA1 OT #1 reverse	GACCAAAGGGGTAGGCGTAG	M
Tip60 sgRNA1 OT #3 forward	CACGCTGTTTTCTGGCGTACA	M
Tip60 sgRNA1 OT #3 reverse	AGGATGGACAGTGCAGTTGG	M

Tip60 sgRNA1 OT #4 forward	CAGGGGCATAAAGCCCAAACG	M
Tip60 sgRNA1 OT #4 reverse	AGTAGTCTTCTGTAGTTGTTGCTCT	M
Tip60 sgRNA1 OT #5 forward	CGTTTTCTGCGCACGGAGTTG	M
Tip60 sgRNA1 OT #5 reverse	TTCACCTACCACCTCGACCT	M
Tip60 sgRNA2 OT #1 forward	CCTGGGGAGAGGGTGTTATTGAC	M
Tip60 sgRNA2 OT #1 reverse	CTGGCAGTGGCAGAAAGAATC	M
Tip60 sgRNA2 OT #2 forward	CACAGGAGGGGTGGGAATACG	M
Tip60 sgRNA2 OT #2 reverse	GGACACTCGGGGAAGAGTTT	M
Tip60 sgRNA2 OT #4 forward	CAGAGGACTAGGCGAGGTGAT	M
Tip60 sgRNA2 OT #4 reverse	ACACAGCAATTTCCAGGAGGA	M
Tip60 sgRNA2 OT #5 forward	CTTGGTCCAAGACTCTCCAGG	M
Tip60 sgRNA2 OT #5 reverse	TTGACACACTGGAATGGGCT	M
Tip60 sgRNA2 OT #7 forward	CTGCTTTCCTACGTACGCACT	M
Tip60 sgRNA2 OT #7 reverse	CTGCCGACCAGGCCATAAAT	M

Table 5: Quantitative PCR primer.

mRNA	**Primer sequence (5'-3')**	**Species**
Tip60 exon3, 4 forward	GATGAGTGGCCCCTGGC	M
Tip60 exon3, 4 reverse	GCTCGTGAGTCACCCATTCA	M
Tip60 exon8 forward	CCACAAGAGCTTACCACGCT	M
Tip60 exon8 reverse	AGGGTGCCGAAGATCACATT	M
Tip60 exon11 forward	GGGCTATGGCAAGCTGCTTATT	M
Tip60 exon11 reverse	GCCAAGATCTGACAGGGGTTT	M
Genomic *Tip60* exon3, 4 forward	TGAATGGGTGACTCACGAGC	M
Genomic *Tip60* exon3, 4 reverse	GGGACCTACTCACCACCTCT	M
Gapdh forward	TTCACCACCATGGAGAAGGC	M
Gapdh reverse	CCCTTTTGGCTCCACCCT	M
Hsp90ab1 forward	ACCTGGGAACCATTGCTAAG	M
Hsp90ab1 reverse	AGAATCCGACACCAAACTGC	M
Rpl13 forward	TGAGGACCTCTGTGAACTTGC	M
Rpl13 reverse	GGAGAAACGGAAGGAAAAGG	M
Genomic *Ephb4* forward	CGCTAGCCTCAAAATCGTGG	M

Genomic *Ephb4* forward	GGAACACCAACAGAGACCAGT	M
TIP60 exon8 forward	CAACCACCGCTCAACGAAAC	H
TIP60 exon8 reverse	AGAAGTACCACGGCTTGAGG	H
TIP60 exon11 forward	CTAACCCTGCCTCCCTACCA	H
TIP60 exon11 reverse	TGGTCTGGGACCAGTAGCTT	H
GAPDH forward	TGCACCACCAACTGCTTAGC	H
GAPDH reverse	GGCATGGACTGTGGTCATGAG	H
HSP90AB1 forward	AATTGACATCATCCCCAACCCT	H
HSP90AB1 reverse	CCAAACTGCCCAATCATGGAG	H

Table 6: sgRNA oligonucleotides for cloning into *FgH1tUTG* vector.

sgRNA target	**Sense**	**antisense**	**Specificity**
TIP60 sgRNA1	TCCCGCCGGCAC	AAACCGGCTTGA	H/M
	CGCCTCAAGCCG	GGCGGTGCCGGC	
TIP60 sgRNA2	TCCCCTGCCTCC	AAACCGGCGCTG	H/M
	CTACCAGCGCCG	GTAGGGAGGCAG	
TIP60 sgRNA3	TCCCGCTTGCCG	AAACGCGCCGGG	H
	TAGCCCCGGCGC	GCTACGGCAAGC	
Tip60 sgRNA4	TCCCGCTTGCCA	AAACGCGCCGGG	M
	TAGCCCCGGCGC	GCTATGGCAAGC	

Table 7: Nextera i5 and i7 indexing primer and generic p5 and p7 sequencing primer used in CUT&Tag sequencing experiments (Mezger et al., 2018).

Name	**Index sequence**	**Full sequence**
v2_P5.60	TACTGACC	AATGATACGGCGACCACCGAGATCTACACTACT
		GACCTCGTCGGCAGCGTCAGATGTGTAT
v2_P5.61	CGATAGGG	AATGATACGGCGACCACCGAGATCTACACCGA
		TAGGGTCGTCGGCAGCGTCAGATGTGTAT
v2_P5.62	ACTTAGAA	AATGATACGGCGACCACCGAGATCTACACACTT
		AGAATCGTCGGCAGCGTCAGATGTGTAT

v2_P5.79	CTCCGAAC	AATGATACGGCGACCACCGAGATCTACACCTCC GAACTCGTCGGCAGCGTCAGATGTGTAT
v2_P7.60	TTTAATGC	CAAGCAGAAGACGGCATACGAGATGCATTAAA GTCTCGTGGGCTCGGAGATGTG
v2_P7.63	ATGATGAT	CAAGCAGAAGACGGCATACGAGATATCATCAT GTCTCGTGGGCTCGGAGATGTG
v2_P7.65	TAACAACA	CAAGCAGAAGACGGCATACGAGATTGTTGTTA GTCTCGTGGGCTCGGAGATGTG
v2_P7.67	CATCGACC	CAAGCAGAAGACGGCATACGAGATGGTCGATG GTCTCGTGGGCTCGGAGATGTG
v2_P7.69	CGGCCAAT	CAAGCAGAAGACGGCATACGAGATATTGGCCG GTCTCGTGGGCTCGGAGATGTG
v2_P7.78	CGCCGTGC	CAAGCAGAAGACGGCATACGAGATGCACGGCG GTCTCGTGGGCTCGGAGATGTG
v2_P7.80	CATTTCGA	CAAGCAGAAGACGGCATACGAGATTCGAAATG GTCTCGTGGGCTCGGAGATGTG
v2_P7.81	GCTTGCCA	CAAGCAGAAGACGGCATACGAGATTGGCAAGC GTCTCGTGGGCTCGGAGATGTG
v2_P7.82	TTCTACCA	CAAGCAGAAGACGGCATACGAGATTGGTAGAA GTCTCGTGGGCTCGGAGATGTG
v2_P7.86	ACCACAAC	CAAGCAGAAGACGGCATACGAGATGTTGTGGT GTCTCGTGGGCTCGGAGATGTG
Illumina P5	N/A	AATGATACGGCGACCACCGA
Illumina P7	N/A	CAAGCAGAAGACGGCATACGAGAT

3.3.7 PCR programs

Table 8: PCR programs for PCR reactions.

Program	Temperature	Time	No. of cycles

Y repeat	94	2 min	1
	94	30 s	
	68	30 s	5
	72	1 min	
	94	30 s	
	60	30 s	22
	72	30 s	
	72	5 min	1
Cre	94	3 min	1
	94	30 s	
	60	30s	30
	72	1 min	
	72	10 min	1
Tip60 lox	94	3 min	1
	94	30 s	
	62	30 s	34
	72	30 s	
	72	5 min	1
Tip60 genetrap	94	3 min	1
	94	30 s	
	55	30 s	34
	72	30 s	
	72	5 min	1
Tp53	94	3 min	1

	94	30 s	
	55	30 s	34
	72	30 s	
	72	5 min	1
Cdkn2a	94	3 min	1
	94	30 s	
	55	30 s	34
	72	30 s	
	72	5 min	1
1st NGS PCR	95	2 min	1
	95	15	
	60	15	18
	72	30	
	72	5 min	1
2nd NGS PCR	95	2 min	1
	95	15	
	60	15	24
	72	30	
	72	5 min	1

3.4 Microscopy

3.4.1 Live-cell imaging

Cells were imaged using a live cell imaging system (IncuCyte S3) at 37°C and 5% CO_2 using a 10X objective for up to 4 days. For 3D confocal live cell time-lapse imaging, cells were cultured in 8-well tissue culture chambers (Sarstedt, 94.6140.802) and stained with 1 μM SiR-DNA stain (Spirochrome, SC007) and 1 μM verapamil (Spirochrome, SC007). Cells were imaged every 5 min for a total of 24 h using a confocal microscope (Leica SP8) and analysed using an image analysis software (NIH ImageJ Fiji, v1.52h).

3.4.2 Histology

E5.5 uteri and *NestinCre* embryo brains were dissected, fixed in Bouin's solution and paraffin embedded. Serial 7 μm sections were collected and stained with haematoxylin and eosin. Serial sections were examined and all concepti were photographed using a compound microscope (Axioplan 2, Carl Zeiss) using a digital camera (AxioCam HR, Carl Zeiss).

3.4.3 SA-β-galactosidase staining by X-gal

Senescence-associated (SA)-β-galactosidase activity was assessed by 5-bromo-4-chloro-3-indolyl-β-D-galactopyranoside (X-gal) staining performed with the Senescence β-Galactosidase Staining Kit (CST, 9860) according to the manufacturer's instruction. Briefly, cells were cultured in 6-well plates, washed twice with PBS, fixed with 1.5 ml 1X fixative solution for 15 min at RT, washed twice with PBS, stained with 2 ml 1X staining solution (pH=6.0), sealed with parafilm (Merck, P7793), incubated at 37°C

overnight in a dry incubator and analysed by light microscopy. SA-β-galactosidase positive and negative cells were counted in triplicates in 3 images with at least 300 nuclei per replicate using an image analysis software (NIH ImageJ Fiji, v1.52h). Cells were irradiated with 32 Gy using a Theratron Phoenix Co-60 Teletherapy Gamma unit (Best Theratronics, Theratron Phoenix) and cultured for 5 days prior staining as positive controls.

3.4.4 Immunofluorescence

Inner cell mass outgrowths from blastocysts grown in gelatine-coated chamber slides (Millipore, PEZGS0416) were washed in PBS, fixed in 2% (v/v) paraformaldehyde (PFA; Sigma, 158127-500G) in PBS for 15 min at RT, washed twice in PBS, incubated in 0.2% (v/v) Triton X-100 (Sigma, T8787) in PBS for 15 min, blocked in PBSG (0.25% (w/v) gelatine (Sigma, G-1890) in PBS) for 15 min, stained with primary antibody (Table 9) in PBSG for 1 h, washed 4 x 5 min in PBS, stained with secondary antibody in PBSG for 1 h in the dark, washed in PBS, stained with 0.1 µg/µl DAPI (Sigma, 10236276001) in PBS for 5 min, washed twice in PBS for 5 min and washed in MQ-H_2O. Chamber slide walls were removed, and slides mounted in 30 µl Dako fluorescent mounting medium (Dako, S3032). Images of blastocysts were acquired on a compound fluorescence microscope (Axioplan 2, Carl Zeiss) using a digital camera (AxioCam HR, Carl Zeiss).

3.4.5 Primary and secondary antibodies

Table 9: Primary and secondary antibodies used in immunofluorescence (IF), western blotting (WB) and CUT&Tag-sequencing.

Primary antibody	Host	Target	IF	WB	CUT &Tag

Abcam, ab214725	rabbit	H2AZK4ac	1:500	1:2000	-
Abcam, ab214730	rabbit	H2AZK7ac	1:500	1:1000	-
Diagenode, C15210012	rabbit	H2AZK7ac	-	1:2000	1:250
Millipore, ABE1363	rabbit	H2AZK4-7-11ac	-	1:2000	-
Diagenode, C15410173	rabbit	H2AZK4-7-11ac	-	1:3000	1:250
CST, D3V1I	rabbit	H2AZK4-7ac	-	-	1:200
Active Motif, AB_2615081	rabbit	H2AZ	-	1:3000	1:200
Abcam, ab4174	rabbit	H2AZ	1:200	1:750	-
Abcam, ab45152	rabbit	H2AK5ac	1:500	1:4000	-
Abcam, ab4729	rabbit	H2AK27ac	1:500	-	-
Millipore, 07-327	rabbit	H4K5ac	1:500	1:5000	-
Millipore, 07-328	rabbit	H4K8ac	1:500	1:5000	1:100
Abcam, ab46983	rabbit	H4K12ac	1:500	1:20000	-
Millipore, 07-329	rabbit	H4K16ac	1:500	1:7500	1:100
Merck Millipore 06-598	rabbit	H4ac	-	1:1000	1:50
Abcam, ab10799	mouse	H3	-	1:7000	1:50
CST, mAB9649	rabbit	H3K9ac	1:500	-	-
Abcam, ab4441	rabbit	H3K9ac	-	1:8000	-
Millipore, 07-353	rabbit	H3K14ac	1:500	-	-
CST, D4B9	rabbit	H3K14ac	-	1:1000	-
Abcam, ab1191	rabbit	H3K18ac	-	1:1000	-
Merck Millipore 07-355	rabbit	H3K23ac	-	-	1:50
Abcam, ab4729	rabbit	H3K27ac	-	1:2000	-
Millipore, 07-473	rabbit	H3K4me3	-	1:7500	-
CST, 9733	rabbit	H3K27me3	-	-	1:50
Millipore, 16-193	mouse	phospho-H2AX	1:800	-	-
CST, 54020 13546	rabbit	RNAPII S2/S5	-	-	1:50

Merck, 17-672	mouse	RNAPII	-	-	1:100
Secondary antibody	**Type**	**Target**	**IF**	**WB**	**CUT &Tag**
ThermoFisher, A-21206	donkey	α-rabbit A488	1:5000	-	-
ThermoFisher, SA1001	-	Streptavidin-FITC	1:500	-	-
LiCor, 926-32211	goat	α-rabbit-IRDye800CW	-	1:8000	-
LiCor, 925-68020	goat	α-mouse-IRDye680LT	-	1:16000	-
Antibodies online, ABIN101961	guinea pig	α-rabbit IgG	-	-	1:100
abcam, ab46540	rabbit	α-mouse-IgG	-	-	1:100

3.5 Flow Cytometry

3.5.1 Fluorescence activated cell sorting (FACS)

Cells were collected in a single cell suspension and sorted by WEHI FACS Facility technicians into vials with the cell type-specific growth medium supplemented with 100 U/ml penicillin and 100 μg/ml streptomycin (Gibco, 15140163)

3.5.2 Live/Dead cell staining

To quantify live and dead cells, cells were collected, washed twice in PBS, stained in 10 μM ethidium homodimer-1 (EthD-1) and 0.2 μM calcein [(acetyloxy)methyl ester] (calcein AM; both ThermoFisher, L3224) in PBS for 15 min and analysed by flow cytometry using a LSRII Fortessa Cell Analyzer (Biosciences, 647465) without compensation.

3.5.3 TMRE staining

Tetramethylrhodamine, ethyl ester (TMRE) is a red-orange fluorescent dye that accumulates in active mitochondria. To identify live cells, cells were treated with 50 nM TMRE (Abcam, ab113852) for 30 min, trypsinized, washed with FACS buffer (150 mM NaCl, 3.7 mM KCl, 2.5 mM $CaCl_2$, 1.2 mM $MgSO_4$, 14.8 mM HEPES, 1.2 mM KH_2PO_4, pH 7.2), supplemented with 2% (v/v) FBS (SAFC, 12003C), and analysed by flow cytometry using a LSRII Fortessa Cell Analyzer (Biosciences, 647465) without compensation. Additionally, cells were treated with 100 μM FCCP (Abcam, ab113852) as a negative control 10 min prior to TMRE stain. FCCP (carbonyl cyanide 4-(trifluoromethoxy) phenylhydrazone) interferes with the mitochondrial proton gradient so that TMRE cannot accumulate in the mitochondrial membrane.

3.5.4 Annexin-V staining

To identify early and late apoptotic cells, cells were collected, washed twice in PBS, stained with 5 μl phycoerythrin (PE)-conjugated annexin-V, a phospholipid-binding protein (BD Bioscience, 556421) and 0.5 μg/ml DAPI (Sigma, 10236276001) in 100 μl annexin-V binding buffer (BD Bioscience, 559763) for 15 min at RT, and diluted with 400 μl annexin-V binding buffer and analysed by flow cytometry using a LSRII Fortessa Cell Analyzer (Biosciences, 647465).

3.5.5 BrdU incorporation

For BrdU incorporation analysis of the DNA synthesis phase of the cell cycle, cells were cultured in the presence of 10 μM BrdU for 1 h, then trypsinized, washed once with PBS,

resuspended in PBS, fixed by dropwise adding -20°C 100% EtOH to a final concentration of 75% EtOH while gently vortexing, and stored at 4°C for up to 7 days. Fixed cells were washed twice with FACS buffer, treated with 2 M HCl for 1 h, washed twice with FACS buffer, stained with 1:20 anti-BrdU antibody (Invitrogen, 17-5071-41) for 30 min, washed twice with FACS buffer, stained with DNA stain (7-AAD; BD Biosciences, 559925; 1:20 dilution) and analysed by flow cytometry using a LSRII Fortessa Cell Analyzer (Biosciences, 647465).

3.5.6 γH2AX staining

For γH2AX staining, cells were trypsinized and washed twice with PBS. $1x10^5$ cells were fixed and permeabilized in 100 µl FOXP3 fixation and permeabilization solution (ThermoFisher, 00-5523-00) according to the manufacturer's instruction, incubated for 1 h, washed twice with FACS buffer, resuspended in 500 µl FACS buffer containing anti-γH2AX primary antibody (Merck, 16-193) in a 1:400 dilution, and incubated overnight at 4°C on a roller. Stained cells were washed twice in FACS buffer and resuspended in 100 µl FACS buffer containing secondary streptavidin-A647 conjugate (ThermoFisher, S21374) in a 1:400 dilution, and incubated for 1 h at 4°C. Stained cells were washed twice with FACS buffer, resuspended in 200 µl FACS buffer containing 25 µg/ml RNAse (Merck, 10109142001) and 0.5 µg/ml DAPI (Sigma, 10236276001), and analysed by flow cytometry using a LSRII Fortessa Cell Analyzer (Biosciences, 647465). No compensation was needed. As a positive control, wild-type MEFs were UV-irradiated with 20 mJ using a UV crosslinker (Biorad, GS Gene linker UV chamber, 808BR, 1989) and allowed to recover in the cell culture incubator for 30 min. γH2AX signals were

assessed separately for cells with 2n and 4n DNA content and normalized to the respective control value.

3.6 Biochemical

3.6.1 Acid protein extraction and quantification

To recover a protein preparation enriched in histones, acid protein extraction was performed as described (Sidoli et al., 2016). All reagents used were chilled on ice. Adherent cells were washed twice with PBS, nuclei were extracted for 5 min on ice in nuclear isolation wash buffer (15 mM Tris-HCl, 60 mM KCl, 15 mM NaCl, 5 mM $MgCl_2$, 1 mM $CaCl_2$, and 250 mM sucrose, pH=7.5 (HCl-adjusted) freshly supplemented with 1 protease inhibitor cocktail tablet (PIC, Roche, 11697498001) per 10 ml, 1 mM PMSF (Roche, 10837091001), 1 mM DTT (Supelco, 646563), and 5 mM sodium butyrate (Sigma, 303410)) supplemented with 0.2% (v/v) NP-40 Alternative (Millipore, 492016), scraped from the plate and collected in a 1.5 ml tube, centrifuged for 5 min at 2500x *g* at 4°C, washed trice with nuclear isolation wash buffer (without NP-40 Alternative), lysed for 2 h on ice in 100 µl 0.4 N H_2SO_4 (Sigma, 339741) per $5x10^6$ cells and centrifuged for 10 min at 10,000 x *g*. Nuclear protein lysate supernatants were transferred to new tubes and centrifuged for 5 min at 10,000 x *g*. The supernatant was transferred to another new tube with 0.5 volumes of 100% TCA (Sigma, T0699) to achieve 33% (v/v) final concentration of TCA in the nuclear protein lysates. The tubes were inverted several times and incubated for 2 h or overnight on ice. Precipitated acid extracted proteins were collected by centrifugation for 10 min at 10,000 x *g*, washed once with 1 ml acidic acetone (0.1% (v/v) HCl in acetone), spun down for 2 min at 17,300 x *g*, washed trice with 100% acetone, air dried for 5 to 15 min, resuspended in 100 µl sterile MQ-H_2O per $5x10^6$ cells,

spun down for 2 min at 10,000 x *g*. The supernatant was transferred to a new tube, aliquoted to avoid freeze thaw cycles, and snap frozen at -80°C. The protein concentrations were quantified using a Bradford assay according to the manufacturer's instruction (Biorad, 5000204).

3.6.2 Cell fractionation protein extraction

Cells were fractioned using the subcellular protein fractionation kit for cultured cells (Thermo Scientific, 78840) according to the manufacturer's instructions. All buffers were freshly supplemented with 1 protease inhibitor cocktail tablet (PIC, Roche, 11697498001) per 10 ml, 1 mM PMSF (Roche, 10837091001), 1 mM DTT (Supelco, 646563), and 5 mM sodium butyrate (Sigma, 303410). Briefly, cells were washed twice with ice cold PBS, scraped in ice cold PBS, resuspended in 10 volumes of cytoplasmic extraction buffer (CEB) and incubated on ice for 10 min with gentle mixing. Nuclei were spun down for 5 min at 3,000 x *g*. The supernatant was collected as the cytosolic fraction and stored at -80°C. Nuclei were resuspended in 10 volumes of membrane extraction buffer (MEB), vortexed for 5 s and incubated for 10 min with gentle mixing. Nuclei were collected for 5 min at 3,000 x *g* and washed with another 5 volumes of MEB, resuspended in 5 volumes of nuclear extraction buffer (NEB), vortexed for 15 s and incubated at 4°C for 30 min with gentle mixing. The lysate was centrifuged for 5 min at 5000 x *g*. The supernatant was collected as the soluble nuclear fraction and stored at -80°C. The pellet was washed with another 5 volumes of NEB and resuspended in chromatin bound extraction buffer (NEB supplemented with 5 mM $CaCl_2$ and 3,000 U/ml micrococcal nuclease (MNase)), pipetted 10 times to break up the pellet, vortexed for 15 s, incubated for 5 min at 37°C, vortexed again for 15 s and spun down for 5 min at 16,000 x *g*. The supernatant was collected as the chromatin fraction and stored at -80°C. A possible

follow-up step to extract nuclear cytoskeletal proteins was omitted. The protein concentration was quantified using a Bradford assay according to manufacturer's instruction (Biorad, 5000204). Samples were diluted up to 1:5.

3.6.3 SDS-PAGE and western immunoblotting

Protein extracts were prepared with 2X SDS sample buffer (0.08 M Tris-HCl, pH 6.8, 2.5% (w/v) sodium dodecyl sulphate, 8% (v/v) glycerol, 4 mM 2-mercaptoethanol, 0.02% (w/v) bromophenol blue), incubated for 5 min at 95°C, separated by SDS-PAGE using 4-12% (w/v) Bis-Tris polyacrylamide gels (Invitrogen, NP0321BOX) at 110 V in MES running buffer (NP0002, Invitrogen), and transferred onto hydrophobic PVDF membranes (MERCK, IPFL00010) or Odyssey® nitrocellulose membranes (Li-Cor, 926-31090), using transfer equipment (BioRad, 170-3930) in western transfer buffer (150 mM glycine, 20 mM Tris, 20% (v/v) methanol in MQ-H_2O) at 90 V for 1.5 h. Membranes were blocked in Odyssey Blocking Solution (Li-Cor, 927-40000), for 1 h at 4°C, incubated with primary antibodies (Table 9) overnight in Intercept (PBS) Blocking Buffer (Li-Cor Biosciences, 927-70001), supplemented with 0.1% Tween-20 at 4°C, washed in PBST (PBS, 0.1% (v/v) Tween-20) 5 times for 5 min, incubated with 1:8,000 anti-rabbit-IRDye-800CW (Li-Cor, 925-32211) and 1:16,000 anti-mouse-IRDye-680LT (Li-Cor Biosciences, 925-68020) IgG secondary antibody in Intercept (PBS) Blocking Buffer (Li-Cor Biosciences, 927-70001), supplemented with 0.1% Tween-20 at RT for 1 h, and washed in PBST 5 times for 5 min and washed in PBS 5 times for 5 min. Protein bands were detected using the Odyssey CLx Imaging System (Li-Cor Biosciences, model 9140) and quantified using the Odyssey CLx 1.0.18 software (Li-Cor Biosciences). Protein bands were quantified by subtracting background intensity above and below the band and normalizing to indicated total protein or housekeeping proteins. Normalized intensities

of treated samples were divided by control values to calculate fold changes. Fold changes were log_{10}-transformed for statistical analysis. Unpaired two-tailed t test or two-way ANOVA were used to test for statistically significant differences between indicated values.

3.7 Statistical analysis

Statistical analysis was carried out using the Prism v8.0a software, if not stated otherwise. Statistical methods are stated in the figure legends. Data are presented as mean ± SEM, unless indicated otherwise. Individual experimental replicates are represented by circles in the bar graphs.

Chapter 4 Inducible *TIP60* deletion systems

4.1 Genetic deletion or mutation of the *Tip60* gene in human cells and mice

To investigate the roles of TIP60 in cellular processes, I removed endogenous TIP60 from cells by genomic deletion. Due to the lethal nature of *Tip60* deletion, the absence of specific TIP60 inhibitor and the known off-target artefacts of siRNA knockdown, I generated dox-inducible CRISPR/Cas9 mutant *TIP60* cells and utilized a characterized tamoxifen-inducible Cre/*loxP Tip60* knockout in mice. In addition, I will present data generated using a *Tip60* genetrap allele in mice.

4.2 Inducible *ERT2* deletion of exons 3 and 4 of the *Tip60* gene

Prior to commencing my PhD, two *loxP* sites were inserted into the *Tip60* locus of C57BL/6 mESCs by CRISPR/Cas9-mediated mutagenesis and used to create mice with the *Tip60*^{fl} allele by the Melbourne Advanced Genome Editing Centre (MAGEC) at WEHI (Figure 4.1A). Two sgRNAs of the sequence GTACGGAGATGATCCGGGCG and TGGAAGCTACGCCTGCAACT were used to create double-stranded breaks within the *Tip60* locus to stimulate homologous recombination. A donor vector with 2 kbp of homology arms was used to introduce *loxP* sequences disrupting the sgRNA binding sites to prevent cleavage of the target allele, and restriction sites for diagnostic digests. 602 bp containing exon 3 and exon 4 of *Tip60* were flanked with *loxP* sites to facilitate a frameshift disruption of TIP60 synthesis. All splice variants of *Tip60* contain exon 2 and exon 3 (Figure 1.7A). No other genes are found in this locus. Founder mice (F0) were screened for the correct insertion of *loxP* sites and backcrossed to C57BL/6 wild-type males to produce targeted F1 offspring. Germline transmission was assessed by genotyping PCR and selected mice were used to screen for correct positioning of *loxP* sites by diagnostic digest and further sequenced by next generation sequencing (NGS).

I utilized inducible *RosaCreERT2* (*ERT2*) transgenic mice (Seibler et al., 2003) crossed to *Tip60*^{fl} mice to isolate primary murine embryonic fibroblasts (MEFs).

MEFs are lineage-committed multipotent stem cells, giving rise to adipogenic, chondrogenic, and osteogenic tissue (Dastagir et al., 2014). Primary MEFs s undergo cellular senescence in standard culturing conditions (20% O_2), but can be cultured long-term in low oxygen incubator (3% O_2) to extend their ability to proliferate and differentiate (Parrinello et al., 2003). Utilizing primary cells reduces common cell culture artifacts that can be seen in cell lines that have been cultured for decades and thus resemble the physiological situation more closely.

In cell cultures Cre-ERT2 was induced with 4-hydroxy-tamoxifen (4-OHT). The IC_{50} of 4-OHT treatment for 5 days for cell survival MEFs was 7.4 ± 0.7 µM (Figure 4.1B). *Tip60*$^{fl/fl}$*;ERT2*, *Tip60*$^{fl/+}$*;ERT2* and *Tip60*$^{+/+}$*;ERT2* control MEFs were isolated and induced with 250 nM 4-OHT for 1 to 5 days resulting in deletion of exons 3 and 4 of the *Tip60* gene. Induced cultures are referred to as *Tip60*$^{iKO/iKO}$*;ERT2*. Deletion of the *loxP* flanked DNA was shown by genotyping PCR (Figure 4.1C). Due to lack of commercially available TIP60 antibody, I performed *Tip60* RT-qPCR with primers spanning exon 3 and exon 4 of *Tip60*, which showed that no *Tip60* mRNA containing exon 3 and exon 4 could be detected in *Tip60*$^{iKO/iKO}$*;ERT2* MEFs after 3 days of tamoxifen treatment (Figure 4.1D), indicating that *Tip60* mRNA is translated with a frameshift leading to a non-sense protein sequence.

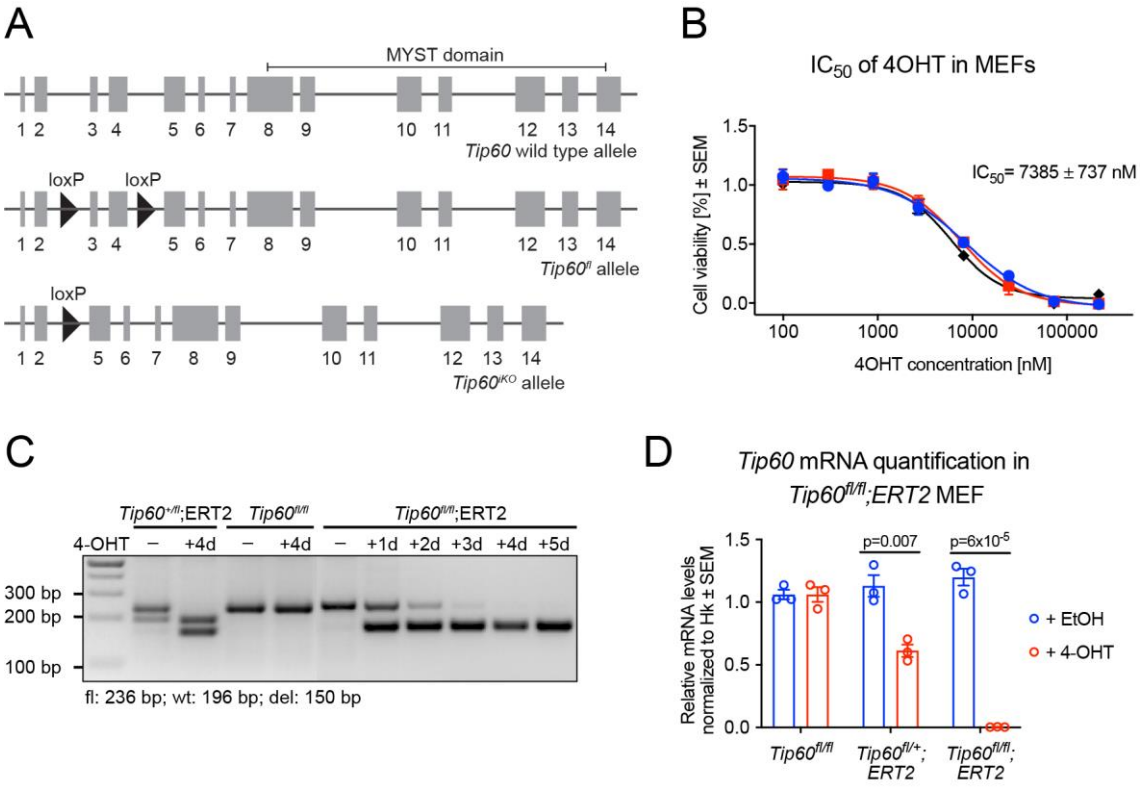

Figure 4.1: *ERT2/loxP*-mediated deletion of exons 3 and 4 of the *Tip60* gene. (A) Schematic drawing of the conditional *Tip60* allele. Exons are represented by numbered grey boxes. Exons 3 and 4 are flanked by *loxP* sites (*Tip60^{fl}* allele). In combination with tamoxifen induced *ERT2*, *Tip60^{fl}* leads to deletion of exon 3 and 4 resulting in a frameshift and so generating the induced knockout *Tip60^{iKO}* allele. (**B)** Effect of 4-OHT on MEF cell viability after 3 days of treatment in 3 independent MEF clones (red, blue, and black line). Each dot represents mean ± SEM of 4 technical replicates. An IC_{50} value of 7.4 ± 0.7 µM for the effect of 4-OHT on cell viability has been determined. (**C)** Representative DNA gel of three-way PCR genotyping of *Tip60^{+}* (wild-type), *Tip60^{fl}*, and *Tip60^{iKO}* (induced knockout) alleles, shown here in 4-OH-tamoxifen (4-OHT) and vehicle (EtOH) treated MEFs. Upon 4-OHT treatment of MEFs, the sequence flanked by *loxP* sites (which yielded a 236 bp band) is excised to produce the deleted allele (yielding a 150 bp band). This process is completed over the course of 3 days. (**D)** RT-qPCR assessment of *Tip60* mRNA levels normalized to the housekeeping (Hk) gene *Hsp90ab1* in *Tip60$^{+/+}$;ERT2*, *Tip60$^{iKO/+}$;ERT2*, and *Tip6$^{iKO/iKO}$;ERT2* MEFs induced with tamoxifen (4-OHT) for 3 days. Means ± SEM of three biological replicates (each assessed in triplicate) are displayed and analysed by unpaired two-tailed t test.

4.3 Inducible CRISPR/Cas9 mutation of the *Tip60* gene

In parallel to the recombinase induced *Tip60* knockout, I mutated *Tip60* utilizing an inducible CRISPR/Cas9 system, involving inducible sgRNA expression in combination with constitutively expressed Cas9 (Aubrey et al., 2015). Two different sgRNAs, sgRNA1 and sgRNA2, targeting exons 8 and 11 of the *Tip60* gene, respectively, were designed (Figure 4.2A). Exons 8 and exon 11 encode parts of the MYST domain, harbouring the characteristic acetyltransferase activity. The sgRNA sequences were designed to be able to target both the human and murine *TIP60* locus. sgRNAs were cloned into the lentiviral transfer vector *FgH1tUTG*. *FgH1tUTG* facilitates the stable transduction of dox-inducible transgene expressing the sgRNAs into target cells alongside a constitutively expressed *GFP* marker gene. For *Cas9* expression I utilized the lentiviral transfer vector *FUCas9Cherry* (Addgene plasmid # 70182; http://n2t.net/addgene:70182; RRID:Addgene_70182) (Aubrey et al., 2015), mediating constitutive expression of Cas9 alongside a constitutive mCherry marker. Using lentiviral transduction, I integrated the sgRNA expressing transgene under the dox inducible promoter as well as the constitutively expressed *Cas9* gene (hereafter referred to as g1/C9 for sgRNA#1 and g2/C9 for sgRNA#2 or g/C9 for merged data from g1 and g2) into MEFs, HEK293 cells and U2OS cells. Cell lines containing only the sgRNA transgene, lacking Cas9, were used as controls (hereafter referred to as g1 and g2 or g for merged data). The integration of the Cas9 and sgRNA constructs was monitored by the expression of the fluorescence markers mCherry and GFP, respectively, and sorted for high intensity by FACS to acquire homogenous, double positive populations (Figure 4.2B). Cells were treated with dox to induce sgRNA transcription and mutation of the *Tip60* locus. Induced cultures are referred to as *iC-Tip60* cells. Insertion and deletion (indel) mutations were analysed in the bulk population via high throughput sequencing, using a threshold of at

least 25 reads per sequence (Figure 4.2C). After 24 hours of dox induction, the indel frequency reached 60% and after 48 hours it plateaued at around 85% in MEFs (Figure 4.2D). Both sgRNAs showed a similar dynamic and efficiency. Based on these data and considering two alleles per cell, homozygous knockout of *Tip60* is predicted to occur at a rate of at least 72% [$0.85^2 = 0.7225$]. This rate is likely higher, since it is more likely that if Cas9 is active in a cell, it will delete both alleles. Notably, indels that were less frequent than 25 reads were not counted, potentially underestimating the indel frequency. Guide only controls showed no indel activity. Assessment of the top four predicted off-target loci for each sgRNA in the mouse genome, identified by WTSI Genome Editing (WGE) (Hodgkins et al., 2015), showed no indel activity (Figure 4.2E). RT-qPCR analysis of *iC-Tip60* MEFs showed a reduction of *Tip60* mRNA in bulk MEFgC/9 cultures after 3 days of induction (Figure 4.2F), indicating increased non-sense mediated decay of mutated Tip60 *mRNA* or inefficient transcription. Notably, remaining *Tip60* mRNA potentially consists of both wildtype and mutated mRNA in *iC-Tip60* MEFs.

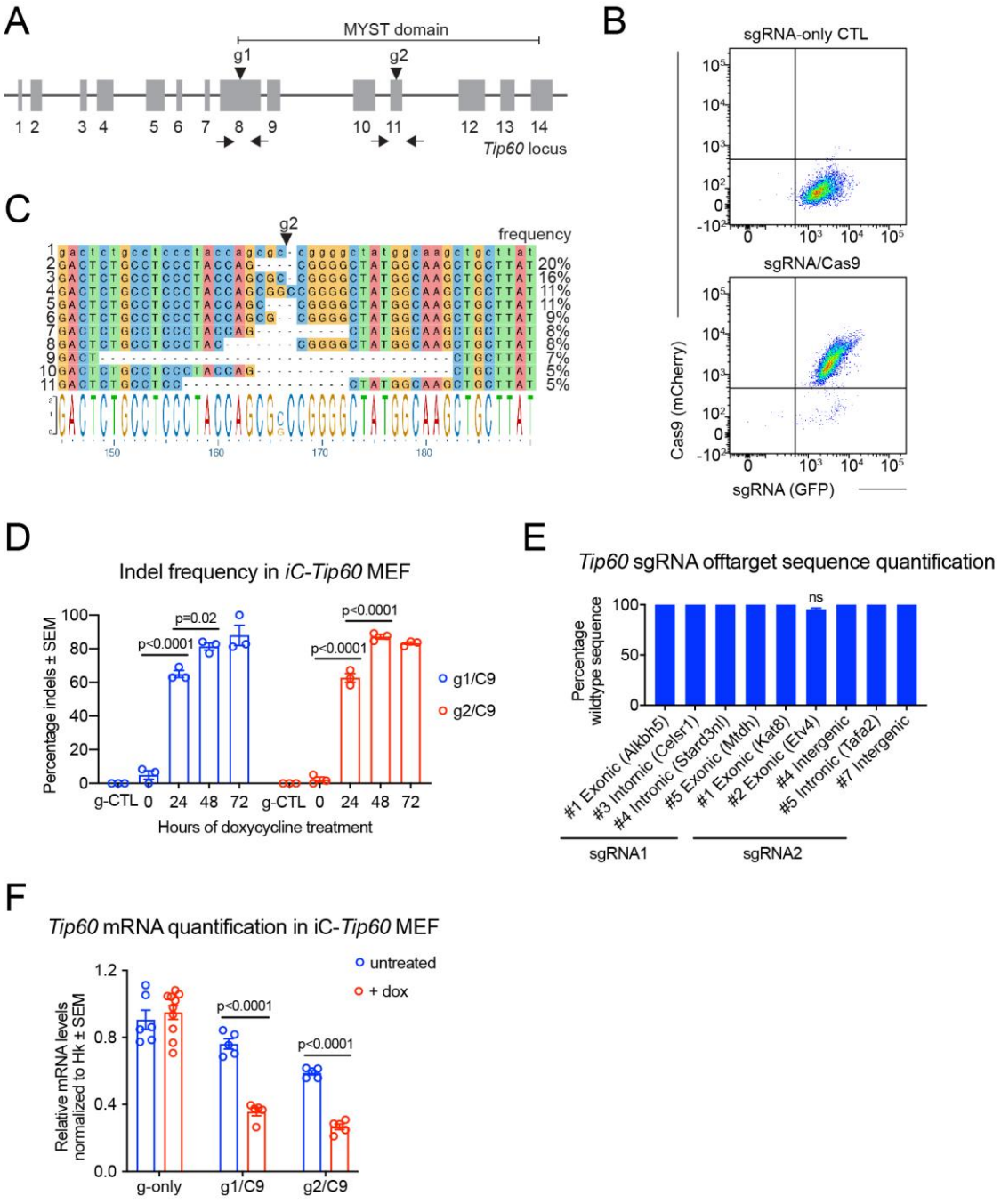

Figure 4.2: CRISPR/Cas9-mediated mutation of the *Tip60* gene. (A) Inducible CRISPR *Tip60* (*iC-Tip60*) mutation system, with sgRNA PAM sites represented by black arrowheads (g1 and g2). Upon dox induction, sgRNA1 or sgRNA2 is transcribed, leading to CRISPR/Cas9 mediated indels in exon 8 and exon 11, respectively. **(B)** FACS plots of the Cas9 and sgRNA positive MEFs. Cas9 and sgRNAs were co-expressed with the marker proteins mCherry and GFP, respectively, to allow sorting of double positive (MEFg/C9) and GFP positive sgRNA-only control cells (g-only CTL). **(C)** Representative indel sequence analysis of *iC-Tip60* MEFs after 3 days of dox induction of sgRNA#2 (g2). The sequences are displayed in decreasing frequency and aligned to the wild-type sequence (1st row, lower case letters). Indels are shown as a percentage of all sequences with at least 25 reads (total of 502 out of 3052 reads). **(D)** Quantification of

indel frequencies in dox induced CRISPR *Tip60* mutated MEFs (*iC-Tip60* MEFs) for each sgRNA#1 and sgRNA#2 and sgRNA-only controls (g1/C9, g2/C9, and g-CTL). DNA was sequenced after 24, 48, and 72 hours of dox treatment. The frequency indicates populations of indels of all sequences with at least 25 reads. Means ± SEM of 3 technical replicates for each sgRNA are displayed and were analysed by one-way ANOVA with time as the independent factor and Benjamini and Hochberg correction. **(E)** Assessment of potential off-target effect. Quantification of wild-type frequencies at potential off-target loci for each sgRNA in *iC-Tip60* MEFg1/C9 and MEFg2/C9 after 3 days of dox treatment as a percentage of all sequences with at least 25 reads. No off-target indel activity was detected. **(F)** RT-qPCR assessment of *Tip60* mRNA levels, normalized to *Hsp90ab1*, in *iC-Tip60* and control MEFs (MEFg/C9 and g-only control) induced with dox for 3 days. Means ± SEM of 3 biological replicates, each assessed in triplicate and analysed by unpaired two-tailed t test. Note, the *Tip60* mRNA detected in the *iC-Tip60* is assumed to contain mutations corresponding to the *Tip60* gene mutations detected in these cells displayed in (C,D).

4.4 Conclusion to Chapter 4

In conclusion, I generated and characterized two inducible *TIP60* knockout systems. The *ERT2/loxP*-mediated deletion of *Tip60* lead to complete deletion of exon 3 and exon 4 introducing a frameshift and leading to completely different translation compared to the physiological TIP60 protein sequence. Thus, the *ERT2/loxP* induced *Tip60* recombination represents a *Tip60* allele lacking all functional domains producing a null allele. Induction of the CRISPR/Cas9 system resulted in mutations in 80% of exon 8 or exon 11 of *Tip60*. These mutations partly lead to non-sense mediated decay of *Tip60* mRNA. Thus, I predict the induced CRISPR mutation of *Tip60* resulted in cell cultures with a large proportion of *Tip60* null cells and some wildtype, heterozygous, or silently mutated *Tip60* cells. The dynamic of maximum *Tip60* deletion was reached after 3 – 4 days of induction and comparable between the *ERT2/loxP* system and induced CRISPR mutation system.

Chapter 5 The cellular functions of TIP60

5.1 Effects of *TIP60* deletion on cell proliferation

I am utilizing the inducible genetic deletion of *TIP60* to investigate the effects of genetic loss of *TIP60* on cell proliferation in a range of murine and human cell types.

5.1.1 *Tip60* deletion causes cell proliferation arrest in MEFs

Treatment of *Tip60$^{fl/fl}$;ERT2* and *Tip60$^{+/fl}$;ERT2* MEFs with 4-OHT for 3 days followed by passaging in culture for 2 weeks in absence of 4-OHT resulted in complete growth arrest in *Tip60$^{iKO/iKO}$;ERT2* MEFs, whereas heterozygous *Tip60$^{+/iKO}$;ERT2* control MEFs continued to proliferate normally, similar to vehicle (EtOH) treated cells (Figure 5.1A). *Tip60$^{iKO/iKO}$;ERT2* MEFs retained the ability to adhere to the cell culture plastic after passaging and no excessive floating cells were observed compared to *Tip60$^{+/iKO}$;ERT2* control MEFs, suggesting an absence of cell death. *Tip60$^{iKO/iKO}$;ERT2* MEF morphology closely resembled senescent MEFs (Figure 5.1B), characterized by flattened and extended cytoplasm (Salama et al., 2014; Sheikh et al., 2015).

The inducible CRISPR *Tip60* mutated MEFs (*iC-Tip60*) were continuously cultured in dox supplemented medium for 9 days. *iC-Tip60* cells displayed growth arrest after 3 days of dox treatment compared to cells expressing only sgRNA without Cas9 (Figure 5.1C). No difference between g-only control MEFs and untreated MEFg/C9 suggest that constitutive Cas9 expression had no effect on cell proliferation. After 5 days of dox treatment *iC-Tip60* MEFs closely resemble *ERT2* mediated *Tip60* knockout MEFs with an extended and flat cell morphology (Figure 5.1D). In conclusion, both inducible TIP60 knockout methods result in strikingly similar dynamics with respect to growth arrest and morphological phenotype.

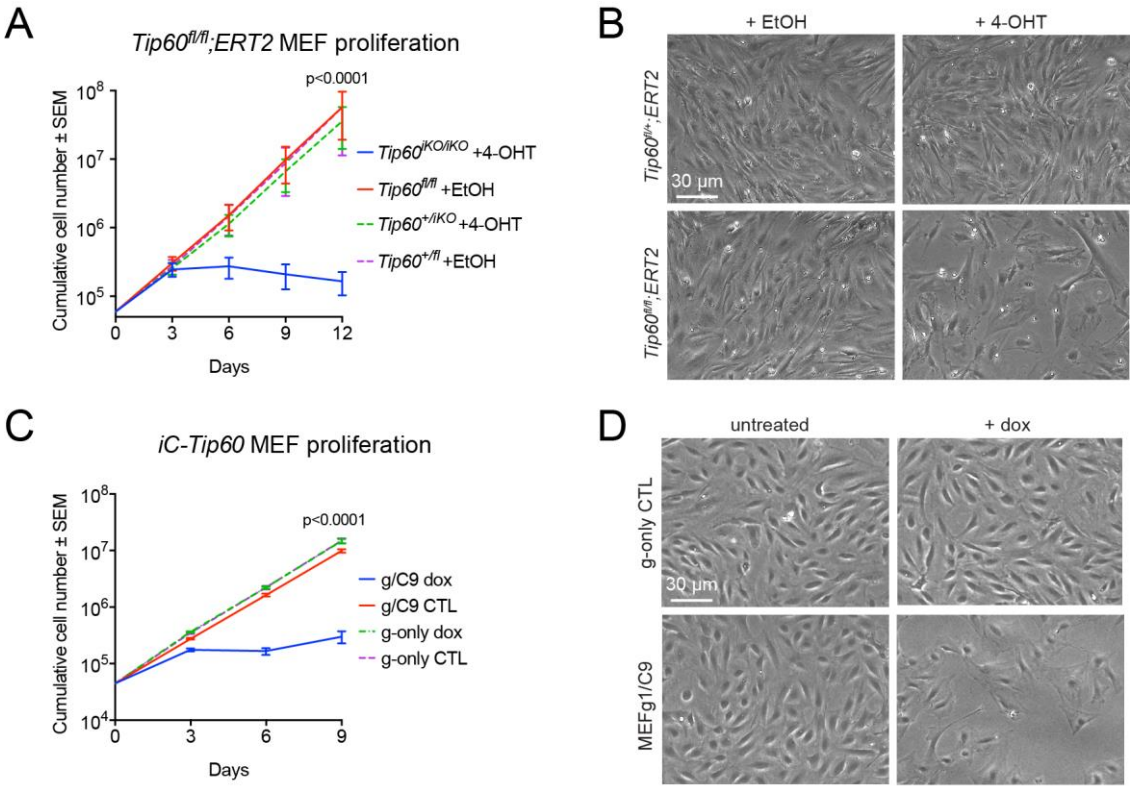

Figure 5.1: *Tip60* deletion causes cell proliferation arrest in murine cells. (A) Proliferation of *Tip60*$^{fl/fl}$*;ERT2* MEFs. 4-OHT induced homozygous *Tip60* knockout led to cell cycle arrest after 3 days. Cells were treated for 3 days with 4-OHT before culturing in normal growth medium for the rest of the experiment. The slopes of log transformed growth curves were calculated from 3 to 12 days and compared using an unpaired two-tailed t test. Data are presented as means ± SEM of cell isolates from 3 individual mouse embryos per genotype. **(B)** Representative phase contrast images of *Tip60*$^{fl/+}$*;ERT2* and *Tip60*$^{fl/fl}$*;ERT2* MEFs untreated and 5 days after 4-OHT induction of *Tip60* deletion. **(C)** Proliferation of *iC-Tip60* MEFs. Data from both sgRNAs were similar and so were combined. Dox induced *Tip60* mutation led to proliferation arrest after 3 days. Means ± SEM of 3 independent replicates for each of 2 sgRNAs are displayed. The slopes of log transformed growth curves were calculated from 3 to 9 days and compared by unpaired two-tailed t test. **(D)** Representative phase contrast images of *iC-Tip60* MEFs and g-only controls (g/C9 and g-only CTL) 5 days after dox induction of *Tip60* mutation.

5.1.2 *Tip60* deletion causes cell proliferation arrest in human cell lines

To determine the effects of loss of TIP60 in human cells, I induced CRISPR/Cas9-mediated *TIP60* mutation in the human embryonic kidney 293 (HEK293) cells and human U2OS osteosarcoma cell line. HEK293 cells are non-cancerous human embryonic

cells allowing me to compare the effect of TIP60 mutation in human cells with my findings in murine cells. To investigate the effect of loss of TIP60 in human cancer cells, I utilize U2OS cells, which allow highly efficient CRISPR/Cas9-mediated mutation of target genes.

Tip60 mRNA is strongly reduced in human *TIP60* mutant cells after 3 days of dox induction (Figure 5.2A). *iC-Tip60* U2OS and *iC-Tip60* HEK293 cells were continuously cultured in dox supplemented medium for 15 and 16 days, respectively, and cell proliferation and morphology were assessed. *TIP60* deletion led to a drastic slowing in cell growth (Figure 5.2B). The timing of the effects of loss of TIP60 were similar in human and mouse cells. However, the growth curves of the human cells retained a slight upwards slope, suggesting an incomplete growth arrest. Phase contrast microscopy of *iC-TIP60* U2OS cells revealed a similar flattened, extended phenotype to *Tip60* deleted MEFs in U2OS cells (Figure 5.2C). *iC-TIP60* HEK293 cells displayed reduced adherence to the tissue culture surface and about 24% and 20% of cells lost contact assessed 4 and 8 days after dox treatment just before splitting consecutive passages, respectively (Figure 5.2D). Notably, the absolute cell numbers combining adherent cells and floating cells were reduced by 40% and 73% after 4 days and 8 days, respectively, compared to g-only CTL cells, indicating, that the reduction in cell number in *TIP60* knockout HEK293 is not explained solely by detaching cells, but also partly by proliferation arrest.

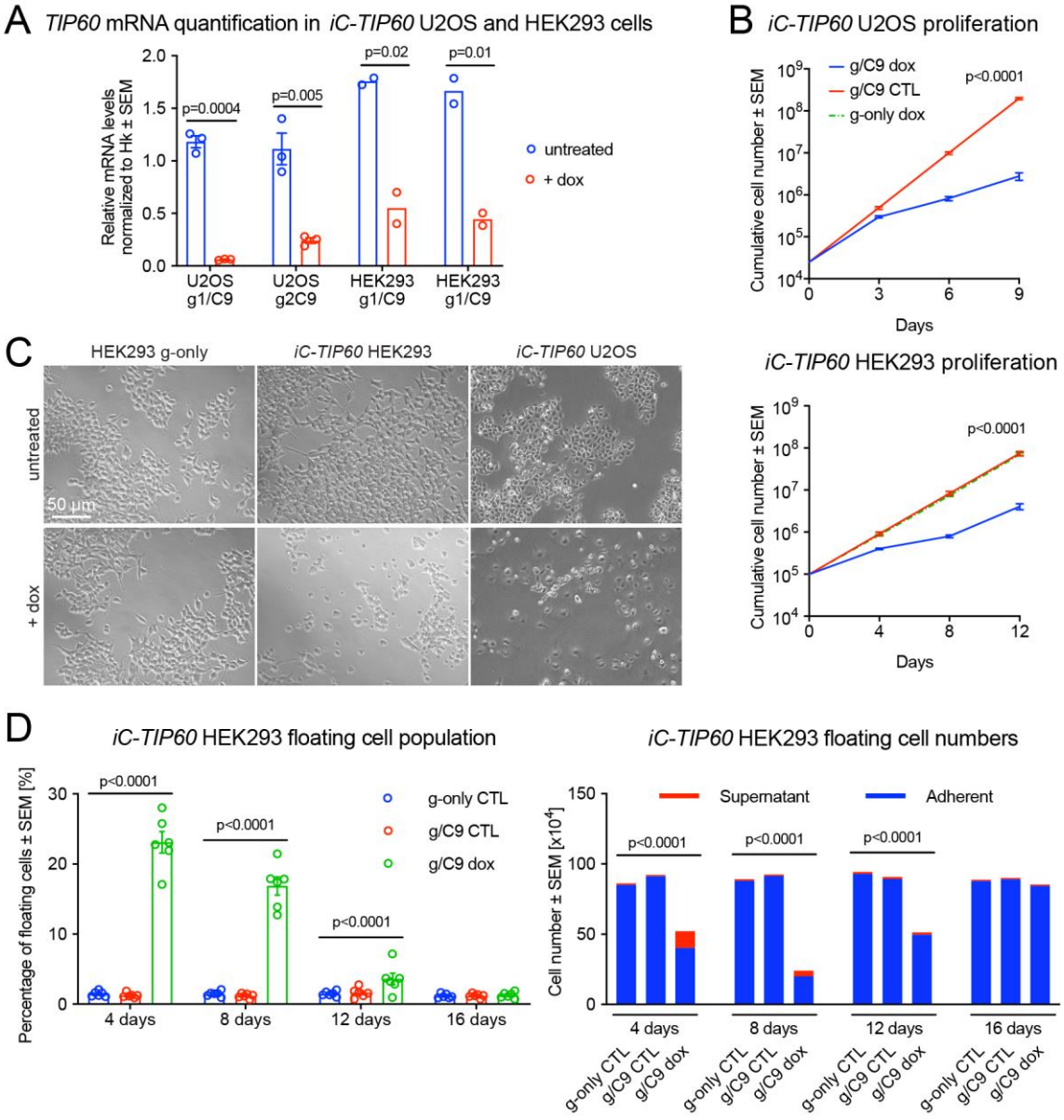

Figure 5.2: *TIP60* deletion causes cell proliferation arrest in normal and cancerous human cells. (A) RT-qPCR assessment of *TIP60* mRNA levels normalized to *Hsp90ab1* in *iC-TIP60* U2OS and HEK293 cells induced with dox for 3 days. Means ± SEM of at least two experiments (each assessed in triplicates) are displayed and analysed by unpaired two-tailed t test. **(B)** Proliferation of human cell lines (HEK293 and U2OS) transfected with Cas9 and *TIP60* guide RNAs (HEK293g/C9 and U2OSg/C9). Data from two different guide RNAs, sgRNA#1 and sgRNA#2, were similar and thus combined such that the means ± SEM are derived from 2 guides, each assessed in triplicate. The slopes of log transformed growth curves were calculated from 3 to 9 days (U2OS) and 3 to 12 days (HEK293 cells) and compared by unpaired two-tailed t test. **(C)** Representative phase contrast images of *iC-TIP60* HEK293 and U2OS 5 days after dox induction of *TIP60* mutation. **(D)** Cell counts of floating cells in culture supernatants of continuous *iC-TIP60* HEK293 cultures after dox induction. Percentage of floating cells (left) and combined absolute cell numbers of adherent and floating cells (right) are displayed.

5.1.3 Induced CRISPR-mediated *TIP60* mutation is incomplete

Unlike ERT2 induced Tip60 deleted MEFs, CRISPR/Cas9-induced *TIP60* mutant cell cultures displayed outgrowth of cells after approximately 3 passages. *iC-TIP60* MEFs proliferation returned to levels similar to control cells after 12 days of continuous culturing in dox supplemented medium (Figure 5.3A). Similarly, *iC-TIP60* U2OS and HEK293 cells returned to normal proliferation rates after 9 and 8 days, respectively. Notably, the CRISPR/Cas9 mutation is not complete as indicated by the indel frequencies and a small portion of cells must be considered *Tip60* heterozygous or wild-type (Figure 5.3B). Congruently, when I assessed outgrowth culture cells for indels by high throughput-sequencing I observed lower indel frequencies in the outgrowth cultures compared to time points early after dox induction. A possible reason for the outgrowth seen in CRISPR mutant cells might be due to a selection for indels not leading to dysfunctional TIP60 protein or nonsense mediated decay of *Tip60* mRNA, such as silent mutations in the sgRNA target area, especially the PAM site, protecting the locus from Cas9 mediated cleavage. In addition, failure to delete can be due to low Cas9 expression, as previously reported (Aubrey et al., 2015). Viral transgenes are prone to silencing, especially when silencing provides a proliferative advantage, essentially exerting a selection pressure. Cas9 and sgRNA transgene silencing was confirmed by the observed in loss of fluorescence markers GFP and mCherry, indicating loss of sgRNA and Cas9 expression, respectively (Figure 5.3C). Further, cells have been shown to mitigate CRISPR-mediated mutation of genes by skipping mutated exons or reinitiate translation leading to N-terminally truncated proteins (Smits et al., 2019).

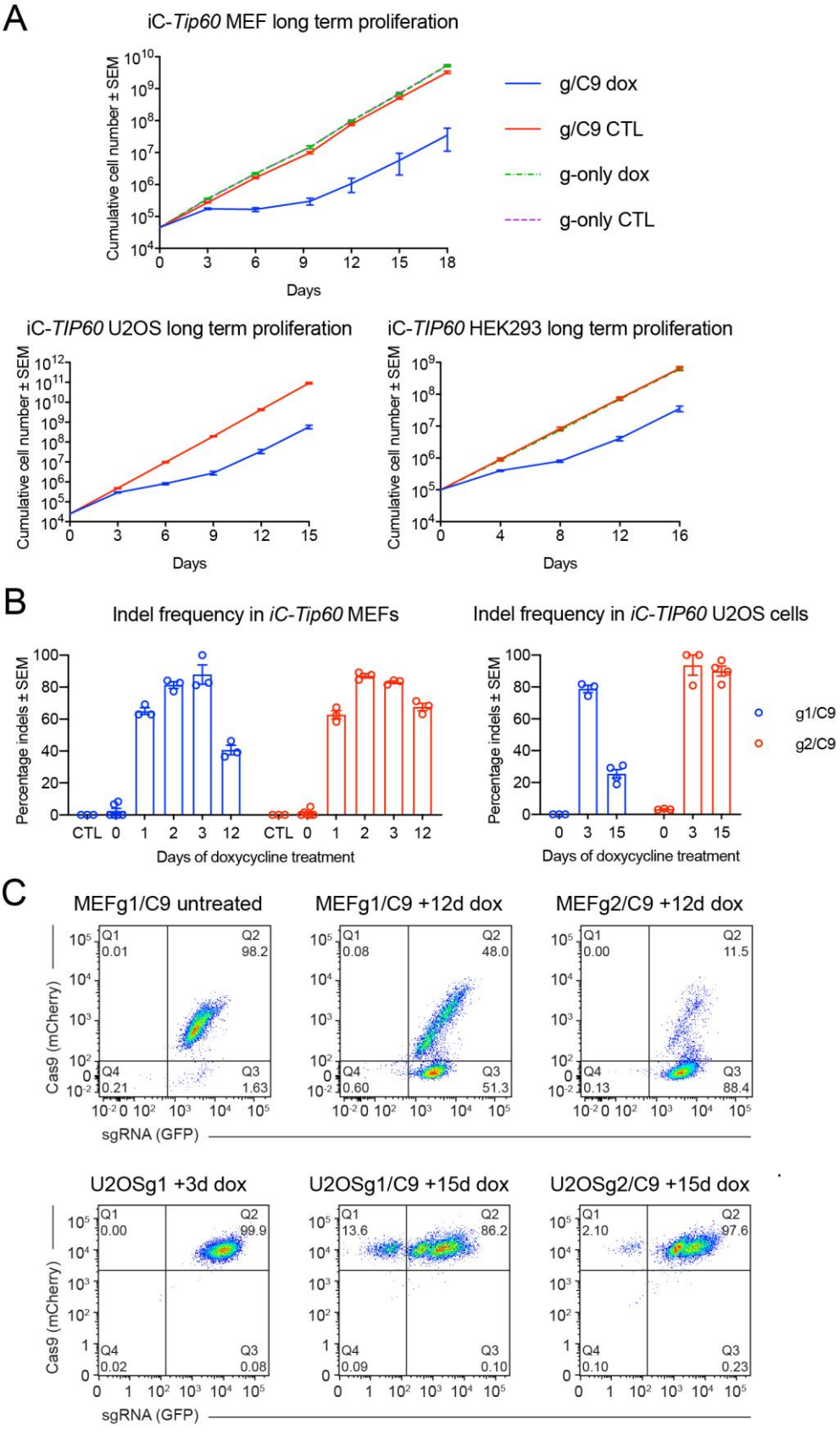

Figure 5.3: Serial passaging of *iC-TIP60* cells results in the outgrowth of cells that avoided loss of TIP60. (A) Cell proliferation curves for *iC-TIP60* MEF, U2OS and

HEK293 cells show outgrowth of cells after 12 days, 9 days, and 8 days, respectively. Cells were cultured continuously in dox supplemented medium and were counted at every passage. Data from two different guide RNAs, sgRNA#1 and sgRNA#2, were similar and thus combined such that the means ± SEM are derived from 2 guides, each assessed in triplicate. The slopes of log transformed growth curves were calculated from 12 days (MEF), 9 days (U2OS) and 8 days (HEK293) onwards and compared by unpaired two-tailed t test. No significant difference in proliferation was observed after serial passaging of *iC-TIP60* cultures compared to control cultures. **(B)** Indel frequencies of long term *iC-TIP60* MEF and U2OS cultures show varying levels of indels after prolonged culturing. **(C)** FACS analysis of long term *iC-TIP60* MEF and U2OS cultures show partial loss of GFP and mCherry marker, indicating silencing or loss of the sgRNA or Cas9 transgene, respectively.

5.2 Effects of *Tip60* deletion on cell viability and cell cycle progression

5.2.1 *Tip60* deletion does not affect cell survival

TIP60 has been reported to have both pro-apoptotic and pro-survival functions. TIP60 acetylates p53, leading to p53-mediated apoptosis (Tang, 2006 #95;Sykes, 2006 #96;Kaya-Okur, 2019 #223}. Binding of HIV tat protein to TIP60 in HIV infected cells abolished TIP60-mediated apoptosis (Col et al., 2005). Although. TIP60 knockout lead to pre-implantation lethality with increased apoptosis in mice (Hu et al., 2009), an increase in floating cells was only observed in *iC-TIP60* HEK293 cultures and not in *iC-Tip60* MEFs or *iC-TIP60* U2OS cells. I assessed cell death and apoptosis in *TIP60* mutant cultures using three different tests, namely a calcein AM live/EthD-1 dead cell assay, a TMRE live/dead cell assay and staining for early- and late-apoptotic cells via annexin-V flow cytometric analysis, showing that cell survival was not affected in U2OS or adherent or floating HEK293 cells after 3 days of dox treatment (Figure 5.4A-C). While the absolute number of dead floating cells in HEK293 cultures increased dramatically, the percentage of dead cells did not change compared to control cultures, indicating that

detached cells undergo loss-of-contact induced cell death in both genotypes (Figure 5.4B).

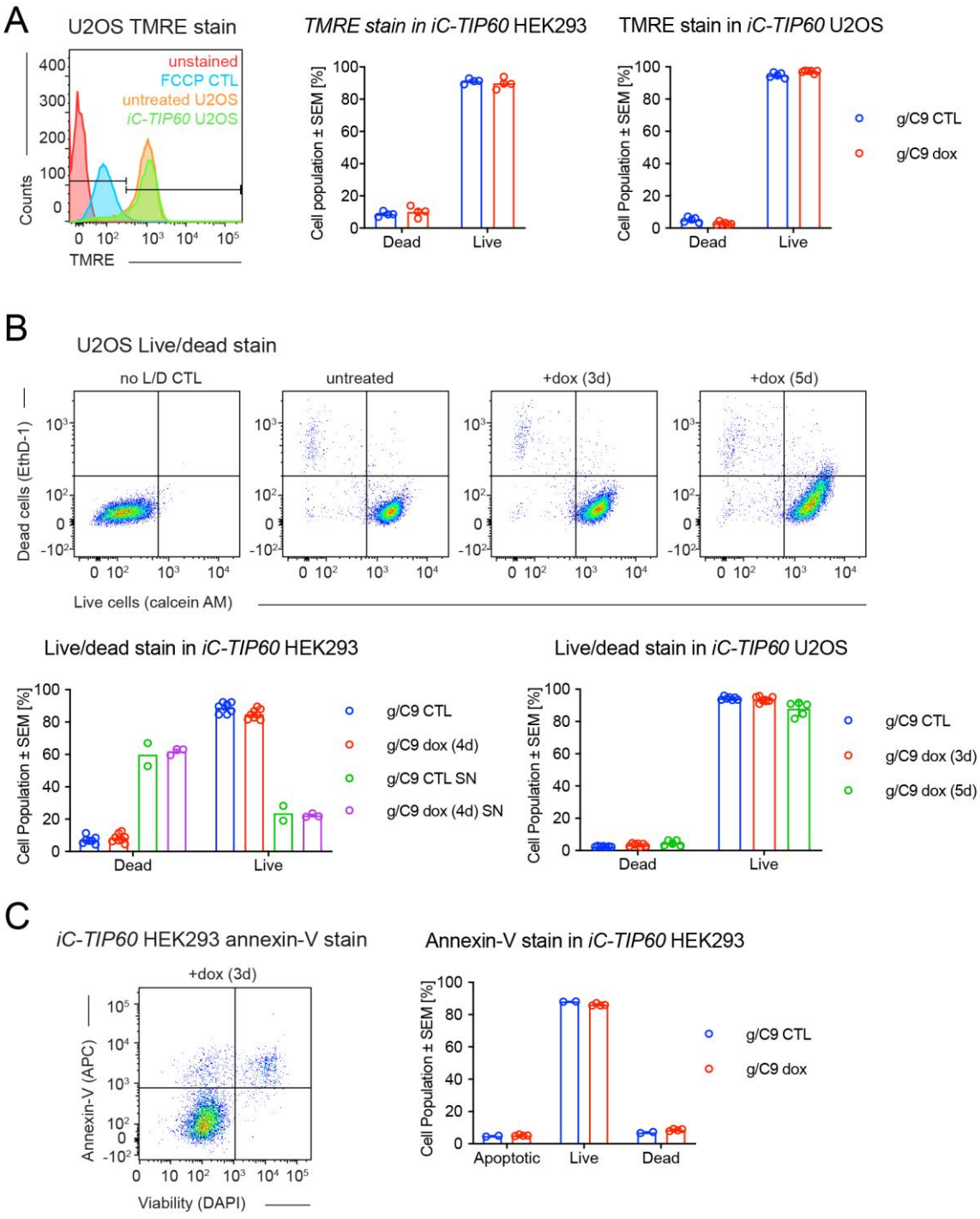

Figure 5.4: *Tip60* deletion does not affect cell survival. **(A)** *iC-TIP60* HEK293 and *iC-TIP60* U2OS cells and their respective controls were stained with tetramethyl-rhodamine, ethyl ester (TMRE) and analysed by flow cytometry. TMRE stains intact, active, negatively charged mitochondria. Apoptotic processes lead to loss of TMRE staining. No

change in TMRE staining was observed after loss of TIP60 in HEK293 cells or U2OS cells. Mitochondria depolarized with carbonyl cyanide 4-(trifluoromethoxy) phenylhydrazone (FCCP) were used as a negative control for TMRE staining. **(B)** *iC-TIP60* HEK293 and *iC-TIP60* U2OS cells and their respective controls were stained with ethidium homodimer-1 (EthD-1) and calcein AM (calcein [(acetyloxy)methyl ester]) and analysed by flow cytometry to provide a second assessment of live and dead cell populations. No change in EtD-1/calcein AM staining was observed after loss of TIP60 in HEK293 cells or U2OS cells. Additionally, for *iC-TIP60* HEK293 cultures, floating cells were collected and analysed independently (SN = supernatant). **(C)** *iC-TIP60* and control HEK293 cells were stained with annexin V and DAPI to provide a third assessment of cell death and assessment of apoptotic cell death. No change in annexin V or DAPI staining was observed after loss of TIP60 in HEK293 cells or U2OS cells. **(A-C)** Means ± SEM of a minimum of 3 independent replicates analysed by unpaired two-tailed t test.

5.2.2 *Tip60* deletion does not cause DNA damage

TIP60 plays an essential role in early steps of the DNA damage response (DDR) by acetylating ATM (Sun et al., 2005). To assess if *Tip60* deletion alters the DDR, I performed γH2AX staining on $Tip60^{iKO/iKO}$*;ERT2* MEFs 3 days after 4-OHT induction. γH2AX was not increased in *Tip60* knockout MEFs (Figure 5.5A), suggesting that accumulation of unrepaired DNA damage was not a factor in the observed proliferation defect, especially in light of previous observations that ERT2 increases burden DNA damage in cells (Janbandhu et al., 2014).

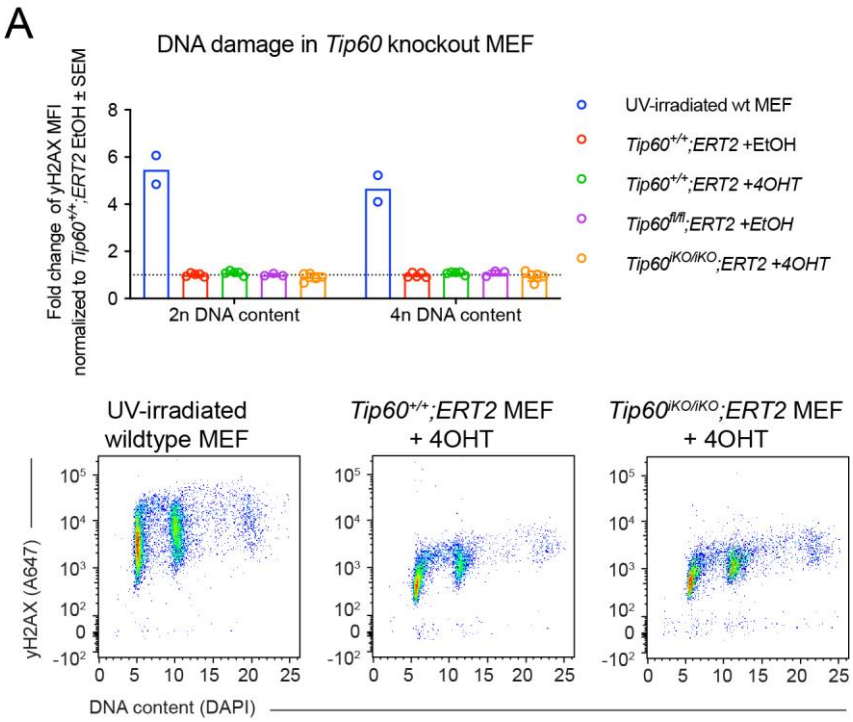

Figure 5.5: *Tip60* deletion does not cause DNA damage. (A) Quantification of DNA damage indicated by γH2AX in *Tip60*$^{iKO/iKO}$*;ERT2* MEFs 3 days after 4-OHT induction by C_{12}FDG staining detected using flow cytometry. The mean fluorescence intensity (MFI) of γH2AX was normalized to vehicle (EtOH) treated *Tip60*$^{+/+}$*;ERT2* MEFs. UV-irradiated cells were used as γH2AX positive control. Due to increased DNA content of G2/M-phase cells, γH2AX MFI was evaluated separately for 2n and >2n cell population as indicated by DNA stain. No increase in γH2AX was observed in *Tip60* deleted MEFs. Representative FACS plots are shown. A minimum of 3 replicates for each genotype were assessed, except the positive control (n=2).

5.2.3 *Tip60* deletion causes cell cycle arrest and leads to a failure to progress to metaphase

To investigate the possibility that the decline (rather than arrest) in cell growth was a combination of cells undergoing cell cycle arrest and cells escaping the deletion of TIP60, I performed live cell imaging and tracking of individual cell divisions using the IncuCyte live cell imaging system. Untreated U2OS control cells displayed several cell divisions during the time of imaging of 4 days and grew into a confluent culture (Figure 5.6A and B). Most *iC-TIP60* U2OS cells demonstrated a final cell division before complete

proliferation arrest and did not grow into a confluent culture. Some *iC-TIP60* U2OS cells maintained normal division rates, which might be due to silencing of the viral Cas9 and sgRNA or the creation of indels that do not affect TIP60 protein function, such as deletion of 3 or 6 nucleotides, as I observed in MEFs in 20% and 8% of the sequencing reads, respectively (Figure 4.2D). No detaching cells were observed, suggesting that cell death did not occur.

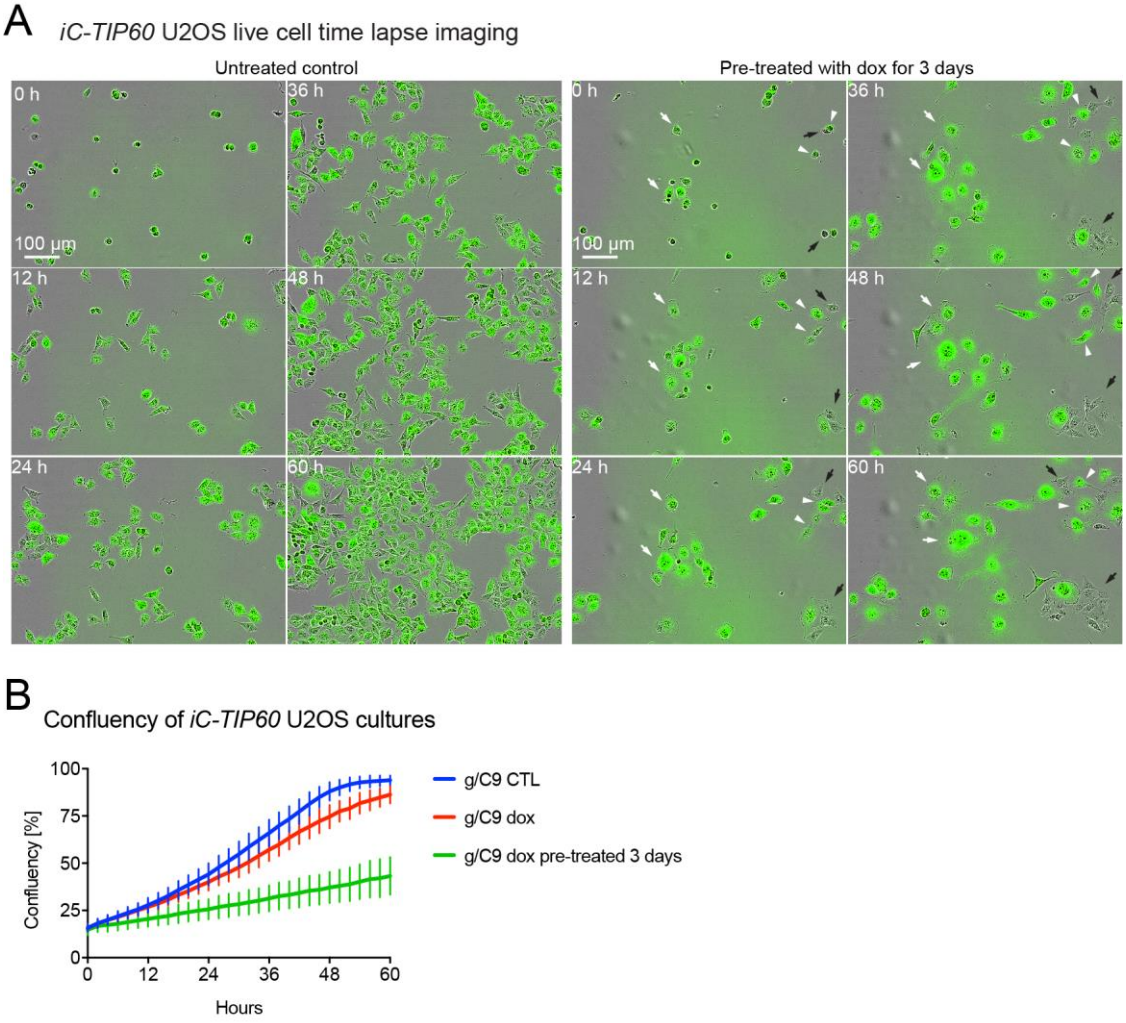

Figure 5.6: iC-TIP60 U2OS cells display cell division defect. (A) Representative still images of live-cell time-lapse imaging of *iC-TIP60* and control U2OS cells over a period of 60 h after 3 days of pre-treatment with dox. While control cells actively divided and increased in numbers (left two columns), the majority of *iC-TIP60* cells did not divide (right two columns; white arrow) during the 60 h time-lapse imaging period. Some *iC-TIP60* cells divided only once (white arrowhead), but some cells displayed normal

division rates (black arrow). No detaching or disintegrating cells were observed, indicating absence of cell death. **(B)** Automatic image analysis via the IncuCyte S3 Software (V2018B) was used to calculate the density of cells, determined by space occupied by cells compared to total imaged area. Means ± SD of 4 images for each of 4 experiments were analysed.

To better understand the effects of loss of TIP60 on cell function, I analysed the cell cycle in populations of *iC-Tip60* MEFs and *iC-TIP60* U2OS cells and their respective controls by BrdU incorporation. In *iC-Tip60* MEFs S-phase cells were reduced 2-fold compared to control cells 5 days after induced *Tip60* mutation (Figure 5.7A). The polyploidy of MEFs prevented me from distinguishing further between G1-phase and G2/M-phase results. Compared to control U2OS cells, *iC-TIP60* U2OS cells showed a 2-fold decrease in S-phase cells, a 47% increase in G2/M-phase cells, a 34% increase in G1-phase cells and an 8-fold increase in cells with a DNA content >2N, indicating endoreplication (Figure 5.7B). Decreasing S-phase and increasing G1-phase and G2/M-phase populations in *iC-TIP60* cells suggests that cells in G1-phase were unable to enter S-phase and arrested in G1, whereas cells in S-phase progressed to G2/M and either arrested then or displayed dysfunctional mitosis.

To investigate the cell cycle phenotype in more detail, I performed high-resolution 3D confocal live cell imaging of dividing *iC-TIP60* U2OS cells. Compared to U2OS control cells, which underwent mitosis normally within 25 min, *iC-TIP60* U2OS cells revealed severely prolonged chromosome condensation of 4 h 45 min and ultimately showed a failure to localize chromosomes to a metaphase plate, failed to divide and instead endoreplicated (Figure 5.7C).

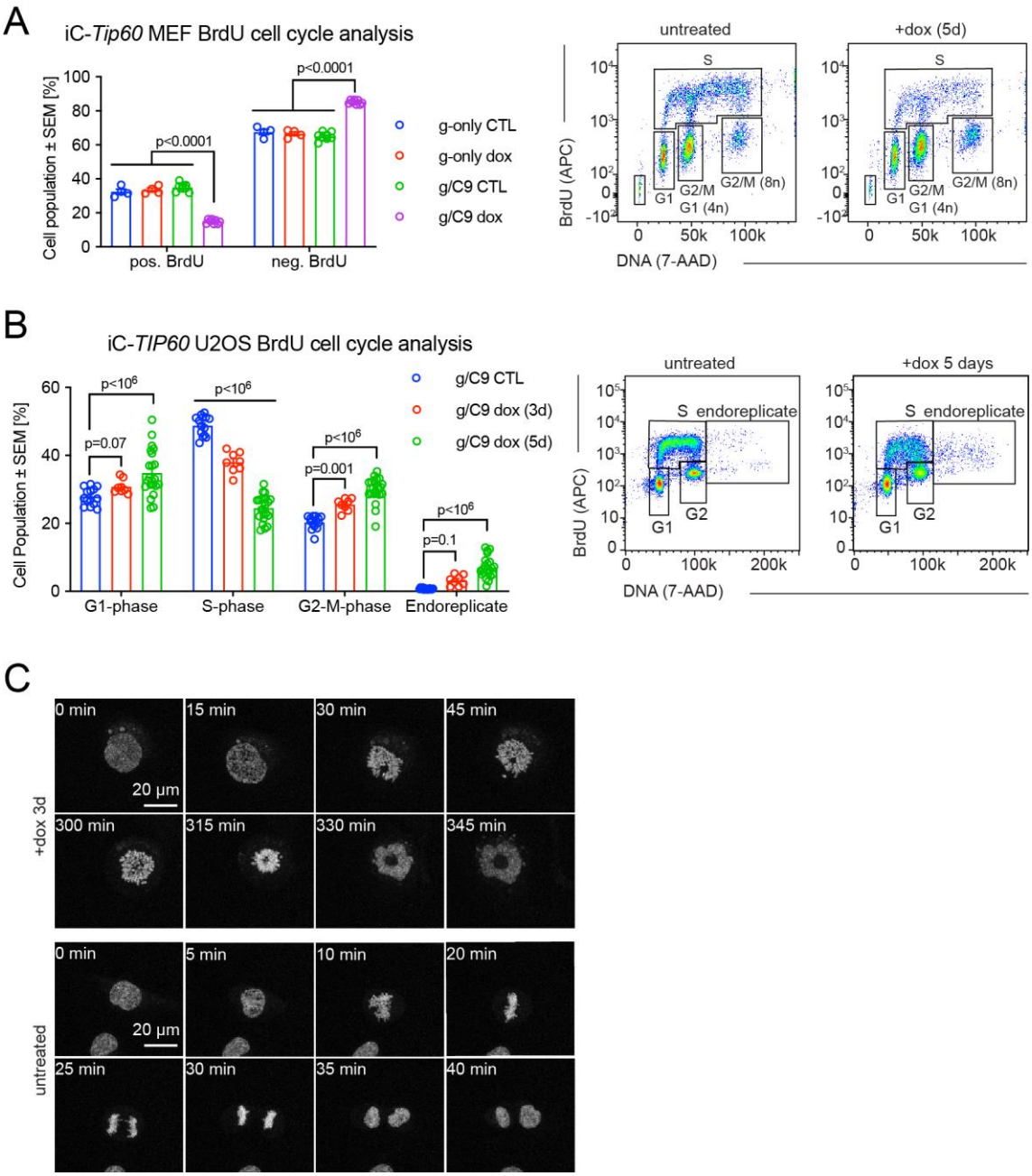

Figure 5.7: *Tip60* deletion causes cell cycle arrest and leads to failure to progress to metaphase. (A) Flow cytometry cell cycle analysis of *iC-Tip60* MEFs after 5 days of dox treatment assessing BrdU incorporation and DNA content. Additional DNA peaks represent endoreplicated MEFs and therefore populations were identified as either G1, G1 (4n) + G2/M, G2/M (4n), and S-phase. Due to overlapping G2/M (2n) and G1 (4n) populations, only S-phase populations were quantified. Means ± SEM of 3 independent replicates are displayed and were analysed by unpaired two-tailed t-test. **(B)** Flow cytometric cell cycle analysis of BrdU incorporation and DNA content of *iC-TIP60* and control U2OS cells. Cells with >4n DNA content suggested endoreplicating cells. Means ± SEM of at least 4 replicates for each sgRNA analysed by two-way ANOVA with cell cycle phase and duration of dox treatment as independent factors and with Benjamini and Hochberg correction. **(C)** Representative maximum intensity projection still images of

3D confocal live cell time-lapse imaging of *iC-TIP60* and control U2OS after 3 days of dox treatment showing an endoreplicating cell with prolonged chromosome condensation of 3 hours compared to control U2OS division completed in < 1 h.

5.2.4 *Tip60* deletion causes cellular senescence

I assessed SA-β-galactosidase (β-gal) activity in *iC-TIP60* U2OS cells and *TIP60*$^{iKO/iKO}$*;ERT2* MEFs, which can serve as a marker of cellular senescence in certain cell types such as human fibroblasts (Serrano et al., 1996). *TIP60* deletion led to increased β-gal positive cell populations in *TIP60*$^{iKO/iKO}$*;ERT2* MEFs and *iC-TIP60* U2OS cells after prolonged treatment of 6 days with 4-OHT or dox, respectively (Figure 5.8A). *TIP60*$^{iKO/iKO}$*;ERT2* MEFs showed a 2.4-fold increase ($p=10^{-4}$) in β-gal positive cells 6 days after 4-OHT induction compared to control MEFs, while iC-TIP60 U2OS cells showed a 5-fold increase. However, total percentages of β-gal positive cells 6 days after induced *TIP60* deletion was 5-fold higher in MEFs (21%) compared to U2OS cells (4%).

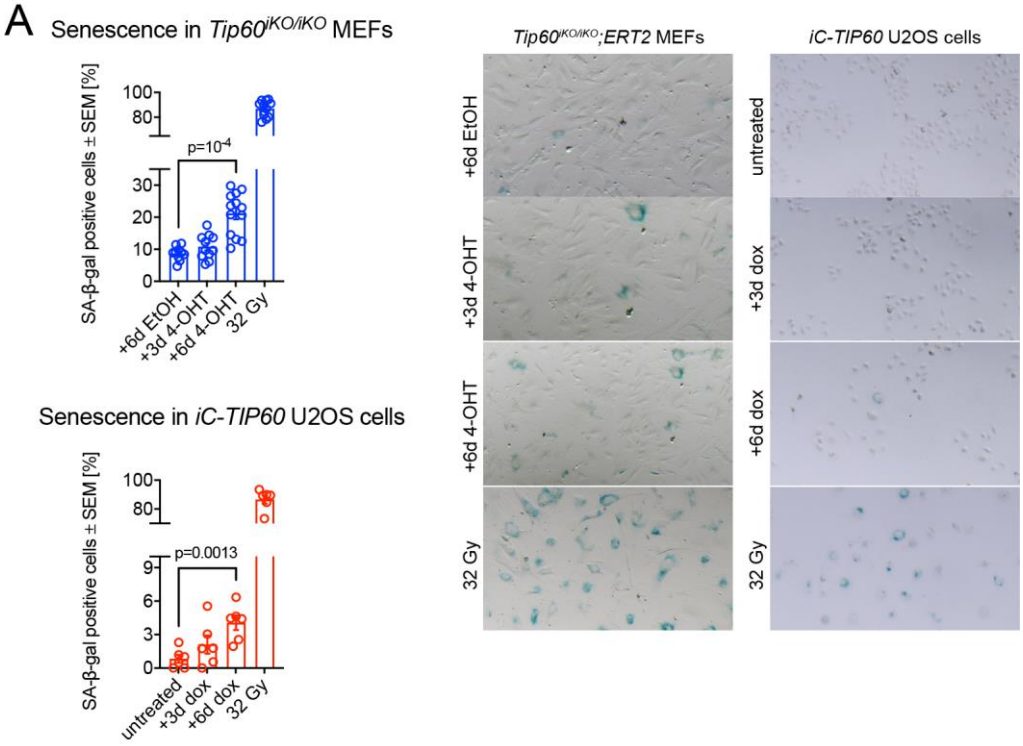

Figure 5.8: SA-β-gal assessment in *TIP60* mutant cells. (A) SA-β-galactosidase (β-gal) staining of *iC-TIP60* U2OS cells and *TIP60*$^{iKO/iKO}$*;ERT2* MEFs 3 and 6 days after *TIP60* deletion compared to untreated control cells. Cells irradiated with 32 Gy were stained as positive controls. Means ± SEM of β-gal positive cell populations for at least 2 images of 3 replicates with at least 200 counted cells per replicate are displayed and analysed by unpaired two-tailed t-test.

5.2.5 Loss of TIP60 causes cell cycle arrest even in the absence of the cell regulators p53, INK4A and ARF

TP53, p16^{INK4A} and 14^{ARF} (p19^{ARF} in mice) are essential cell cycle regulators and tumour suppressors that are commonly mutated in cancer (Kandoth et al., 2013; Ma et al., 2018). Furthermore, *Trp53* and *Cdkn2a* are known to be important for the induction of senescence in MEFs (Efeyan et al., 2007; Ferbeyre et al., 2002; Jacobs et al., 1999). However, there is evidence that alternative avenues for TP53-independent tumour suppression exist (Li et al., 2012a). To determine a possible relevance of the cell cycle arrest observed in the absence of TIP60 to *TP53* or *CDKN2A/CDKN2B* mutant cancers,

I investigated if the observed proliferation arrest in *TIP60* mutant cells depended on the ARF-TP53 tumour suppressor pathway (Figure 5.9A). I deleted the *Tip60* gene in MEFs already lacking p53 (*Trp53*$^{-/-}$ MEFs) or INK4A-ARF (*Cdkn2*$^{-/-}$ MEFs). In *Trp53*$^{-/-}$ MEFg1/C9 cells indel frequency reached 80% after only 24 hours of dox induction (Figure 5.9B), presenting a marginally faster dynamic compared to wild-type MEFs. Interestingly, a similar cell growth arrest compared to wild-type MEFs was observed in *Tip60* deleted *Trp53*$^{-/-}$ MEFs and *Tip60* deleted *Cdkn2a*$^{-/-}$ MEFs compared to *Trp53*$^{-/-}$ or *Cdkn2a*$^{-/-}$ control MEFs, indicating a TRP53 and p16^{INK4A}/p19^{ARF}-independent mechanism of cell cycle arrest in the absence of TIP60 (Figure 5.9C). The morphology was indistinguishable from *Tip60*-only deleted MEFs with senescence-like features (Figure 5.9D).

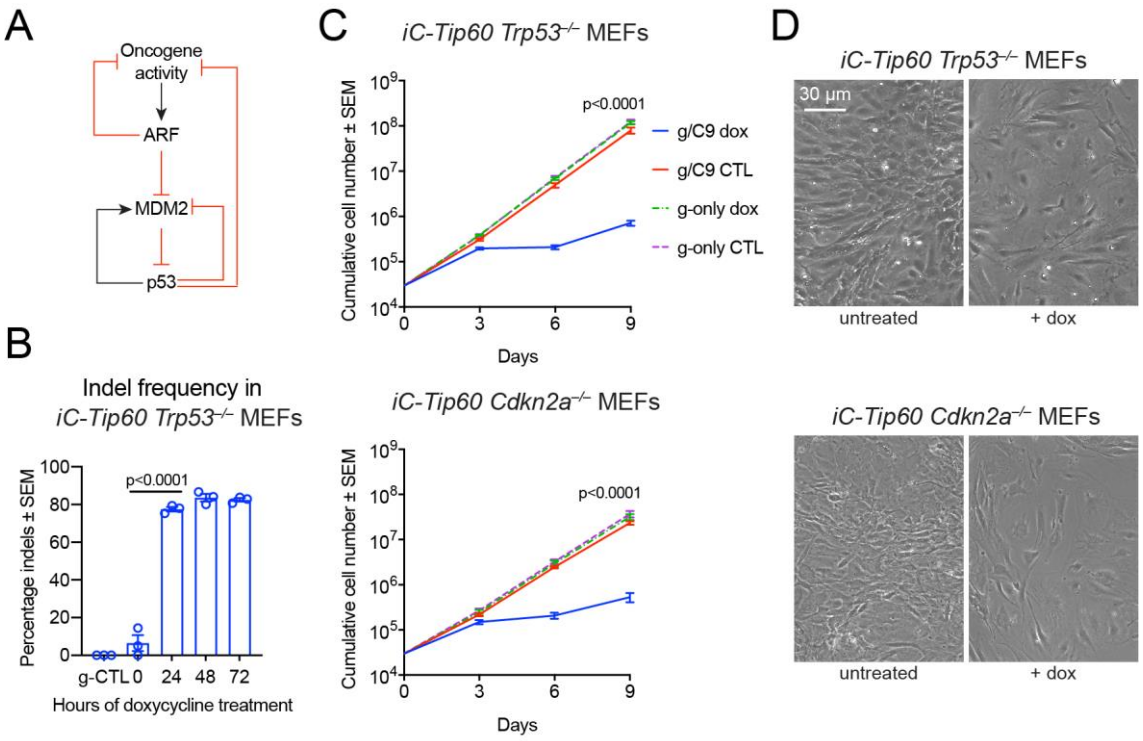

Figure 5.9: Loss of TIP60 causes cell cycle arrest even in the absence of the cell regulators TP53 or p16^{INK4A} and p19^{ARF}. Schematic drawing of the p19^{ARF}, MDM2 and TP53 pathway. **(B)** Quantification of indel frequencies in *iC-Tip60 Trp53*$^{-/-}$ MEFs and *Trp53*$^{-/-}$ guide-only control cells. The frequency indicates populations of indels of all

sequences with at least 25 reads. Means ± SEM of 3 technical replicates analysed by one-way ANOVA with time as the independent factor and Benjamini and Hochberg correction. **(C)** Proliferation of *iC-Tip60 Trp53*$^{-/-}$ MEFs and *iC-Tip60 Cdkn2a*$^{-/-}$ MEFs, lacking p53 or p16^{INK4A} and p19^{ARF}, respectively, compared to *Tip60* intact controls. Means ± SEM of data were derived using two different guide RNAs, sgRNA#1 and sgRNA#2, each assessed in triplicate. Dox induced *Tip60* mutation led to growth arrest after 3 days, independent of TP53, and p16^{INK4A} and p19^{ARF} status. The slopes of log transformed growth curves were calculated from 3 to 9 days and slopes were compared by unpaired two-tailed t test. **(D)** Representative phase contrast images *iC-Tip60 Trp53*$^{-/-}$ MEFs and *iC-Tip60 Cdkn2a*$^{-/-}$ MEFs with their respective control MEFs 5 days after dox treatment. Note the flattened and extended phenotype of *iC-Tip60* cells.

This finding could potentially have bearing on the suitability of TIP60 as a target for the development of new cancer therapeutics, as the *TP53* gene is mutated in 42% of cancers (Kandoth et al., 2013) and *CDKN2A* encoding p16^{INK4A} and p19^{ARF}, is mutated in 3.6% in a pan-cancer study (Kandoth et al., 2013) and in up to 78% in specific paediatric leukaemia (Ma et al., 2018).

5.3 Effects of *Tip60* deletion in blastocysts and mESC

5.3.1 *Tip60* knockout blastocysts fail to form inner cell mass outgrowths

Loss of TIP60 leads to pre-implantation lethality (Hu et al., 2009). To extend the previous observations reported by Hu and colleagues and determine the time of embryonic lethality as well as the consequences of loss of TIP60 on conceptus morphology, the offspring of intercrosses of mice carrying a *Tip60* genetrap allele (*Tip60*$^{gt/+}$; Figure 5.10A) were examined by Honours student Catherine Pitt. *Tip60*$^{gt/gt}$ homozygous embryos were absent at E6.5, E9.5 and weaning (Figure 5.10B). One quarter of the concepti of *Tip60*$^{gt/+}$ x *Tip60*$^{gt/+}$ matings had an abnormal morphology at E5.5. These anomalies occurred at the Mendelian frequency expected for *Tip60*$^{gt/gt}$ embryos (Figure 5.10C). The abnormal

morphology observed included a lack of structure, decreased cell number and pyknotic nuclei, indicating cell death. Confirming data previously reported by Hu and colleagues (Hu et al., 2009), *Tip60*$^{gt/gt}$ blastocysts were unable to form inner cell mass (ICM) outgrowths *in vitro* (Figure 5.10D, E). Heterozygous *Tip60* genetrap embryos formed ESC outgrowth and displayed no morphological differences. Heterozygous *Tip60* genetrap ICM outgrowths were not delayed compared to wild-type controls.

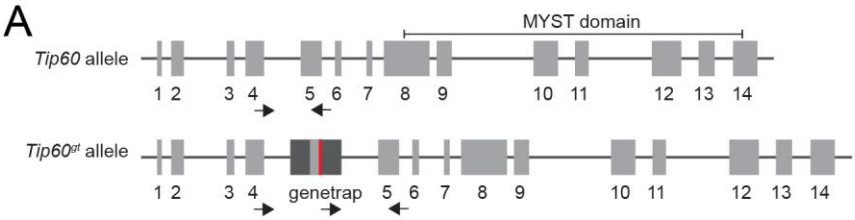

B

Developmental age	Number and (%) of offspring per genotype				
	Tip60$^{+/+}$	*Tip60*$^{+/gt}$	*Tip60*$^{gt/gt}$	Total	*Tip60*$^{gt/gt}$ missing Pbinom
Weaning	14 (33%)	29 (67%)	0	43	$4x10^{-6}$
E9.5	24 (40%)	36 (60%)	0	60	$<10^{-6}$
E6.5	14 (27%)	38 (73%)	0	52	$<10^{-6}$

C

Intercross	Wildtype morphology	Abnormal morphology	Pbinom
Tip60$^{+/+}$	25 (92%)	2 (8%)	
Tip60$^{+/gt}$	22 (73%)	8 (27%)	p=0.001

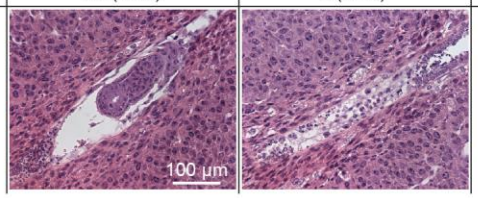

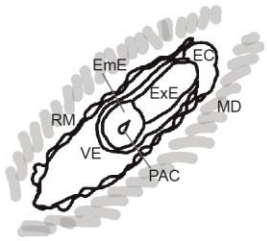

D

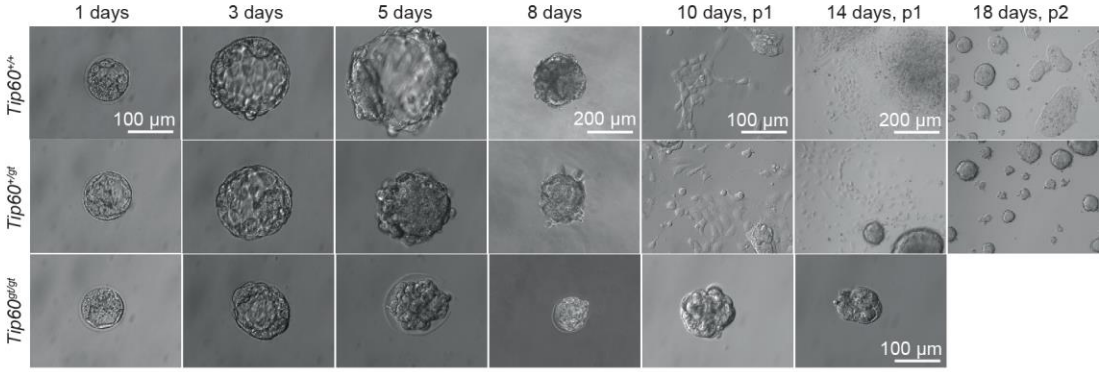

E

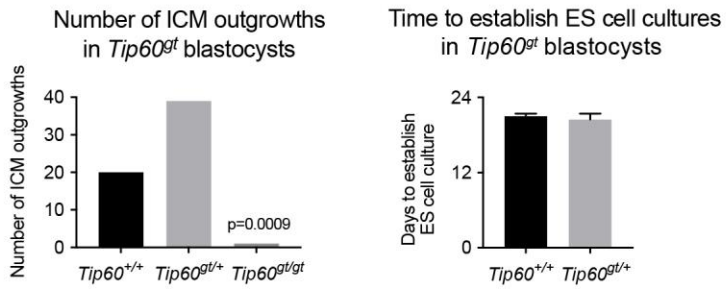

Figure 5.10: Homozygous *Tip60* genetrap blastocysts fail to form inner cell mass outgrowths and ES cells. (A) *Tip60* gene trap allele. The gene trap construct harbours a 3' splice acceptor site and a stop codon, facilitating splicing into the genetrap construct and use of a stop codon, leading to premature termination of the mRNA. **(B)** Peri-implantation lethality of *Tip60*$^{gt/gt}$ mice was observed to be identical to the published null

allele (Hu et al., 2009), suggesting that the genetrap allele is also a null allele. **(C)** *Tip60*^{gt} homozygous embryos were absent by E6.5 among offspring from *Tip60*$^{gt/+}$ x *Tip60*$^{gt/+}$ crosses. *Tip60*^{gt} heterozygous embryos occurred at the expected rate. The p value for the cumulative probability distribution being different from the expected Mendelian distribution (pbinom) is displayed for the missing *Tip60*$^{gt/gt}$ offspring specifically. **(D)** Representative images of cultures of *Tip60*$^{gt/gt}$, *Tip60*$^{gt/-}$ and *Tip60*$^{+/+}$ E3.5 blastocysts to ES cells derivation. E3.5 embryos derived from *Tip60*$^{gt/+}$ x *Tip60*$^{gt/+}$ crosses were plated in culture. *Tip60*$^{gt/-}$ and *Tip60*$^{+/+}$ blastocysts formed inner cell mass (ICM) outgrowths, which were dissociated after 8 days. *Tip60*$^{gt/gt}$ blastocysts failed to grow in culture. Despite being morphologically normal at E3.5, *Tip60*$^{gt/gt}$ blastocysts failed to produce inner cell mass outgrowths. **(E)** Number of blastocysts with observed ICM outgrowth per genotype indicated and time to establish ES cell cultures from E3.5 embryos derived from *Tip60*$^{gt/+}$ x *Tip60*$^{gt/+}$ crosses. *Tip60*$^{gt/gt}$ did not form ES cell cultures. Interestingly *Tip60*$^{gt/-}$ heterozygous blastocysts show no delay in establishing ES cell cultures. Outgrowths from 60 E3.5 embryos were genotyped, and the genotype distribution was analysed by Chi-squared test. The data were generated by Honours student Catherine Pitt.

5.3.2 TIP60 depletion causes abnormal morphology and proliferation arrest in mESC

To better understand the effects of *Tip60* deletion in embryonic stem cells, I isolated ESC from *Tip60*$^{fl/fl}$*;ERT2* and *Tip60*$^{+/+}$*;ERT2* mouse blastocysts and cultured these in 2i medium. Induction of *Tip60*$^{fl/fl}$*;ERT2* ESCs with 4-OHT led to complete deletion of the *loxP* flanked genomic regions after 3 days (Figure 5.11A). Loss of TIP60 caused proliferation arrest in ESCs after 3 days of 4-OHT induction, similar to *Tip60*$^{fl/fl}$*;ERT2* MEFs (Figure 5.11B). TIP60 heterozygosity had no effect on cell proliferation or morphology of *Tip60*$^{iKO/+}$*;ERT2* ESCs, which grew in round, protuberant colonies typical of ESCs (Figure 5.11B, C). *Tip60*$^{iKO/iKO}$*;ERT2* ESCs, however, displayed an abnormal flattened, epithelium-like morphology and grew as monolayer, rather than in multi-layered colonies (Figure 5.11C). In conclusion, *Tip60* deletion caused proliferative arrest in ESCs highly resembling the effects of loss of TIP60 on MEFs.

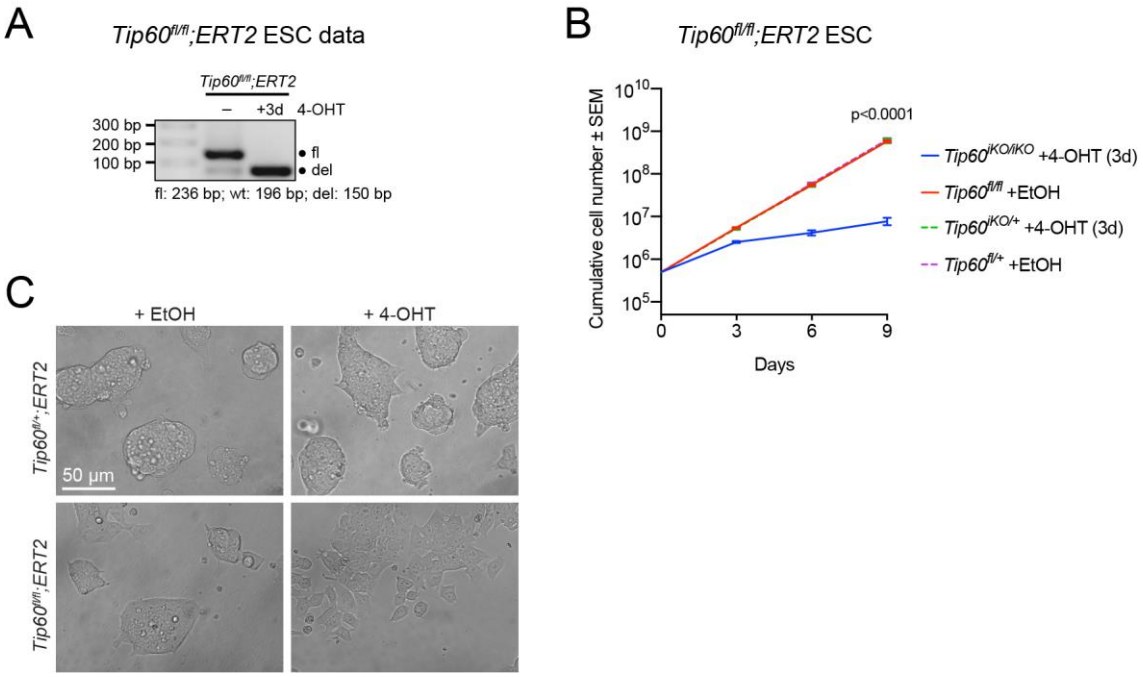

Figure 5.11: *Tip60* deletion leads to an arrest of cell proliferation and abnormal morphology in ESCs. (A) Representative DNA gel of three-way PCR genotyping of uninduced *Tip60*^{fl} and induced *Tip60*^{iKO} alleles in 4-OHT and EtOH treated ESCs. **(B)** Proliferation of *Tip60*$^{fl/+}$*;ERT2* and *Tip60*$^{fl/fl}$*;ERT2* mESCs. 4-OHT induced homozygous *Tip60* knockout leads to cell cycle arrest after 3 days. Cells were treated for 3 days with 4-OHT before culturing in normal growth medium for the rest of the experiment. The slopes of log transformed growth curves were calculated from 3 to 9 days and compared using an unpaired two-tailed t test. Data are presented as means ± SEM of cell isolates from 3 individual mouse embryos per genotype. **(B)** Representative phase contrast images of *Tip60*$^{fl/+}$*;ERT2* and *Tip60*$^{fl/fl}$*;ERT2* mESCs untreated and 3 days after 4-OHT induction of *Tip60* deletion.

5.4 Discussion to chapter 5

In this study, I deleted *TIP60* in normal mouse cells and human cells and in cells lacking the tumour suppressors TP53, p16^{INK4A} and p19^{ARF} to investigate the role of TIP60. Under all conditions, I demonstrated cell cycle arrest upon *TIP60* deletion in G1 or G2/M phase of the cell cycle and increased endoreplication. I show that the cell cycle arrest induced by loss of TIP60 is independent of TP53, p16^{INK4A} and p19^{ARF}. While in this study loss of TIP60 caused cell cycle arrest, TIP60 has previously been reported to induce cell cycle

arrest, either as a co-activator of TP53 at target genes such as CDKN1A ($p21^{CIP1/WAF1}$) (Legube et al., 2004), or in a TP53-independent manner (Eymin et al., 2006) after genotoxic stress in the context of DNA repair. The active role of TIP60 in inducing cell cycle arrest in the context of genotoxic stress appears to involve specific molecular mechanisms, including interaction with DNA damage repair proteins (Sun et al., 2005). In contrast, the data presented here, suggest that the loss of TIP60 causes cell cycle arrest in a range of cell cycle phases as well as dysfunctional mitosis due in a manner independent of tumour suppressor and cell cycle regulators. Notably, DNA damage was not increased in *Tip60* deleted MEFs, excluding accumulation of DNA damage as a factor causing cell cycle arrest. Instead, senescence-associated (SA)-β-galactosidase activity was increased in the absence of TIP60.

Interestingly, while cell cycle arrest occurred rapidly after loss of TIP60, cell survival was not affected. The TP53-independent nature of the cell cycle arrest caused by loss of TIP60 is noteworthy, as some aspects of TP53 function appear to be dependent on TIP60 (Kruse and Gu, 2009; Sykes et al., 2006; Tang et al., 2006). These two findings are not mutually exclusive, as TIP60 appears to be essential for many cell functions.

In contrast to human and mouse cells *in vitro*, which did not exhibit cell death, we observed pyknotic nuclei in *Tip60* null peri-implantation embryos *in vivo*, which is consistent with a previous report (Hu et al., 2009), and indicates that diverse cell types might undergo different fates upon loss of TIP60, which include cell cycle arrest or apoptotic cell death.

In conclusion, the data presented here support roles of TIP60 as essential for cell proliferation in human (HEK293, U2OS) and mouse (MEFs, ESC) cells and for cell

survival in late blastocysts peri-implantation mouse embryos. My data do not suggest that the absence of TIP60 results in an obvious increase in DNA damage, although I did not induce DNA damage to specifically challenge the DNA damage repair machinery. It is noteworthy however, that the two different outcomes of loss of TIP60 observed, namely cell death in peri-implantation embryos and cell cycle arrest in cultured human and mouse cells, as well as the nature of the cell cycle arrest in various phases of the cell cycle favours a more general requirement for TIP60 in cell function, rather than specific roles in cell cycle progression or cell survival. I hypothesise that this general role of TIP60 is a requirement for efficient gene expression, which I will explore in Chapter 8. However, before I address the role of TIP60 in gene expression, I will report its role in histone acetylation in the next chapter.

Chapter 6 TIP60 histone acetylation targets

6.1 TIP60 is essential for histone H2AZ lysine 7 acetylation in human and mouse cells

Previously proposed TIP60 histone acetylation targets comprise a wide range of histones, including the canonical histones H4, H3, and H2A as well as the histone variant H2AZ. Other MYST family members have been shown to acetylate specific histone targets (Voss and Thomas, 2018). Furthermore, most studies utilized *in vitro* assays, RNAi depletion, or overexpression systems to assess TIP60 acetylation targets. In this chapter, I investigate the effects of genetic loss of TIP60 on the acetylation of histone residues via western blots on acid extracted proteins from TIP60 null cells. Initially, Elizabeth Allan conducted a cell-free acetylation assay with and without recombinant human TIP60 and recombinant histone H2AZ protein and confirmed that TIP60 can directly acetylate H2AZ *in vitro* (Figure 6.1A). This also showed that the antibody recognizes acetylated H2AZ and did not cross-react with the unmodified form.

Next, I analysed histone extracts from *Tip60*$^{fl/+}$*;ERT2* and *Tip60*$^{fl/fl}$*;ERT2* MEFs 3 days post 4-OHT induction (Figure 6.1B). *Tip60*$^{iKO/iKO}$*;ERT2* MEFs showed a 5-fold reduction in pan-H2AZK4-7-11ac, 5-fold in H2AZK7ac, and 2-fold reduction in H2AZK4ac (Figure 6.1C). Importantly, total H2AZ protein levels remained unchanged. These findings supported a major role of TIP60 in H2AZ acetylation, as previously proposed, but also demonstrated that other HATs contribute to H2AZK4 acetylation. In addition, I examined other proposed TIP60 histone acetylation targets: H2AK5ac and H4K5ac were decreased by 10%, and 20%, respectively, but no significant alterations in H4K8, H4K12, H4K16, H3K9, H3K14, H3K18 and H3K27 acetylation levels were observed (Figure 6.1C). No difference in any acetylation marks was observed between EtOH and 4-OHT treated heterozygous *Tip60*$^{+/iKO}$*;ERT2* MEFs.

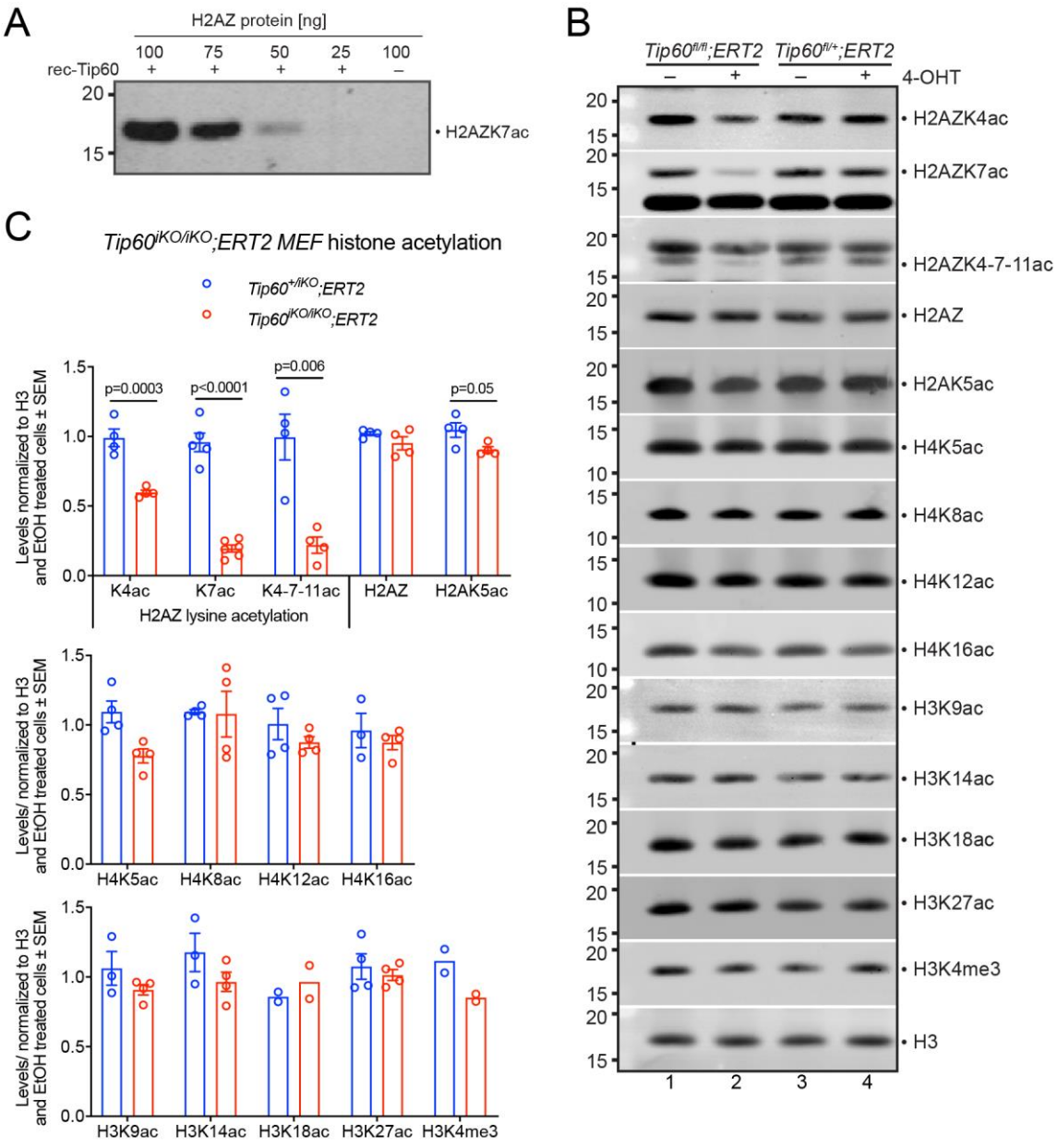

Figure 6.1: TIP60 is essential for histone H2AZ lysine 7 acetylation in MEFs. (A) Cell-free acetylation assay analysed by western blot showing full-length recombinant H2AZ histone, with (lane 1-4) and without recombinant TIP60 (lane 5). **(B)** Representative western blots of acid extracted proteins from *Tip60$^{fl/+}$;ERT2 MEFs* (lanes 3,4 7 and 8) and *Tip60$^{fl/fl}$;ERT2* MEFs (lanes 1, 2, 5 and 6) treated with vehicle (EtOH, –) or 4-hydroxytamoxifen (4-OHT, +) to induce Cre recombination (generating *Tip6$^{iKO/+}$;ERT2* and *Tip60$^{iKO/iKO}$;ERT2* MEFs) for 3 days and probed for H2AZK4ac, H2AZK7ac, H2AZK4-7-11ac, H2AK5ac, total H2AZ, and H4K5ac. Blots were probed for pan-H3 as a loading control. **(C)** Fold change of histone lysine acetylation levels normalized to total H3 protein between EtOH and 4-OHT treated cells after 3 days of 4-OHT treatment. Shown are *Tip60$^{+/iKO}$;ERT2* control MEFs and *Tip60$^{iKO/iKO}$;ERT2* MEFs. Means ± SEM of 2 to 8 independent experiments are shown. Fold changes were log

transformed and analysed by unpaired two-tailed t test. The data in **(A)** were generated by Elizabeth Allan.

CRISPR *TIP60* knockout cell cultures display similar results. Comparing control MEFs and MEFs treated with dox for 1, 2 and 3 days, a progressive 7-fold decrease in H2AZK7ac and a 2-fold decline in H2AZK4ac were observed (p=0.0001 and p=0.002, respectively; Figure 6.2A, B). The time dependent manner of reduction in H2AZ acetylation after genomic deletion of *Tip60* supports a direct dependence on TIP60. I observed a comparably modest reduction in H4K12ac after *Tip60* mutation (p=0.03), but not in H2AK5ac, H4 acetylation marks (H4K5ac, H4K8ac, H4K16ac) or H3 acetylation marks (H3K9ac, H3K14ac, H3K27ac) (Figure 6.2B).

TIP60 mutation in HEK293 cells caused a 4-fold reduction in H2AZK7ac (p=0.0008), a 2-fold decrease in H2AZK4ac (p=0.01) and a 13-fold reduction H2AZK4-7-11ac (p=0.02, Figure 6.2C), but no change in the total H2AZ protein levels. H4K16ac (p=0.03) and H4K8ac (p=0.047) were both reduced by 37%, but other histone lysine acetylation levels were unchanged (Figure 6.2C).

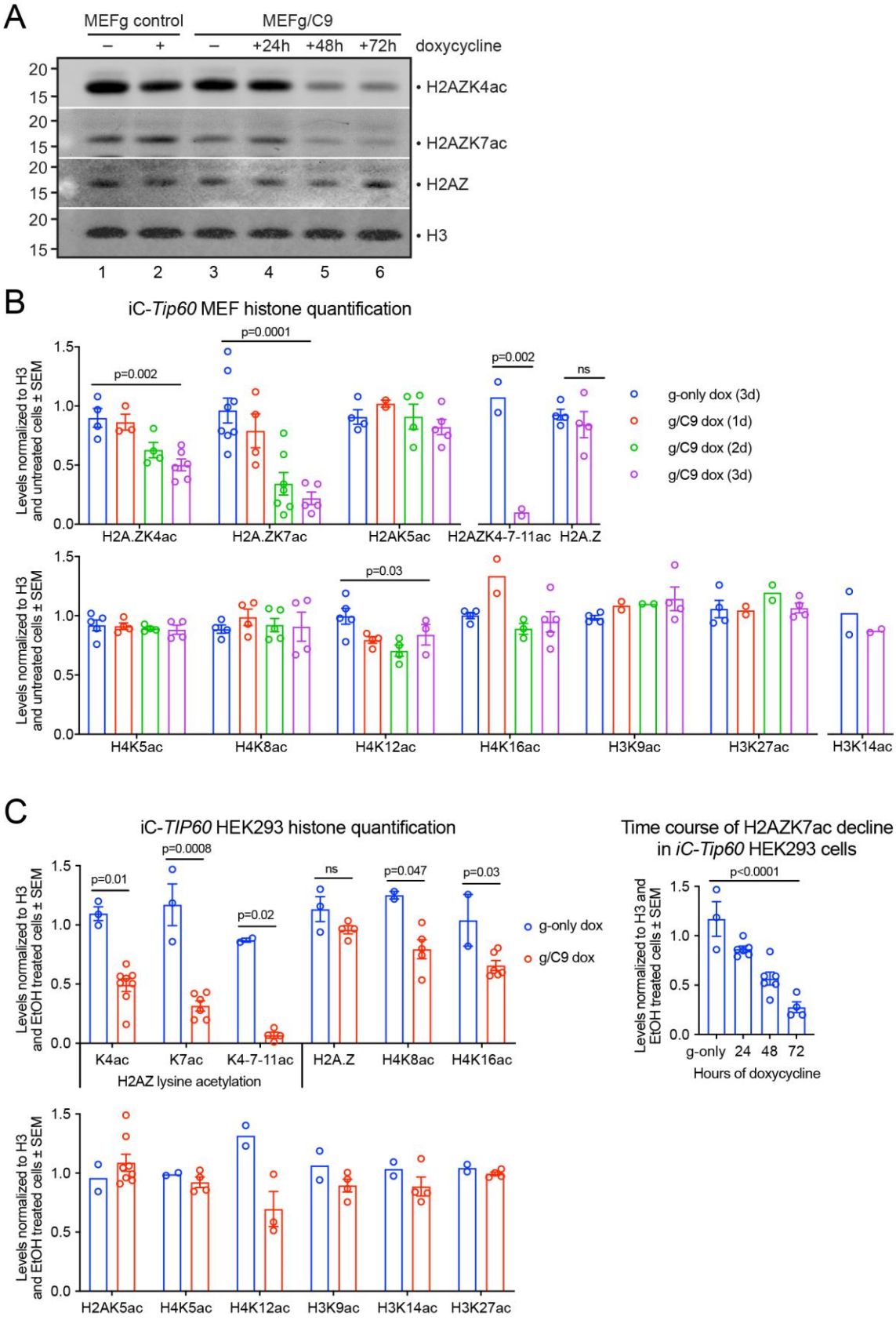

Figure 6.2: Histone H2AZ lysine 7 acetylation is reduced in induced CRISPR-mediated *TIP60* mutated mouse and human cells. (A) Representative western blots of acid extracted proteins from *iC-Tip60* MEF (lane 3-6) and sgRNA (g)-only control MEFs

(lane 1, 2) untreated (–) or treated with dox (+) to induce *Tip60* knockout for the indicated times and probed for acetylated histones. Blots were probed for pan-H3 as a loading control. **(B)** Fold changes of histone lysine acetylation levels normalized to H3 between *iC-Tip60* and control MEF. Data from sgRNA#1 and sgRNA#2 were similar and thus combined. **(C)** Fold change of histone lysine acetylation levels normalized to H3 between *iC-TIP60* and control HEK293 cells after 3 days of dox treatment and time course of H2AZK7ac decline. Data from sgRNA#1 and sgRNA#2 were similar and thus combined. Means ± SEM of 2 to 8 independent experiments are shown **(B, C)**. Fold changes were log transformed and analysed by unpaired two-tailed t test for samples comparing untreated with 3 days treated cells or one-way ANOVA with time as the independent factor and Benjamini and Hochberg correction for time course samples.

Similar to wild-type MEFs, deletion of *Tip60* in *Cdnk2a*$^{-/-}$ or *Trp53*$^{-/-}$ MEFs resulted in a reduction in H2AZK4, H2AZK7 and H2AZK4-11 acetylation (Figure 6.3E). In addition to the profound effects on H2AZ acetylation, I found a modest reduction in H4K12ac and H4K16ac in *Tip60* deleted *Cdkn2*$^{-/-}$ MEFs compared to control MEFs, that were not observed in *Tip60* deleted *Trp53*$^{-/-}$ MEFs.

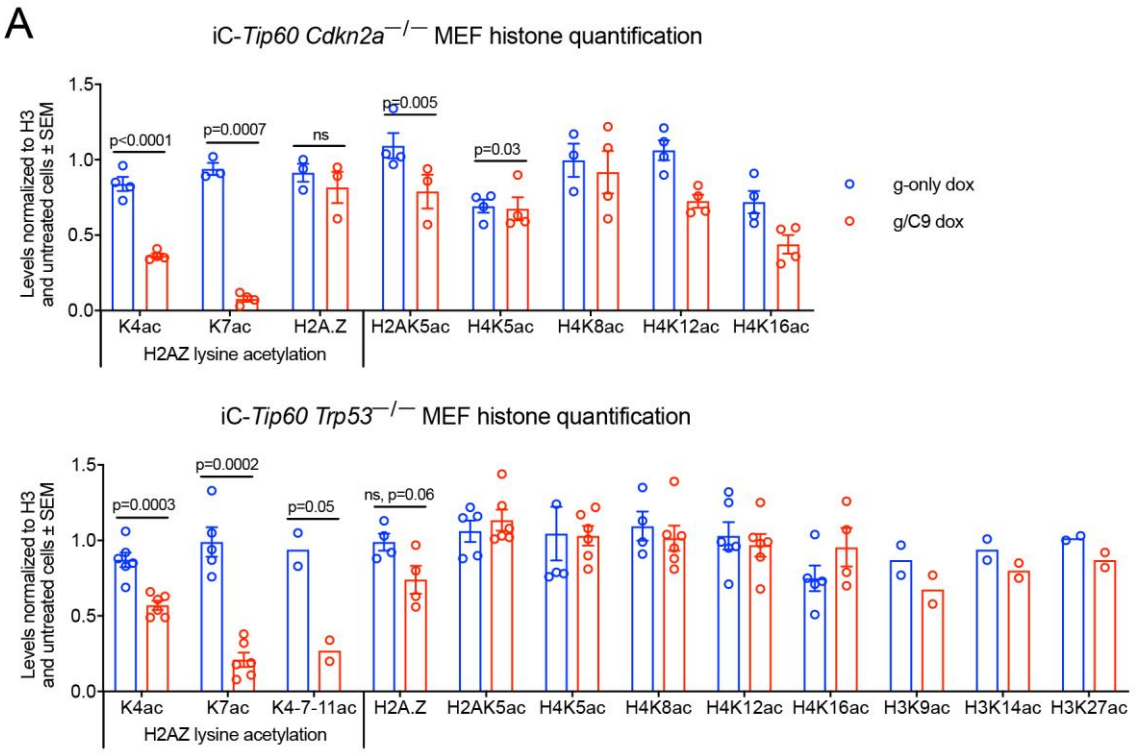

Figure 6.3: H2AZ acetylation is reduced in *iC-Tip60 Trp53*$^{-/-}$ and *Cdkn2a*$^{-/-}$ cells(A). Fold change of H2AZ and specific lysine acetylation levels normalized to H3 between *iC-Tip60 Trp53*$^{-/-}$ and control MEFs, as well as *iC-Tip60 Cdkn2a*$^{-/-}$ and control MEFs after 3 days of dox treatment to induce *Tip60* mutation. Data from sgRNA#1 and sgRNA#2 were similar and thus combined. Fold changes were log transformed and analysed by unpaired two-tailed t test.

6.2 TIP60 is essential for histone H2AZK7 acetylation in early mouse embryos *ex vivo*

To gain an insight if TIP60 affected the acetylation of similar histone lysine residues *in vivo* as in cultured cell lines, the histone acetylation levels in *Tip60*$^{gt/+}$ x *Tip60*$^{gt/+}$ intercross E3.5 blastocysts were assessed by Honours student Catherine Pitt and research assistant Samantha Eccles. *Tip60*$^{gt/gt}$ E3.5 blastocysts cultured for only 1 day showed no change in any histone acetylation marks, suggesting persistent maternal TIP60 at this stage (data not shown). Consequently, blastocysts were cultured for 3 days to allow a decline in maternal TIP60 protein before assessing histone acetylation by

immunofluorescence. Previous genotyping had associated *Tip60*$^{gt/gt}$ blastocysts with an abnormal morphology, characterized by a lack of ICM outgrowth (Figure 6.4A). Blastocysts with abnormal morphology displayed reduced H2AZK4ac, H2AZK7ac, and H4K16ac based on quantification of the mean fluorescence intensity (MFI) per nucleus (Figure 6.4B). The effects of the presumed lack of TIP60 on H2AZ acetylation were congruent with the western blot data from *Tip60* deleted cells, albeit less pronounced in amplitude.

The very early pre-implantation lethality of the *Tip60* null embryos prevented us from examining germline *Tip60* deleted embryos at a later stage of development. While Ms Pitt and Ms Eccles were not able to detect an effect of loss of TIP60 immediately *ex vivo*, presumably because of the necessity to allow time for the maternal TIP60 protein to decline, these data obtained in *ex vivo* short term cultures suggest that TIP60 is required for H2AZ acetylation in vivo, as well as in cultured cell lines.

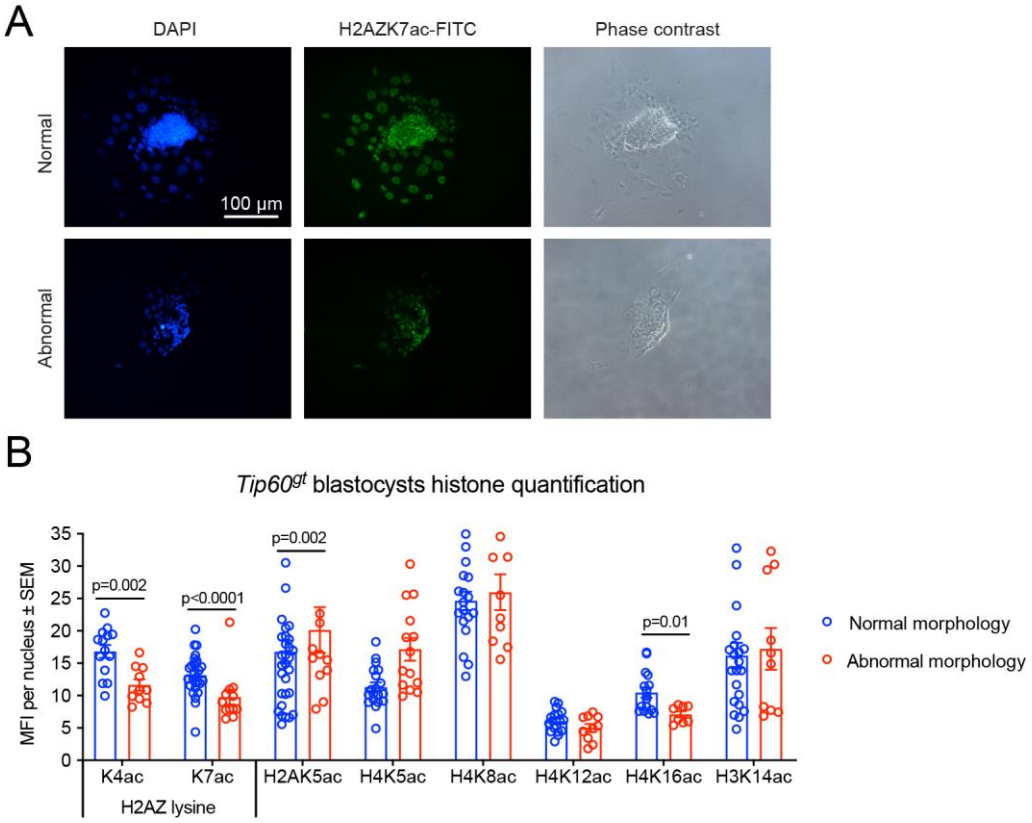

Figure 6.4: TIP60 is essential for histone H2AZK7 acetylation in mouse embryos *ex vivo*. (A) Representative epifluorescence images of E3.5 blastocysts derived from histone *Tip60*$^{gt/+}$ x *Tip60*$^{gt/+}$ matings cultured for 3 days and stained with antibodies against H2AZK7ac and DAPI. Blastocyst cultures with a normal inner cell mass outgrowth and with an abnormal morphology without inner cell mass outgrowth [associated with homozygous mutation of *Tip60* in comparable experiments (Figure 5.10D)] are shown. **(B)** Quantification of histone lysine acetylation in *Tip60*^{gt} knockout blastocyst cells. The mean fluorescence intensity (MFI) per nucleus was calculated by averaging the intensity of stained nuclei normalized to the area relative to background signal. Blastocyst cultures with normal inner cell outgrowth and lacking inner cell outgrowth [associated with homozygous mutation of *Tip60* in comparable experiments (Fig S5)] were assessed separately. The nuclei from a minimum of 8 blastocysts per genotype were analysed. Fold changes were log transformed and analysed by unpaired two-tailed t test. Data were generated by Samantha Eccles.

6.3 Loss of TIP60 does not affect levels of chromatin bound H2AZ

As mentioned before, H2AZ is a non-canonical histone variant and expressed and deposited into chromatin independent of the cell cycle (Nekrasov et al., 2012; Wu and

Bonner, 1981). Deposition and eviction of H2AZ-H2B dimers into chromatin is dependent on chromatin remodelling complexes (Gevry et al., 2007; Obri et al., 2014; Papamichos-Chronakis et al., 2011; Ruhl et al., 2006). Due to the role of the TIP60-containing NuA4 complex in H2AZ deposition and eviction, I investigated global chromatin bound H2AZ levels in *iC-TIP60* U2OS cells. Three days after dox treatment cells were fractionated into cytosolic, soluble nuclear, and chromatin bound fractions. The success of the cell fractionation was tested by staining with a-tubulin for cytosolic fractions and RNAPII for chromatin bound fraction (Figure 6.5A). Fractions were analysed for H2AZ and H2AZK4-7-11ac levels by loading equal amounts of protein fractions (Figure 6.5B). Histone were overwhelmingly restricted to the chromatin bound fraction H2AZ levels (Figure 6.5C). Only a small proportion of H2AZ was detected in the cytosol, representing 5.9% and 3.0% of total H2AZ in control and *iC-TIP60* U2OS cells, respectively. Very little or no H2AZ was detected in soluble nuclear fractions. Acetylated H2AZ or H3 were not detectable in the soluble nuclear and cytosolic fractions (Figure 6.5C). The chromatin bound level of H2AZ were unaffected by loss of TIP60. In contrast, H2AZK4-7-11ac levels were reduced by 85% (Figure 6.5C), congruent with my findings represented in Figure 6.1, Figure 6.2, and Figure 6.3 of western blots of acid extracted histone fractions in a range of *TIP60* deleted cell lines. Interestingly, global chromatin bound H3 levels remained unchanged in iC-TIP60 U2OS cells compared to controls cells, suggesting that TIP60 deletion had no major effect on global nucleosome occupancy. Further, these findings suggest that previous results in histone extracted from whole nuclei largely represent chromatin bound histones.

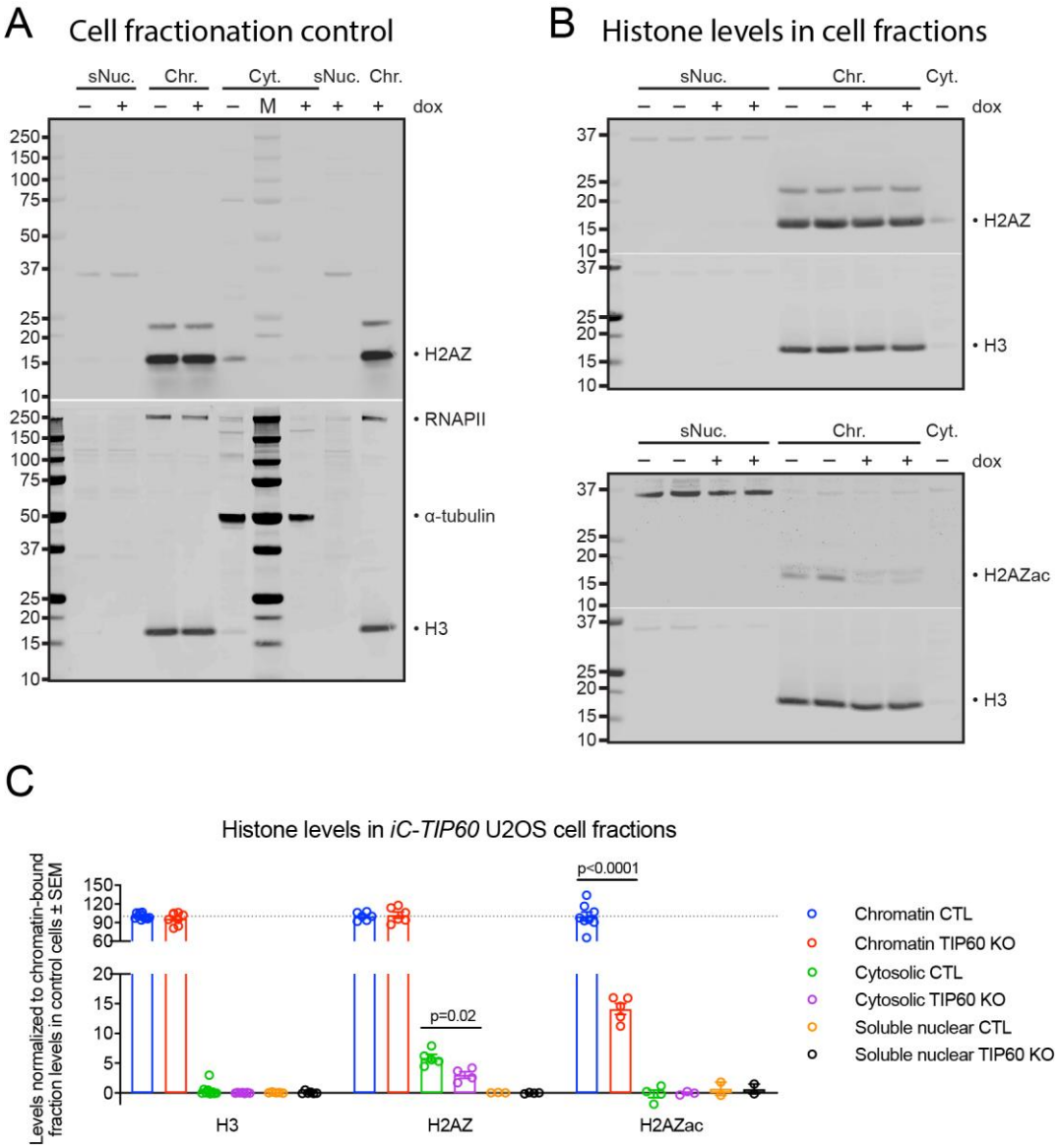

Figure 6.5: TIP60 depletion does not alter global chromatin bound H2AZ levels. (A) Western blot on subcellular fractions of *iC-TIP60* U2OS cells 3 days after dox induction and untreated control cells stained for H3, and H2AZ; α-tubulin and RNAPII were used to differentiate between cytosolic and chromatin bound fractions, respectively. **(B)** Western blot of 8 µg of fractionated cell lysates stained for H3, H2AZ, H2AZK4-7-11ac, and α-tubulin. **(C)** Quantification of H3, H2AZ and H2AZK4-7-11ac levels in *iC-TIP60* U2OS cells normalized to chromatin bound fractions in untreated control (CTL) cells. Means ± SEM of 2 to 6 independent experiments are shown. Fold changes were log transformed and analysed by unpaired two-tailed t test.

6.4 Discussion to chapter 6

Loss of TIP60 results in a marked decline in H2AZK7 acetylation and a reduction in H2AZK4 acetylation. These were the only two histone acetylation residues that were consistently affected in all human and mouse cell types examined here. My results are consistent with previous reports that showed that TIP60 is required for the acetylation of H2AZ and gene activation in human, mouse and insect cells (Dalvai et al., 2013; Giaimo et al., 2018; Kusch, 2004; Kusch et al., 2014). However, TIP60 has also been reported to be required for the acetylation of other histones. TIP60 has been proposed to acetylate H2AK5, H3K14 and H4 on K5, K8, K12 and K16 in cell-free assays using N-terminal histone peptides assessed by mass spectrometry (Kimura and Horikoshi, 1998). However, cell-free histone acetylation assays typically overestimate the range of acetylation targets (Voss and Thomas, 2018).

Compared to the profound and consistent reduction in H2AZ acetylation upon *Tip60* deletion in all cell types, alterations in H4 lysine acetylation observed in these experiments were variable between cell types and not present in in all cell types. Various other HATs are known to acetylate H4 lysines and redundancy between those HATs might conceal a potential effect of loss of TIP60 on genome-wide H4 acetylation (Voss and Thomas, 2018). Alternatively, the profound and consistent reduction in H2AZ acetylation upon *Tip60* deletion in all cell types and the fact that changes in H4 acetylation were not present in all cell types could indicate that the effects of *Tip60* deletion on H4 acetylation may be indirect or restricted to specific cell types.

Robust reduction of H2AZK4ac to about half the levels in TIP60 depleted cells compared to control cells, suggest that other HATs can acetylate H2AZK4. MOF, which is the MYST family member most closely related to TIP60, could be considered a potential

candidate. Loss of MOF leads to similar peri-implantation lethality as loss of TIP60. The effects of loss of MOF on histone acetylation were assessed by immunofluorescence in pre-implantation embryos; a complete loss of H4K16ac was observed. Other histone acetylation marks, however, were not affected, including H4K5ac, H4K8ac, H4K12ac, H3K9ac, and H3K14ac (Thomas et al., 2008). H4K16 acetylation has been well established as the major target of MOF in human cells (Taipale et al., 2005) and in the fruit fly (Smith et al., 2000). In yeast, deletion of Sas2 (yeast homologe to human MOF) did not alter H2AZ modification (Babiarz et al., 2006). Gcn5, however, was reported to acetylate H2AZ in yeast (Millar et al., 2006) and human (Semer et al., 2019) and p300 deletion reduced H2AZ acetlyation in cancer cell lines (Colino-Sanguino et al., 2019). Previous studies primarily utilize pan H2AZK4-7-11 acetylation antibodies and thus did not differentiate between possible distinct functions of acetylation of these three H2AZ lysine residues.

Cell fractionation experiments revealed an 85% reduction of H2AZac specifically in the chromatin bound fractions, while acetylated H2AZ was not detectable in the soluble nuclear or cytosolic fractions, suggesting that H2AZ may only be acetylated in the nucleus. Previous work suggested that TIP60 is required for H2AZ deposition on DNA (Gevry et al., 2007), and that H2AZ incorporation destabilises the nucleosome (Henikoff et al., 2009), leading to higher nucleosome turnover (Dion et al., 2007). It was shown that acetylation of histones supports the subsequent deposition or eviction of H2AZ, with H2AK5ac, H3K14ac, and H3K27ac correlating with deposition of H2AZ (Choi et al., 2009; Hsu et al., 2018a; Hsu et al., 2018b; Wang et al., 2009a) and H3K56ac correlating with eviction of H2AZ (Watanabe et al., 2013). However, the role of H2AZ acetylation in H2AZ deposition and eviction is unknown. I found that total H2AZ levels in the

chromatin bound fraction were not affected by loss of TIP60, suggesting that loss of TIP60 neither leads to decreased H2AZ levels due to defective H2AZ deposition, nor to increased chromatin bound H2AZ due to defective eviction of H2AZ. Nevertheless, analysing global chromatin bound H2AZ levels by western blot might not reveal aberrant localization of H2AZ in the chromatin landscape, which will need to be investigated by ChIP-seq experiments.

Null deletion of the *H2az* gene in mice results in an abnormal inner cell mass phenotype and preimplantation lethality in mice (Faast et al., 2001) similar to the *Tip60* null phenotype. The mitotic defect and increased endoreplication indicate that *Tip60*$^{-/-}$ cells were able to synthesize DNA, but failed to arrange chromosomes in a metaphase plate, followed by a failure of chromosome segregation. These observations may mirror the knockout phenotype of the loss of the yeast homologue of TIP60, *esa1*. *Esa1* null or catalytic inactive mutants display a budding phenotype characterized by improper DNA segregation and aberrant spindle orientation accompanied by incomplete nucleus and microtubule extension through the bud neck (Clarke et al., 1999). In this context it is interesting that TIP60-mediated acetylation of aurora B kinase, the catalytic subunit of the chromosome passenger complex, promotes accurate chromosome segregation in mitosis (Mo et al., 2016).

H2AZ has been shown to play an important role in centromere formation (Greaves et al., 2007) and H2AZ depletion has been linked to abnormal nuclear chromatin organisation, as well as lagging chromosomes and chromosome bridges during cell division in mammalian cells (Rangasamy et al., 2004). The mitosis defect upon loss of TIP60 that I observed, could reflect a requirement for TIP60-dependent acetylation of H2AZ in

centromere and spindle formation. At least in *Schizosaccharomyces pombe*, non-acetylateable mutant *pht1* (H2AZ analogue) leads to 50% of chromosome segregation defects compared to *pht1*Δ (Kim et al., 2009), suggesting an important role of H2AZ acetylation in chromosome segregation. A later study, however, suggested that the function of H2AZ in chromosome segregation is not due to direct deposition at the centromeres, but rather an indirect effect through regulation of expression of proteins important for chromosome segregation (Hou et al., 2010). My data showing that cells lacking TIP60 and H2AZ acetylation arrest in various stages of the cell cycle and not just in mitosis supports this latter hypothesis.

Chapter 7 H2AZ acetylation in cell proliferation

7.1 Introduction

In this chapter, I analyse the link between loss of H2AZ acetylation and proliferation arrest in TIP60 depleted cells.

7.2 HDACi treatment of TIP60 deleted cells

To determine if inhibiting the decline in H2AZ acetylation might rescue the observed cell proliferation defect in *TIP60* knockout cells, I treated *iC-TIP60* U2OS cells with the HDAC inhibitors (HDACi) trichostatin A (TSA) and sodium butyrate (NaBu) while simultaneously inducing *TIP60* mutation with dox and assessed cell proliferation by MTS assay. Four days of doxycycline induced *TIP60* mutation led to a 20 – 25% reduction in viable cells (Figure 7.1A), congruent with previous observations (Figure 5.2). At the higher concentrations both, TSA and NaBu, induced cell death irrespective of TIP60 status. The EC_{50} for inducing cell death by TSA or NaBu was not different in control and *iC-TIP60* U2OS cells (TSA-control: 87.5 ± 1.6 nM; TSA-*iC-TIP60*: 83.8 ± 4.7 nM; p=0.5; NaBu-control: 4.0 ± 0.04 mM; NaBu-*iC-TIP60*: 4.9 ± 0.4 mM; p=0.07). HDACi treatment with lower concentrations of NaBu (<1000 µM) or TSA (<50 nM) had no effect on cell proliferation and did not rescue the cell proliferation defect in *iC-TIP60* cells. Higher HDACi concentrations reduced the number of viable cells in control and *TIP60* knockout cells, suggesting a dominant effect of HDACi treatment on viable cell numbers. Percentage of viable cells in *iC-TIP60* U2OS cells compared to control cells were only increased when treated with 250 nM TSA (TSA-control: 5.0%; TSA- *iC-TIP60*: 7.5%; $p=10^{-5}$) or 10 mM NaBu (NaBu-control: 16.4%; NaBu-*iC-TIP60*: 21.7%; $p=2x10^{-4}$).

Western blot analysis of histone acetylation levels in cells treated with HDACi and dox to induce mutation of *TIP60* revealed that treatment with 6 nM or 30 nM TSA did not lead to an increase in H2AZac levels in *TIP60* mutated cells after 3 days of treatment (Figure 7.1B). However, treatment with 1 mM or 5 mM NaBu resulted in an increase H2AZac levels in *TIP60* mutant cells above wild-type levels. Interestingly, unmodified H2AZ was slightly increased in NaBu treated cells irrespective of TIP60 status. These data indicate that the proliferation arrest phenotype caused by *Tp60* mutation was not rescued by the increase in H2AZ acetylation by NaBu inhibition of HDACs. Therefore, the cell arrest observed in the absence of TIP60 might be independent of the role of TIP60 in histone acetylation. However, the increase in H2AZ acetylation levels upon NaBu treatment may lead to unregulated acetylation, which does not compensate for the loss of endogenous H2AZ acetylation patterns in *TIP60* mutant cells. Furthermore, HDACi treatment may affect other cellular functions, independent of H2AZ acetylation that might obstruct efforts to revert the cell cycle arrest in *TIP60* mutant cells.

To distinguish between these possibilities, I generated catalytically inactive TIP60 and examined its effects on histone acetylation and cell cycle progression in the next section.

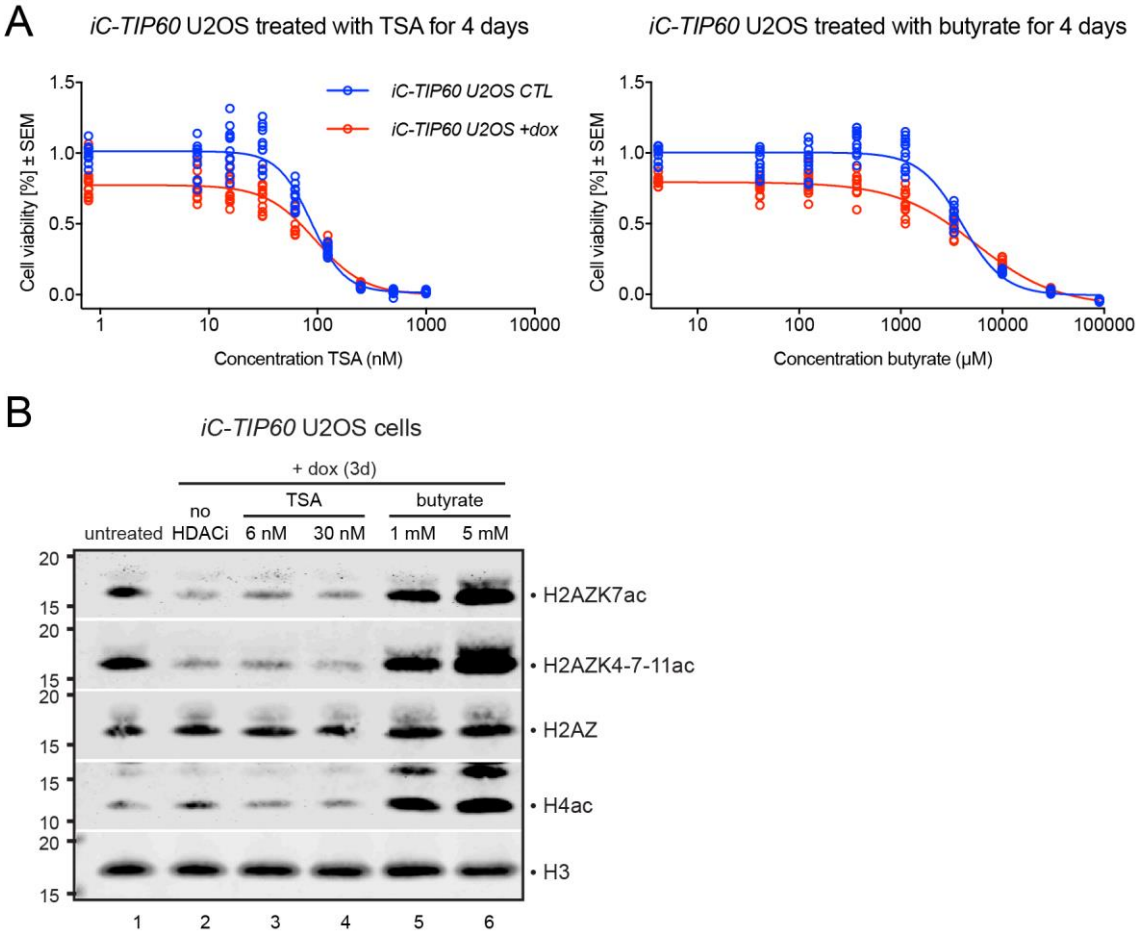

Figure 7.1: HDAC treatment does not rescue cell proliferation in *TIP60* deleted cells. **(A)** MTS assay of *iC-U2OS* cells treated with dox and/or HDAC inhibitors (TSA and NaBu) for 4 days. Absorbance values were normalized to untreated control cells. Each condition was measured in 4 replicates per plate in a minimum of 3 independent plates and analysed by . **(B)** Western blot staining for H2AZK7ac, H2AZK4-7-11ac, H2AZ, H4ac, and H3 in *iC-U2OS* cells treated with dox and/or HDAC inhibitors (TSA and NaBu) for 4 days. Data from sgRNA#1 and sgRNA#2 were combined.

7.3 Catalytic inactive TIP60 complementation

7.3.1 Overexpression constructs for TIP60

To understand the role of the HAT activity of TIP60 and thus H2AZ acetylation in cellular processes, I used my inducible *ERT2/loxP* and inducible *iC-TIP60* mutation system and complemented the loss of endogenous TIP60 with overexpression of wild-type TIP60 or

two variants of catalytically inactive TIP60, namely TIP60$^{Q377E, G380E}$ and TIP60^{E403Q}. I designed three lentiviral transfer constructs, with TIP60 fused to a 3XFlag-tag at the C-terminus and co-translated GFP under the control of a CMV promotor as well as a neomycin resistance cassette under the control of a *PGK1* promoter (Figure 7.2A). To utilize these constructs with the inducible CRISPR/Cas9 system targeting the endogenous *TIP60* locus, I equipped my constructs encoding the wild-type and the catalytically inactive TIP60 each with a silent mutation within the PAM-site to render these exogenous TIP60 sequences resistance to CRISPR/Cas9 mutation. To enable this, I designed a new *TIP60* targeting sgRNA (sgRNA3) shifted only a few bp downstream from sgRNA2, targeting exon 11 of *Tip60*, which was cloned into the vector system described previously. TIP60 overexpression in *Tip60$^{fl/fl}$;ERT2* MEFs and 4-OHT induced deletion of endogenous *Tip60* results in cells expressing either no TIP60, or wildtype TIP60^{WT}, or mutant ciTIP60^{E403Q} (Figure 7.2B).

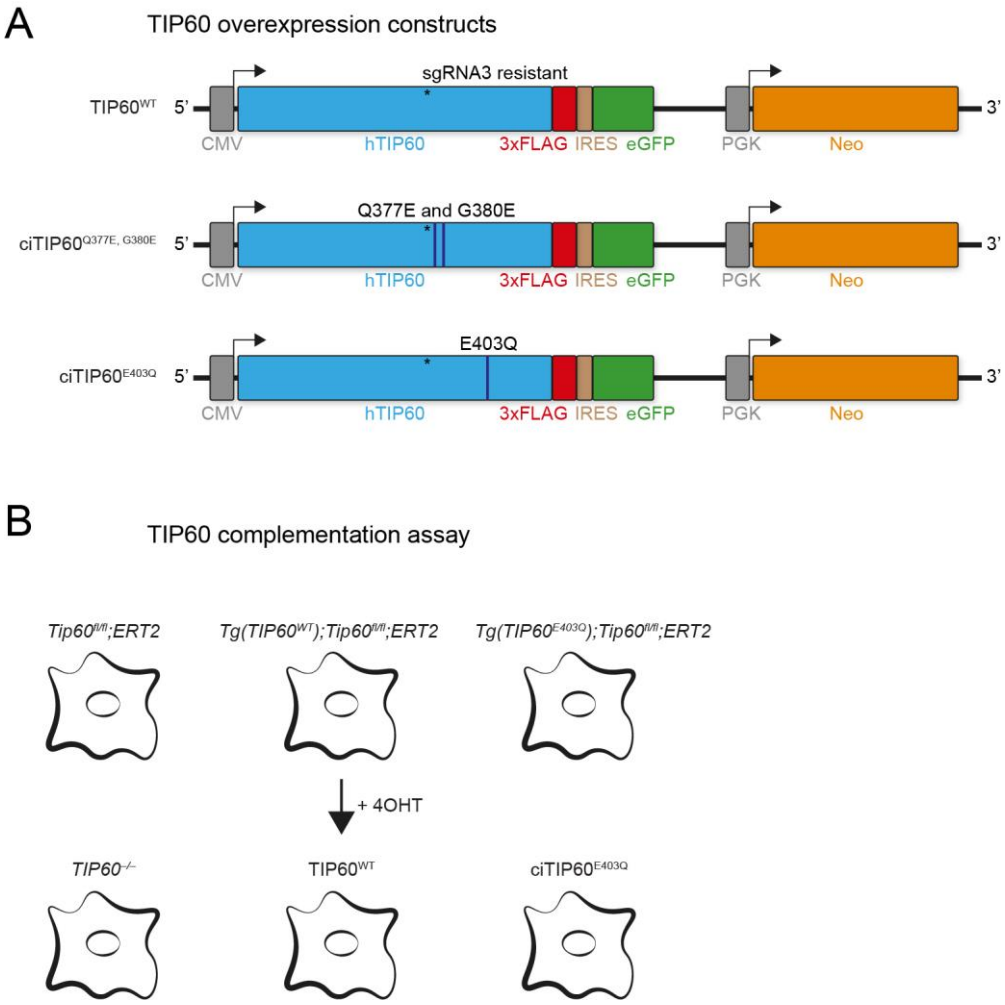

Figure 7.2: TIP60 complementation assay with catalytically inactive and wild-type TIP60 overexpression constructs. (A) Schematic drawing showing TIP60 overexpression cassettes stably transduced into CRISPR/Cas9-inducible *TIP60* mutation cells. Three constructs expressing human wild-type TIP60 isoform 2 and two different catalytically inactive mutants of TIP60, TIP60$^{Q377E,\ G380E}$ and TIP60^{E403Q} are shown. The asterisk marks a silent mutation in the PAM site used by sgRNA3 (indicated by an asterix), rendering the TIP60 transgenes immune to CRISPR/Cas9 deletion. A 3XFlag-tag is fused to the C-terminus of TIP60. A GFP and a neomycin-cassette serve as selection markers after lentiviral transduction. **(B)** Schematic of un-complemented *Tip60$^{fl/fl}$;ERT2*, and TIP60 complemented *Tg(Tip60^{WT});Tip60$^{fl/fl}$;ERT2*, and *Tg(Tip60^{E403Q});Tip60$^{fl/fl}$;ERT2* MEFs. Treatment with 4-OHT leads to induced genetic deletion of endogenous *Tip60* resulting in Tip60$^{-/-}$ MEFs and MEFs expressing only wildtype TIP60^{WT} or mutant ciTIP60^{E403Q}.

7.3.2 The HAT activity of TIP60 is indispensable for cell proliferation

I transduced each of the three constructs into *TIP60$^{fl/fl}$;ERT2* MEFs cells. Induction of these cells with 4-OHT and dox, respectively, mutated the endogenous *TIP60* gene and replaced endogenous TIP60 protein with the exogenous variant. Successful deletion of endogenous TIP60 in *TIP60$^{fl/fl}$;ERT2* MEFs expressing either no exogenous TIP60 (control), TIP60^{WT} or TIP60^{E403Q} is shown in a three-way genotyping PCR (Figure 7.3A). Complete deletion of endogenous Tip60 was achieved after 4 days of 4-OHT treatment. Expression of exogenous TIP60 was assessed by western blot using a FLAG-tag specific antibody. Uniform expression of exogenous TIP60 was observed in *Tg(Tip60^{WT});Tip60$^{fl/fl}$;ERT2* MEFs, *Tg(Tip60$^{Q377E,\ G380E}$);Tip60$^{fl/fl}$;ERT2* MEFs, and *Tg(Tip60^{E403Q});Tip60$^{fl/fl}$;ERT2* MEFs (Figure 7.3B). Expression of exogenous TIP60^{WT} or catalytically inactive TIP60 mutants (ciTIP60) did not alter proliferation rates in control MEFs (Figure 7.3C). Treatment with 4-OHT for 3 days, however, lead to the previously observed proliferation arrest resulting from loss of TIP60 in un-complemented MEFs (Figure 5.1) and comparable proliferation arrest in ciTIP60^{E403Q} and ciTIP60$^{Q377E,\ G380E}$ complemented MEFs. TIP60^{WT} complemented MEFs displayed no decrease in cell proliferation. The cell morphology characterized by flat and spread out cells was observed in un-complemented and ciTIP60 complemented MEFs, but not in TIP60^{WT} complemented MEFs (Figure 7.3D). These data suggest that exogenous expression of wildtype TIP60 rescues the Tip60 deletion phenotype in cell proliferation and that the catalytic activity of TIP60 is indispensable for cell proliferation in MEFs.

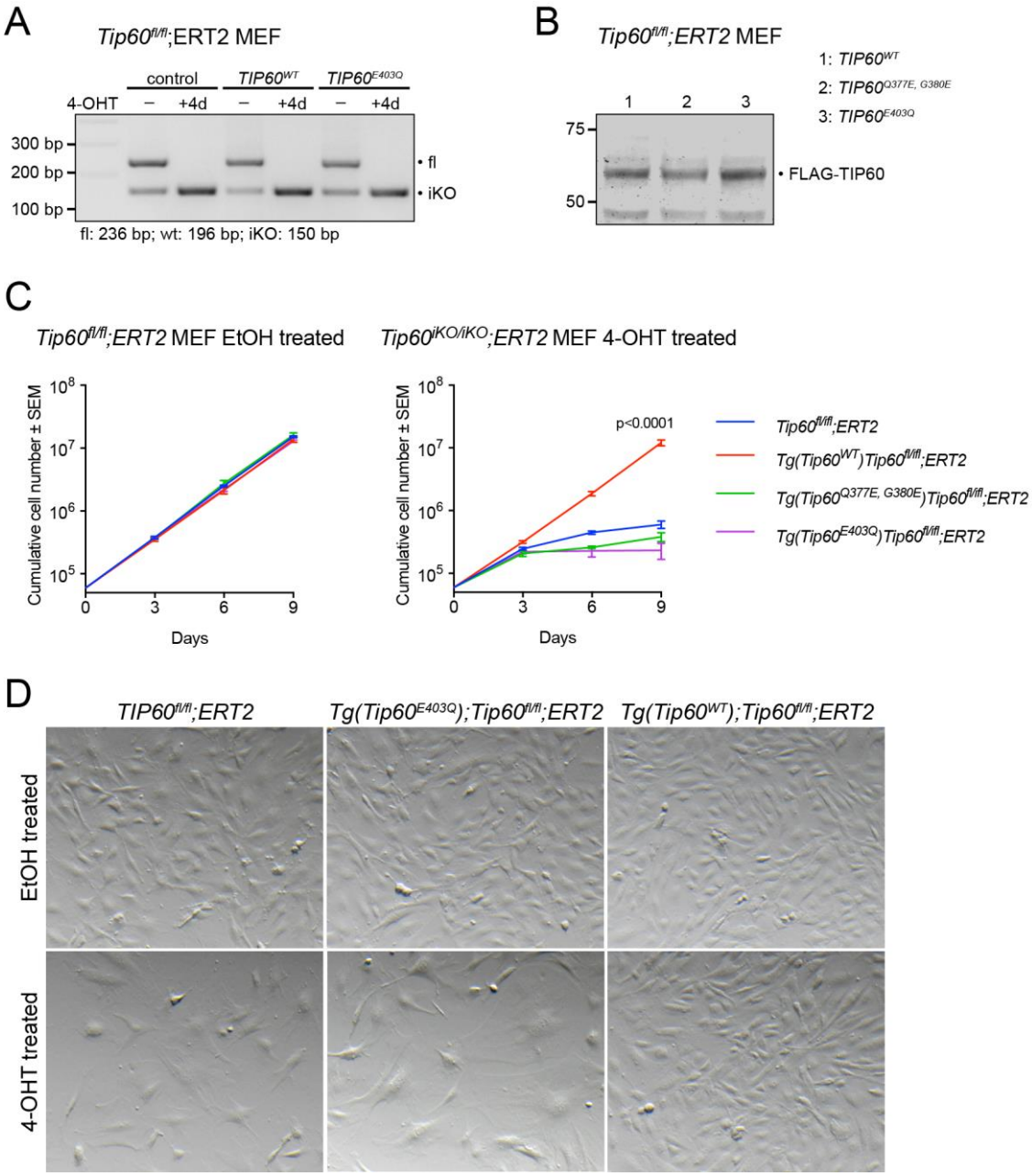

Figure 7.3: The acetyltransferase activity of TIP60 is essential for cell proliferation in MEFs. (A) Representative DNA gel of three-way PCR genotyping of *Tip60^{fl}* and *Tip60^{iKO}* alleles in *Tip60$^{fl/fl}$;ERT2*, *Tg(Tip60^{WT});Tip60$^{fl/fl}$;ERT2*, and *Tg(Tip60^{E403Q});Tip60$^{fl/fl}$;ERT2* MEFs 4 days after 4-OHT treatment. **(B)** Western blot of whole cell extracts from *Tg(Tip60^{WT});Tip60$^{fl/fl}$;ERT2*, *Tg(Tip60$^{Q377E, G380E}$);Tip60$^{fl/fl}$;ERT2*, and *Tg(Tip60^{E403Q});Tip60$^{fl/fl}$;ERT2* MEFs probed for FLAG-tag TIP60 protein **(C)** Proliferation of *Tip60$^{fl/fl}$;ERT2*, *Tg(Tip60^{WT});Tip60$^{fl/fl}$;ERT2*, and *Tg(Tip60^{E403Q});Tip60$^{fl/fl}$;ERT2* MEFs. Overexpression of wildtype or catalytically inactive TIP60 in EtOH treated MEFs had no effect on proliferation. 4-OHT induced deletion of endogenous *Tip60* led to cell cycle arrest after 3 days in un-complemented MEFs as well as MEFs complemented with catalytically inactive TIP60. Complementation with wildtype TIP60 rescued the proliferation arrest upon 4-OHT

treatment. Cells were treated for 3 days with 4-OHT before culturing in normal growth medium for the rest of the experiment. The slopes of log transformed growth curves were calculated from 3 to 9 days and compared using an unpaired two-tailed t test. Data are presented as means ± SEM of 3 replicates per condition. **(D)** Representative phase contrast images of *TIP60$^{fl/fl}$;ERT2*, *Tg(Tip60^{WT});Tip60$^{fl/fl}$;ERT2*, and *Tg(Tip60^{E403Q});Tip60$^{fl/fl}$;ERT2* MEFs untreated and 4 days after 4-OHT induction of endogenous *Tip60* mutation.

7.3.3 H2AZ acetylation depends on the catalytic activity of TIP60

I investigate H2AZ and H2AZ acetylation levels in *Tip60$^{fl/fl}$;ERT2* MEFs complemented with catalytically inactive TIP60 or wild-type TIP60. Western blot analysis of *Tip60$^{fl/fl}$;ERT2*, *Tg(Tip60^{WT});Tip60$^{fl/fl}$;ERT2*, and *Tg(Tip60^{E403Q});Tip60$^{fl/fl}$;ERT2* MEFs 4 days after 4-OHT treatment revealed the rescue of H2AZ acetylation by exogenous human wild-type TIP60, but no rescue was observed when catalytically inactive TIP60^{E403Q} mutant was expressed (Figure 7.4A). H2AZ levels remained unchanged in these cells. These observations show that E403Q mutation leads to catalytically inactive TIP60 and loss of H2AZ acetylation correlates with lack of proliferation in MEFs.

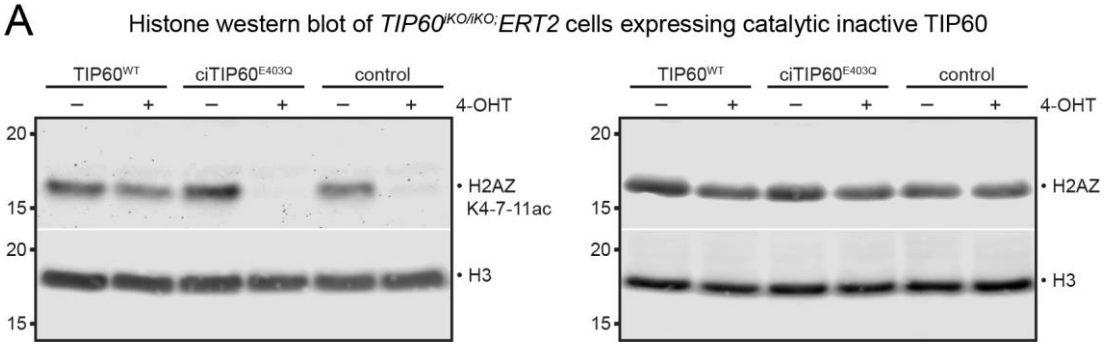

Figure 7.4: The catalytic activity of TIP60 is indispensable for H2AZ acetylation. (A) Western blots of acid extracted proteins from *Tip60$^{fl/fl}$;ERT2*, *Tg(Tip60^{WT});Tip60$^{fl/fl}$;ERT2*, and *Tg(Tip60^{E403Q});Tip60$^{fl/fl}$;ERT2* MEFs 4 days after 4-OHT treatment. Blots were probed for H2AZ and H2AZK4-7-11ac, as well as H3 as a loading control.

7.4 Discussion to chapter 7

In this chapter I sought to determine if it is the acetylation by TIP60 that was required for continued cell cycle progression. The treatment of *TIP60* mutant U2OS cells with the HDACi NaBu, but not TSA, restored the H2AZ acetylation signal as assessed by western blots. However, TSA concentrations were slightly below the EC_{50} of 87.5 nM and increasing the TSA concentrations could ameliorate global H2AZ acetylation. Both TSA and NaBu are pan-HDAC inhibitors with specificity towards HDACs of class I (HDAC1, 2, and 3), class IIa (HDAC4, 7, and 9), and class IIb (HDAC6) (Cacabelos and Torrellas, 2016; Davie, 2003). Despite apparent rescue of the H2AZ acetylation levels, NaBu did not rescue the proliferation defect in TIP60 depleted cells. This suggested that the cell cycle arrest observed in the absence of TIP60 might not be mediated simply by the loss of H2AZ acetylation, which was also observed in the absence of TIP60. However, it is also possible that, while NaBu restored global levels of H2AZac, it may not have restored the H2AZac at specific genomic sites where TIP60 is required to acetylate H2AZ.

Expressing catalytically inactive TIP60 mutants was shown to lead to embryonic lethality in fruit flies (Lorbeck et al., 2011) and mice (Acharya et al., 2017). Interestingly, murine ES cells expressing a catalytically inactive mutant of TIP60 are able to proliferate, but not differentiate (Acharya et al., 2017). The difference in effects between the complete loss of TIP60 and the loss of its catalytic activity suggests that it may not simply be the catalytic activity alone that is required for cell cycle progression. In this context, it is noteworthy that in ES cells TIP60 is bound to genes decorated with the bivalent marks H3K4 and K27 trimethylation (Fazzio et al., 2008), which are poised to become active, suggesting that TIP60 itself may be poised for activation at these loci. However, the correlation between H2AZ and H3K27me3 found in ESCs is completely reversed in neuronal precursor cells (Creyghton et al., 2008), suggesting that the functions of H2AZ

differs between ESC and other cell types. H2AZ is not essential for ESC proliferation, but differentiation (Creyghton et al., 2008), while other cell types rely on H2AZ to proliferate (Maruyama et al., 2012; Rangasamy et al., 2004; Rispal et al., 2019). Congruent with these findings, H2AZ was shown to be lost from the zygotic genome after fertilization and re-expressed in the morula stage, just before the first step of cell differentiation commences (Nashun et al., 2010). In conclusion, this suggests that H2AZ and potentially its TIP60-dependent acetylation play different roles in undifferentiated ESCs and other cell types. An indication that H2AZ acetylation is not essential for cell proliferation was shown in DT40 cells overexpressing non-acetylable H2AZ mutant (5 N-terminal lysines are replaced with arginines), which rescued the observed proliferation defect of H2AZ knockout (Kusakabe et al., 2016).

MEFs expressing only catalytically inactive TIP60 displayed the same proliferation arrest as uncomplemented *Tip60$^{iKO/iKO}$;ERT2* MEFs cells, showing that the catalytic activity of TIP60 is indispensable for cell proliferation in MEFs. The major reduction of H2AZ acetylation in *Tg(Tip60^{E403Q});Tip60$^{fl/fl}$* supports the essential role of TIP60 acetylation activity in H2AZ acetylation. Rescue of H2AZ acetylation levels and proliferation by complementing *Tip60$^{iKO/iKO}$;ERT2* MEFs with human wildtype TIP60 shows that exogenous human TIP60 can functionally substitute endogenous murine TIP60. Importantly, these data suggest that TIP60 HAT inhibitors may have utility as anti-cancer drugs.

Chromosome segregation defects and early embryonic lethality is shared between TIP60 and H2AZ knockouts, but the role of H2AZ during the cell cycle is not well understood. Here I showed data supporting the idea that the lack of H2AZ acetylation might be

sufficient in causing defects in cell proliferation, however, TIP60 acetyltransferase activity might have additional functions other than H2AZ acetylation that are essential in cell proliferation.

Chapter 8 TIP60 in transcription regulation

8.1 Introduction

Interestingly, TIP60 and H2AZ share many roles in transcription, supporting the functional link between TIP60 and H2AZ and potential importance of TIP60 mediated acetylation of H2AZ. This link might extend from co-regulating selected transcription factors, to a general role in transcription of most transcriptionally active genes. H2AZ might be deposited at gene promoters to facilitate rapid activation of gene expression after induction through consequent eviction of H2AZ. In this chapter I investigate the effect of loss of TIP60 on gene expression.

8.2 TIP60 is required for normal gene expression in murine and human cells

8.2.1 *Tip60* deletion leads to differential expression of many genes in MEFs

To assess the effects of loss of TIP60 on gene expression, I performed RNA-sequencing profiling of *Tip60*$^{+/+}$*;ERT2* control and *Tip60*$^{fl/fl}$*;ERT2* cells 3 days and 5 days after 4-OHT treatment. The bioinformatics analysis of my dataset was conducted by Dr Alexandra Garnham and Prof Gordon Smyth. Multidimensional scaling (MDS) indicated that samples clustered by genotypes and segregated between genotype in the first dimension (Figure 8.1A). A total of 8238 genes were differentially expressed (DE) in *Tip60*$^{iKO/iKO}$*;ERT2* cells compared to control cells over both time points (Table 12, Table 13, and Figure 8.1B). DE genes after 3 days and 5 days were highly correlated ($p = 5x10^{-5}$, Figure 8.1C). For the subsequent analysis I concentrated on genes DE 3 days after induction of *Tip60* deletion to examine the primary effects of loss of TIP60. At 3 days after induction of *Tip60* deletion, a total of 6311 genes were DE, with approximately half downregulated (3428). Of the top 50 DE genes ranked by FDR, 92% were downregulated

(Figure 8.1D). Among the top 500 DE genes I found 77.6% were downregulated, suggesting a significance bias towards transcriptional repression in the absence of TIP60.

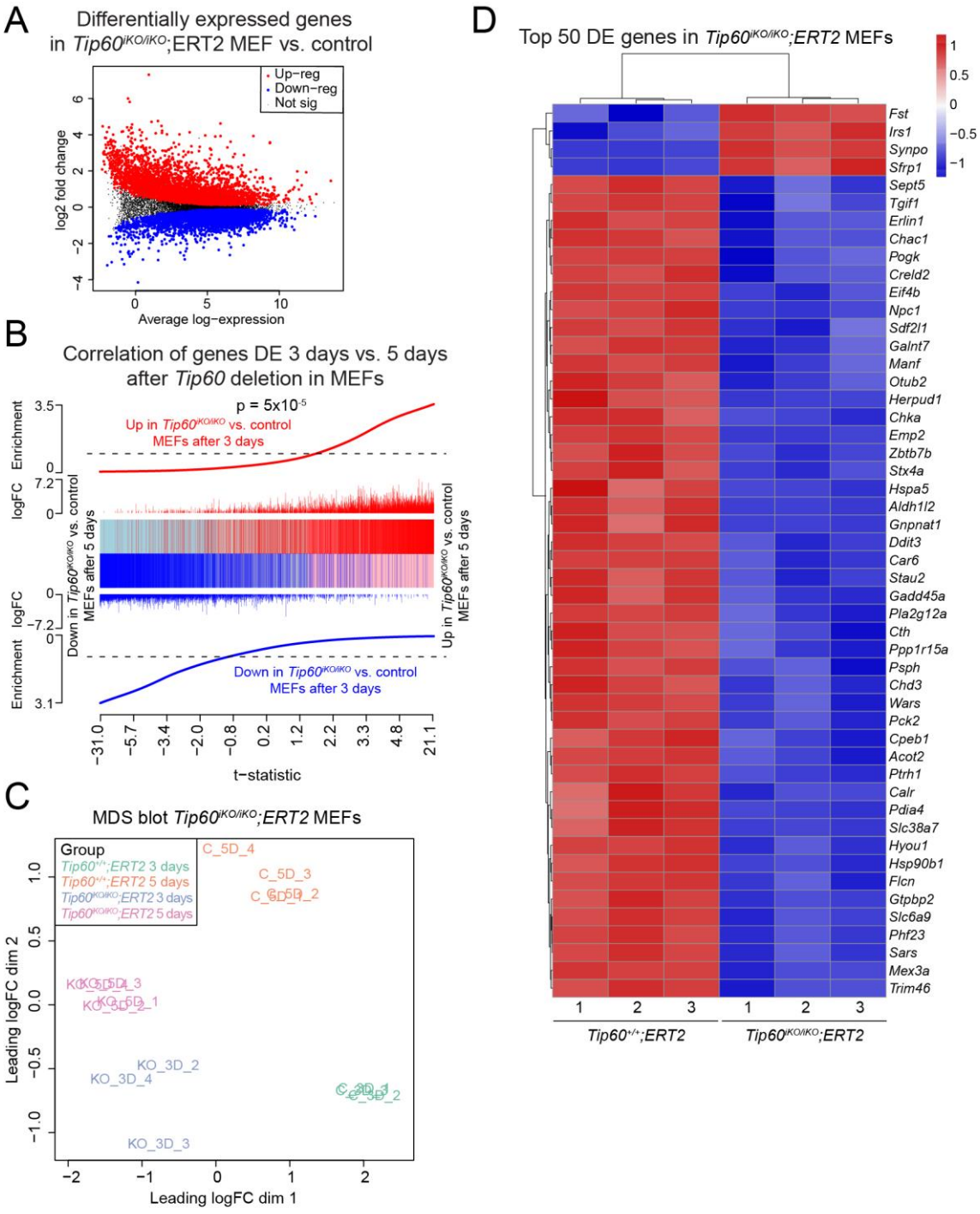

Figure 8.1: General analysis of RNA-sequencing results of *Tip60$^{iKO/iKO}$;ERT2* vs. *Tip60$^{+/+}$;ERT2* MEFs treated with 4-OHT for 3 and 5 days. (A) Multi-dimensional scaling plot of *Tip60$^{+/+}$;ERT2* and *Tip60$^{iKO/iKO}$;ERT2* MEF samples after 3 and 5 days of 4-OHT treatment to induced *Tip60* knockout. The distance between each pair of samples

is computed as the leading fold change, defined as the root-mean-square of the largest 500 log2 fold changes between that pair of samples. **(B)** Mean-difference plot showing the log2 fold change vs. average log2 counts-per-million of each gene in *Tip60$^{iKO/iKO}$;ERT2* MEFs vs. *Tip60$^{+/+}$;ERT2* control MEFs after treatment for 3 days with 4-OHT. **(C)** Barcode enrichment plot showing correlation of the transcriptional profiles induced by *Tip60* deletion after either 3 days or 5 days in MEFs. Genes are ordered according to differential expression at 5 days from most down-regulated (left) to most up-regulated (right) in *Tip60* deleted vs. control cells. The x-axis shows moderated t-statistics. Vertical red and blue bars show the location of genes in the dataset 3 days post *Tip60* deletion and the corresponding log2-fold-changes are indicated by the length of the bars. The blue and red worms indicate the enrichment of vertical bars relative to the 5 day dataset. The ROAST p-value for positive correlation is indicated. A high similarity in the effects of loss of TIP60 deletion at 3 days compared to 5 days after induction of *Tip60* deletion with 4-OHT treatment was observed. **(D)** Heatmap of the top 50 DE genes by FDR in *Tip60$^{iKO/iKO}$;ERT2* vs. *Tip60$^{+/+}$;ERT2* control MEFs after 3 days of 4-OHT treatment. Figure elements were generated by Dr Alexandra Garnham.

Apart from *Tip60* (*Kat5*) itself, *Kat2a*, *p300*, and *Kat7* mRNA levels were moderately reduced in *Tip60$^{iKO/iKO}$;ERT2* cells compared to control cells. No compensatory upregulation of a *KAT* gene was seen (Figure 8.2A). No significant changes in mRNA levels of the large NuA4 scaffold proteins TRRAP and EP400 or in other subunits of NuA4 complex, such as *Brd8*, *Ruvbl1*, *Epc2*, *Yeats4*, *Ing3*, *Vps72*, *Actl6a* (*Baf53a*), *Morf4l1* (*Mrg15*) and *Meaf6* were observed. The NuA4 subunits *Epc1* and *Dmap1* were upregulated, *Morf4l2*, *Yeats2* and *Ruvbl2* downregulated in *Tip60$^{iKO/iKO}$;ERT2* cells compared to control cells.

To better understand the cell cycle dysregulation observed in *Tip60$^{iKO/iKO}$;ERT2* cells, I examined cyclin (*Ccn*), cyclin-dependent kinase (*Cdk*), and cyclin-dependent kinase inhibitor (*Cdkn*) genes, as well as G1/ S transition promoting factor genes in my RNA-sequencing data set (Figure 8.2B). Cyclin genes were upregulated in *Tip60$^{iKO/iKO}$;ERT2* cells compared to control cells, including cyclin E, A and B genes, which peak in the G1/S transition, G2 and G2/M transition, respectively, while *Cdk2*, and *Cdk4* were downregulated. Interestingly *Cdkn1a* encoding p21$^{CIP1/WAF1}$ was downregulated, while

Cdkn2b and *Cdkn2c* encoding $p15^{INK4B}$ and $p18^{INK4C}$, respectively were upregulated in *Tip60*$^{iKO/iKO}$*;ERT2* cells compared to control cells. G1/S transitioning factors were mostly upregulated in *Tip60*$^{iKO/iKO}$*;ERT2* cells compared to control cells, possibly reflecting that cells accumulated in G1 phase in the absence of TIP60. BCL2 family genes and TRP53 target genes were generally downregulated in the absence of TIP60 in MEFs, including TRP53 target genes *Bax* and *Bak*, and only *Bim* was upregulated (Figure 8.2C), consistent with my observation that the TRP53 pathway was not required for the cell cycle arrest caused by the absence of TIP60 (Figure 5.9). Cell adhesion genes and collagen genes were strongly upregulated, up to 25-fold in *Tip60*$^{iKO/iKO}$*;ERT2* cells compared to control cells (Figure 8.2D). This notably included cell substrate adhesion genes, such as integrin and collagen genes, with 30% of the genes within this biological process upregulated ($p = 0.0002$; Table 17).

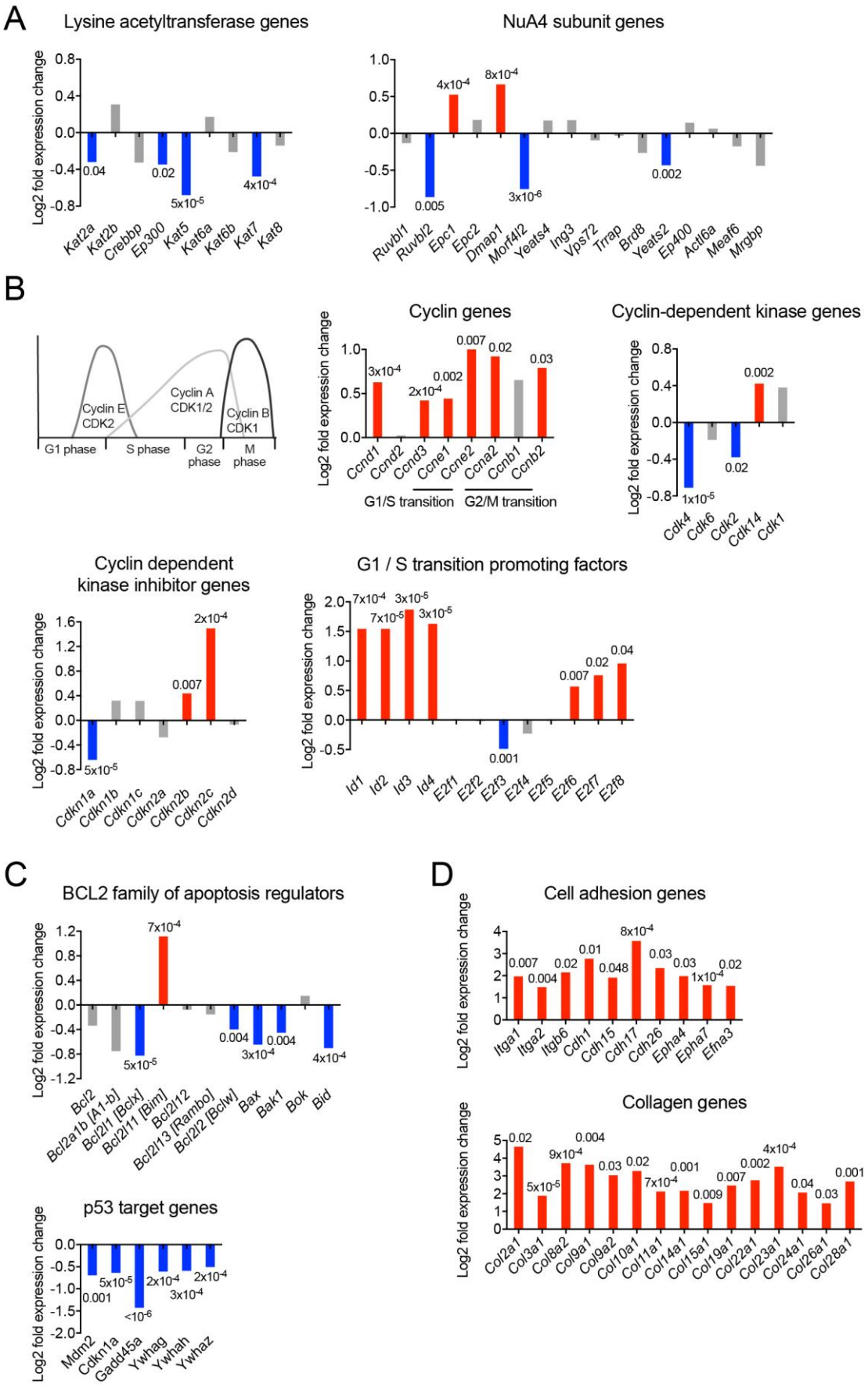
A
Lysine acetyltransferase genes
Log2 fold expression change
0.04
0.02
5x10-5
4x10-4
Kat2a Kat2b Crebbp Ep300 Kat5 Kat6a Kat6b Kat7 Kat8
NuA4 subunit genes
4x10-4
8x10-4
0.005
3x10-6
0.002
Ruvbl1 Ruvbl2 Epc1 Epc2 Dmap1 Morf4l2 Yeats4 Ing3 Vps72 Trrap Brd8 Yeats2 Ep400 Actl6a Meaf6 Mrgbp
B
Cyclin E CDK2
Cyclin A CDK1/2
Cyclin B CDK1
G1 phase
S phase
G2 phase
M phase
Cyclin genes
3x10-4
2x10-4
0.002
0.007
0.02
0.03
Ccnd1 Ccnd2 Ccnd3 Ccne1 Ccne2 Ccna2 Ccnb1 Ccnb2
G1/S transition
G2/M transition
Cyclin-dependent kinase genes
0.002
0.02
1x10-5
Cdk4 Cdk6 Cdk2 Cdk14 Cdk1
Cyclin dependent kinase inhibitor genes
2x10-4
0.007
5x10-5
Cdkn1a Cdkn1b Cdkn1c Cdkn2a Cdkn2b Cdkn2c Cdkn2d
G1 / S transition promoting factors
7x10-4
7x10-5
3x10-5
3x10-5
0.007
0.02
0.04
0.001
Id1 Id2 Id3 Id4 E2f1 E2f2 E2f3 E2f4 E2f5 E2f6 E2f7 E2f8
C
BCL2 family of apoptosis regulators
7x10-4
5x10-5
0.004
3x10-4
0.004
4x10-4
Bcl2 Bcl2a1b [A1-b] Bcl2l1 [Bclx] Bcl2l11 [Bim] Bcl2l12 Bcl2l13 [Rambo] Bcl2l2 [Bclw] Bax Bak1 Bok Bid
p53 target genes
0.001
5x10-5
<10-6
2x10-4
3x10-4
2x10-4
Mdm2 Cdkn1a Gadd45a Ywhag Ywhah Ywhaz
D
Cell adhesion genes
0.007
0.004
0.02
0.01
0.048
8x10-4
0.03
0.03
1x10-4
0.02
Itga1 Itga2 Itgb6 Cdh1 Cdh15 Cdh17 Cdh26 Epha4 Epha7 Efna3
Collagen genes
0.02
5x10-5
9x10-4
0.004
0.03
0.02
7x10-4
0.001
0.009
0.007
0.002
4x10-4
0.04
0.03
0.001
Col2a1 Col3a1 Col8a2 Col9a1 Col9a2 Col10a1 Col11a1 Col14a1 Col15a1 Col19a1 Col22a1 Col23a1 Col24a1 Col26a1 Col28a1

Figure 8.2: Effect of *Tip60* deletion on the expression of individual genes in MEF. (A-D) Results for specific groups of genes with FDR indicated in the graphs. Blue bars, significantly downregulated, red bars significantly upregulated, grey bars represent genes not significantly changed. **(A)** Histone lysine acetyltransferase (KAT) genes and TIP60 complex, i.e. NuA4 complex subunit genes. **(B)** Schematic drawing of cyclins and cyclin-dependent kinase activity during mitotic cell cycle and mRNA level changes of cell cycle related genes, including cyclin genes, cyclin-dependent kinase genes, and cyclin-dependent kinase inhibitor genes in *Tip60*$^{iKO/iKO}$*;ERT2* vs. *Tip60*$^{+/+}$*;ERT2* control MEFs. FDR values are indicated in the graph. **(C)** BCL2 family of apoptosis regulator genes and TRP53 target genes. **(D)** Cell-substrate adhesion genes and collagen genes.

Among the top 10 enriched biological processes 8 were downregulated and these were gene expression, protein translation and associated processes, consistent with the fact that MEFs enter cell cycle arrest after loss of TIP60, in which metabolism and protein synthesis is reduced. Only 2 processes were upregulated, which related to tissue development (Figure 8.3A, Table 17). Specific signalling pathways were upregulated, including TGFß and the WNT signalling pathways (Table 21). Examining transcription and gene expression processes more specifically, I found that these were on the whole downregulated in the absence of TIP60, with several processes related to regulation of gene transcription on the DNA level, such as transcription, DNA-template, nucleic acid-template transcription, transcriptional regulatory region DNA binding (Figure 8.3B, Table 16).

Pathways downregulated in *Tip60* $^{iKO/iKO}$;ERT2 MEFs after 5 days of 4-OHT treatment included TRP53-signaling, cell cycle regulation, apoptosis and necroptosis, congruent with the observation that TIP60 knockout MEFs neither proliferate, nor undergo apoptosis or other forms of cell death, but rather enter cell cycle arrest.

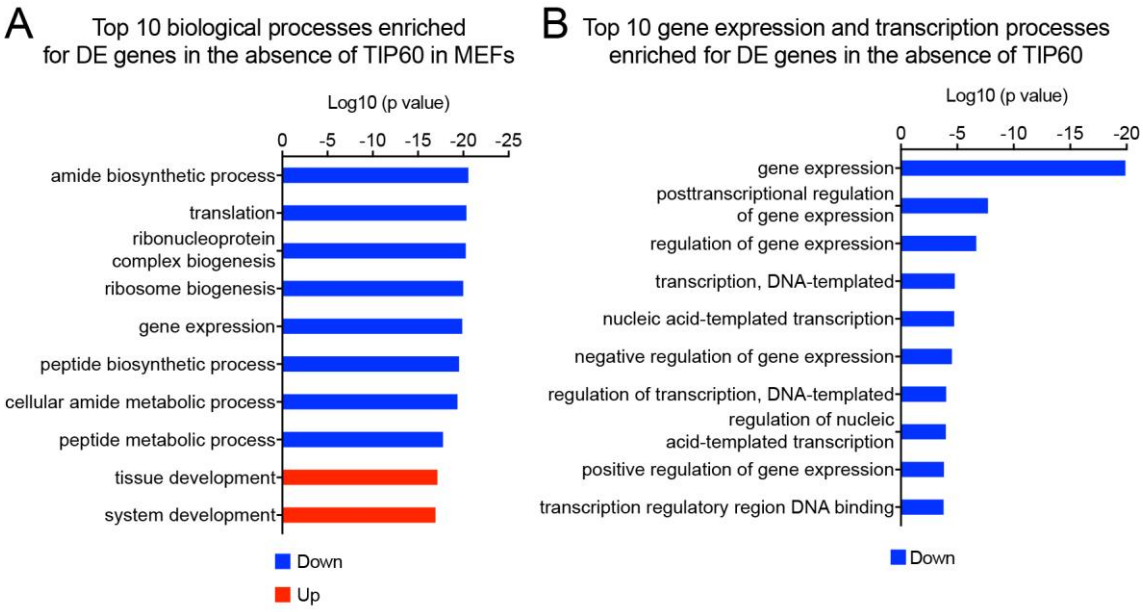

Figure 8.3: Effect of *Tip60* deletion on biological processes in MEF. (A) Top 10 biological processes (GO terms) enriched for genes differentially expressed in the absence of TIP60 in MEFs. **(B)** Top 10 gene expression and transcription processes (GO terms) enriched for genes DE in the absence of TIP60 in MEFs.

8.2.2 *TIP60* deletion leads to large dysregulation of transcription in HEK293 cells

In HEK293 samples clustered by genotypes and segregated between genotypes in the first dimension (Figure 8.4A). The expression changes in HEK293 cells, where *TIP60* was deleted using either sgRNA#1 or sgRNA#2 were highly correlated 3 days after induction of *TIP60* deletion (Figure 8.4B) and data from the two sgRNAs were combined for all further analyses. In the absence of TIP60, 6236 genes were differentially expressed between *iC-TIP60* and control HEK293 cells, with approximately half downregulated (DR) and upregulated (UR) (Table 14, Table 15). However, the amplitude of change was higher in a subset of UR genes compared to the DR genes (Figure 8.4C). The top two UR genes were ephrin B2 and protocadherin 9. Indeed, 13 members of the protocadherin gene family were UR (Table 15).

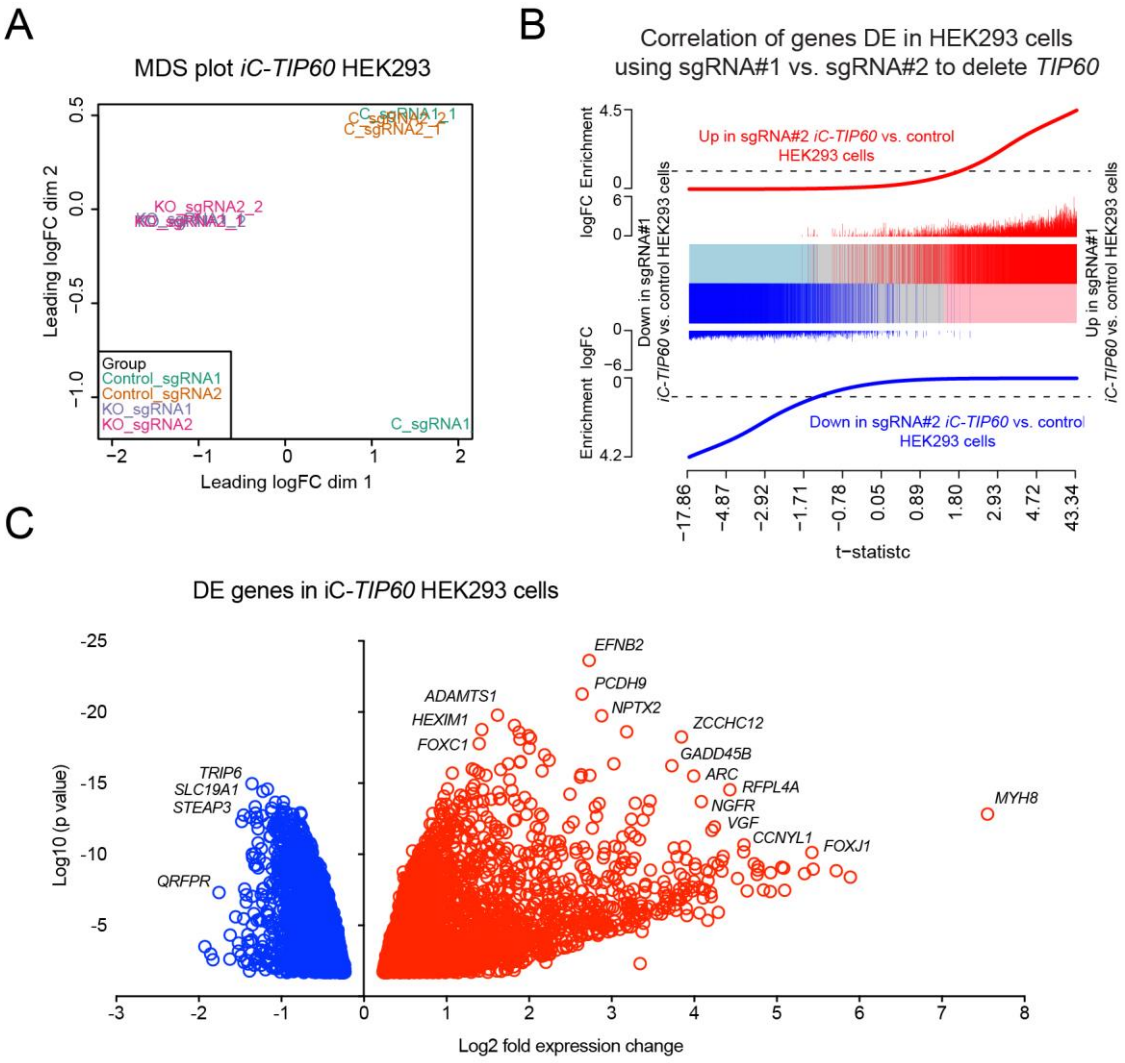

Figure 8.4: General analysis of RNA-sequencing results from *iC-TIP60* vs. control HEK293 cells after 3 days of dox treatment to induced *Tip60* deletion. (A) Multi-dimensional scaling plot of RNA-sequencing data from 2 replicates for each of two sgRNA control and *iC-TIP60* HEK293 cells after 3 days of dox induction comparing the effects of sgRNA#1 and sgRNA#2. **(B)** Barcode enrichment plot showing strong correlation of the transcriptional profiles induced by *TIP60* deletion after 3 days with either sgRNA1 or sgRNA2 in HEK293 cells. Genes are ordered according to differential expression induced with sgRNA#1 from most down-regulated (left) to most up-regulated (right) in *TIP60* deletion vs. control cells. The x-axis shows moderated t-statistics. Vertical red and blue bars show genes in the dataset with sgRNA#2 induced *TIP60* deletion and the corresponding log2-fold-changes are also shown. The blue and red worms indicate relative enrichment of vertical bars. The ROAST p-value for positive correlation is indicated. The effects of *TIP60* mutation using the two sgRNAs were highly similar. To focus on effects supported by both sgRNAs, both datasets were combined for further analyses. **(C)** Volcano plot displaying genes significantly DE in *iC-TIP60* vs.

control HEK293 cells. Results from both sgRNAs were combined. Graphs in panels A and B were generated by Dr Alexandra Garnham.

Similar to the findings in MEFs, NuA4 subunit and KAT genes were not greatly dysregulated in HEK293 cells (Figure 8.5A). Cell cycle and mitosis processes and genes were predominantly downregulated in the absence of TIP60 (Figure 8.5B, Table 18), congruent with the observed cell cycle arrest after TIP60 mutation (Figure 5.2). However, the cyclin A1 gene was 10-fold upregulated in HEK293 cells lacking TIP60, possibly indicating accumulation of cells arrested in G2 phase, while cyclin dependent kinase genes were generally downregulated (Figure 8.5C). Cell senescence processes and genes were upregulated, including TP53 target genes, e.g. *CDKN1A* and GADD45, as well as *CDKN1C, CDKN2B* and *CDKN2D,* encoding $p21^{CIP1/WAF1}$, $p57^{KIP2}$, $p15^{INK4B}$ and $p19^{INK4D}$, respectively, were up to 13-fold upregulated (Figure 8.5D). Some BCL2 family genes were downregulated in HEK239 cells lacking TIP60 (Figure 8.5E), similar to *Tip60* deleted MEFs (Figure 8.2C).

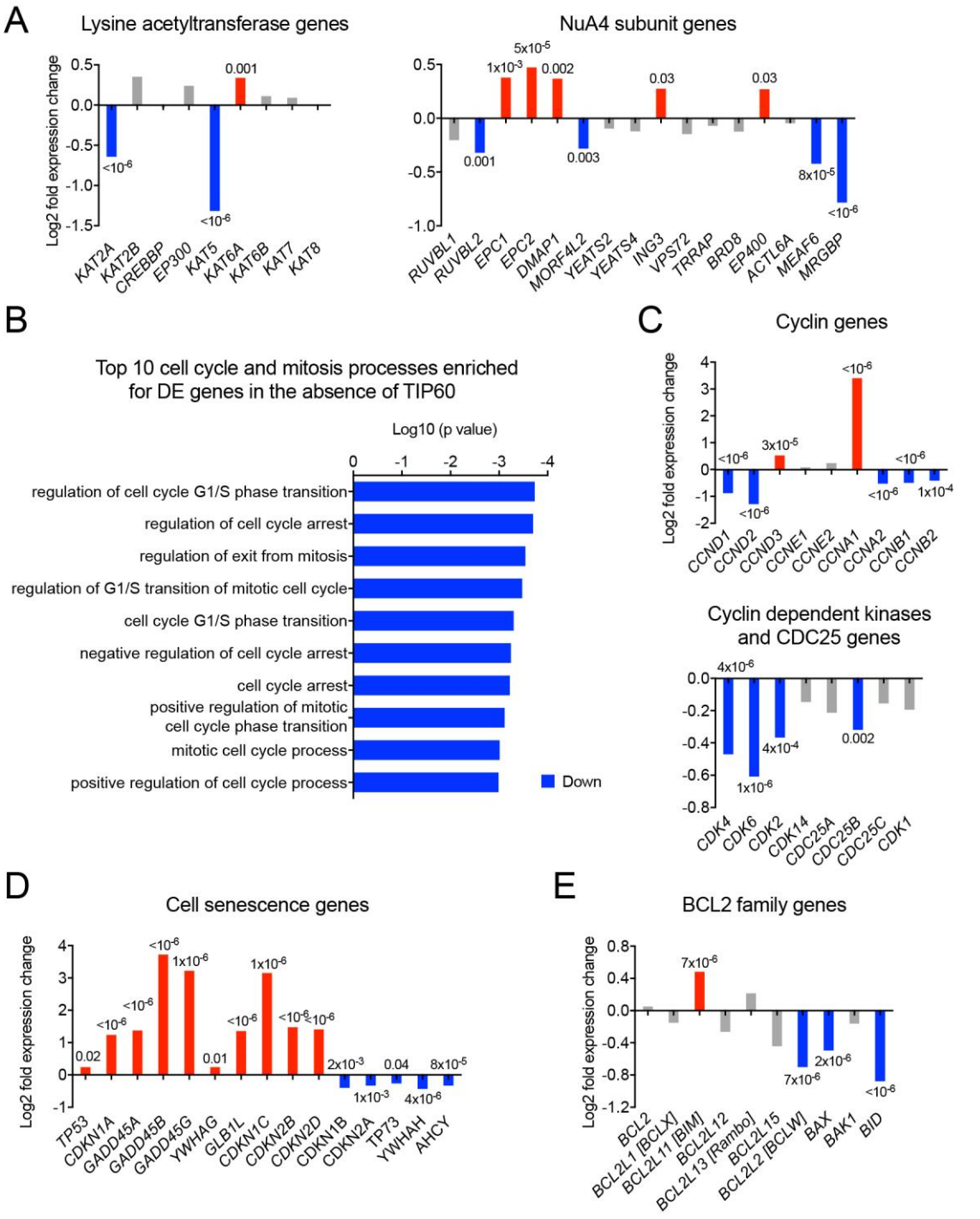

Figure 8.5: Effect of *TIP60* deletion on the expression of individual genes in HEK293 cells. (A, C-E) Results for specific groups of genes with FDR indicated in the graphs. Blue bars, significantly downregulated, red bars significantly upregulated, grey bars represent genes not significantly affected based on FDRs. **(A)** Histone lysine acetyltransferase (KAT) genes and TIP60 complex, i.e. NuA4 complex subunit genes. **(B)** The top 10 cell cycle and mitosis processes (GO terms) were downregulated in *iC-TIP60* HEK293 cells compared to control cells. **(C)** Cyclin genes, cyclin dependent kinase genes and the *CDC25* gene. **(E)** Cell senescence genes. **(F)** BCL2 family genes.

TIP60 deleted HEK293 had a large proportion of cells that lifted off the cell culture plastic. However, the proportion of dead cells was not increased (Figure 5.4B), suggesting a primary failure in cell-substrate adhesion. However, genes encoding cell-cell adhesion proteins, in particular of the protocadherin, cadherin and ephrin receptor families were upregulated in the absence of TIP60 (Figure 8.6B). Indeed, 33% of genes with the annotation "cell adhesion" were upregulated in the absence of TIP60 ($p < 10^{-6}$; Table 19), suggesting perhaps a futile attempt to compensate for an impaired cell adhesion.

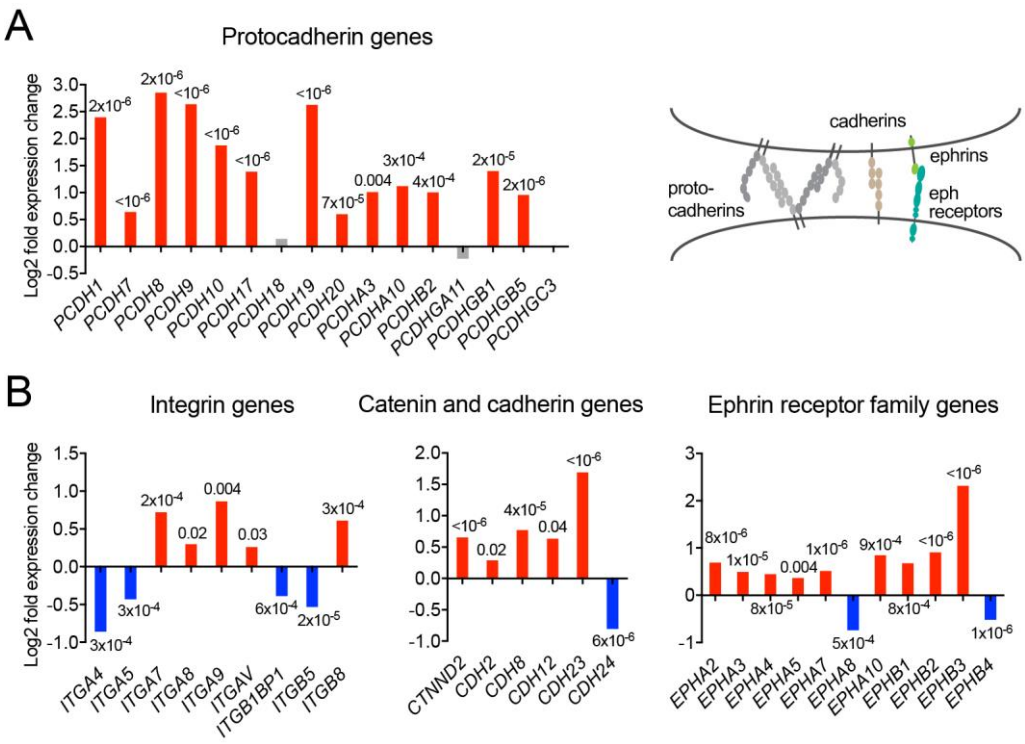

Figure 8.6: Effect of *TIP60* deletion on the expression of cell adhesion and cell interaction genes in HEK293 cells. (A, B) Results for specific groups of genes with FDR indicated in the graphs. Blue bars, significantly downregulated, red bars significantly upregulated, grey bars represent genes not significantly affected based on FDRs. **(A)** Expression level changes of protocadherin genes in *iC-TIP60* vs. control HEK293 and schematic drawing of cell-cell adhesion interaction upregulated in the absence of TIP60. **(B)** Cell-cell adhesion genes.

Six of the top 10 biological processes were downregulated in HEK293 cells lacking TIP60; these were metabolic processes, whereas organ development processes were upregulated (Figure 8.7A, Table 18). Similarly, among the KEGG pathways affected, metabolic pathways ($p < 10^{-6}$) and the cell cycle ($p = 6x10^{-5}$; Table 22) were downregulated, whereas cell adhesion molecules were upregulated ($p = 5x10^{-4}$; Table 23). Gene expression and transcription processes were comprehensively downregulated with the sole exception of the upregulation of the process "positive regulation of transcription from RNAPII promoters in response to endoplasmic reticulum stress" (Figure 8.7B).

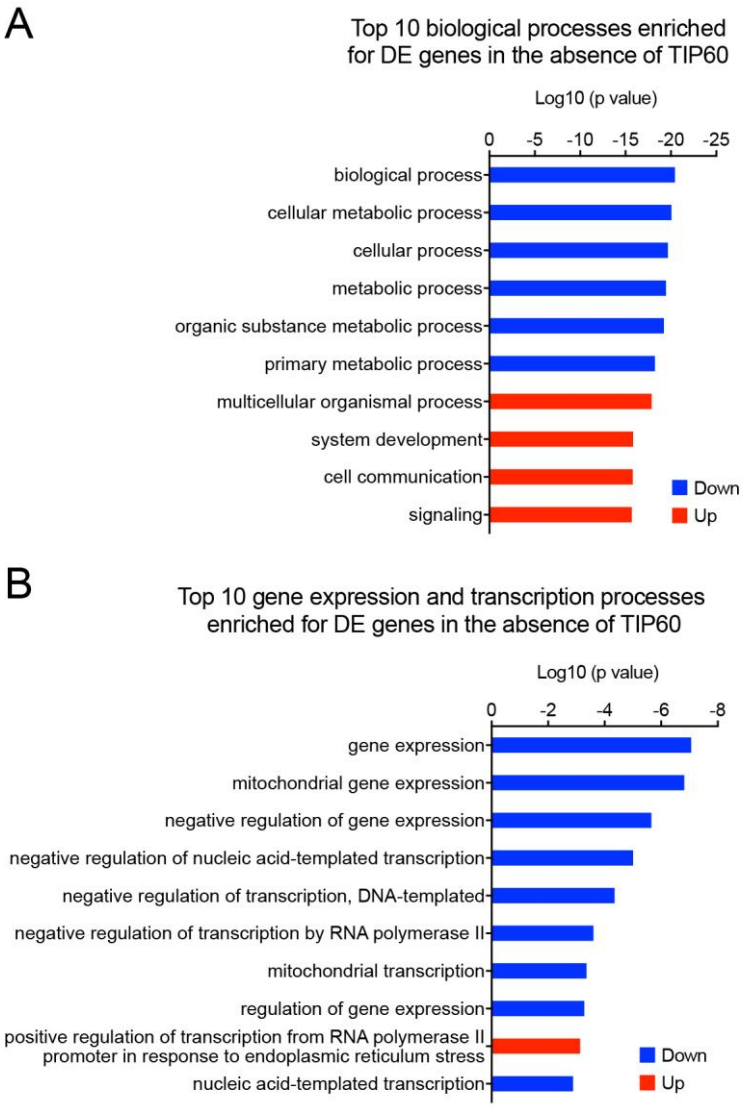

Figure 8.7: Effect of *TIP60* deletion on biological processes in HEK293 cells. (A) Top 10 biological processes (GO terms) enriched for genes differentially expressed in the absence of TIP60. **(B)** Top 10 gene expression and transcription processes (GO terms) in *iC-TIP60* vs. control HEK293 cells.

In conclusion, many genes essential for basic cell functions appear to be dependent on TIP60. Nevertheless, other genes were expressed at normal levels or even upregulated in the absence of TIP60, suggesting that TIP60 is not simply required for all transcription.

8.3 Assessment of the effects of *TIP60* deletion on the genomic distribution of acetylated H2AZ and acetylated H4

8.3.1 Determining the conditions for CUT&Tag assessment of the effects of loss of TIP60 on the genomic location of H2AZ and H2AZac

To assess the effects of *TIP60* deletion on the genomic distribution of acetylated H2AZ and acetylated H4, I performed CUT&Tag sequencing on *iC-TIP60* U2OS cells. *D. melanogaster* S2 cells were used as a spike-in and mixed with target cells in a fixed ratio. This was to enable us to determine if there was a global reduction in H2AZ acetylation by providing a standard for comparison between samples. I first investigated the effect of the CUT&Tag procedure on H2AZ acetylation levels and the affinity of my antibodies to H2AZ in human cells and its orthologues in *D. melanogaster* S2 cells. Although anticipated to be a potential source of artefacts, I tested trypsinization because it would have allowed a more quantitative mixing of test cells with S2 spike-in cells. However, trypsinisation, as well as prolonged incubation in CUT&Tag antibody staining buffer without NaBu severely reduces acetylation signal of H2AZ (Figure 8.8A). S2 cell H2Av was recognized by the H2AZK-4-7-11ac antibody targeting the N-terminal lysines, but not by the pan-H2AZ antibody, which binds to the unmodified C-terminal domain (Figure 8.8A). Inhibiting HDACs in trypsinised cells during the CUT&Tag procedure via NaBu protected H2AZ acetylation (Figure 8.8B). I therefore performed CUT&Tag experiments with scraped cells and in the presence of NaBu.

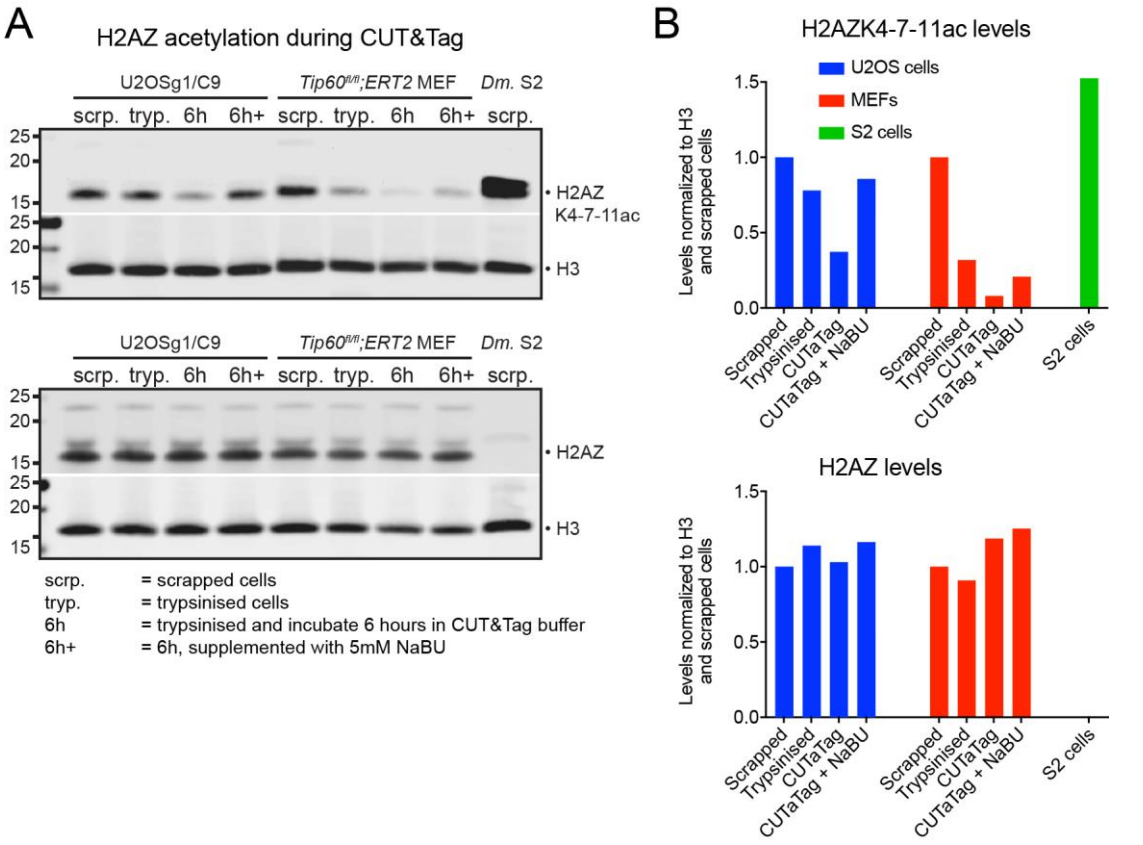

Figure 8.8: Determining the conditions for CUT&Tag assessment of the effects of loss of TIP60 on the genomic location of H2AZ and H2AZac. (A) Western blot of histone extracts from *iC-TIP60* U2OS cells, *Tip60$^{fl/fl}$;ERT2* MEFs, and S2 cells stained for H3, H2AZ, and H2AZK4-7-11ac comparing trypsinized cells, scraped cells and cells incubated in CUT&Tag buffer for 6 hours with and without NaBu. **(B)** Quantification of H2AZ and H2AZK4-7-11ac histone levels normalized to H3. Trypsinization and prolonged incubation in CUT&Tag antibody staining buffer without NaBu severely reduces acetylation of H2AZ. *D. melanogaster* H2Av is recognized by the H2AZK-4-7-11ac antibody, which targets the acetylated N-terminal lysines, but not by the H2AZ antibody, which binds to the unmodified C-terminal domain.

8.3.2 H2AZ acetylation is reduced at TSS upon *TIP60* deletion

I generated CUT&Tag sequencing data for H2AZ, H2AZK4-7ac, H2AZK4-7-11ac, H4K8ac, and H4K16ac in *iC-TIP60* U2OS and control U2OS cells with S2 *D. melanogaster* spike in cells. The quality control, read alignment, read counts, generation of BAM files, normalization to spike-in reads, and differential decoration analysis of my CUT&Tag dataset was conducted by Dr Alexandra Garnham and Prof Gordon Smyth.

The total mapped reads per library and subdivision of uniquely mapped reads per species are displayed in Table 24 and Figure 8.9A. A global reduction of H2AZ acetylation by 80 - 90% was observed in *iC-TIP60* U2OS compared to control U2OS cells using two different antibodies, namely against H2AZK4-7ac and H2AZK4-7-11ac (Figure 8.9B). H2AZ, H4K8ac, and H4K16ac were slightly reduced but did not reach significance. These data suggest that global occupancy of acetylated H2AZ is drastically reduced in cells lacking TIP60, congruent with the global reduction of acetylated H2AZ seen by western blot (Figure 6.5).

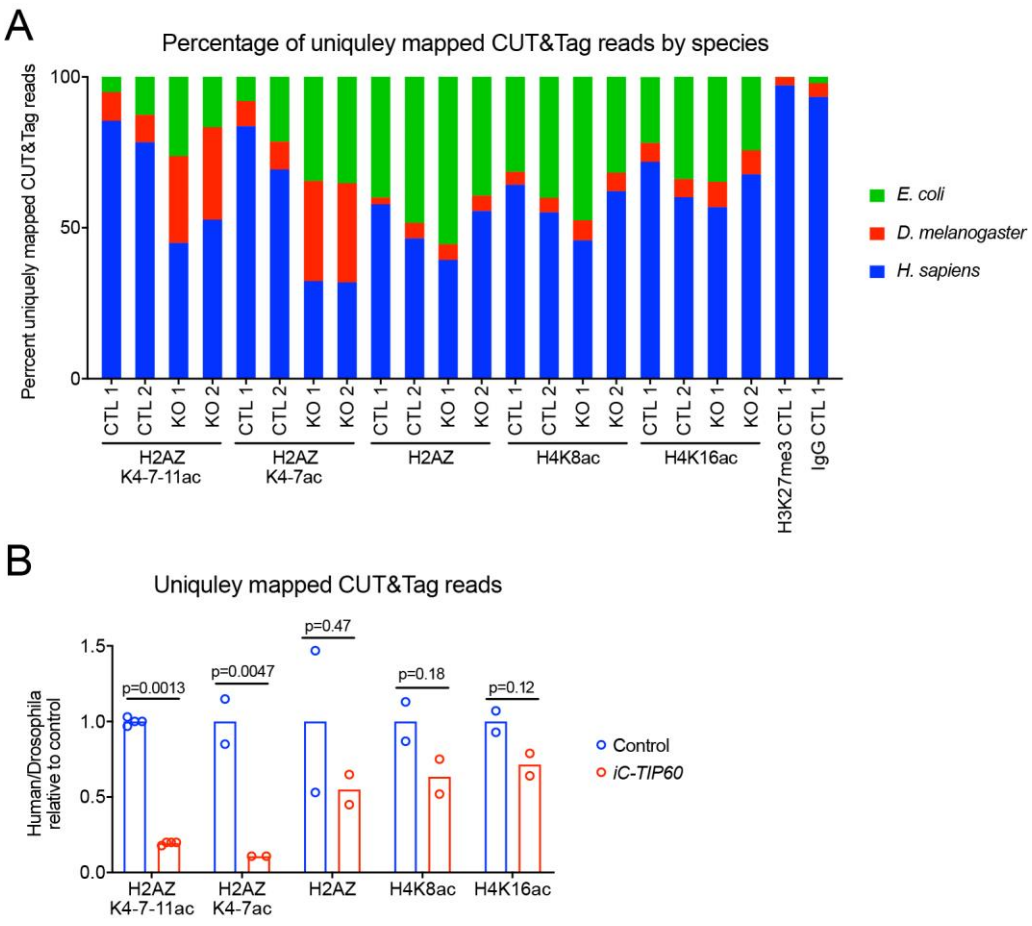

Figure 8.9: H2AZ acetylation is reduced in *TIP60* deleted cells. (A) CUT&Tag sequencing read percentages of uniquely mapped reads to the *E. coli*, *D. melanogaster*, or *H. sapiens* genome. spike-in *D. melanogaster* serves as a spike in while E *coli* is carried over from pAG-Tn5. CUT&Tag sequencing for H3K27me3 and IgG CTL samples were performed with commercial pAG-Tn5, which contains no carry-over *E. coli* DNA, while

other samples were performed with pAG-Tn5 kindly donated by the Henikoff laboratory and contains *E. coli* DNA indicating the ratio between added pAG-Tn5 and enriched genomic fragments from other species. **(B)** CUT&Tag sequencing reads in *iC-TIP60* U2OS cells as fraction of spike-in S2 *D. melanogaster* cells normalized to control U2OS cells using antibodies detecting H2AZK4-7-11ac, H2AZK4-7ac, total H2AZ, H4K8ac, and H4K16ac. Replicates from sgRNA1 and sgRNA2 were similar and thus combined. Fold changes are displayed as mean ± SEM and analysed by log transformation followed by multiple t-test with Benjamini and Hochberg correction.

I used the BAM files prepared by Alexandra Garnham to produce wiggle plots using SeqMonk (v1.45.1). CUT&Tag peaks were found primarily at the TSS of genes for H2AZ, acetylated H2AZ, H4K8ac, and H4K16ac, while H3K27me3 was found across gene bodies and intergenic regions (Figure 8.10A). H3K27me3 is a well-known chromatin mark for inactive genes (Barski et al., 2007; Bernstein et al., 2002; Bernstein et al., 2005; Bernstein et al., 2006; Boyer et al., 2006; Mikkelsen et al., 2007; Rea et al., 2000). Interestingly, I found peaks for H2AZ, H2AZK4-7-11ac, H2AZK4-7ac, H4K8ac, and H4K16ac at TSS of genes not decorated with H3K27me3, indicating that these peaks accumulated at TSS of active genes. Differential decoration analysis at the TSS of genes, characterized as a 2000 bp region around the 5' end of genes, of each mark in *iC-TIP60* U2OS cells versus control cells revealed a global reduction with an average fold change of 57% and 69% in H2AZK4-7-11ac and H2AZK4-7ac, respectively (Figure 8.10B). Occupancy of H2AZ and H4K8ac at the TSS remained unchanged, while H4K16ac was reduced to 50%. I found an even distribution of fold changes around the means. This data suggests that changes in histone acetylation observed in *TIP60* knockout cells are not loci specific, but rather across all TSS that are decorated by the respective mark.

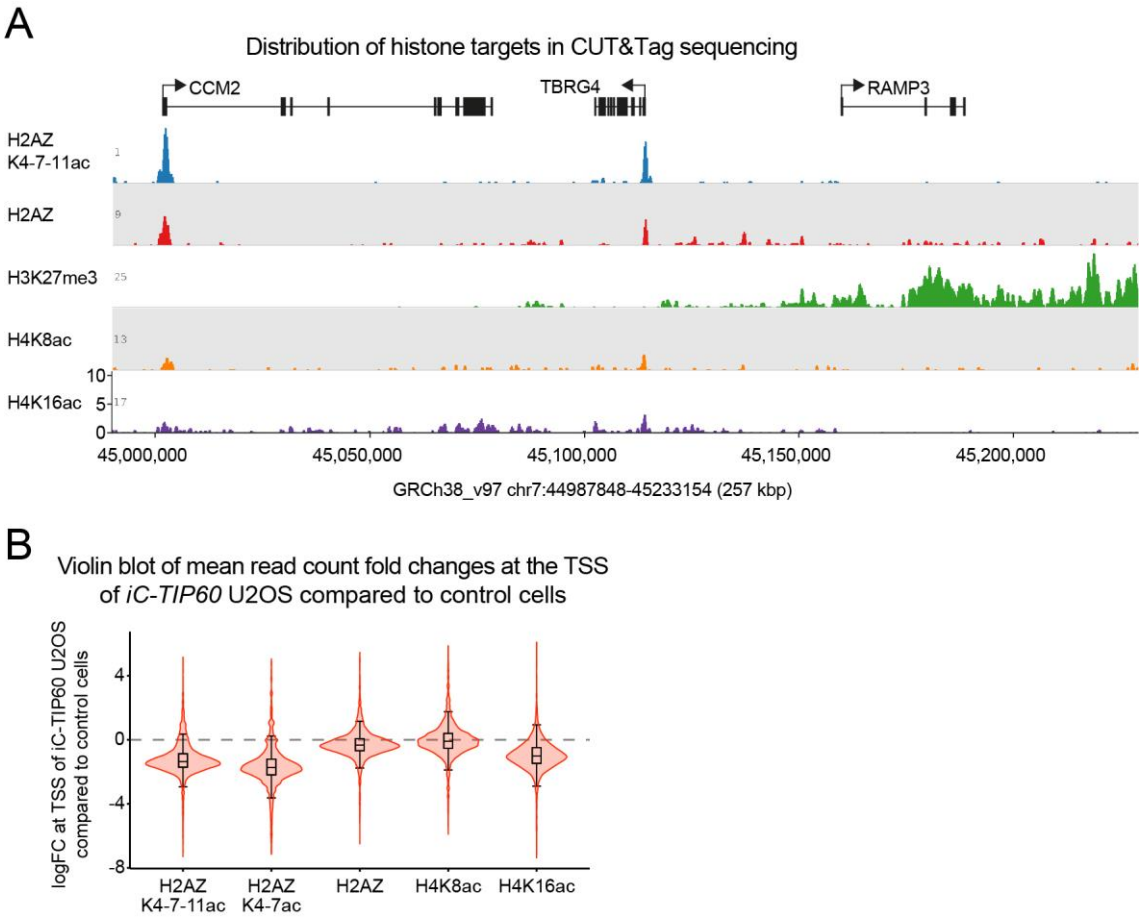

Figure 8.10: H2AZ acetylation is reduced at the TSS in TIP60 deleted cells. (A) Wiggle plot of the chromatin landscape in a 257kbp genomic region. Shown are CUT&Tag peaks for H2AZK4-7-11ac, H2AZ, H3K27me3, H4K8ac, and H4K16ac. H3K27me3 is commonly used as a positive control in CUT&Tag sequencing and is found over inactive regions. The IgG control sample resulted in no comparable read counts. All other marks were found in sharp peaks mainly over transcription start sites of genes. **(B)** CUT&Tag sequencing reads were quantified in a 2000 bp window around the 5' end of genes, marking the TSS. The distributions of probe value fold changes (logFC) between *iC-TIP60* U2OS and control cells are displayed as violin plots, with respective box plots inside.

8.4 Discussion to chapter 8

The RNA-sequencing data of TIP60-deficient cells compared to control cells supports a broad role of TIP60 in gene transcription, congruent with the role of H2AZ acetylation in transcription (Giaimo et al., 2019). Thousands of genes relied on TIP60 for normal expression levels in MEFs, including protein translation, ribosome biogenesis and general

gene expression. In contrast, tissue development, including skeletal and cartilage genes, as well as specific pathways, e.g. the TGFß pathway and the WNT pathway, both involved in mesodermal tissue development (Kimelman, 2006), were upregulated. Therefore, MEFs that arrest in the cell cycle due to the absence of TIP60 were able to express genes commensurate with a mesodermal development program. Furthermore, I observed increased expression of a large number of genes encoding cell adhesion and extracellular matrix proteins, congruent with the well spread and firmly attached, although senescent, morphology of the *Tip60* deleted MEFs. Cell cycle arrest in more than one phase of the cell cycle and dysfunctional mitosis suggest that the observed cell cycle arrest is not due to effects on a single cell cycle regulatory mechanism, but is rather due to a broad transcriptional dysregulation of multiple genes required in different phases of the cell cycle for a range of cellular mechanisms. The RNA-sequencing results further supports my finding that even *Trp53*$^{-/-}$ cells undergo cell cycle arrest after loss of TIP60, namely that the p19^{ARF}-TRP53 tumour suppressor pathway is not engaged in the cell cycle arrest induced in the absence of TIP60 in MEFs. In fruit flies, overexpression of a catalytically inactive form of TIP60 leads to a plethora of dysregulated metabolic and signalling pathways (Lorbeck et al., 2011).

Chapter 9 General discussion and conclusion

9.1 Conclusion

In my PhD projects I have established two inducible TIP60 knockout systems and characterized the immediate effects of loss of TIP60 on cultured human and mouse cells. Although cultured cells do not fully resemble the *in vivo* situation, they provide more cellular context for HAT activities compared to previously used recombinant protein acetylation assays. To further reduce the risk of culture artefacts often seen in cancer cell lines, some of which have been cultured for more than half a century, I also used primary cells isolated from mouse embryos and foetuses. Most data, however, were surprisingly similar in human and mouse cells, suggesting a general role of TIP60 largely independent of cellular environment. One such general function might be a role in facilitating efficient transcription through H2AZ acetylation. Identifying H2AZK7 and H2AZK4 as endogenous histone acetylation targets of TIP60 in a number of human and mouse cell types under a variety of conditions is an important step in understanding the role of TIP60 and its histone acetylation function. A comparison between previously published TIP60 histone acetylation targets with histone acetylation targets that were found to be reduced upon loss of TIP60 in this study is displayed in Table 10. Furthermore, identification of H2AZK7 acetylation as a biomarker and the finding that loss of TIP60 induces cell cycle arrest independent of the tumour suppressors TP53, $p16^{INK4A}$ and $p19^{ARF}$ are essential steps for the assessment of TIP60 as a potential therapeutic target. Investigating TIP60 as a therapeutic target and developing small molecules modulating its activity might have implications in a wide range of diseases, such as obesity, diabetes and other metabolic diseases (Iyer et al., 2012).

Table 10: TIP60 histone acetylation targets. Summary of TIP60 histone acetylation targets found reduced in genetic loss of TIP60 systems in this study compared to

previously published TIP60 histone acetylation targets. [+] indicates that acetylation target was reduced in only some of the assessed cell types and to a minor extent; +++ indicates consistent reduction of acetylation target; – indicates no effect on acetylation target upon loss of TIP60.

Acetylation	**Found in this study**	**Reference**
H2A K5	[+]	(Kimura and Horikoshi, 1998; Jacquet et al. 2016; Jeong et al. 2011)
H2AZ K4-7-11	+++	(Dalvai et al. 2013; Giaimo et al. 2018)
H2AZ K4	+++	N/A
H2AZ K7	+++	N/A
H3 K14	–	(Kimura and Horikoshi, 1998)
H4 K4-8-12-16	N/A	(Ikura et al. 2000; Jacquet et al. 2016)
H4 K5	[+]	(Kimura and Horikoshi, 1998)
H4 K8	[+]	(Kimura and Horikoshi, 1998)
H4 K12	[+]	(Kimura and Horikoshi, 1998)
H4 K16	[+]	(Kimura and Horikoshi, 1998)

H2AZ was shown to accumulate at the promoter region of genes (Barski et al., 2007). The accumulation of H2AZ, however, correlated with both decreased barrier for RNAPII transcription (Weber et al., 2014) as well as paused RNAPII (Day et al., 2016). These contradicting observations might be due to differential H2AZ PTMs such as acetylation, which was shown to accumulate at NICD-ER target genes, while H2AZ occupancy decreased (Giaimo et al., 2018). Thus, I hypothesise a possible function of TIP60 in activating gene transcription via H2AZ acetylation at paused RNAPII promoters (Figure 9.1A). To verify this hypothesis, I will have to establish whether loss of TIP60 results in a global reduction of transcription. This can be achieved through RNA-sequencing experiments utilizing a spike-in to standardize between samples and so assess potential global reduction in mRNA upon *TIP60* deletion.

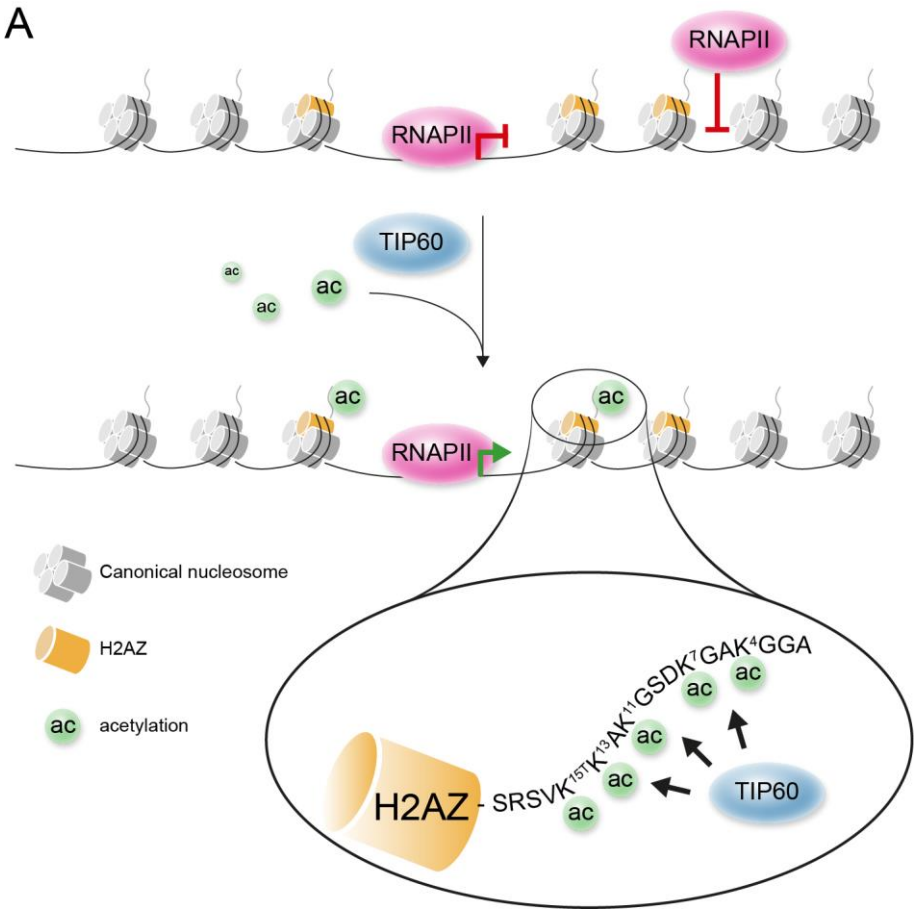

Figure 9.1: Proposed role of TIP60 in gene transcription. (A) Schematic drawing showing a closed chromatin organisation and paused RNAPII with unmodified H2AZ. Upon gene activation, H2AZ is acetylated by TIP60 at N-terminal lysines, which is associated with open and accessible chromatin structure and active gene transcription.

Global histone modification patterns can be used as prognostic markers to classify glioma types (Liu et al., 2010) and lung cancer (Barlesi et al., 2007), suggesting that H2AZ acetylation might be useful as a prognostic marker itself. Importantly, various KATs have been shown to be dysregulated in cancer and prognostic marker for poor survival, for example hMOF (Song et al., 2011), GCN5 (Chen et al., 2013a), and EP300 (Hou et al., 2012) in non-small-cell lung carcinoma (NSCLC). Studies showed that EP300 inhibition leads to impaired DNA damage response in melanoma cells and increased DNA damage induced apoptosis (Yan et al., 2013).

Previous studies showed an increase of apoptosis in *Tip60* knockout blastocysts (Hu et al., 2009), while I observed no increase in apoptosis upon induced deletion of *TIP60* in cultured cells, suggesting that the cellular environment or cell type plays an important role in regulating TIP60 functions. Further, loss of TIP60 was shown to correlate with increased DNA damage accumulation and reduced apoptosis upon DNA damage inducing treatment (Sun et al., 2005; Sun et al., 2009). The lack of DNA damage accumulation upon loss of TIP60 in this study, shows that loss of TIP60 alone does not lead to DNA damage in normal culture conditions.

9.2 Discrepancies with previous studies

In this study, I found that a major effect of loss of TIP60 was a profound reduction in H2AZ acetylation. H2A and H4 acetylation was either not altered or reduced only modestly and only in some of cell types, but not in all experiments. In contrast, previous reports proposed H4 as a direct TIP60 acetylation target (Kimura and Horikoshi, 1998). While I cannot exclude the possibility that TIP60 contributes to H4 acetylation, H4 certainly did not appear to be the major target. Alternatively, the critical function of TIP60 in H4 acetylation may be compensated for by functional redundancies with other HATs. The discrepancies in arriving at different major acetylation targets for TIP60 might stem from differences in experimental approaches and methods deployed, such as cell-free acetylation assay vs. assessment within the cellular context, RNAi knockdown vs. genetic deletion, ChIP-seq, western blots and TIP60 overexpression. While cell-free assays allow the conclusion that TIP60 can acetylate H4 (Kimura and Horikoshi, 1998), they do not predict if TIP60 acetylates H4 in the context of the TIP60 complex in a cell. However, the fact that I found H2AZ acetylation most affected by loss of TIP60 in the context of

different cell types does not rule out the possibility that the acetylation of H2AZ might be affected indirectly by the loss of TIP60. Nevertheless, I showed here (Figure 6.1) and others showed previously (Colino-Sanguino et al., 2019) that TIP60 can acetylated H2AZ in a cell-free system. Therefore, it is highly likely that H2AZ is a major acetylation target of TIP60 in cells. In addition, H4 appears to be a lesser target in the cell types used in these experiments. The plasticity of organisms may explain some of the discrepancies, where if an important protein is deleted from a cell, other mechanisms are upregulated to compensate for the lack of that protein, which might be cell type specific and dependent on the method deployed to facilitate the deletion.

Murine ESC expressing a catalytic inactive TIP60 mutant were shown to proliferate, albeit slower compared to wildtype mESC (Acharya et al., 2017). One possibility for this discrepancy is that ESCs might depend on different KATs other than TIP60 compared to more differentiated cell types and redundancies between HATs might be wider in ESCs. Further, H2AZ acetylation might be essential for cell proliferation in differentiated cells, but not ESC or H2AZ acetylation is mediated through different HATs in ESC upon loss of TIP60.

9.3 Limitations and open questions

In this study, I induced the mutation or deletion of the *TIP60* gene, which does not allow for investigation of acetylation dynamics, which have been shown to be in the minutes to hours range (Weinert et al., 2018).

Although, H2AZ itself was shown to play an important role in cell division and acetylation is critical for the function of H2AZ. The investigation of acetylation of key proteins required for chromosome dynamics during mitosis, such as α-tubulin, aurora

kinases, condensin and other centromere interacting proteins in *TIP60* knockout cells might uncover novel roles of TIP60 in cell division, in addition to and possibly independent of its function as a transcriptional co-regulator.

Methylation of H2AZ lysines 4 and 7 has been reported to suppress gene transcription (Binda et al., 2013). The investigation of the effects of TIP60 on the potentially opposing effects of methylation and acetylation of H2AZ lysines 4 and 7 might help to clarify its role in gene transcription and in particular its role at bivalent genes in ESC, which were shown to harbour both modifications (Ku et al., 2012).

Furthermore, the induced CRISPR/Cas9 *TIP60* knockout or catalytically inactive TIP60 can be used to model potential TIP60 inhibition in combination with current cancer therapeutics to assess a potential synergistic effect in a wide range of cancers.

9.4 Significance of the research

The research results presented here advances the understanding of the molecular and cellular functions of TIP60. The finding that loss of either TIP60 entirely or the histone acetylation function of TIP60 leads to cell cycle arrest suggest that TIP60-specific small molecule inhibitors might be useful for the treatment of cancer. The observation that cell cycle arrest due to the loss of TIP60 is independent of the tumour suppressors TP53, $p16^{INK4A}$ and $p19^{ARF}$ suggests that inhibition of TIP60 could be useful in the treatment of the many cancers that have loss of function mutation in the *TP53* or null mutations of the *CDKN2A/CDKN2B* locus encoding $p16^{INK4A}$, $p19^{ARF}$ and $p15^{Ink4b}$. There may be a potential use for TIP60 inhibitors as an anti-cancer drug target, whereby inhibition of TIP60 may sensitize cells to DNA damage inducing agents. Another opportunity for TIP60 inhibition in cancer treatment may present itself in cancers with low expression

levels of TIP60, by inducing a cell-lethal loss of TIP60 in the cancer cells, while keeping viable cells above the lethal TIP60 threshold (Brown et al., 2016; Gao et al., 2014).

The identification of the acetylation targets of TIP60 is an essential step in the development of TIP60-specific inhibitors. In this context, work presented in this thesis suggests that H2AZ lysine 7 acetylation would be a particularly specific read-out for TIP60 function. The broader characterization of TIP60 illuminates its role in development and embryonic stem cell biology.

Chapter 10 Appendix

10.1 Total number of RNA-sequencing reads per library

Table 11: Total number of mapped reads per RNA-sequencing library.

Library	**Number of mapped sequencing reads**
Tip60$^{iKO/iKO}$;ERT2 MEF 3 days 1 (KO_3D_1)	25966327
Tip60$^{iKO/iKO}$;ERT2 MEF 3 days 2 (KO_3D_2)	44844743
Tip60$^{iKO/iKO}$;ERT2 MEF 3 days 3 (KO_3D_3)	2512975
Tip60$^{iKO/iKO}$;ERT2 MEF 3 days 4 (KO_3D_4)	11942530
Tip60$^{iKO/iKO}$;ERT2 MEF 5 days 1 (KO_5D_1)	31552772
Tip60$^{iKO/iKO}$;ERT2 MEF 5 days 2 (KO_5D_2)	15649991
Tip60$^{iKO/iKO}$;ERT2 MEF 5 days 3 (KO_5D_3)	22524297
Tip60$^{iKO/iKO}$;ERT2 MEF 5 days 4 (KO_5D_4)	18205962
Tip60$^{+/+}$;ERT2 MEF 3 days 1 (C_3D_1)	10586113
Tip60$^{+/+}$;ERT2 MEF 3 days 2 (C_3D_2)	15022993
Tip60$^{+/+}$;ERT2 MEF 3 days 3 (C_3D_3)	12731188
Tip60$^{+/+}$;ERT2 MEF 3 days 4 (C_3D_4)	8554774
Tip60$^{+/+}$;ERT2 MEF 5 days 1 (C_5D_1)	17673369
Tip60$^{+/+}$;ERT2 MEF 5 days 2 (C_5D_2)	22268708
Tip60$^{+/+}$;ERT2 MEF 5 days 3 (C_5D_3)	6987679
Tip60$^{+/+}$;ERT2 MEF 5 days 4 (C_5D_4)	16435287
iC-TIP60 HEK293 sgRNA#1 1 (KO_sgRNA1_1)	19567415
iC-TIP60 HEK293 sgRNA#1 2 (KO_sgRNA1_2)	15411602
iC-TIP60 HEK293 sgRNA#2 1 (KO_sgRNA2_1)	21735884
iC-TIP60 HEK293 sgRNA#2 2 (KO_sgRNA2_2)	17414394
HEK293 sgRNA#1 1 (C_sgRNA1_1)	14557407
HEK293 sgRNA#1 2 (C_sgRNA1_2)	4387017
HEK293 sgRNA#2 1 (C_sgRNA2_1)	16987280
HEK293 sgRNA#2 2 (C_sgRNA2_2)	14425801

10.2 Genes differentially expressed in TIP60 depleted cells

Table 12: Top 50 genes downregulated in *Tip60$^{iKO/iKO}$;ERT2* MEF vs. *Tip60$^{+/+}$;ERT2* MEFs 3 days after tamoxifen treatment

Symbol	Full name	Log^{2}FC	FDR
Emp2	epithelial membrane protein 2	-2.4	1.47E-09
Aldh1l2	aldehyde dehydrogenase 1 family, member L2	-2.6	2.59E-09
Pck2	phosphoenolpyruvate carboxykinase 2 (mitochondrial)	-2.2	9.12E-09
Slc6a9	solute carrier family 6 (neurotransmitter transporter, glycine), member 9	-3.1	9.20E-09
Ppp1r15a	protein phosphatase 1, regulatory subunit 15A	-2.1	1.61E-08
Hsp90b1	heat shock protein 90, beta (Grp94), member 1	-1.9	1.61E-08
Acot2	acyl-CoA thioesterase 2	-2.1	2.34E-08
Trim46	tripartite motif-containing 46	-2.4	2.44E-08
Cth	cystathionase (cystathionine gamma-lyase)	-2.4	4.04E-08
Sdf2l1	stromal cell-derived factor 2-like 1	-1.8	4.04E-08
Ddit3	DNA-damage inducible transcript 3	-2.0	4.23E-08
Zbtb7b	zinc finger and BTB domain containing 7B	-1.4	4.23E-08
Cpeb1	cytoplasmic polyadenylation element binding protein 1	-2.2	4.23E-08
Erlin1	ER lipid raft associated 1	-1.3	5.27E-08
Chac1	ChaC, cation transport regulator 1	-1.9	5.28E-08
Phf23	PHD finger protein 23	-1.6	5.28E-08
Sars	seryl-aminoacyl-tRNA synthetase	-1.5	5.28E-08
Hspa5	heat shock protein 5	-1.9	6.82E-08
Pla2g12a	phospholipase A2, group XIIA	-1.5	6.82E-08
Flcn	folliculin	-1.3	7.22E-08
Stx4a	syntaxin 4A (placental)	-1.5	1.07E-07
Creld2	cysteine-rich with EGF-like domains 2	-2.1	1.25E-07
Manf	mesencephalic astrocyte-derived neurotrophic factor	-1.6	1.25E-07
Chka	choline kinase alpha	-1.5	1.25E-07

Gadd45a	growth arrest and DNA-damage-inducible 45 alpha	-1.4	1.57E-07
Hyou1	hypoxia up-regulated 1	-1.5	1.73E-07
Tgif1	TGFB-induced factor homeobox 1	-1.4	1.84E-07
Chd3	chromodomain helicase DNA binding protein 3	-1.1	1.84E-07
Pdia4	protein disulfide isomerase associated 4	-1.8	2.01E-07
Pogk	pogo transposable element with KRAB domain	-1.2	2.01E-07
Mex3a	mex3 RNA binding family member A	-1.0	2.01E-07
Gtpbp2	GTP binding protein 2	-1.3	2.08E-07
Psph	phosphoserine phosphatase	-2.0	2.30E-07
Wars	tryptophanyl-tRNA synthetase	-1.6	2.30E-07
Slc38a7	solute carrier family 38, member 7	-1.7	2.35E-07
Calr	calreticulin	-1.5	2.38E-07
Car6	carbonic anhydrase 6	-2.8	2.44E-07
Galnt7	polypeptide N-acetylgalactosaminyltransferase 7	-1.2	2.91E-07
Stau2	staufen double-stranded RNA binding protein 2	-1.6	2.92E-07
Sep-05	septin 5	-1.5	2.94E-07
Npc1	NPC intracellular cholesterol transporter 1	-1.2	2.94E-07
Ptrh1	peptidyl-tRNA hydrolase 1 homolog	-1.4	3.17E-07
Dlg2	discs large MAGUK scaffold protein 2	-2.8	3.18E-07
Herpud1	homocysteine-inducible, endoplasmic reticulum stress-inducible, ubiquitin-like domain member 1	-1.9	3.18E-07
Cyb5r1	cytochrome b5 reductase 1	-1.7	3.18E-07
Otub2	OTU domain, ubiquitin aldehyde binding 2	-1.6	3.18E-07
Gnpnat1	glucosamine-phosphate N-acetyltransferase 1	-1.5	3.18E-07
Ticam1	toll-like receptor adaptor molecule 1	-1.3	3.18E-07
Gga2	golgi associated, gamma adaptin ear containing, ARF binding protein 2	-1.2	3.18E-07
Eif4b	eukaryotic translation initiation factor 4B	-0.9	3.18E-07

Table 13: Top 50 genes upregulated in *Tip60$^{iKO/iKO}$;ERT2* MEF vs. *Tip60$^{+/+}$;ERT2* MEFs 3 days after tamoxifen treatment

Symbol	**Full name**	**Log$_2$FC**	**FDR**

Synpo	synaptopodin	1.9	9.12E-09
Sfrp1	secreted frizzled-related protein 1	3.9	4.54E-08
Fst	follistatin	2.5	1.84E-07
Irs1	insulin receptor substrate 1	1.6	3.17E-07
Cd248	CD248 antigen, endosialin	1.6	3.87E-07
Plau	plasminogen activator, urokinase	1.7	5.92E-07
Daam2	dishevelled associated activator of morphogenesis 2	1.9	5.92E-07
Ldhb	lactate dehydrogenase B	1.8	6.92E-07
Lrrc32	leucine rich repeat containing 32	1.6	6.95E-07
Krt80	keratin 80	1.4	9.95E-07
H19	H19, imprinted maternally expressed transcript	1.9	9.95E-07
Snx18	sorting nexin 18	1.0	1.32E-06
Fras1	Fraser extracellular matrix complex subunit 1	2.2	1.35E-06
Mylk	myosin, light polypeptide kinase	3.8	1.56E-06
Tmem260	transmembrane protein 260	1.4	1.60E-06
Camk2g	calcium/calmodulin-dependent protein kinase II gamma	1.0	1.72E-06
Fzd1	frizzled class receptor 1	1.8	1.72E-06
Peg3	paternally expressed 3	2.4	1.73E-06
Ngly1	N-glycanase 1	1.1	1.77E-06
Abat	4-aminobutyrate aminotransferase	2.2	1.90E-06
Zhx1	zinc fingers and homeoboxes 1	1.8	2.14E-06
Snai1	snail family zinc finger 1	1.3	2.27E-06
Kctd12	potassium channel tetramerisation domain containing 12	2.1	2.30E-06
Mdga1	MAM domain containing glycosylphosphatidylinositol anchor 1	2.0	2.63E-06

Mknk2	MAP kinase-interacting serine/threonine kinase 2	1.2	2.65E-06
Ctnnb1	catenin (cadherin associated protein), beta 1	0.7	2.65E-06
Arrdc3	arrestin domain containing 3	1.7	2.65E-06
Rdh10	retinol dehydrogenase 10 (all-trans)	1.7	2.65E-06
Pcca	propionyl-Coenzyme A carboxylase, alpha polypeptide	1.3	2.67E-06
Tmem100	transmembrane protein 100	6.1	3.47E-06
Tmem2	transmembrane protein 2	1.4	3.51E-06
Bahcc1	BAH domain and coiled-coil containing 1	1.0	3.57E-06
Enpp4	ectonucleotide pyrophosphatase/phosphodiesterase 4	1.5	3.62E-06
Smarca2	SWI/SNF related, matrix associated, actin dependent regulator of chromatin, subfamily a, member 2	1.2	3.90E-06
Zfp503	zinc finger protein 503	1.4	4.06E-06
Lmo7	LIM domain only 7	1.4	4.09E-06
Fstl1	follistatin-like 1	1.3	4.50E-06
Lima1	LIM domain and actin binding 1	1.0	4.60E-06
Emilin1	elastin microfibril interfacer 1	2.1	4.64E-06
Recql	RecQ protein-like	1.1	4.67E-06
Cpd	carboxypeptidase D	1.0	4.69E-06
Lrp11	low density lipoprotein receptor-related protein 11	1.9	4.69E-06
Ext2	exostoses (multiple) 2	0.8	4.74E-06
Tln2	talin 2	0.9	4.92E-06
Egfr	epidermal growth factor receptor	2.0	5.03E-06
Sgk1	serum/glucocorticoid regulated kinase 1	1.0	5.94E-06
Sdc1	syndecan 1	1.2	6.03E-06
Dkk3	dickkopf WNT signaling pathway inhibitor 3	2.7	6.03E-06

Igfbp5	insulin-like growth factor binding protein 5	2.2	6.27E-06
B230118H07Rik	RIKEN cDNA B230118H07 gene	1.3	6.37E-06

Table 14: Top 50 genes downregulated in *iC-TIP60* vs. control HEK293 cells 3 days after dox treatment

Symbol	**Full name**	**Log^{2}FC**	**FDR**
TRIP6	thyroid hormone receptor interactor 6	-1.4	4.58E-13
SLC19A1	solute carrier family 19 member 1	-1.2	1.00E-12
STEAP3	STEAP3 metalloreductase	-1.2	1.28E-12
ANP32A	acidic nuclear phosphoprotein 32 family member A	-1.0	5.03E-12
B4GALT2	beta-1,4-galactosyltransferase 2	-1.1	5.32E-12
KAT5	lysine acetyltransferase 5	-1.3	9.10E-12
ITPR3	inositol 1,4,5-trisphosphate receptor type 3	-1.1	1.09E-11
TUB	tubby bipartite transcription factor	-1.0	1.11E-11
DBNDD1	dysbindin domain containing 1	-1.1	1.77E-11
COL4A1	collagen type IV alpha 1 chain	-1.0	1.79E-11
RAC3	Rac family small GTPase 3	-0.9	1.79E-11
CKB	creatine kinase B	-0.8	2.09E-11
JAG2	jagged 2	-1.3	2.14E-11
HDGF	heparin binding growth factor	-1.0	2.30E-11
FAM136A	family with sequence similarity 136 member A	-0.9	2.34E-11
SCD	stearoyl-CoA desaturase	-0.9	2.36E-11
ALDOA	aldolase, fructose-bisphosphate A	-0.8	2.41E-11
NME3	NME/NM23 nucleoside diphosphate kinase 3	-1.5	2.59E-11
ANP32E	acidic nuclear phosphoprotein 32 family member E	-1.0	2.63E-11
METTL7A	methyltransferase like 7A	-1.2	2.81E-11
LRFN4	leucine rich repeat and fibronectin type III domain containing 4	-1.4	3.39E-11
SNTB1	syntrophin beta 1	-1.3	3.42E-11
ADGRL1	adhesion G protein-coupled receptor L1	-1.0	3.48E-11

ASIC1	acid sensing ion channel subunit 1	-1.0	3.74E-11
DHCR7	7-dehydrocholesterol reductase	-0.9	4.05E-11
CARM1	coactivator associated arginine methyltransferase 1	-0.8	4.31E-11
KCTD15	potassium channel tetramerization domain containing 15	-1.1	4.43E-11
SLC25A1	solute carrier family 25 member 1	-0.9	4.75E-11
B4GALNT4	beta-1,4-N-acetyl-galactosaminyltransferase 4	-1.5	5.86E-11
ACAT2	acetyl-CoA acetyltransferase 2	-0.9	6.07E-11
TMEM123	transmembrane protein 123	-1.0	6.07E-11
SOX12	SRY-box 12	-1.3	6.34E-11
UBL4A	ubiquitin like 4A	-1.0	6.68E-11
DBN1	drebrin 1	-1.0	6.83E-11
MEX3A	mex-3 RNA binding family member A	-1.2	7.27E-11
AK4	adenylate kinase 4	-1.0	7.60E-11
CDC42EP1	CDC42 effector protein 1	-1.1	8.27E-11
CCND1	cyclin D1	-0.9	8.55E-11
NPM3	nucleophosmin/nucleoplasmin 3	-1.0	8.57E-11
TYRO3	TYRO3 protein tyrosine kinase	-1.0	8.73E-11
CYBA	cytochrome b-245 alpha chain	-0.9	8.83E-11
COL4A2	collagen type IV alpha 2 chain	-0.8	9.03E-11
ZNF618	zinc finger protein 618	-1.1	9.62E-11
CDCA7	cell division cycle associated 7	-0.8	1.00E-10
ANP32B	acidic nuclear phosphoprotein 32 family member B	-0.8	1.02E-10
TRABD	TraB domain containing	-1.1	1.13E-10
MICALL1	MICAL like 1	-0.8	1.13E-10
LMNB1	lamin B1	-0.8	1.24E-10
SLC18B1	solute carrier family 18 member B1	-1.1	1.29E-10
CCND2	cyclin D2	-1.3	1.42E-10

Table 15: Top 50 genes upregulated in *iC-TIP60* vs. control HEK293 cells 3 days after dox treatment

Symbol	**Full name**	**Log^{2}FC**	**FDR**
EFNB2	ephrin B2	2.7	3.26E-20
PCDH9	protocadherin 9	2.6	3.79E-18
ADAMTS1	ADAM metallopeptidase with thrombospondin type 1 motif 1	1.6	6.45E-17
NPTX2	neuronal pentraxin 2	2.9	6.45E-17
HEXIM1	hexamethylene bisacetamide inducible 1	1.8	2.52E-16
FOXC1	forkhead box C1	1.4	4.04E-16
TUBB3	tubulin beta 3 class III	3.2	4.62E-16
PCDH10	protocadherin 10	1.9	4.62E-16
KCTD12	potassium channel tetramerization domain containing 12	2.0	7.13E-16
ZCCHC12	zinc finger CCHC-type containing 12	3.8	8.12E-16
TSC22D2	TSC22 domain family member 2	2.0	8.95E-16
HIST1H2BK	histone cluster 1 H2B family member k	1.9	9.54E-16
IRS2	insulin receptor substrate 2	1.4	1.88E-15
FZD8	frizzled class receptor 8	2.0	3.60E-15
NPTXR	neuronal pentraxin receptor	2.2	9.97E-15
NRARP	NOTCH regulated ankyrin repeat protein	2.2	2.22E-14
BMP2	bone morphogenetic protein 2	1.9	2.55E-14
SERPINE2	serpin family E member 2	1.9	2.66E-14
KCNC3	potassium voltage-gated channel subfamily C member 3	3.0	3.15E-14
JUN	Jun proto-oncogene, AP-1 transcription factor subunit	1.7	3.15E-14
GADD45B	growth arrest and DNA damage inducible beta	3.7	4.14E-14
ZIC2	Zic family member 2	1.3	6.45E-14
CITED2	Cbp/p300 interacting transactivator with Glu/Asp rich carboxy-terminal domain 2	1.7	6.83E-14
ZSWIM6	zinc finger SWIM-type containing 6	1.3	7.25E-14

TENT5C	terminal nucleotidyltransferase 5C	2.2	7.82E-14
PCDH17	protocadherin 17	1.4	1.04E-13
SPEN	spen family transcriptional repressor	1.1	1.04E-13
PCDH19	protocadherin 19	2.6	1.29E-13
CDKN2B	cyclin dependent kinase inhibitor 2B	1.5	1.37E-13
HIST1H1C	histone cluster 1 H1 family member c	2.7	1.37E-13
ARC	activity regulated cytoskeleton associated protein	4.0	1.45E-13
MAP2	microtubule associated protein 2	2.6	1.77E-13
H1F0	H1 histone family member 0	1.8	2.49E-13
CEMIP2	cell migration inducing hyaluronidase 2	1.3	5.74E-13
PNPLA8	patatin like phospholipase domain containing 8	1.3	9.77E-13
H2AFX	H2A histone family member X	1.0	9.86E-13
RFPL4A	ret finger protein like 4A	4.4	1.03E-12
WDR47	WD repeat domain 47	1.4	1.03E-12
TUFT1	tuftelin 1	1.8	1.16E-12
ERRFI1	ERBB receptor feedback inhibitor 1	1.6	1.51E-12
CLU	clusterin	1.3	1.81E-12
SERPINI1	serpin family I member 1	2.5	1.95E-12
LGR5	leucine rich repeat containing G protein-coupled receptor 5	1.2	2.21E-12
TUBB4B	tubulin beta 4B class IVb	1.0	2.47E-12
RND3	Rho family GTPase 3	1.2	2.64E-12
FAM222A	family with sequence similarity 222 member A	1.9	2.93E-12
SORBS1	sorbin and SH3 domain containing 1	1.7	3.50E-12
EFR3B	EFR3 homolog B	1.6	3.78E-12
ZNF711	zinc finger protein 711	1.5	3.89E-12
TPPP	tubulin polymerization promoting protein	1.8	4.12E-12

10.3 GO terms for biological processes dysregulated in TIP60 depleted cells

Table 16: Top50 GO terms in *Tip60$^{iKO/iKO}$;ERT2* MEF vs. *Tip60$^{+/+}$;ERT2* MEFs for biological processes enriched among genes downregulated in the absence of TIP60 3 days after tamoxifen treatment

GO number	Go term	%	p
GO:0043604	amide biosynthetic process	41%	2.68E-21
GO:0006412	translation	42%	4.47E-21
GO:0022613	ribonucleoprotein complex biogenesis	46%	5.06E-21
GO:0042254	ribosome biogenesis	50%	9.78E-21
GO:0010467	gene expression	29%	1.29E-20
GO:0043043	peptide biosynthetic process	41%	2.89E-20
GO:0043603	cellular amide metabolic process	38%	4.33E-20
GO:0006518	peptide metabolic process	39%	1.60E-18
GO:0044267	cellular protein metabolic process	29%	1.74E-16
GO:0044237	cellular metabolic process	27%	4.15E-16
GO:0034660	ncRNA metabolic process	42%	6.04E-16
GO:0016072	rRNA metabolic process	50%	6.48E-16
GO:0044271	cellular nitrogen compound biosynthetic process	29%	1.67E-15
GO:0034641	cellular nitrogen compound metabolic process	28%	2.77E-15
GO:0044238	primary metabolic process	27%	4.35E-15
GO:0002181	cytoplasmic translation	64%	1.73E-14
GO:0043170	macromolecule metabolic process	27%	2.00E-14
GO:0006364	rRNA processing	50%	2.94E-14
GO:0006807	nitrogen compound metabolic process	27%	6.04E-14
GO:0009058	biosynthetic process	28%	7.00E-14
GO:0071704	organic substance metabolic process	27%	1.29E-13
GO:1901576	organic substance biosynthetic process	28%	1.37E-13
GO:0044260	cellular macromolecule metabolic process	27%	1.41E-13
GO:0019538	protein metabolic process	28%	2.15E-13
GO:0042273	ribosomal large subunit biogenesis	66%	2.45E-13
GO:0044249	cellular biosynthetic process	28%	7.11E-13
GO:0034470	ncRNA processing	42%	1.29E-12

GO:0008152	metabolic process	26%	1.64E-12
GO:0006396	RNA processing	35%	2.32E-12
GO:0042274	ribosomal small subunit biogenesis	63%	4.96E-12
GO:1901564	organonitrogen compound metabolic process	28%	5.55E-12
GO:0009059	macromolecule biosynthetic process	28%	7.04E-12
GO:0034645	cellular macromolecule biosynthetic process	28%	1.10E-11
GO:1901566	organonitrogen compound biosynthetic process	32%	1.14E-11
GO:0016070	RNA metabolic process	28%	1.64E-11
GO:0046907	intracellular transport	32%	6.68E-11
GO:0051649	establishment of localization in cell	31%	8.84E-11
GO:0051641	cellular localization	30%	1.14E-10
GO:0031329	regulation of cellular catabolic process	36%	1.40E-10
GO:0016569	covalent chromatin modification	38%	3.14E-10
GO:0006914	autophagy	39%	4.49E-10
GO:0061919	process utilizing autophagic mechanism	39%	4.49E-10
GO:0009894	regulation of catabolic process	34%	6.69E-10
GO:0016570	histone modification	38%	9.24E-10
GO:0006325	chromatin organization	35%	1.01E-09
GO:0090304	nucleic acid metabolic process	28%	1.01E-09
GO:0042255	ribosome assembly	61%	1.75E-09
GO:0016192	vesicle-mediated transport	32%	3.79E-09
GO:0006810	transport	28%	4.34E-09
GO:0051234	establishment of localization	28%	4.65E-09

Table 17: Top50 GO terms in *Tip60$^{iKO/iKO}$;ERT2* MEF vs. *Tip60$^{+/+}$;ERT2* MEF for biological processes enriched among genes upregulated in the absence of TIP60 3 days after tamoxifen treatment

GO number	**GO term**	**%**	**p**
GO:0009888	tissue development	30%	7.08E-18
GO:0048731	system development	26%	1.16E-17
GO:0048513	animal organ development	27%	5.59E-17
GO:0032501	multicellular organismal process	24%	1.47E-16

GO:0009653	anatomical structure morphogenesis	27%	3.98E-16
GO:0009887	animal organ morphogenesis	31%	1.67E-14
GO:0001501	skeletal system development	36%	5.39E-14
GO:0007275	multicellular organism development	25%	6.36E-14
GO:0051216	cartilage development	46%	6.10E-13
GO:0072359	circulatory system development	30%	6.89E-13
GO:0032502	developmental process	24%	9.35E-13
GO:0030198	extracellular matrix organization	43%	1.01E-12
GO:0048856	anatomical structure development	24%	1.30E-12
GO:0035295	tube development	30%	1.64E-12
GO:0007166	cell surface receptor signaling pathway	27%	3.33E-12
GO:0061448	connective tissue development	41%	3.49E-12
GO:0007167	enzyme linked receptor protein signaling pathway	31%	1.04E-11
GO:0030154	cell differentiation	25%	1.06E-11
GO:0043062	extracellular structure organization	40%	1.56E-11
GO:0035239	tube morphogenesis	30%	2.14E-11
GO:0001503	ossification	37%	2.27E-11
GO:0007155	cell adhesion	29%	4.49E-11
GO:0003008	system process	29%	5.44E-11
GO:0022610	biological adhesion	29%	7.29E-11
GO:0002062	chondrocyte differentiation	51%	7.51E-11
GO:0048598	embryonic morphogenesis	32%	8.93E-11
GO:0072001	renal system development	38%	9.70E-11
GO:0001655	urogenital system development	37%	1.52E-10
GO:0048705	skeletal system morphogenesis	39%	3.63E-10
GO:0048869	cellular developmental process	24%	4.75E-10
GO:0001944	vasculature development	31%	5.05E-10
GO:0035107	appendage morphogenesis	42%	5.08E-10
GO:0035108	limb morphogenesis	42%	5.08E-10
GO:0007507	heart development	32%	5.83E-10
GO:0001822	kidney development	38%	6.23E-10
GO:0048729	tissue morphogenesis	31%	6.36E-10

GO:0072358	cardiovascular system development	30%	7.80E-10
GO:0010463	mesenchymal cell proliferation	58%	1.22E-09
GO:0001568	blood vessel development	31%	1.42E-09
GO:0048646	anatomical structure formation involved in morphogenesis	29%	1.49E-09
GO:0051239	regulation of multicellular organismal process	25%	1.78E-09
GO:0050673	epithelial cell proliferation	34%	1.79E-09
GO:0060485	mesenchyme development	38%	2.01E-09
GO:0023052	signaling	24%	2.51E-09
GO:0060349	bone morphogenesis	50%	2.96E-09
GO:0007154	cell communication	24%	4.10E-09
GO:0048762	mesenchymal cell differentiation	38%	1.17E-08
GO:0048736	appendage development	39%	1.50E-08
GO:0060173	limb development	39%	1.50E-08
GO:0035113	embryonic appendage morphogenesis	42%	1.89E-08

Table 18: Top50 GO terms in *iC-TIP60* vs. control HEK293 cells for biological processes enriched among genes downregulated in the absence of TIP60 3 days after dox treatment

GO number	**Go term**	**%**	**p**
GO:0008150	biological_process	22%	3.32E-21
GO:0044237	cellular metabolic process	23%	8.34E-21
GO:0009987	cellular process	22%	2.13E-20
GO:0008152	metabolic process	23%	3.40E-20
GO:0071704	organic substance metabolic process	23%	5.88E-20
GO:0044238	primary metabolic process	23%	5.79E-19
GO:0006807	nitrogen compound metabolic process	23%	8.63E-16
GO:0034641	cellular nitrogen compound metabolic process	24%	1.10E-14
GO:1901360	organic cyclic compound metabolic process	24%	4.68E-13
GO:1901576	organic substance biosynthetic process	24%	5.30E-13
GO:0009058	biosynthetic process	24%	7.74E-13
GO:0044249	cellular biosynthetic process	23%	4.55E-12
GO:0046483	heterocycle metabolic process	23%	8.34E-12

GO:0006725	cellular aromatic compound metabolic process	23%	1.57E-11
GO:0006139	nucleobase-containing compound metabolic process	23%	1.75E-11
GO:0051276	chromosome organization	28%	7.83E-11
GO:0044271	cellular nitrogen compound biosynthetic process	24%	2.65E-10
GO:0044283	small molecule biosynthetic process	31%	4.81E-10
GO:0044281	small molecule metabolic process	26%	8.68E-10
GO:1902653	secondary alcohol biosynthetic process	56%	1.82E-09
GO:0043170	macromolecule metabolic process	22%	2.38E-09
GO:0044260	cellular macromolecule metabolic process	23%	3.19E-09
GO:0016126	sterol biosynthetic process	54%	3.65E-09
GO:0006695	cholesterol biosynthetic process	54%	1.39E-08
GO:0010558	negative regulation of macromolecule biosynthetic process	27%	1.98E-08
GO:0009890	negative regulation of biosynthetic process	26%	2.39E-08
GO:0031327	negative regulation of cellular biosynthetic process	26%	3.35E-08
GO:0019222	regulation of metabolic process	23%	4.92E-08
GO:0080090	regulation of primary metabolic process	23%	5.06E-08
GO:2000113	negative regulation of cellular macromolecule biosynthetic process	26%	7.30E-08
GO:0010467	gene expression	23%	8.48E-08
GO:0051172	negative regulation of nitrogen compound metabolic process	25%	8.71E-08
GO:1901362	organic cyclic compound biosynthetic process	23%	8.82E-08
GO:1902652	secondary alcohol metabolic process	43%	9.11E-08
GO:0090304	nucleic acid metabolic process	23%	1.38E-07
GO:0016125	sterol metabolic process	42%	1.47E-07
GO:0140053	mitochondrial gene expression	39%	1.51E-07
GO:0008203	cholesterol metabolic process	43%	1.53E-07
GO:0009124	nucleoside monophosphate biosynthetic process	38%	2.19E-07
GO:1990542	mitochondrial transmembrane transport	45%	2.23E-07
GO:0031323	regulation of cellular metabolic process	23%	2.60E-07
GO:0051171	regulation of nitrogen compound metabolic process	23%	2.82E-07

GO:1901566	organonitrogen compound biosynthetic process	25%	3.56E-07
GO:0031324	negative regulation of cellular metabolic process	25%	3.96E-07
GO:0010605	negative regulation of macromolecule metabolic process	24%	5.64E-07
GO:1901564	organonitrogen compound metabolic process	23%	7.30E-07
GO:0009156	ribonucleoside monophosphate biosynthetic process	37%	8.03E-07
GO:0045934	negative regulation of nucleobase-containing compound metabolic process	26%	8.23E-07
GO:0060255	regulation of macromolecule metabolic process	23%	8.89E-07
GO:0006325	chromatin organization	28%	1.18E-06

Table 19: Top50 GO terms in *iC-TIP60* vs. control HEK293 cells for biological processes enriched among genes upregulated in the absence of TIP60 3 days after dox treatment

GO number	**Go term**	**%**	**p**
GO:0032501	multicellular organismal process	27%	1.30E-18
GO:0048731	system development	28%	1.40E-16
GO:0007154	cell communication	27%	1.58E-16
GO:0023052	signaling	27%	2.04E-16
GO:0006928	movement of cell or subcellular component	31%	1.48E-15
GO:0007275	multicellular organism development	28%	1.76E-15
GO:0003008	system process	33%	7.70E-15
GO:0048856	anatomical structure development	27%	2.68E-14
GO:0032502	developmental process	27%	1.32E-13
GO:0022610	biological adhesion	33%	5.69E-13
GO:0009653	anatomical structure morphogenesis	29%	6.35E-13
GO:0007155	cell adhesion	33%	6.95E-13
GO:0040011	locomotion	31%	8.44E-13
GO:0007166	cell surface receptor signaling pathway	29%	9.52E-13
GO:0030154	cell differentiation	28%	1.83E-12
GO:0007165	signal transduction	27%	3.00E-12
GO:0120036	plasma membrane bounded cell projection organization	31%	6.18E-12

GO:0048869	cellular developmental process	28%	6.52E-12
GO:0030030	cell projection organization	31%	1.01E-11
GO:0035239	tube morphogenesis	34%	1.13E-11
GO:0048870	cell motility	31%	1.44E-11
GO:0051674	localization of cell	31%	1.44E-11
GO:0035295	tube development	33%	4.12E-11
GO:0050877	nervous system process	35%	8.09E-11
GO:0007267	cell-cell signaling	31%	8.14E-11
GO:0023051	regulation of signaling	28%	1.75E-10
GO:0007399	nervous system development	29%	2.01E-10
GO:0098916	anterograde trans-synaptic signaling	36%	2.04E-10
GO:0007268	chemical synaptic transmission	36%	2.04E-10
GO:0010646	regulation of cell communication	28%	2.33E-10
GO:0099537	trans-synaptic signaling	36%	3.04E-10
GO:0099536	synaptic signaling	36%	3.70E-10
GO:0009888	tissue development	30%	3.87E-10
GO:0048513	animal organ development	28%	4.16E-10
GO:0072359	circulatory system development	32%	5.32E-10
GO:0048468	cell development	29%	1.60E-09
GO:0072358	cardiovascular system development	34%	1.87E-09
GO:0048514	blood vessel morphogenesis	35%	1.88E-09
GO:0016477	cell migration	31%	1.95E-09
GO:0009605	response to external stimulus	29%	1.96E-09
GO:0001525	angiogenesis	37%	2.00E-09
GO:0051239	regulation of multicellular organismal process	28%	2.89E-09
GO:0061564	axon development	35%	2.99E-09
GO:0048646	anatomical structure formation involved in morphogenesis	32%	3.05E-09
GO:0001944	vasculature development	34%	3.47E-09
GO:0009966	regulation of signal transduction	27%	5.99E-09
GO:0007409	axonogenesis	36%	6.22E-09
GO:0001568	blood vessel development	34%	8.02E-09

GO:0048699	generation of neurons	30%	9.78E-09
GO:0032879	regulation of localization	28%	1.23E-08

10.4 KEGG pathways dysregulated in TIP60 depleted cells

Table 20: KEGG pathways in *Tip60$^{iKO/iKO}$;ERT2* MEF vs. *Tip6$^{+/+}$;ERT2* MEFs enriched among genes downregulated in the absence of TIP60 3 days after tamoxifen treatment

KEGG number	**Pathway**	**%**	**p**
path:mmu03010	Ribosome	63%	1.37E-21
path:mmu04141	Protein processing in endoplasmic reticulum	50%	3.87E-12
path:mmu03008	Ribosome biogenesis in eukaryotes	58%	1.04E-09
path:mmu01230	Biosynthesis of amino acids	55%	2.76E-07
path:mmu04071	Sphingolipid signaling pathway	47%	7.32E-07
path:mmu04144	Endocytosis	38%	3.66E-06
path:mmu04722	Neurotrophin signaling pathway	43%	9.79E-06
path:mmu04014	Ras signaling pathway	38%	1.39E-05
path:mmu04370	VEGF signaling pathway	52%	1.39E-05
path:mmu04072	Phospholipase D signaling pathway	42%	2.22E-05
path:mmu04150	mTOR signaling pathway	40%	2.42E-05
path:mmu04666	Fc gamma R-mediated phagocytosis	45%	3.50E-05
path:mmu04142	Lysosome	40%	0.000154
path:mmu04721	Synaptic vesicle cycle	49%	0.000193
path:mmu05163	Human cytomegalovirus infection	35%	0.000395
path:mmu05223	Non-small cell lung cancer	44%	0.000445
path:mmu00970	Aminoacyl-tRNA biosynthesis	48%	0.000557
path:mmu03013	RNA transport	36%	0.000571
path:mmu05220	Chronic myeloid leukemia	41%	0.000744
path:mmu03020	RNA polymerase	54%	0.000754
path:mmu05230	Central carbon metabolism in cancer	44%	0.000845
path:mmu04660	T cell receptor signaling pathway	41%	0.001306
path:mmu05152	Tuberculosis	37%	0.001334
path:mmu04218	Cellular senescence	35%	0.001469

path:mmu04664	Fc epsilon RI signaling pathway	43%	0.002157
path:mmu04650	Natural killer cell mediated cytotoxicity	40%	0.002361
path:mmu05214	Glioma	40%	0.002469
path:mmu05211	Renal cell carcinoma	40%	0.002469
path:mmu04066	HIF-1 signaling pathway	38%	0.002529
path:mmu00564	Glycerophospholipid metabolism	39%	0.002714
path:mmu04728	Dopaminergic synapse	37%	0.002733
path:mmu05212	Pancreatic cancer	39%	0.002862
path:mmu04720	Long-term potentiation	41%	0.003775
path:mmu05100	Bacterial invasion of epithelial cells	39%	0.004025
path:mmu04966	Collecting duct acid secretion	56%	0.004138
path:mmu00520	Amino sugar and nucleotide sugar metabolism	43%	0.004236
path:mmu04662	B cell receptor signaling pathway	40%	0.004462
path:mmu04145	Phagosome	35%	0.004826
path:mmu05213	Endometrial cancer	40%	0.004905
path:mmu04910	Insulin signaling pathway	35%	0.005186
path:mmu04068	FoxO signaling pathway	35%	0.005574
path:mmu01521	EGFR tyrosine kinase inhibitor resistance	38%	0.005593
path:mmu00051	Fructose and mannose metabolism	47%	0.005887
path:mmu04926	Relaxin signaling pathway	35%	0.00599
path:mmu05167	Kaposi sarcoma-associated herpesvirus infection	33%	0.00717
path:mmu04915	Estrogen signaling pathway	36%	0.007182
path:mmu05231	Choline metabolism in cancer	36%	0.007343
path:mmu04070	Phosphatidylinositol signaling system	36%	0.007343
path:mmu01200	Carbon metabolism	35%	0.007993
path:mmu04140	Autophagy - animal	34%	0.009856
path:mmu04137	Mitophagy - animal	38%	0.010078
path:mmu04062	Chemokine signaling pathway	33%	0.010504
path:mmu00600	Sphingolipid metabolism	42%	0.011097
path:mmu05170	Human immunodeficiency virus 1 infection	32%	0.011516
path:mmu04625	C-type lectin receptor signaling pathway	36%	0.012323

path:mmu04012	ErbB signaling pathway	36%	0.013244
path:mmu04010	MAPK signaling pathway	30%	0.015081
path:mmu01522	Endocrine resistance	35%	0.016306
path:mmu00510	N-Glycan biosynthesis	39%	0.0171
path:mmu04912	GnRH signaling pathway	36%	0.01711
path:mmu05142	Chagas disease (American trypanosomiasis)	35%	0.018948
path:mmu05219	Bladder cancer	41%	0.020087
path:mmu04922	Glucagon signaling pathway	35%	0.02043
path:mmu04979	Cholesterol metabolism	41%	0.021037
path:mmu00010	Glycolysis / Gluconeogenesis	38%	0.0216
path:mmu04917	Prolactin signaling pathway	37%	0.021851
path:mmu05215	Prostate cancer	34%	0.022651
path:mmu04210	Apoptosis	33%	0.023403
path:mmu05210	Colorectal cancer	34%	0.024465
path:mmu04520	Adherens junction	35%	0.025635
path:mmu04371	Apelin signaling pathway	32%	0.027263
path:mmu05216	Thyroid cancer	40%	0.027451
path:mmu05218	Melanoma	35%	0.029848
path:mmu05162	Measles	33%	0.030781
path:mmu05014	Amyotrophic lateral sclerosis (ALS)	38%	0.03088
path:mmu04015	Rap1 signaling pathway	31%	0.031215
path:mmu05140	Leishmaniasis	37%	0.033238
path:mmu04730	Long-term depression	37%	0.033238
path:mmu00440	Phosphonate and phosphinate metabolism	67%	0.033315
path:mmu04151	PI3K-Akt signaling pathway	29%	0.034682
path:mmu00565	Ether lipid metabolism	39%	0.037457
path:mmu05132	Salmonella infection	34%	0.039107
path:mmu05161	Hepatitis B	31%	0.041785
path:mmu04919	Thyroid hormone signaling pathway	32%	0.042315
path:mmu00030	Pentose phosphate pathway	42%	0.04414
path:mmu04933	AGE-RAGE signaling pathway in diabetic complications	33%	0.044336

path:mmu01524	Platinum drug resistance	34%	0.045992

Table 21: KEGG pathways in *Tip60$^{iKO/iKO}$;ERT2* MEF vs. *Tip6$^{+/+}$;ERT2* MEFs enriched among genes upregulated in the absence of TIP60 3 days after tamoxifen treatment

KEGG number	**Pathway**	**%**	**p**
path:mmu04974	Protein digestion and absorption	58%	7.93E-10
path:mmu05217	Basal cell carcinoma	49%	4.29E-06
path:mmu04934	Cushing syndrome	37%	8.64E-06
path:mmu05226	Gastric cancer	37%	2.06E-05
path:mmu00410	beta-Alanine metabolism	58%	4.87E-05
path:mmu04976	Bile secretion	47%	0.000165
path:mmu04512	ECM-receptor interaction	39%	0.000222
path:mmu05200	Pathways in cancer	27%	0.000322
path:mmu04350	TGF-beta signaling pathway	38%	0.000379
path:mmu04310	Wnt signaling pathway	34%	0.000396
path:mmu04964	Proximal tubule bicarbonate reclamation	64%	0.00043
path:mmu00340	Histidine metabolism	64%	0.00043
path:mmu05205	Proteoglycans in cancer	31%	0.000448
path:mmu04360	Axon guidance	31%	0.00059
path:mmu05146	Amoebiasis	37%	0.000626
path:mmu00380	Tryptophan metabolism	50%	0.000699
path:mmu05225	Hepatocellular carcinoma	31%	0.001072
path:mmu05224	Breast cancer	32%	0.001339
path:mmu02010	ABC transporters	44%	0.001433
path:mmu00980	Metabolism of xenobiotics by cytochrome P450	44%	0.001433
path:mmu03460	Fanconi anemia pathway	39%	0.0015
path:mmu04390	Hippo signaling pathway	31%	0.001667
path:mmu04060	Cytokine-cytokine receptor interaction	31%	0.001677
path:mmu00512	Mucin type O-glycan biosynthesis	50%	0.001806
path:mmu04971	Gastric acid secretion	38%	0.001979
path:mmu00982	Drug metabolism - cytochrome P450	44%	0.00226

path:mmu05165	Human papillomavirus infection	27%	0.002443
path:mmu05414	Dilated cardiomyopathy (DCM)	35%	0.002894
path:mmu04924	Renin secretion	37%	0.003328
path:mmu04916	Melanogenesis	34%	0.0034
path:mmu04960	Aldosterone-regulated sodium reabsorption	44%	0.003932
path:mmu00563	Glycosylphosphatidylinositol (GPI)-anchor biosynthesis	46%	0.004278
path:mmu04610	Complement and coagulation cascades	39%	0.004576
path:mmu05410	Hypertrophic cardiomyopathy (HCM)	35%	0.004912
path:mmu04550	Signaling pathways regulating pluripotency of stem cells	31%	0.007508
path:mmu04340	Hedgehog signaling pathway	38%	0.009097
path:mmu04530	Tight junction	29%	0.011092
path:mmu05412	Arrhythmogenic right ventricular cardiomyopathy (ARVC)	34%	0.01204
path:mmu00360	Phenylalanine metabolism	55%	0.01258
path:mmu04911	Insulin secretion	33%	0.0147
path:mmu04972	Pancreatic secretion	33%	0.017289
path:mmu05204	Chemical carcinogenesis	36%	0.020522
path:mmu04740	Olfactory transduction	38%	0.021935
path:mmu00640	Propanoate metabolism	38%	0.021935
path:mmu03430	Mismatch repair	41%	0.022146
path:mmu04970	Salivary secretion	32%	0.025162
path:mmu04925	Aldosterone synthesis and secretion	31%	0.025775
path:mmu00280	Valine, leucine and isoleucine degradation	33%	0.034363
path:mmu00350	Tyrosine metabolism	40%	0.034966
path:mmu04927	Cortisol synthesis and secretion	32%	0.041285
path:mmu04270	Vascular smooth muscle contraction	28%	0.042316
path:mmu04068	FoxO signaling pathway	27%	0.046765
path:mmu04614	Renin-angiotensin system	43%	0.04694
path:mmu04520	Adherens junction	29%	0.047432

path:mmu04933	AGE-RAGE signaling pathway in diabetic complications	28%	0.04893

Table 22: KEGG pathways in *iC-TIP60* vs. control HEK293 cells enriched among genes downregulated in the absence of TIP60 3 days after dox treatment

KEGG number	**Pathway**	**%**	**p**
path:hsa01100	Metabolic pathways	27%	1.53E-07
path:hsa00240	Pyrimidine metabolism	39%	3.96E-05
path:hsa04110	Cell cycle	36%	5.68E-05
path:hsa01230	Biosynthesis of amino acids	40%	0.000381
path:hsa00230	Purine metabolism	32%	0.000418
path:hsa00900	Terpenoid backbone biosynthesis	55%	0.00065
path:hsa04115	p53 signaling pathway	38%	0.000662
path:hsa00310	Lysine degradation	38%	0.001743
path:hsa01200	Carbon metabolism	33%	0.001937
path:hsa00270	Cysteine and methionine metabolism	41%	0.002556
path:hsa00100	Steroid biosynthesis	53%	0.002903
path:hsa00983	Drug metabolism - other enzymes	39%	0.005318
path:hsa00860	Porphyrin and chlorophyll metabolism	47%	0.007439
path:hsa00010	Glycolysis / Gluconeogenesis	37%	0.007899
path:hsa03008	Ribosome biogenesis in eukaryotes	33%	0.00811
path:hsa03030	DNA replication	39%	0.008139
path:hsa04932	Non-alcoholic fatty liver disease (NAFLD)	29%	0.008557
path:hsa04914	Progesterone-mediated oocyte maturation	32%	0.009932
path:hsa01212	Fatty acid metabolism	36%	0.010115
path:hsa05010	Alzheimer disease	29%	0.010434
path:hsa01040	Biosynthesis of unsaturated fatty acids	45%	0.011118
path:hsa00280	Valine, leucine and isoleucine degradation	36%	0.012795
path:hsa00071	Fatty acid degradation	37%	0.016163
path:hsa00620	Pyruvate metabolism	38%	0.022104
path:hsa04211	Longevity regulating pathway	31%	0.022297
path:hsa00650	Butanoate metabolism	42%	0.025552

path:hsa04723	Retrograde endocannabinoid signaling	28%	0.030123
path:hsa00480	Glutathione metabolism	35%	0.03084
path:hsa00514	Other types of O-glycan biosynthesis	40%	0.035174
path:hsa04114	Oocyte meiosis	28%	0.041866
path:hsa04068	FoxO signaling pathway	27%	0.042501
path:hsa03013	RNA transport	26%	0.045581
path:hsa04714	Thermogenesis	25%	0.0461
path:hsa04977	Vitamin digestion and absorption	43%	0.047163
path:hsa05200	Pathways in cancer	24%	0.047592

Table 23: KEGG pathways in *iC-TIP60* vs. control HEK293 cells enriched among genes upregulated in the absence of TIP60 3 days after dox treatment

KEGG number	**Pathway**	**%**	**p**
path:hsa05322	Systemic lupus erythematosus	67%	9.57E-12
path:hsa05034	Alcoholism	42%	3.42E-06
path:hsa04970	Salivary secretion	52%	1.34E-05
path:hsa04080	Neuroactive ligand-receptor interaction	42%	1.48E-05
path:hsa04911	Insulin secretion	47%	2.66E-05
path:hsa05202	Transcriptional misregulation in cancer	38%	4.35E-05
path:hsa05150	Staphylococcus aureus infection	73%	4.60E-05
path:hsa04060	Cytokine-cytokine receptor interaction	40%	7.89E-05
path:hsa04010	MAPK signaling pathway	33%	0.000112
path:hsa04925	Aldosterone synthesis and secretion	43%	0.000154
path:hsa04971	Gastric acid secretion	45%	0.000352
path:hsa05031	Amphetamine addiction	47%	0.000355
path:hsa05020	Prion diseases	60%	0.000377
path:hsa04514	Cell adhesion molecules (CAMs)	41%	0.000538
path:hsa04919	Thyroid hormone signaling pathway	38%	0.000587
path:hsa04928	Parathyroid hormone synthesis, secretion and action	38%	0.000817
path:hsa04918	Thyroid hormone synthesis	44%	0.001023
path:hsa04915	Estrogen signaling pathway	37%	0.001187

path:hsa05030	Cocaine addiction	47%	0.002302
path:hsa04726	Serotonergic synapse	39%	0.002518
path:hsa04020	Calcium signaling pathway	34%	0.003543
path:hsa04924	Renin secretion	41%	0.003631
path:hsa04725	Cholinergic synapse	36%	0.005374
path:hsa04976	Bile secretion	42%	0.006225
path:hsa05321	Inflammatory bowel disease (IBD)	45%	0.007105
path:hsa04380	Osteoclast differentiation	35%	0.007162
path:hsa04610	Complement and coagulation cascades	46%	0.007248
path:hsa04145	Phagosome	34%	0.007602
path:hsa05414	Dilated cardiomyopathy (DCM)	37%	0.007674
path:hsa05323	Rheumatoid arthritis	40%	0.007795
path:hsa04216	Ferroptosis	42%	0.008921
path:hsa04650	Natural killer cell mediated cytotoxicity	37%	0.009531
path:hsa05416	Viral myocarditis	43%	0.009963
path:hsa05203	Viral carcinogenesis	31%	0.010097
path:hsa02010	ABC transporters	44%	0.01038
path:hsa04960	Aldosterone-regulated sodium reabsorption	44%	0.01038
path:hsa05310	Asthma	100%	0.011852
path:hsa04024	cAMP signaling pathway	32%	0.012171
path:hsa04310	Wnt signaling pathway	32%	0.012403
path:hsa05164	Influenza A	32%	0.013828
path:hsa05145	Toxoplasmosis	34%	0.014904
path:hsa04923	Regulation of lipolysis in adipocytes	39%	0.015599
path:hsa05140	Leishmaniasis	38%	0.016765
path:hsa04612	Antigen processing and presentation	40%	0.016915
path:hsa04727	GABAergic synapse	36%	0.017502
path:hsa05330	Allograft rejection	63%	0.018413
path:hsa04210	Apoptosis	32%	0.021191
path:hsa04713	Circadian entrainment	34%	0.022454
path:hsa04022	cGMP-PKG signaling pathway	31%	0.023381
path:hsa04672	Intestinal immune network for IgA production	50%	0.023641

path:hsa04972	Pancreatic secretion	35%	0.026138
path:hsa04721	Synaptic vesicle cycle	36%	0.026182
path:hsa04510	Focal adhesion	29%	0.02664
path:hsa05162	Measles	33%	0.026791
path:hsa05320	Autoimmune thyroid disease	67%	0.027146
path:hsa05332	Graft-versus-host disease	67%	0.027146
path:hsa04927	Cortisol synthesis and secretion	36%	0.028969
path:hsa04974	Protein digestion and absorption	35%	0.03515
path:hsa04810	Regulation of actin cytoskeleton	29%	0.035689
path:hsa05224	Breast cancer	30%	0.036298
path:hsa04360	Axon guidance	29%	0.038605
path:hsa04540	Gap junction	33%	0.03861
path:hsa04740	Olfactory transduction	38%	0.043435
path:hsa05130	Pathogenic Escherichia coli infection	35%	0.043504
path:hsa04916	Melanogenesis	32%	0.044276
path:hsa04973	Carbohydrate digestion and absorption	41%	0.044354
path:hsa04921	Oxytocin signaling pathway	30%	0.044914
path:hsa04659	Th17 cell differentiation	32%	0.045164
path:hsa05146	Amoebiasis	32%	0.045164
path:hsa00534	Glycosaminoglycan biosynthesis - heparan sulfate / heparin	42%	0.047981
path:hsa04961	Endocrine and other factor-regulated calcium reabsorption	36%	0.049011

10.5 Total number of mapped reads per CUT&Tag library

Table 24: Total number of mapped reads per CUT&Tag library and subdivided by uniquely mapped reads per species.

Library	**Number of uniquely mapped sequencing reads**			
	Total	*H. sapiens*	*D. melanogaster*	*E. coli*
iC-TIP60 U2OSg1 control H2AZK4-7-11ac	8504100	7231571	800755	429024

iC-TIP60 U2OSg2 control H2AZK4-7-11ac	8561817	6668753	783104	1066582
iC-TIP60 U2OSg1 KO H2AZK4-7-11ac	6135341	2744741	1760245	1596954
iC-TIP60 U2OSg2 KO H2AZK4-7-11ac	3722353	1949730	1134295	618118
iC-TIP60 U2OSg1 control H2AZK4-7ac	4071760	3390251	337310	325488
iC-TIP60 U2OSg2 control H2AZK4-7ac	4176216	2879607	387024	889721
iC-TIP60 U2OSg1 KO H2AZK4-7ac	2213318	712549	731506	759042
iC-TIP60 U2OSg2 KO H2AZK4-7ac	1964805	624154	643374	688349
iC-TIP60 U2OSg1 control H2AZ	7179687	4125194	165026	2853561
iC-TIP60 U2OSg2 control H2AZ	8506536	3928537	441402	4088764
iC-TIP60 U2OSg1 KO H2AZ	4321923	1693417	220087	2386535
iC-TIP60 U2OSg2 KO H2AZ	6795090	3754220	342894	2658398
iC-TIP60 U2OSg1 control H4K8ac	4567993	2922479	194570	1430454
iC-TIP60 U2OSg2 control H4K8ac	3122626	1713702	147589	1246149
iC-TIP60 U2OSg1 KO H4K8ac	2998455	1367766	199145	1418387
iC-TIP60 U2OSg2 KO H4K8ac	4499754	2782847	277091	1418979
iC-TIP60 U2OSg1 control H4K16ac	8895096	6353215	555080	1932224

iC-TIP60 U2OSg2 control H4K16ac		11031665	6597907	665034	3707213
iC-TIP60 U2OSg1 KO H4K16ac		8188451	4627658	676370	2835401
iC-TIP60 U2OSg2 KO H4K16ac		4349355	2925796	346166	1049673
iC-TIP60 U2OSg1 control H3K27me3		8397551	8110135	235875	26
iC-TIP60 U2OSg1 control IgG		50439	46627	2274	1005

Chapter 11 References

References

Abney, J.R., Cutler, B., Fillbach, M.L., Axelrod, D., and Scalettar, B.A. (1997). Chromatin dynamics in interphase nuclei and its implications for nuclear structure. J Cell Biol *137*, 1459-1468.

Acharya, D., Hainer, S.J., Yoon, Y., Wang, F., Bach, I., Rivera-Perez, J.A., and Fazzio, T.G. (2017). KAT-Independent Gene Regulation by Tip60 Promotes ESC Self-Renewal but Not Pluripotency. Cell Rep *19*, 671-679.

Acharya, D., Nera, B., Milstone, Z.J., Bourke, L., Yoon, Y., Rivera-Pérez, J.A., Trivedi, C.M., and Fazzio, T.G. (2018). TIP55, a splice isoform of the KAT5 acetyltransferase, is essential for developmental gene regulation and organogenesis. Scientific Reports *8*, 14908.

Adam, M., Robert, F., Larochelle, M., and Gaudreau, L. (2001). H2A.Z is required for global chromatin integrity and for recruitment of RNA polymerase II under specific conditions. Mol Cell Biol *21*, 6270-6279.

Adamowicz, M., Vermezovic, J., and d'Adda di Fagagna, F. (2016). NOTCH1 Inhibits Activation of ATM by Impairing the Formation of an ATM-FOXO3a-KAT5/Tip60 Complex. Cell Rep *16*, 2068-2076.

Akhtar, A., and Becker, P.B. (2000). Activation of Transcription through Histone H4 Acetylation by MOF, an Acetyltransferase Essential for Dosage Compensation in Drosophila. Molecular cell *5*, 367-375.

Albert, I., Mavrich, T.N., Tomsho, L.P., Qi, J., Zanton, S.J., Schuster, S.C., and Pugh, B.F. (2007). Translational and rotational settings of H2A.Z nucleosomes across the Saccharomyces cerevisiae genome. Nature *446*, 572-576.

Allahverdi, A., Yang, R., Korolev, N., Fan, Y., Davey, C.A., Liu, C.-F., and Nordenskiöld, L. (2011). The effects of histone H4 tail acetylations on cation-induced chromatin folding and self-association. Nucleic Acids Research *39*, 1680-1691.

Allfrey, V.G., Faulkner, R., and Mirsky, A.E. (1964). Acetylation and Methylation of Histones and Their Possible Role in the Regulation of Rna Synthesis. Proc Natl Acad Sci U S A *51*, 786-794.

Aubrey, B.J., Kelly, G.L., Kueh, A.J., Brennan, M.S., O'Connor, L., Milla, L., Wilcox, S., Tai, L., Strasser, A., and Herold, M.J. (2015). An inducible lentiviral guide RNA platform enables the identification of tumor-essential genes and tumor-promoting mutations in vivo. Cell Rep *10*, 1422-1432.

Auger, A.a., Galarneau, L., Altaf, M., Nourani, A., Doyon, Y., Utley, R.T., Cronier, D., Allard, S.p., and Côté, J. (2008). Eaf1 Is the Platform for NuA4 Molecular Assembly That Evolutionarily Links Chromatin Acetylation to ATP-Dependent Exchange of Histone H2A Variants. Molecular and Cellular Biology *28*, 2257-2270.

Babiarz, J.E., Halley, J.E., and Rine, J. (2006). Telomeric heterochromatin boundaries require NuA4-dependent acetylation of histone variant H2A.Z in Saccharomyces cerevisiae. Genes Dev *20*, 700-710.

Badri, K.R., Zhou, Y., Dhru, U., Aramgam, S., and Schuger, L. (2008). Effects of the SANT domain of tension-induced/inhibited proteins (TIPs), novel partners of the histone acetyltransferase p300, on p300 activity and TIP-6-induced adipogenesis. Mol Cell Biol *28*, 6358-6372.

Bakkenist, C.J., and Kastan, M.B. (2003). DNA damage activates ATM through intermolecular autophosphorylation and dimer dissociation. Nature *421*, 499-506.

Bakkenist, C.J., and Kastan, M.B. (2004). Initiating cellular stress responses. Cell *118*, 9-17.

Baldi, S., and Becker, P.B. (2013). The variant histone H2A.V of Drosophila--three roles, two guises. Chromosoma *122*, 245-258.

Banin, S., Moyal, L., Shieh, S., Taya, Y., Anderson, C.W., Chessa, L., Smorodinsky, N.I., Prives, C., Reiss, Y., Shiloh, Y., *et al.* (1998). Enhanced phosphorylation of p53 by ATM in response to DNA damage. Science *281*, 1674-1677.

Bannister, A.J., Schneider, R., Myers, F.A., Thorne, A.W., Crane-Robinson, C., and Kouzarides, T. (2005). Spatial distribution of di- and tri-methyl lysine 36 of histone H3 at active genes. J Biol Chem *280*, 17732-17736.

Bararia, D., Trivedi, A.K., Zada, A.A.P., Greif, P.A., Mulaw, M.A., Christopeit, M., Hiddemann, W., Bohlander, S.K., and Behre, G. (2008). Proteomic identification of the MYST domain histone acetyltransferase TIP60 (HTATIP) as a co-activator of the myeloid transcription factor C/EBPα. Leukemia *22*, 800-807.

Barlesi, F., Giaccone, G., Gallegos-Ruiz, M.I., Loundou, A., Span, S.W., Lefesvre, P., Kruyt, F.A., and Rodriguez, J.A. (2007). Global histone modifications predict prognosis of resected non small-cell lung cancer. J Clin Oncol *25*, 4358-4364.

Barski, A., Cuddapah, S., Cui, K., Roh, T.Y., Schones, D.E., Wang, Z., Wei, G., Chepelev, I., and Zhao, K. (2007). High-resolution profiling of histone methylations in the human genome. Cell *129*, 823-837.

Barzily-Rokni, M., Friedman, N., Ron-Bigger, S., Isaac, S., Michlin, D., and Eden, A. (2011). Synergism between DNA methylation and macroH2A1 occupancy in epigenetic silencing of the tumor suppressor gene p16(CDKN2A). Nucleic Acids Res *39*, 1326-1335.

Bassi, C., Li, Y.T., Khu, K., Mateo, F., Baniasadi, P.S., Elia, A., Mason, J., Stambolic, V., Pujana, M.A., Mak, T.W., *et al.* (2016). The acetyltransferase Tip60 contributes to mammary tumorigenesis by modulating DNA repair. Cell Death Differ *23*, 1198-1208.

Belotserkovskaya, R. (2003). FACT Facilitates Transcription-Dependent Nucleosome Alteration. Science *301*, 1090-1093.

Ben-Hattar, J., and Jiricny, J. (1988). Methylation of single CpG dinucleotides within a promoter element of the Herpes simplex virus tk gene reduces its transcription in vivo. Gene *65*, 219-227.

Berman, H.M., Westbrook, J., Feng, Z., Gilliland, G., Bhat, T.N., Weissig, H., Shindyalov, I.N., and Bourne, P.E. (2000). The Protein Data Bank. Nucleic Acids Res *28*, 235-242.

Berndsen, C.E., Albaugh, B.N., Tan, S., and Denu, J.M. (2007). Catalytic mechanism of a MYST family histone acetyltransferase. Biochemistry *46*, 623-629.

Bernstein, B.E., Humphrey, E.L., Erlich, R.L., Schneider, R., Bouman, P., Liu, J.S., Kouzarides, T., and Schreiber, S.L. (2002). Methylation of histone H3 Lys 4 in coding regions of active genes. Proc Natl Acad Sci U S A *99*, 8695-8700.

Bernstein, B.E., Kamal, M., Lindblad-Toh, K., Bekiranov, S., Bailey, D.K., Huebert, D.J., McMahon, S., Karlsson, E.K., Kulbokas, E.J., 3rd, Gingeras, T.R., *et al.* (2005). Genomic maps and comparative analysis of histone modifications in human and mouse. Cell *120*, 169-181.

Bernstein, B.E., Mikkelsen, T.S., Xie, X., Kamal, M., Huebert, D.J., Cuff, J., Fry, B., Meissner, A., Wernig, M., Plath, K., *et al.* (2006). A bivalent chromatin structure marks key developmental genes in embryonic stem cells. Cell *125*, 315-326.

Binda, O., Sevilla, A., LeRoy, G., Lemischka, I.R., Garcia, B.A., and Richard, S. (2013). SETD6 monomethylates H2AZ on lysine 7 and is required for the maintenance of embryonic stem cell self-renewal. Epigenetics *8*, 177-183.

Blaess, S., Corrales, J.D., and Joyner, A.L. (2006). Sonic hedgehog regulates Gli activator and repressor functions with spatial and temporal precision in the mid/hindbrain region. Development *133*, 1799-1809.

Bohm, V., Hieb, A.R., Andrews, A.J., Gansen, A., Rocker, A., Toth, K., Luger, K., and Langowski, J. (2011). Nucleosome accessibility governed by the dimer/tetramer interface. Nucleic Acids Res *39*, 3093-3102.

Boudreault, A.A., Cronier, D., Selleck, W., Lacoste, N., Utley, R.T., Allard, S., Savard, J., Lane, W.S., Tan, S., and Cote, J. (2003). Yeast enhancer of polycomb defines global Esa1-dependent acetylation of chromatin. Genes Dev *17*, 1415-1428.

Bowman, B.R., Moure, C.M., Kirtane, B.M., Welschhans, R.L., Tominaga, K., Pereira-Smith, O.M., and Quiocho, F.A. (2006). Multipurpose MRG Domain Involved in Cell Senescence and Proliferation Exhibits Structural Homology to a DNA-Interacting Domain. Structure *14*, 151-158.

Boyarchuk, E., Filipescu, D., Vassias, I., Cantaloube, S., and Almouzni, G. (2014). The histone variant composition of centromeres is controlled by the pericentric heterochromatin state during the cell cycle. Journal of Cell Science *127*, 3347-3359.

Boyer, L.A., Langer, M.R., Crowley, K.A., Tan, S., Denu, J.M., and Peterson, C.L. (2002). Essential role for the SANT domain in the functioning of multiple chromatin remodeling enzymes. Molecular cell *10*, 935-942.

Boyer, L.A., Latek, R.R., and Peterson, C.L. (2004). The SANT domain: a unique histone-tail-binding module? Nat Rev Mol Cell Biol *5*, 158-163.

Boyer, L.A., Plath, K., Zeitlinger, J., Brambrink, T., Medeiros, L.A., Lee, T.I., Levine, S.S., Wernig, M., Tajonar, A., Ray, M.K., *et al.* (2006). Polycomb complexes repress developmental regulators in murine embryonic stem cells. Nature *441*, 349-353.

Bradbury, L.H.G.P.S.H.R.M.P.Y.E.M. (1993). Studies of the DNA binding properties of histone H4 amino terminus. The Journal of Biological Chemistry *268*, pp. 305-314.

Brady, M.E., Ozanne, D.M., Gaughan, L., Waite, I., Cook, S., Neal, D.E., and Robson, C.N. (1999). Tip60 Is a Nuclear Hormone Receptor Coactivator. Journal of Biological Chemistry *274*, 17599-17604.

Brown, James A.L., Bourke, E., Eriksson, Leif A., and Kerin, Michael J. (2016). Targeting cancer using KAT inhibitors to mimic lethal knockouts. Biochemical Society Transactions *44*, 979-986.

Brunelle, M., Nordell Markovits, A., Rodrigue, S., Lupien, M., Jacques, P.E., and Gevry, N. (2015). The histone variant H2A.Z is an important regulator of enhancer activity. Nucleic Acids Res *43*, 9742-9756.

Burma, S., Chen, B.P., Murphy, M., Kurimasa, A., and Chen, D.J. (2001). ATM phosphorylates histone H2AX in response to DNA double-strand breaks. J Biol Chem *276*, 42462-42467.

Cacabelos, R., and Torrellas, C. (2016). Pharmacoepigenomics. In Medical Epigenetics, T.O. Tollefsbol, ed. (Boston: Academic Press), pp. 585-617.

Cai, Y., Jin, J., Florens, L., Swanson, S.K., Kusch, T., Li, B., Workman, J.L., Washburn, M.P., Conaway, R.C., and Conaway, J.W. (2005). The Mammalian YL1 Protein Is a Shared Subunit of the TRRAP/TIP60 Histone Acetyltransferase and SRCAP Complexes. Journal of Biological Chemistry *280*, 13665-13670.

Cai, Y., Jin, J., Tomomori-Sato, C., Sato, S., Sorokina, I., Parmely, T.J., Conaway, R.C., and Conaway, J.W. (2003). Identification of new subunits of the multiprotein mammalian TRRAP/TIP60-containing histone acetyltransferase complex. J Biol Chem *278*, 42733-42736.

Cao, X., and Sudhof, T.C. (2001). A transcriptionally [correction of transcriptively] active complex of APP with Fe65 and histone acetyltransferase Tip60. Science *293*, 115-120.

Casas-Delucchi, C.S., van Bemmel, J.G., Haase, S., Herce, H.D., Nowak, D., Meilinger, D., Stear, J.H., Leonhardt, H., and Cardoso, M.C. (2012). Histone hypoacetylation is required to maintain late replication timing of constitutive heterochromatin. Nucleic Acids Research *40*, 159-169.

Chan, H.M., Narita, M., Lowe, S.W., and Livingston, D.M. (2005). The p400 E1A-associated protein is a novel component of the p53 --> p21 senescence pathway. Genes Dev *19*, 196-201.

Chen, B., Yusuf, M., Hashimoto, T., Estandarte, A.K., Thompson, G., and Robinson, I. (2017). Three-dimensional positioning and structure of chromosomes in a human prophase nucleus. Sci Adv *3*, e1602231.

Chen, G., Cheng, Y., Tang, Y., Martinka, M., and Li, G. (2012). Role of Tip60 in human melanoma cell migration, metastasis, and patient survival. J Invest Dermatol *132*, 2632-2641.

Chen, J. (2016). The Cell-Cycle Arrest and Apoptotic Functions of p53 in Tumor Initiation and Progression. Cold Spring Harb Perspect Med *6*, a026104.

Chen, L., Wei, T., Si, X., Wang, Q., Li, Y., Leng, Y., Deng, A., Chen, J., Wang, G., Zhu, S., *et al.* (2013a). Lysine acetyltransferase GCN5 potentiates the growth of non-small cell lung cancer via promotion of E2F1, cyclin D1, and cyclin E1 expression. J Biol Chem *288*, 14510-14521.

Chen, P.B., Hung, J.H., Hickman, T.L., Coles, A.H., Carey, J.F., Weng, Z., Chu, F., and Fazzio, T.G. (2013b). Hdac6 regulates Tip60-p400 function in stem cells. Elife *2*, e01557.

Chevillard-Briet, M., Quaranta, M., Grézy, A., Mattera, L., Courilleau, C., Philippe, M., Mercier, P., Corpet, D., Lough, J., Ueda, T., *et al.* (2014). Interplay between chromatin-modifying enzymes controls colon cancer progression through Wnt signaling. Human molecular genetics *23*, 2120-2131.

Cho, H.J., Li, H., Linhares, B.M., Kim, E., Ndoj, J., Miao, H., Grembecka, J., and Cierpicki, T. (2018). GAS41 Recognizes Diacetylated Histone H3 through a Bivalent Binding Mode. ACS Chemical Biology *13*, 2739-2746.

Choi, J., Heo, K., and An, W. (2009). Cooperative action of TIP48 and TIP49 in H2A.Z exchange catalyzed by acetylation of nucleosomal H2A. Nucleic Acids Res *37*, 5993-6007.

Choudhary, C., Kumar, C., Gnad, F., Nielsen, M.L., Rehman, M., Walther, T.C., Olsen, J.V., and Mann, M. (2009). Lysine Acetylation Targets Protein Complexes and Co-Regulates Major Cellular Functions (American Association for the Advancement of Science), pp. 834.

Clarke, A.S., Lowell, J.E., Jacobson, S.J., and Pillus, L. (1999). Esa1p Is an Essential Histone Acetyltransferase Required for Cell Cycle Progression. Molecular and Cellular Biology *19*, 2515-2526.

Col, E., Caron, C., Chable-Bessia, C., Legube, G., Gazzeri, S., Komatsu, Y., Yoshida, M., Benkirane, M., Trouche, D., and Khochbin, S. (2005). HIV-1 Tat targets Tip60 to impair the apoptotic cell response to genotoxic stresses. The EMBO Journal *24*, 2634-2645.

Colino-Sanguino, Y., Cornett, E.M., Moulder, D., Smith, G.C., Hrit, J., Cordeiro-Spinetti, E., Vaughan, R.M., Krajewski, K., Rothbart, S.B., Clark, S.J., *et al.* (2019). A Read/Write Mechanism Connects p300 Bromodomain Function to H2A.Z Acetylation. iScience *21*, 773-788.

Conerly, M.L., Teves, S.S., Diolaiti, D., Ulrich, M., Eisenman, R.N., and Henikoff, S. (2010). Changes in H2A.Z occupancy and DNA methylation during B-cell lymphomagenesis. Genome Res *20*, 1383-1390.

Creyghton, M.P., Cheng, A.W., Welstead, G.G., Kooistra, T., Carey, B.W., Steine, E.J., Hanna, J., Lodato, M.A., Frampton, G.M., Sharp, P.A., *et al.* (2010). Histone H3K27ac separates active from poised enhancers and predicts developmental state. Proc Natl Acad Sci U S A *107*, 21931-21936.

Creyghton, M.P., Markoulaki, S., Levine, S.S., Hanna, J., Lodato, M.A., Sha, K., Young, R.A., Jaenisch, R., and Boyer, L.A. (2008). H2AZ Is Enriched at Polycomb Complex Target Genes in ES Cells and Is Necessary for Lineage Commitment. Cell *135*, 649-661.

Csankovszki, G., Nagy, A., and Jaenisch, R. (2001). Synergism of Xist RNA, DNA methylation, and histone hypoacetylation in maintaining X chromosome inactivation. J Cell Biol *153*, 773-784.

Dahlin, J.L., Nelson, K.M., Strasser, J.M., Barsyte-Lovejoy, D., Szewczyk, M.M., Organ, S., Cuellar, M., Singh, G., Shrimp, J.H., Nguyen, N., *et al.* (2017). Assay interference and off-target liabilities of reported histone acetyltransferase inhibitors. Nature Communications *8*, 1527.

Dai, C., Shi, D., and Gu, W. (2013). Negative regulation of the acetyltransferase TIP60-p53 interplay by UHRF1 (ubiquitin-like with PHD and RING finger domains 1). J Biol Chem *288*, 19581-19592.

Dai, C., Tang, Y., Jung, S.Y., Qin, J., Aaronson, S.A., and Gu, W. (2011). Differential effects on p53-mediated cell cycle arrest vs. apoptosis by p90. Proc Natl Acad Sci U S A *108*, 18937-18942.

Dalvai, M., Bellucci, L., Fleury, L., Lavigne, A.C., Moutahir, F., and Bystricky, K. (2013). H2A.Z-dependent crosstalk between enhancer and promoter regulates cyclin D1 expression. Oncogene *32*, 4243-4251.

Dastagir, K., Reimers, K., Lazaridis, A., Jahn, S., Maurer, V., Strauß, S., Dastagir, N., Radtke, C., Kampmann, A., Bucan, V., *et al.* (2014). Murine embryonic fibroblast cell lines differentiate into three mesenchymal lineages to different extents: new models to investigate differentiation processes. Cell Reprogram *16*, 241-252.

Davie, J.R. (2003). Inhibition of histone deacetylase activity by butyrate. J Nutr *133*, 2485S-2493S.

Day, D.S., Zhang, B., Stevens, S.M., Ferrari, F., Larschan, E.N., Park, P.J., and Pu, W.T. (2016). Comprehensive analysis of promoter-proximal RNA polymerase II pausing across mammalian cell types. Genome Biology *17*, 120.

Deguchi, K., Ayton, P.M., Carapeti, M., Kutok, J.L., Snyder, C.S., Williams, I.R., Cross, N.C., Glass, C.K., Cleary, M.L., and Gilliland, D.G. (2003). MOZ-TIF2-

induced acute myeloid leukemia requires the MOZ nucleosome binding motif and TIF2-mediated recruitment of CBP. Cancer Cell *3*, 259-271.

Dhillon, N., Oki, M., Szyjka, S.J., Aparicio, O.M., and Kamakaka, R.T. (2006). H2A.Z functions to regulate progression through the cell cycle. Mol Cell Biol *26*, 489-501.

Dion, M.F., Kaplan, T., Kim, M., Buratowski, S., Friedman, N., and Rando, O.J. (2007). Dynamics of Replication-Independent Histone Turnover in Budding Yeast. Science *315*, 1405-1408.

Domaschenz, R., Kurscheid, S., Nekrasov, M., Han, S., and Tremethick, D.J. (2017). The Histone Variant H2A.Z Is a Master Regulator of the Epithelial-Mesenchymal Transition. Cell Rep *21*, 943-952.

Dong, Y., Isono, K.I., Ohbo, K., Endo, T.A., Ohara, O., Maekawa, M., Toyama, Y., Ito, C., Toshimori, K., Helin, K., *et al.* (2017). EPC1/TIP60-Mediated Histone Acetylation Facilitates Spermiogenesis in Mice. Mol Cell Biol *37*, e00082-00017.

Doyon, Y., Cayrou, C., Ullah, M., Landry, A.-J., Côté, V., Selleck, W., Lane, W.S., Tan, S., Yang, X.-J., and Côté, J. (2006). ING Tumor Suppressor Proteins Are Critical Regulators of Chromatin Acetylation Required for Genome Expression and Perpetuation. Molecular cell *21*, 51-64.

Doyon, Y., Selleck, W., Lane, W.S., Tan, S., and Cote, J. (2004). Structural and functional conservation of the NuA4 histone acetyltransferase complex from yeast to humans. Mol Cell Biol *24*, 1884-1896.

Draker, R., Ng, M.K., Sarcinella, E., Ignatchenko, V., Kislinger, T., and Cheung, P. (2012). A combination of H2A.Z and H4 acetylation recruits Brd2 to chromatin during transcriptional activation. PLoS Genet *8*, e1003047.

Draker, R., Sarcinella, E., and Cheung, P. (2011). USP10 deubiquitylates the histone variant H2A.Z and both are required for androgen receptor-mediated gene activation. Nucleic Acids Res *39*, 3529-3542.

Du, Y., Liu, Z., Cao, X., Chen, X., Chen, Z., Zhang, X., Zhang, X., and Jiang, C. (2017). Nucleosome eviction along with H3K9ac deposition enhances Sox2 binding during human neuroectodermal commitment. Cell Death & Differentiation *24*, 1121-1131.

Dyda, F., Klein, D.C., and Hickman, A.B. (2000). GCN5-related N-acetyltransferases: a structural overview. Annu Rev Biophys Biomol Struct *29*, 81-103.

Efeyan, A., Ortega-Molina, A., Velasco-Miguel, S., Herranz, D., Vassilev, L.T., and Serrano, M. (2007). Induction of p53-Dependent Senescence by the MDM2 Antagonist Nutlin-3a in Mouse Cells of Fibroblast Origin. Cancer Research *67*, 7350-7357.

Eirin-Lopez, J.M., Gonzalez-Romero, R., Dryhurst, D., Ishibashi, T., and Ausio, J. (2009). The evolutionary differentiation of two histone H2A.Z variants in chordates (H2A.Z-1 and H2A.Z-2) is mediated by a stepwise mutation process that affects three amino acid residues. BMC evolutionary biology *9*, 31.

El-Deiry, W. (1993). WAF1, a potential mediator of p53 tumor suppression. Cell *75*, 817-825.

Eymin, B., Claverie, P., Salon, C., Leduc, C., Col, E., Brambilla, E., Khochbin, S., and Gazzeri, S. (2006). p14ARF activates a Tip60-dependent and p53-independent ATM/ATR/CHK pathway in response to genotoxic stress. Mol Cell Biol *26*, 4339-4350.

Faast, R., Thonglairoam, V., Schulz, T.C., Beall, J., Wells, J.R.E., Taylor, H., Matthaei, K., Rathjen, P.D., Tremethick, D.J., and Lyons, I. (2001). Histone variant

H2A.Z is required for early mammalian development. Current Biology *11*, 1183-1187.

Fan, J.Y., Gordon, F., Luger, K., Hansen, J.C., and Tremethick, D.J. (2002). The essential histone variant H2A.Z regulates the equilibrium between different chromatin conformational states. Nature Structural Biology *9*, 172-176.

Fan, J.Y., Rangasamy, D., Luger, K., and Tremethick, D.J. (2004). H2A.Z alters the nucleosome surface to promote HP1alpha-mediated chromatin fiber folding. Molecular cell *16*, 655-661.

Farria, A., Li, W., and Dent, S.Y. (2015). KATs in cancer: functions and therapies. Oncogene *34*, 4901-4913.

Farris, S.D., Rubio, E.D., Moon, J.J., Gombert, W.M., Nelson, B.H., and Krumm, A. (2005). Transcription-induced chromatin remodeling at the c-myc gene involves the local exchange of histone H2A.Z. J Biol Chem *280*, 25298-25303.

Fazzio, T.G., Huff, J.T., and Panning, B. (2008). An RNAi screen of chromatin proteins identifies Tip60-p400 as a regulator of embryonic stem cell identity. Cell *134*, 162-174.

Feng, Y., Vlassis, A., Roques, C., Lalonde, M.E., Gonzalez-Aguilera, C., Lambert, J.P., Lee, S.B., Zhao, X., Alabert, C., Johansen, J.V., *et al.* (2016). BRPF3-HBO1 regulates replication origin activation and histone H3K14 acetylation. EMBO J *35*, 176-192.

Ferbeyre, G., de Stanchina, E., Lin, A.W., Querido, E., McCurrach, M.E., Hannon, G.J., and Lowe, S.W. (2002). Oncogenic ras and p53 cooperate to induce cellular senescence. Mol Cell Biol *22*, 3497-3508.

Filippakopoulos, P., Picaud, S., Mangos, M., Keates, T., Lambert, J.P., Barsyte-Lovejoy, D., Felletar, I., Volkmer, R., Muller, S., Pawson, T., *et al.* (2012). Histone recognition and large-scale structural analysis of the human bromodomain family. Cell *149*, 214-231.

Finch, J.T., and Klug, A. (1976). Solenoidal model for superstructure in chromatin. Proceedings of the National Academy of Sciences *73*, 1897-1901.

Finch, J.T., Lutter, L.C., Rhodes, D., Brown, R.S., Rushton, B., Levitt, M., and Klug, A. (1977). Structure of nucleosome core particles of chromatin. Nature *269*, 29-36.

Fisher, K., Southall, S.M., Wilson, J.R., and Poulin, G.B. (2010). Methylation and demethylation activities of a C. elegans MLL-like complex attenuate RAS signalling. Developmental biology *341*, 142-153.

Frank, S.R., Parisi, T., Taubert, S., Fernandez, P., Fuchs, M., Chan, H.M., Livingston, D.M., and Amati, B. (2003). MYC recruits the TIP60 histone acetyltransferase complex to chromatin. EMBO reports *4*, 575-580.

Fyodorov, D.V., Zhou, B.R., Skoultchi, A.I., and Bai, Y. (2018). Emerging roles of linker histones in regulating chromatin structure and function. Nat Rev Mol Cell Biol *19*, 192-206.

Gansen, A., Valeri, A., Hauger, F., Felekyan, S., Kalinin, S., Toth, K., Langowski, J., and Seidel, C.A.M. (2009). Nucleosome disassembly intermediates characterized by single-molecule FRET. Proceedings of the National Academy of Sciences *106*, 15308-15313.

Gao, C., Bourke, E., Scobie, M., Famme, M.A., Koolmeister, T., Helleday, T., Eriksson, L.A., Lowndes, N.F., and Brown, J.A. (2014). Rational design and validation of a Tip60 histone acetyltransferase inhibitor. Sci Rep *4*, 5372.

Garcia-Ramirez, M., Rocchini, C., and Ausio, J. (1995). Modulation of chromatin folding by histone acetylation. J Biol Chem *270*, 17923-17928.

Gasser, R., Koller, T., and Sogo, J.M. (1996). The stability of nucleosomes at the replication fork. J Mol Biol *258*, 224-239.

Gaughan, L., Logan, I.R., Cook, S., Neal, D.E., and Robson, C.N. (2002). Tip60 and Histone Deacetylase 1 Regulate Androgen Receptor Activity through Changes to the Acetylation Status of the Receptor. Journal of Biological Chemistry *277*, 25904-25913.

Gavaravarapu, S., and Kamine, J. (2000). Tip60 inhibits activation of CREB protein by protein kinase A. Biochem Biophys Res Commun *269*, 758-766.

Gevry, N., Chan, H.M., Laflamme, L., Livingston, D.M., and Gaudreau, L. (2007). p21 transcription is regulated by differential localization of histone H2A.Z. Genes Dev *21*, 1869-1881.

Gevry, N., Hardy, S., Jacques, P.E., Laflamme, L., Svotelis, A., Robert, F., and Gaudreau, L. (2009). Histone H2A.Z is essential for estrogen receptor signaling. Genes Dev *23*, 1522-1533.

Giaimo, B.D., Ferrante, F., Herchenröther, A., Hake, S.B., and Borggrefe, T. (2019). The histone variant H2A.Z in gene regulation. Epigenetics & Chromatin *12*, 37.

Giaimo, B.D., Ferrante, F., Vallejo, D.M., Hein, K., Gutierrez-Perez, I., Nist, A., Stiewe, T., Mittler, G., Herold, S., Zimmermann, T., *et al.* (2018). Histone variant H2A.Z deposition and acetylation directs the canonical Notch signaling response. Nucleic Acids Res *46*, 8197-8215.

Gorbsky, G.J. (2015). The spindle checkpoint and chromosome segregation in meiosis. The FEBS journal *282*, 2471-2487.

Gorrini, C., Squatrito, M., Luise, C., Syed, N., Perna, D., Wark, L., Martinato, F., Sardella, D., Verrecchia, A., Bennett, S., *et al.* (2007). Tip60 is a haplo-insufficient tumour suppressor required for an oncogene-induced DNA damage response. Nature *448*, 1063.

Graus-Porta, D., Blaess, S., Senften, M., Littlewood-Evans, A., Damsky, C., Huang, Z., Orban, P., Klein, R., Schittny, J.C., and Muller, U. (2001). Beta1-class integrins regulate the development of laminae and folia in the cerebral and cerebellar cortex. Neuron *31*, 367-379.

Greally, J.M. (2018). A user's guide to the ambiguous word 'epigenetics'. Nature Reviews Molecular Cell Biology *19*, 207-208.

Greaves, I.K., Rangasamy, D., Ridgway, P., and Tremethick, D.J. (2007). H2A.Z contributes to the unique 3D structure of the centromere. Proc Natl Acad Sci U S A *104*, 525-530.

Greenberg, M.V.C., and Bourc'his, D. (2019). The diverse roles of DNA methylation in mammalian development and disease. Nat Rev Mol Cell Biol *20*, 590-607.

Gu, W., and Roeder, R.G. (1997). Activation of p53 sequence-specific DNA binding by acetylation of the p53 C-terminal domain. Cell *90*, 595-606.

Guenther, M.G., Levine, S.S., Boyer, L.A., Jaenisch, R., and Young, R.A. (2007). A chromatin landmark and transcription initiation at most promoters in human cells. Cell *130*, 77-88.

Guillemette, B., Bataille, A.R., Gevry, N., Adam, M., Blanchette, M., Robert, F., and Gaudreau, L. (2005). Variant histone H2A.Z is globally localized to the promoters of inactive yeast genes and regulates nucleosome positioning. PLoS Biol *3*, e384.

Gupta, A., Guerin-Peyrou, T.G., Sharma, G.G., Park, C., Agarwal, M., Ganju, R.K., Pandita, S., Choi, K., Sukumar, S., Pandita, R.K., *et al.* (2008). The mammalian ortholog of Drosophila MOF that acetylates histone H4 lysine 16 is essential for embryogenesis and oncogenesis. Mol Cell Biol *28*, 397-409.

Gursoy-Yuzugullu, O., Ayrapetov, M.K., and Price, B.D. (2015). Histone chaperone Anp32e removes H2A.Z from DNA double-strand breaks and promotes nucleosome reorganization and DNA repair. Proc Natl Acad Sci U S A *112*, 7507-7512.

Halkidou, K., Gnanapragasam, V.J., Mehta, P.B., Logan, I.R., Brady, M.E., Cook, S., Leung, H.Y., Neal, D.E., and Robson, C.N. (2003). Expression of Tip60, an androgen receptor coactivator, and its role in prostate cancer development. Oncogene *22*, 2466-2477.

Harper, J.W., Adami, G.R., Wei, N., Keyomarsi, K., and Elledge, S.J. (1993). The p21 Cdk-interacting protein Cip1 is a potent inhibitor of G1 cyclin-dependent kinases. Cell *75*, 805-816.

Hassig, C.A., Tong, J.K., Fleischer, T.C., Owa, T., Grable, P.G., Ayer, D.E., and Schreiber, S.L. (1998). A role for histone deacetylase activity in HDAC1-mediated transcriptional repression. Proc Natl Acad Sci U S A *95*, 3519-3524.

Hattori, T., Coustry, F., Stephens, S., Eberspaecher, H., Takigawa, M., Yasuda, H., and de Crombrugghe, B. (2008). Transcriptional regulation of chondrogenesis by coactivator Tip60 via chromatin association with Sox9 and Sox5. Nucleic Acids Res *36*, 3011-3024.

Haupt, Y., Maya, R., Kazaz, A., and Oren, M. (1997). Mdm2 promotes the rapid degradation of p53. Nature *387*, 296-299.

Hayakawa, T., Ohtani, Y., Hayakawa, N., Shinmyozu, K., Saito, M., Ishikawa, F., and Nakayama, J.-i. (2007). RBP2 is an MRG15 complex component and down-regulates intragenic histone H3 lysine 4 methylation. Genes to Cells *0*, 070606122915002-???

Hebbes, T.R., Clayton, A.L., Thorne, A.W., and Crane-Robinson, C. (1994). Core histone hyperacetylation co-maps with generalized DNase I sensitivity in the chicken beta-globin chromosomal domain. The EMBO journal *13*, 1823-1830.

Hebbes, T.R., Thorne, A.W., and Crane-Robinson, C. (1988). A direct link between core histone acetylation and transcriptionally active chromatin. EMBO J *7*, 1395-1402.

Heintzman, N.D., Stuart, R.K., Hon, G., Fu, Y., Ching, C.W., Hawkins, R.D., Barrera, L.O., Van Calcar, S., Qu, C., Ching, K.A., *et al.* (2007). Distinct and predictive chromatin signatures of transcriptional promoters and enhancers in the human genome. Nat Genet *39*, 311-318.

Henikoff, S., Henikoff, J.G., Sakai, A., Loeb, G.B., and Ahmad, K. (2009). Genome-wide profiling of salt fractions maps physical properties of chromatin. Genome Res *19*, 460-469.

Henikoff, S., and Smith, M.M. (2015). Histone variants and epigenetics. Cold Spring Harb Perspect Biol *7*, a019364.

Hergeth, S.P., and Schneider, R. (2015). The H1 linker histones: multifunctional proteins beyond the nucleosomal core particle. EMBO reports *16*, 1439-1453.

Hobbs, C.A., Paul, B.A., and Gilmour, S.K. (2002). Deregulation of Polyamine Biosynthesis Alters Intrinsic Histone Acetyltransferase and Deacetylase Activities in Murine Skin and Tumors. Cancer Research *62*, 67-74.

Hobbs, C.A., Wei, G., DeFeo, K., Paul, B., Hayes, C.S., and Gilmour, S.K. (2006). Tip60 Protein Isoforms and Altered Function in Skin and Tumors that Overexpress Ornithine Decarboxylase. Cancer Research *66*, 8116-8122.

Hodawadekar, S.C., and Marmorstein, R. (2007). Chemistry of acetyl transfer by histone modifying enzymes: structure, mechanism and implications for effector design. Oncogene *26*, 5528-5540.

Hodgkins, A., Farne, A., Perera, S., Grego, T., Parry-Smith, D.J., Skarnes, W.C., and Iyer, V. (2015). WGE: a CRISPR database for genome engineering. Bioinformatics *31*, 3078-3080.

Hoek, M., and Stillman, B. (2003). Chromatin assembly factor 1 is essential and couples chromatin assembly to DNA replication in vivo. Proceedings of the National Academy of Sciences *100*, 12183-12188.

Holbert, M.A., Sikorski, T., Carten, J., Snowflack, D., Hodawadekar, S., and Marmorstein, R. (2007). The human monocytic leukemia zinc finger histone acetyltransferase domain contains DNA-binding activity implicated in chromatin targeting. J Biol Chem *282*, 36603-36613.

Hota, S.K., and Bruneau, B.G. (2016). ATP-dependent chromatin remodeling during mammalian development. Development *143*, 2882-2897.

Hou, H., Wang, Y., Kallgren, S.P., Thompson, J., Yates, J.R., 3rd, and Jia, S. (2010). Histone variant H2A.Z regulates centromere silencing and chromosome segregation in fission yeast. J Biol Chem *285*, 1909-1918.

Hou, X., Li, Y., Luo, R.Z., Fu, J.H., He, J.H., Zhang, L.J., and Yang, H.X. (2012). High expression of the transcriptional co-activator p300 predicts poor survival in resectable non-small cell lung cancers. European Journal of Surgical Oncology (EJSO) *38*, 523-530.

Hsu, C.C., Shi, J., Yuan, C., Zhao, D., Jiang, S., Lyu, J., Wang, X., Li, H., Wen, H., Li, W., *et al.* (2018a). Recognition of histone acetylation by the GAS41 YEATS domain promotes H2A.Z deposition in non-small cell lung cancer. Genes Dev *32*, 58-69.

Hsu, C.C., Zhao, D., Shi, J., Peng, D., Guan, H., Li, Y., Huang, Y., Wen, H., Li, W., Li, H., *et al.* (2018b). Gas41 links histone acetylation to H2A.Z deposition and maintenance of embryonic stem cell identity. Cell Discov *4*, 28.

Hsu, T.C. (1962). Differential rate in RNA synthesis between euchromatin and heterochromatin. Experimental Cell Research *27*, 332-334.

Hu, G., Cui, K., Northrup, D., Liu, C., Wang, C., Tang, Q., Ge, K., Levens, D., Crane-Robinson, C., and Zhao, K. (2013). H2A.Z facilitates access of active and repressive complexes to chromatin in embryonic stem cell self-renewal and differentiation. Cell Stem Cell *12*, 180-192.

Hu, Y., Fisher, J.B., Koprowski, S., McAllister, D., Kim, M.S., and Lough, J. (2009). Homozygous disruption of the Tip60 gene causes early embryonic lethality. Developmental dynamics : an official publication of the American Association of Anatomists *238*, 2912-2921.

Hua, S., Kallen, C.B., Dhar, R., Baquero, M.T., Mason, C.E., Russell, B.A., Shah, P.K., Liu, J., Khramtsov, A., Tretiakova, M.S., *et al.* (2008). Genomic analysis of estrogen cascade reveals histone variant H2A.Z associated with breast cancer progression. Molecular Systems Biology *4*, 188.

Huisinga, K.L., Brower-Toland, B., and Elgin, S.C. (2006). The contradictory definitions of heterochromatin: transcription and silencing. Chromosoma *115*, 110-122.

Humbert, J., Salian, S., Makrythanasis, P., Lemire, G., Rousseau, J., Ehresmann, S., Garcia, T., Alasiri, R., Bottani, A., Hanquinet, S., *et al.* (2020). De Novo KAT5 Variants Cause a Syndrome with Recognizable Facial Dysmorphisms, Cerebellar Atrophy, Sleep Disturbance, and Epilepsy. Am J Hum Genet *107*, 564-574.

Ikura, T., Ogryzko, V.V., Grigoriev, M., Groisman, R., Wang, J., Horikoshi, M., Scully, R., Qin, J., and Nakatani, Y. (2000). Involvement of the TIP60 Histone Acetylase Complex in DNA Repair and Apoptosis. Cell *102*, 463-473.

Ikura, T., Tashiro, S., Kakino, A., Shima, H., Jacob, N., Amunugama, R., Yoder, K., Izumi, S., Kuraoka, I., Tanaka, K., *et al.* (2007). DNA damage-dependent acetylation and ubiquitination of H2AX enhances chromatin dynamics. Mol Cell Biol *27*, 7028-7040.

Ishibashi, T., Dryhurst, D., Rose, K.L., Shabanowitz, J., Hunt, D.F., and Ausió, J. (2009). Acetylation of Vertebrate H2A.Z and Its Effect on the Structure of the Nucleosome. Biochemistry *48*, 5007-5017.

Ito, S., Kayukawa, N., Ueda, T., Taniguchi, H., Morioka, Y., Hongo, F., and Ukimura, O. (2018). MRGBP promotes AR-mediated transactivation of KLK3 and TMPRSS2 via acetylation of histone H2A.Z in prostate cancer cells. Biochim Biophys Acta Gene Regul Mech.

Iyer, A., Fairlie, D.P., and Brown, L. (2012). Lysine acetylation in obesity, diabetes and metabolic disease. Immunol Cell Biol *90*, 39-46.

Jackson, J.D., and Gorovsky, M.A. (2000). Histone H2A.Z has a conserved function that is distinct from that of the major H2A sequence variants. Nucleic Acids Res *28*, 3811-3816.

Jacobs, J.J., Kieboom, K., Marino, S., DePinho, R.A., and van Lohuizen, M. (1999). The oncogene and Polycomb-group gene bmi-1 regulates cell proliferation and senescence through the ink4a locus. Nature *397*, 164-168.

Jacquet, K., Fradet-Turcotte, A., Avvakumov, N., Lambert, J.-P., Roques, C., Pandita, Raj K., Paquet, E., Herst, P., Gingras, A.-C., Pandita, Tej K., *et al.* (2016). The TIP60 Complex Regulates Bivalent Chromatin Recognition by 53BP1 through Direct H4K20me Binding and H2AK15 Acetylation. Molecular cell *62*, 409-421.

Janbandhu, V.C., Moik, D., and Fassler, R. (2014). Cre recombinase induces DNA damage and tetraploidy in the absence of loxP sites. Cell Cycle *13*, 462-470.

Jeong, K.W., Kim, K., Situ, A.J., Ulmer, T.S., An, W., and Stallcup, M.R. (2011). Recognition of enhancer element–specific histone methylation by TIP60 in transcriptional activation. Nature Structural & Molecular Biology *18*, 1358-1365.

Jin, C., and Felsenfeld, G. (2007). Nucleosome stability mediated by histone variants H3.3 and H2A.Z. Genes Dev *21*, 1519-1529.

Jin, F., Li, Y., Dixon, J.R., Selvaraj, S., Ye, Z., Lee, A.Y., Yen, C.A., Schmitt, A.D., Espinoza, C.A., and Ren, B. (2013). A high-resolution map of the three-dimensional chromatin interactome in human cells. Nature *503*, 290-294.

Johnson, A.A., Sarthi, J., Pirooznia, S.K., Reube, W., and Elefant, F. (2013). Increasing Tip60 HAT levels rescues axonal transport defects and associated behavioral phenotypes in a Drosophila Alzheimer's disease model. J Neurosci *33*, 7535-7547.

Kadosh, D., and Struhl, K. (1998). Histone deacetylase activity of Rpd3 is important for transcriptional repression in vivo. Genes Dev *12*, 797-805.

Kalkhoven, E. (2004). CBP and p300: HATs for different occasions. Biochem Pharmacol *68*, 1145-1155.

Kamine, J., Elangovan, B., Subramanian, T., Coleman, D., and Chinnadurai, G. (1996). Identification of a cellular protein that specifically interacts with the essential cysteine region of the HIV-1 Tat transactivator. Virology *216*, 357-366.

Kandoth, C., McLellan, M.D., Vandin, F., Ye, K., Niu, B., Lu, C., Xie, M., Zhang, Q., McMichael, J.F., Wyczalkowski, M.A., *et al.* (2013). Mutational landscape and significance across 12 major cancer types. Nature *502*, 333-339.

Kanemaki, M., Kurokawa, Y., Matsu-ura, T., Makino, Y., Masani, A., Okazaki, K.-i., Morishita, T., and Tamura, T.-a. (1999). TIP49b, a New RuvB-like DNA Helicase, Is Included in a Complex Together with Another RuvB-like DNA Helicase, TIP49a. Journal of Biological Chemistry *274*, 22437-22444.

Kaplanis, J., Samocha, K.E., Wiel, L., Zhang, Z., Arvai, K.J., Eberhardt, R.Y., Gallone, G., Lelieveld, S.H., Martin, H.C., McRae, J.F., *et al.* (2020). Evidence for 28 genetic disorders discovered by combining healthcare and research data. Nature *586*, 757-762.

Kaufman, P.D., Kobayashi, R., Kessler, N., and Stillman, B. (1995). The p150 and p60 subunits of chromatin assemblyfactor I: A molecular link between newly synthesized histories and DNA replication. Cell *81*, 1105-1114.

Kaya-Okur, H.S., Wu, S.J., Codomo, C.A., Pledger, E.S., Bryson, T.D., Henikoff, J.G., Ahmad, K., and Henikoff, S. (2019). CUT&Tag for efficient epigenomic profiling of small samples and single cells. Nat Commun *10*, 1930.

Kaypee, S., Sudarshan, D., Shanmugam, M.K., Mukherjee, D., Sethi, G., and Kundu, T.K. (2016). Aberrant lysine acetylation in tumorigenesis: Implications in the development of therapeutics. Pharmacology & Therapeutics *162*, 98-119.

Kebede, A.F., Schneider, R., and Daujat, S. (2015). Novel types and sites of histone modifications emerge as players in the transcriptional regulation contest. The FEBS journal *282*, 1658-1674.

Keogh, M.C., Mennella, T.A., Sawa, C., Berthelet, S., Krogan, N.J., Wolek, A., Podolny, V., Carpenter, L.R., Greenblatt, J.F., Baetz, K., *et al.* (2006). The Saccharomyces cerevisiae histone H2A variant Htz1 is acetylated by NuA4. Genes Dev *20*, 660-665.

Khosravi, R., Maya, R., Gottlieb, T., Oren, M., Shiloh, Y., and Shkedy, D. (1999). Rapid ATM-dependent phosphorylation of MDM2 precedes p53 accumulation in response to DNA damage. Proceedings of the National Academy of Sciences *96*, 14973-14977.

Kim, C.-H., Kim, J.-W., Jang, S.-M., An, J.-H., Song, K.-H., and Choi, K.-H. (2012a). Transcriptional activity of paired homeobox Pax6 is enhanced by histone acetyltransferase Tip60 during mouse retina development. Biochemical and Biophysical Research Communications *424*, 427-432.

Kim, C.H., Kim, J.W., Jang, S.M., An, J.H., Seo, S.B., and Choi, K.H. (2015). The chromodomain-containing histone acetyltransferase TIP60 acts as a code reader, recognizing the epigenetic codes for initiating transcription. Biosci Biotechnol Biochem *79*, 532-538.

Kim, H.S., Vanoosthuyse, V., Fillingham, J., Roguev, A., Watt, S., Kislinger, T., Treyer, A., Carpenter, L.R., Bennett, C.S., Emili, A., *et al.* (2009). An acetylated form of histone H2A.Z regulates chromosome architecture in Schizosaccharomyces pombe. Nat Struct Mol Biol *16*, 1286-1293.

Kim, J.-W., Jang, S.-M., Kim, C.-H., An, J.-H., Kang, E.-J., and Choi, K.-H. (2012b). New Molecular Bridge between RelA/p65 and NF-κB Target Genes via Histone Acetyltransferase TIP60 Cofactor. Journal of Biological Chemistry *287*, 7780-7791.

Kim, J.W., Jang, S.M., Kim, C.H., An, J.H., and Choi, K.H. (2012c). Transcriptional activity of neural retina leucine zipper (Nrl) is regulated by c-Jun N-terminal kinase and Tip60 during retina development. Mol Cell Biol *32*, 1720-1732.

Kim, J.W., Jang, S.M., Kim, C.H., An, J.H., Kang, E.J., and Choi, K.H. (2011). Tip60 regulates myoblast differentiation by enhancing the transcriptional activity of MyoD via their physical interactions. The FEBS journal *278*, 4394-4404.

Kim, J.W., Jang, S.M., Kim, C.H., An, J.H., Kang, E.J., and Choi, K.H. (2012d). New molecular bridge between RelA/p65 and NF-kappaB target genes via histone acetyltransferase TIP60 cofactor. J Biol Chem *287*, 7780-7791.

Kim, J.W., Song, P.I., Jeong, M.H., An, J.H., Lee, S.Y., Jang, S.M., Song, K.H., Armstrong, C.A., and Choi, K.H. (2008). TIP60 represses transcriptional activity of p73beta via an MDM2-bridged ternary complex. J Biol Chem *283*, 20077-20086.

Kim, K., Punj, V., Choi, J., Heo, K., Kim, J.M., Laird, P.W., and An, W. (2013). Gene dysregulation by histone variant H2A.Z in bladder cancer. Epigenetics Chromatin *6*, 34.

Kim, M.S., Merlo, X., Wilson, C., and Lough, J. (2006). Co-activation of atrial natriuretic factor promoter by Tip60 and serum response factor. J Biol Chem *281*, 15082-15089.

Kimelman, D. (2006). Mesoderm induction: from caps to chips. Nature Reviews Genetics *7*, 360-372.

Kimura, A., and Horikoshi, M. (1998). Tip60 acetylates six lysines of a specific class in core histones in vitro. Genes to cells : devoted to molecular & cellular mechanisms *3*, 789-800.

Kimura, H., and Cook, P.R. (2001). Kinetics of core histones in living human cells: little exchange of H3 and H4 and some rapid exchange of H2B. J Cell Biol *153*, 1341-1353.

Klein, B.J., Ahmad, S., Vann, K.R., Andrews, F.H., Mayo, Z.A., Bourriquen, G., Bridgers, J.B., Zhang, J., Strahl, B.D., Cote, J., *et al.* (2018). Yaf9 subunit of the NuA4 and SWR1 complexes targets histone H3K27ac through its YEATS domain. Nucleic Acids Res *46*, 421-430.

Knights, C.D., Catania, J., Di Giovanni, S., Muratoglu, S., Perez, R., Swartzbeck, A., Quong, A.A., Zhang, X., Beerman, T., Pestell, R.G., *et al.* (2006). Distinct p53 acetylation cassettes differentially influence gene-expression patterns and cell fate. J Cell Biol *173*, 533-544.

Kranz, D., Dohmesen, C., and Dobbelstein, M. (2008). BRCA1 and Tip60 determine the cellular response to ultraviolet irradiation through distinct pathways. Journal of Cell Biology *182*, 197-213.

Krummel, K.A., Lee, C.J., Toledo, F., and Wahl, G.M. (2005). The C-terminal lysines fine-tune P53 stress responses in a mouse model but are not required for stability control or transactivation. Proc Natl Acad Sci U S A *102*, 10188-10193.

Kruse, J.-P., and Gu, W. (2009). Modes of p53 Regulation. Cell *137*, 609-622.

Ku, M., Jaffe, J.D., Koche, R.P., Rheinbay, E., Endoh, M., Koseki, H., Carr, S.A., and Bernstein, B.E. (2012). H2A.Z landscapes and dual modifications in pluripotent and multipotent stem cells underlie complex genome regulatory functions. Genome Biol *13*, R85.

Kueh, A.J., Dixon, M.P., Voss, A.K., and Thomas, T. (2011). HBO1 is required for H3K14 acetylation and normal transcriptional activity during embryonic development. Mol Cell Biol *31*, 845-860.

Kueh, A.J., Eccles, S., Tang, L., Garnham, A.L., May, R.E., Herold, M.J., Smyth, G.K., Voss, A.K., and Thomas, T. (2020). HBO1 (KAT7) Does Not Have an Essential Role in Cell Proliferation, DNA Replication, or Histone 4 Acetylation in Human Cells. Mol Cell Biol *40*, MCB.00506-00519.

Kuo, M.H., Zhou, J., Jambeck, P., Churchill, M.E.A., and Allis, C.D. (1998). Histone acetyltransferase activity of yeast Gcn5p is required for the activation of target genes in vivo. Genes & Development *12*, 627-639.

Kusakabe, M., Oku, H., Matsuda, R., Hori, T., Muto, A., Igarashi, K., Fukagawa, T., and Harata, M. (2016). Genetic complementation analysis showed distinct contributions of the N-terminal tail of H2A.Z to epigenetic regulations. Genes to cells : devoted to molecular & cellular mechanisms *21*, 122-135.

Kusch, T. (2004). Acetylation by Tip60 Is Required for Selective Histone Variant Exchange at DNA Lesions. Science *306*, 2084-2087.

Kusch, T., Mei, A., and Nguyen, C. (2014). Histone H3 lysine 4 trimethylation regulates cotranscriptional H2A variant exchange by Tip60 complexes to maximize gene expression. Proc Natl Acad Sci U S A *111*, 4850-4855.

Lane, D.P. (1992). Cancer. p53, guardian of the genome. Nature *358*, 15-16.

Law, C.W., Chen, Y., Shi, W., and Smyth, G.K. (2014). voom: Precision weights unlock linear model analysis tools for RNA-seq read counts. Genome Biol *15*, R29.

Leduc, C., Claverie, P., Eymin, B., Col, E., Khochbin, S., Brambilla, E., and Gazzeri, S. (2006). p14ARF promotes RB accumulation through inhibition of its Tip60-dependent acetylation. Oncogene *25*, 4147-4154.

Lee, C.-K., Shibata, Y., Rao, B., Strahl, B.D., and Lieb, J.D. (2004). Evidence for nucleosome depletion at active regulatory regions genome-wide. Nature Genetics *36*, 900-905.

Lee, D.Y., Hayes, J.J., Pruss, D., and Wolffe, A.P. (1993). A positive role for histone acetylation in transcription factor access to nucleosomal DNA. Cell *72*, 73-84.

Legube, G., Linares, L.K., Lemercier, C., Scheffner, M., Khochbin, S., and Trouche, D. (2002). Tip60 is targeted to proteasome-mediated degradation by Mdm2 and accumulates after UV irradiation. EMBO J *21*, 1704-1712.

Legube, G., Linares, L.K., Tyteca, S., Caron, C., Scheffner, M., Chevillard-Briet, M., and Trouche, D. (2004). Role of the Histone Acetyl Transferase Tip60 in the p53 Pathway. Journal of Biological Chemistry *279*, 44825-44833.

Levine, A.J. (1997). p53, the Cellular Gatekeeper for Growth and Division. Cell *88*, 323-331.

Li, E., Beard, C., and Jaenisch, R. (1993). Role for DNA methylation in genomic imprinting. Nature *366*, 362-365.

Li, G., Levitus, M., Bustamante, C., and Widom, J. (2005). Rapid spontaneous accessibility of nucleosomal DNA. Nat Struct Mol Biol *12*, 46-53.

Li, T., Kon, N., Jiang, L., Tan, M., Ludwig, T., Zhao, Y., Baer, R., and Gu, W. (2012a). Tumor suppression in the absence of p53-mediated cell-cycle arrest, apoptosis, and senescence. Cell *149*, 1269-1283.

Li, Z., Gadue, P., Chen, K., Jiao, Y., Tuteja, G., Schug, J., Li, W., and Kaestner, K.H. (2012b). Foxa2 and H2A.Z mediate nucleosome depletion during embryonic stem cell differentiation. Cell *151*, 1608-1616.

Liao, Y., Smyth, G.K., and Shi, W. (2019). The R package Rsubread is easier, faster, cheaper and better for alignment and quantification of RNA sequencing reads. Nucleic Acids Res *47*, e47.

Lin, Y.-y., Lu, J.-y., Zhang, J., Walter, W., Dang, W., Wan, J., Tao, S.-C., Qian, J., Zhao, Y., Boeke, J.D., *et al.* (2009). Protein Acetylation Microarray Reveals that NuA4 Controls Key Metabolic Target Regulating Gluconeogenesis. Cell *136*, 1073-1084.

Lin, Y.Y., Qi, Y., Lu, J.Y., Pan, X., Yuan, D.S., Zhao, Y., Bader, J.S., and Boeke, J.D. (2008). A comprehensive synthetic genetic interaction network governing yeast histone acetylation and deacetylation. Genes Dev *22*, 2062-2074.

Littau, V.C., Allfrey, V.G., Frenster, J.H., and Mirsky, A.E. (1964). Active and Inactive Regions of Nuclear Chromatin as Revealed by Electron Microscope Autoradiography. Proceedings of the National Academy of Sciences *52*, 93-100.

Liu, B.L., Cheng, J.X., Zhang, X., Wang, R., Zhang, W., Lin, H., Xiao, X., Cai, S., Chen, X.Y., and Cheng, H. (2010). Global histone modification patterns as prognostic markers to classify glioma patients. Cancer Epidemiol Biomarkers Prev *19*, 2888-2896.

Loden, M., and van Steensel, B. (2005). Whole-genome views of chromatin structure. Chromosome research : an international journal on the molecular, supramolecular and evolutionary aspects of chromosome biology *13*, 289-298.

Long, H., Zhang, L., Lv, M., Wen, Z., Zhang, W., Chen, X., Zhang, P., Li, T., Chang, L., Jin, C., *et al.* (2020). H2A.Z facilitates licensing and activation of early replication origins. Nature *577*, 576-581.

Lorbeck, M., Pirooznia, K., Sarthi, J., Zhu, X., and Elefant, F. (2011). Microarray analysis uncovers a role for Tip60 in nervous system function and general metabolism. PloS one *6*, e18412.

Louters, L., and Chalkley, R. (1985). Exchange of histones H1, H2A, and H2B in vivo. Biochemistry *24*, 3080-3085.

Luger, K., Mader, A.W., Richmond, R.K., Sargent, D.F., and Richmond, T.J. (1997). Crystal structure of the nucleosome core particle at 2.8 A resolution. Nature *389*, 251-260.

Luk, E., Ranjan, A., FitzGerald, P.C., Mizuguchi, G., Huang, Y., Wei, D., and Wu, C. (2010). Stepwise Histone Replacement by SWR1 Requires Dual Activation with Histone H2A.Z and Canonical Nucleosome. Cell *143*, 725-736.

Lun, A.T., Chen, Y., and Smyth, G.K. (2016). It's DE-licious: A Recipe for Differential Expression Analyses of RNA-seq Experiments Using Quasi-Likelihood Methods in edgeR. Methods Mol Biol *1418*, 391-416.

Lv, D., Jia, F., Hou, Y., Sang, Y., Alvarez, A.A., Zhang, W., Gao, W.Q., Hu, B., Cheng, S.Y., Ge, J., *et al.* (2017). Histone Acetyltransferase KAT6A Upregulates PI3K/AKT Signaling through TRIM24 Binding. Cancer Res *77*, 6190-6201.

Ma, T. (2000). Cell cycle-regulated phosphorylation of p220NPAT by cyclin E/Cdk2 in Cajal bodies promotes histone gene transcription. Genes & Development *14*, 2298-2313.

Ma, X., Liu, Y., Liu, Y., Alexandrov, L.B., Edmonson, M.N., Gawad, C., Zhou, X., Li, Y., Rusch, M.C., Easton, J., *et al.* (2018). Pan-cancer genome and transcriptome analyses of 1,699 paediatric leukaemias and solid tumours. Nature *555*, 371-376.

Madeira, F., Park, Y.M., Lee, J., Buso, N., Gur, T., Madhusoodanan, N., Basutkar, P., Tivey, A.R.N., Potter, S.C., Finn, R.D., *et al.* (2019). The EMBL-EBI search and sequence analysis tools APIs in 2019. Nucleic Acids Res *47*, W636-W641.

Maeshima, K., Rogge, R., Tamura, S., Joti, Y., Hikima, T., Szerlong, H., Krause, C., Herman, J., Seidel, E., DeLuca, J., *et al.* (2016). Nucleosomal arrays self‐assemble into supramolecular globular structures lacking 30‐nm fibers. The EMBO Journal *35*, 1115-1132.

Maison, C., and Almouzni, G. (2004). HP1 and the dynamics of heterochromatin maintenance. Nat Rev Mol Cell Biol *5*, 296-304.

Marshall, W.F., Dernburg, A.F., Harmon, B., Agard, D.A., and Sedat, J.W. (1996). Specific interactions of chromatin with the nuclear envelope: positional

determination within the nucleus in Drosophila melanogaster. Molecular biology of the cell *7*, 825-842.

Marshall, W.F., Straight, A., Marko, J.F., Swedlow, J., Dernburg, A., Belmont, A., Murray, A.W., Agard, D.A., and Sedat, J.W. (1997). Interphase chromosomes undergo constrained diffusional motion in living cells. Current Biology *7*, 930-939.

Martire, S., and Banaszynski, L.A. (2020). The roles of histone variants in fine-tuning chromatin organization and function. Nature Reviews Molecular Cell Biology *21*, 522-541.

Maruyama, E.O., Hori, T., Tanabe, H., Kitamura, H., Matsuda, R., Tone, S., Hozak, P., Habermann, F.A., von Hase, J., Cremer, C., *et al.* (2012). The actin family member Arp6 and the histone variant H2A.Z are required for spatial positioning of chromatin in chicken cell nuclei. J Cell Sci *125*, 3739-3743.

Matsuda, R., Hori, T., Kitamura, H., Takeuchi, K., Fukagawa, T., and Harata, M. (2010). Identification and characterization of the two isoforms of the vertebrate H2A.Z histone variant. Nucleic Acids Res *38*, 4263-4273.

McAllister, D., Merlo, X., and Lough, J. (2002). Characterization and expression of the mouse tat interactive protein 60 kD (TIP60) gene. Gene *289*, 169-176.

McCarthy, D.J., Chen, Y., and Smyth, G.K. (2012). Differential expression analysis of multifactor RNA-Seq experiments with respect to biological variation. Nucleic Acids Res *40*, 4288-4297.

McGuire, A., Casey, M.C., Shalaby, A., Kalinina, O., Curran, C., Webber, M., Callagy, G., Holian, E., Bourke, E., Kerin, M.J., *et al.* (2019). Quantifying Tip60 (Kat5) stratifies breast cancer. Sci Rep *9*, 3819.

Mendel, J.G. (1865). Experiments in plant hybridization (http://www.esp.org: Electronic Scholarly Publishing Project).

Meneghini, M.D., Wu, M., and Madhani, H.D. (2003). Conserved histone variant H2A.Z protects euchromatin from the ectopic spread of silent heterochromatin. Cell *112*, 725-736.

Messerschmidt, D.M., Knowles, B.B., and Solter, D. (2014). DNA methylation dynamics during epigenetic reprogramming in the germline and preimplantation embryos. Genes Dev *28*, 812-828.

Mezger, A., Klemm, S., Mann, I., Brower, K., Mir, A., Bostick, M., Farmer, A., Fordyce, P., Linnarsson, S., and Greenleaf, W. (2018). High-throughput chromatin accessibility profiling at single-cell resolution. Nature Communications *9*, 3647.

Mikkelsen, T.S., Ku, M., Jaffe, D.B., Issac, B., Lieberman, E., Giannoukos, G., Alvarez, P., Brockman, W., Kim, T.-K., Koche, R.P., *et al.* (2007). Genome-wide maps of chromatin state in pluripotent and lineage-committed cells. Nature *448*, 553-560.

Millar, C.B., Xu, F., Zhang, K., and Grunstein, M. (2006). Acetylation of H2AZ Lys 14 is associated with genome-wide gene activity in yeast. Genes Dev *20*, 711-722.

Mirsky, A.E., and Pollister, A.W. (1946). Chromosin, a Desoxyribose Nucleoprotein Complex of the Cell Nucleus. J Gen Physiol *30*, 117-148.

Mishima, Y., Miyagi, S., Saraya, A., Negishi, M., Endoh, M., Endo, T.A., Toyoda, T., Shinga, J., Katsumoto, T., Chiba, T., *et al.* (2011). The Hbo1-Brd1/Brpf2 complex is responsible for global acetylation of H3K14 and required for fetal liver erythropoiesis. Blood *118*, 2443-2453.

Mitchell, L., Lambert, J.P., Gerdes, M., Al-Madhoun, A.S., Skerjanc, I.S., Figeys, D., and Baetz, K. (2008). Functional dissection of the NuA4 histone

acetyltransferase reveals its role as a genetic hub and that Eaf1 is essential for complex integrity. Mol Cell Biol *28*, 2244-2256.

Mizuguchi, G., Shen, X., Landry, J., Wu, W.H., Sen, S., and Wu, C. (2004). ATP-driven exchange of histone H2AZ variant catalyzed by SWR1 chromatin remodeling complex. Science *303*, 343-348.

Mo, F., Zhuang, X., Liu, X., Yao, P.Y., Qin, B., Su, Z., Zang, J., Wang, Z., Zhang, J., Dou, Z., *et al.* (2016). Acetylation of Aurora B by TIP60 ensures accurate chromosomal segregation. Nature chemical biology *12*, 226-232.

Mo, X., Kowenz-Leutz, E., Laumonnier, Y., Xu, H., and Leutz, A. (2005). Histone H3 tail positioning and acetylation by the c-Myb but not the v-Myb DNA-binding SANT domain. Genes Dev *19*, 2447-2457.

Mohandas, T., Sparkes, R.S., and Shapiro, L.J. (1981). Reactivation of an inactive human X chromosome: evidence for X inactivation by DNA methylation. Science *211*, 393-396.

Monden, T., Kishi, M., Hosoya, T., Satoh, T., Wondisford, F.E., Hollenberg, A.N., Yamada, M., and Mori, M. (1999). p120 acts as a specific coactivator for 9-cis-retinoic acid receptor (RXR) on peroxisome proliferator-activated receptor-gamma/RXR heterodimers. Mol Endocrinol *13*, 1695-1703.

Monden, T., Wondisford, F.E., and Hollenberg, A.N. (1997). Isolation and characterization of a novel ligand-dependent thyroid hormone receptor-coactivating protein. J Biol Chem *272*, 29834-29841.

Murphy, P.J., Wu, S.F., James, C.R., Wike, C.L., and Cairns, B.R. (2018). Placeholder Nucleosomes Underlie Germline-to-Embryo DNA Methylation Reprogramming. Cell *172*, 993-1006.e1013.

Murr, R., Loizou, J.I., Yang, Y.G., Cuenin, C., Li, H., Wang, Z.Q., and Herceg, Z. (2006). Histone acetylation by Trrap-Tip60 modulates loading of repair proteins and repair of DNA double-strand breaks. Nat Cell Biol *8*, 91-99.

Murr, R., Vaissière, T., Sawan, C., Shukla, V., and Herceg, Z. (2007). Orchestration of chromatin-based processes: mind the TRRAP. Oncogene *26*, 5358-5372.

Nagashima, M., Shiseki, M., Pedeux, R.M., Okamura, S., Kitahama-Shiseki, M., Miura, K., Yokota, J., and Harris, C.C. (2003). A novel PHD-finger motif protein, p47ING3, modulates p53-mediated transcription, cell cycle control, and apoptosis. Oncogene *22*, 343-350.

Narkaj, K., Stefanelli, G., Wahdan, M., Azam, A.B., Ramzan, F., Steininger, C.F.D., Jr., Walters, B.J., and Zovkic, I.B. (2018). Blocking H2A.Z Incorporation via Tip60 Inhibition Promotes Systems Consolidation of Fear Memory in Mice. eNeuro *5*, ENEURO.0378-0318.2018.

Nashun, B., Yukawa, M., Liu, H., Akiyama, T., and Aoki, F. (2010). Changes in the nuclear deposition of histone H2A variants during pre-implantation development in mice. Development *137*, 3785-3794.

Nekrasov, M., Amrichova, J., Parker, B.J., Soboleva, T.A., Jack, C., Williams, R., Huttley, G.A., and Tremethick, D.J. (2012). Histone H2A.Z inheritance during the cell cycle and its impact on promoter organization and dynamics. Nature Structural & Molecular Biology *19*, 1076-1083.

Nishibuchi, I., Suzuki, H., Kinomura, A., Sun, J., Liu, N.A., Horikoshi, Y., Shima, H., Kusakabe, M., Harata, M., Fukagawa, T., *et al.* (2014). Reorganization of damaged chromatin by the exchange of histone variant H2A.Z-2. International journal of radiation oncology, biology, physics *89*, 736-744.

Nunan, J., and Small, D.H. (2000). Regulation of APP cleavage by alpha-, beta- and gamma-secretases. FEBS Lett *483*, 6-10.

Nye, C.K., Hanson, R.W., and Kalhan, S.C. (2008). Glyceroneogenesis is the dominant pathway for triglyceride glycerol synthesis in vivo in the rat. J Biol Chem *283*, 27565-27574.

Obri, A., Ouararhni, K., Papin, C., Diebold, M.L., Padmanabhan, K., Marek, M., Stoll, I., Roy, L., Reilly, P.T., Mak, T.W., *et al.* (2014). ANP32E is a histone chaperone that removes H2A.Z from chromatin. Nature *505*, 648-653.

Olins, A.L., and Olins, D.E. (1974). Spheroid Chromatin Units (ngr Bodies). Science *183*, 330-332.

Oudet, P., Gross-Bellard, M., and Chambon, P. (1975). Electron microscopic and biochemical evidence that chromatin structure is a repeating unit. Cell *4*, 281-300.

Paik, W.K., and Kim, S. (1980). Protein Methylation (Wiley).

Pandey, R., and Dou, Y. (2013). H2A.Z Sets the Stage in ESCs. Cell Stem Cell *12*, 143-144.

Papamichos-Chronakis, M., Watanabe, S., Rando, O.J., and Peterson, C.L. (2011). Global regulation of H2A.Z localization by the INO80 chromatin-remodeling enzyme is essential for genome integrity. Cell *144*, 200-213.

Parrinello, S., Samper, E., Krtolica, A., Goldstein, J., Melov, S., and Campisi, J. (2003). Oxygen sensitivity severely limits the replicative lifespan of murine fibroblasts. Nat Cell Biol *5*, 741-747.

Patel, J.H., Du, Y., Ard, P.G., Phillips, C., Carella, B., Chen, C.-J., Rakowski, C., Chatterjee, C., Lieberman, P.M., Lane, W.S., *et al.* (2004). The c-MYC Oncoprotein Is a Substrate of the Acetyltransferases hGCN5/PCAF and TIP60. Molecular and Cellular Biology *24*, 10826-10834.

Pena, P.V., Davrazou, F., Shi, X., Walter, K.L., Verkhusha, V.V., Gozani, O., Zhao, R., and Kutateladze, T.G. (2006). Molecular mechanism of histone H3K4me3 recognition by plant homeodomain of ING2. Nature *442*, 100-103.

Perez-Perri, J.I., Dengler, V.L., Audetat, K.A., Pandey, A., Bonner, E.A., Urh, M., Mendez, J., Daniels, D.L., Wappner, P., Galbraith, M.D., *et al.* (2016). The TIP60 Complex Is a Conserved Coactivator of HIF1A. Cell Rep *16*, 37-47.

Peters, A.H.F.M., Kubicek, S., Mechtler, K., O'Sullivan, R.J., Derijck, A.A.H.A., Perez-Burgos, L., Kohlmaier, A., Opravil, S., Tachibana, M., Shinkai, Y., *et al.* (2003). Partitioning and Plasticity of Repressive Histone Methylation States in Mammalian Chromatin. Molecular cell *12*, 1577-1589.

Petesch, S.J., and Lis, J.T. (2012). Overcoming the nucleosome barrier during transcript elongation. Trends Genet *28*, 285-294.

Phipson, B., Lee, S., Majewski, I.J., Alexander, W.S., and Smyth, G.K. (2016). Robust Hyperparameter Estimation Protects against Hypervariable Genes and Improves Power to Detect Differential Expression. Ann Appl Stat *10*, 946-963.

Pierce, B.A. (2005). Genetics: A Conceptual Approach, 2nd edition edn (New York: W. H. Freeman and Company).

Pirooznia, S.K., Chiu, K., Chan, M.T., Zimmerman, J.E., and Elefant, F. (2012). Epigenetic Regulation of Axonal Growth ofDrosophilaPacemaker Cells by Histone Acetyltransferase Tip60 Controls Sleep. Genetics *192*, 1327-1345.

Raisner, R.M., Hartley, P.D., Meneghini, M.D., Bao, M.Z., Liu, C.L., Schreiber, S.L., Rando, O.J., and Madhani, H.D. (2005). Histone Variant H2A.Z Marks the 5′ Ends of Both Active and Inactive Genes in Euchromatin. Cell *123*, 233-248.

Ran, Q., and Pereira-Smith, O.M. (2000). Identification of an alternatively spliced form of the Tat Interactive Protein (Tip60), Tip60(β). Gene *258*, 141-146.

Rangasamy, D., Berven, L., Ridgway, P., and Tremethick, D.J. (2003). Pericentric heterochromatin becomes enriched with H2A.Z during early mammalian development. EMBO J *22*, 1599-1607.

Rangasamy, D., Greaves, I., and Tremethick, D.J. (2004). RNA interference demonstrates a novel role for H2A.Z in chromosome segregation. Nat Struct Mol Biol *11*, 650-655.

Ransom, M., Dennehey, B.K., and Tyler, J.K. (2010). Chaperoning histones during DNA replication and repair. Cell *140*, 183-195.

Ravens, S., Yu, C., Ye, T., Stierle, M., and Tora, L. (2015). Tip60 complex binds to active Pol II promoters and a subset of enhancers and co-regulates the c-Myc network in mouse embryonic stem cells. Epigenetics Chromatin *8*, 45.

Rea, S., Eisenhaber, F., O'Carroll, D., Strahl, B.D., Sun, Z.-W., Schmid, M., Opravil, S., Mechtler, K., Ponting, C.P., Allis, C.D., *et al.* (2000). Regulation of chromatin structure by site-specific histone H3 methyltransferases. Nature *406*, 593-599.

Ren, Q., and Gorovsky, M.A. (2001). Histone H2A.Z Acetylation Modulates an Essential Charge Patch. Molecular cell *7*, 1329-1335.

Richards, E.J., and Elgin, S.C. (2002). Epigenetic codes for heterochromatin formation and silencing: rounding up the usual suspects. Cell *108*, 489-500.

Richmond, T.J., Finch, J.T., Rushton, B., Rhodes, D., and Klug, A. (1984). Structure of the nucleosome core particle at 7 A resolution. Nature *311*, 532-537.

Rispal, J., Baron, L., Beaulieu, J.F., Chevillard-Briet, M., Trouche, D., and Escaffit, F. (2019). The H2A.Z histone variant integrates Wnt signaling in intestinal epithelial homeostasis. Nat Commun *10*, 1827.

Ritchie, M.E., Phipson, B., Wu, D., Hu, Y., Law, C.W., Shi, W., and Smyth, G.K. (2015). limma powers differential expression analyses for RNA-sequencing and microarray studies. Nucleic Acids Res *43*, e47.

Robbins, E., and Borun, T.W. (1967). The Cytoplasmic Synthesis of Histones in Hela Cells and Its Temporal Relationship to DNA Replication. Proceedings of the National Academy of Sciences *57*, 409-416.

Robinson, M.D., McCarthy, D.J., and Smyth, G.K. (2010). edgeR: a Bioconductor package for differential expression analysis of digital gene expression data. Bioinformatics *26*, 139-140.

Robinson, M.D., and Oshlack, A. (2010). A scaling normalization method for differential expression analysis of RNA-seq data. Genome Biol *11*, R25.

Rogakou, E.P., Pilch, D.R., Orr, A.H., Ivanova, V.S., and Bonner, W.M. (1998). DNA Double-stranded Breaks Induce Histone H2AX Phosphorylation on Serine 139. Journal of Biological Chemistry *273*, 5858-5868.

Rudnizky, S., Bavly, A., Malik, O., Pnueli, L., Melamed, P., and Kaplan, A. (2016). H2A.Z controls the stability and mobility of nucleosomes to regulate expression of the LH genes. Nat Commun *7*, 12958.

Ruhl, D.D., Jin, J., Cai, Y., Swanson, S., Florens, L., Washburn, M.P., Conaway, R.C., Conaway, J.W., and Chrivia, J.C. (2006). Purification of a human SRCAP complex that remodels chromatin by incorporating the histone variant H2A.Z into nucleosomes. Biochemistry *45*, 5671-5677.

Sabari, B.R., Zhang, D., Allis, C.D., and Zhao, Y. (2016). Metabolic regulation of gene expression through histone acylations. Nature Reviews Molecular Cell Biology *18*, 90-101.

Sakaguchi, K., Herrera, J.E., Saito, S.i., Miki, T., Bustin, M., Vassilev, A., Anderson, C.W., and Appella, E. (1998). DNA damage activates p53 through a phosphorylation-acetylation cascade. Genes & Development *12*, 2831-2841.

Sakuraba, K., Yasuda, T., Sakata, M., Kitamura, Y.H., Shirahata, A., Goto, T., Mizukami, H., Saito, M., Ishibashi, K., Kigawa, G., *et al.* (2009). Down-regulation of Tip60 gene as a potential marker for the malignancy of colorectal cancer. Anticancer Res *29*, 3953-3955.

Sakuraba, K., Yokomizo, K., Shirahata, A., Goto, T., Saito, M., Ishibashi, K., Kigawa, G., Nemoto, H., and Hibi, K. (2011). TIP60 as a potential marker for the malignancy of gastric cancer. Anticancer Res *31*, 77-79.

Salama, R., Sadaie, M., Hoare, M., and Narita, M. (2014). Cellular senescence and its effector programs. Genes Dev *28*, 99-114.

Sanford, J.P., Clark, H.J., Chapman, V.M., and Rossant, J. (1987). Differences in DNA methylation during oogenesis and spermatogenesis and their persistence during early embryogenesis in the mouse. Genes & Development *1*, 1039-1046.

Santisteban, M.S., Hang, M., and Smith, M.M. (2011). Histone variant H2A.Z and RNA polymerase II transcription elongation. Mol Cell Biol *31*, 1848-1860.

Santisteban, M.S., Kalashnikova, T., and Smith, M.M. (2000). Histone H2A.Z Regulates Transcription and Is Partially Redundant with Nucleosome Remodeling Complexes. Cell *103*, 411-422.

Santos-Rosa, H., Schneider, R., Bannister, A.J., Sherriff, J., Bernstein, B.E., Emre, N.C., Schreiber, S.L., Mellor, J., and Kouzarides, T. (2002). Active genes are tri-methylated at K4 of histone H3. Nature *419*, 407-411.

Sarcinella, E., Zuzarte, P.C., Lau, P.N., Draker, R., and Cheung, P. (2007). Monoubiquitylation of H2A.Z distinguishes its association with euchromatin or facultative heterochromatin. Mol Cell Biol *27*, 6457-6468.

Seibler, J., Zevnik, B., Kuter-Luks, B., Andreas, S., Kern, H., Hennek, T., Rode, A., Heimann, C., Faust, N., Kauselmann, G., *et al.* (2003). Rapid generation of inducible mouse mutants. Nucleic Acids Res *31*, e12.

Semer, M., Bidon, B., Larnicol, A., Caliskan, G., Catez, P., Egly, J.M., Coin, F., and Le May, N. (2019). DNA repair complex licenses acetylation of H2A.Z.1 by KAT2A during transcription. Nature chemical biology *15*, 992-1000.

Serrano, M., Lee, H., Chin, L., Cordon-Cardo, C., Beach, D., and DePinho, R.A. (1996). Role of the INK4a locus in tumor suppression and cell mortality. Cell *85*, 27-37.

Sharpless, N.E., Ramsey, M.R., Balasubramanian, P., Castrillon, D.H., and DePinho, R.A. (2004). The differential impact of p16INK4a or p19ARF deficiency on cell growth and tumorigenesis. Oncogene *23*, 379-385.

Sheikh, B.N. (2014). Crafting the brain - role of histone acetyltransferases in neural development and disease. Cell Tissue Res *356*, 553-573.

Sheikh, B.N., Phipson, B., El-Saafin, F., Vanyai, H.K., Downer, N.L., Bird, M.J., Kueh, A.J., May, R.E., Smyth, G.K., Voss, A.K., *et al.* (2015). MOZ (MYST3, KAT6A) inhibits senescence via the INK4A-ARF pathway. Oncogene *34*, 5807-5820.

Shelby, R.D., Hahn, K.M., and Sullivan, K.F. (1996). Dynamic elastic behavior of alpha-satellite DNA domains visualized in situ in living human cells. J Cell Biol *135*, 545-557.

Shen, T., Ji, F., Wang, Y., Lei, X., Zhang, D., and Jiao, J. (2018). Brain-specific deletion of histone variant H2A.z results in cortical neurogenesis defects and neurodevelopmental disorder. Nucleic Acids Res *46*, 2290-2307.

Shen, X., Mizuguchi, G., Hamiche, A., and Wu, C. (2000). A chromatin remodelling complex involved in transcription and DNA processing. Nature *406*, 541-544.

Sheridan, A.M., Force, T., Yoon, H.-J., O'Leary, E., Choukroun, G., Taheri, M.R., and Bonventre, J.V. (2001). PLIP, a Novel Splice Variant of Tip60, Interacts with Group IV Cytosolic Phospholipase A2, Induces Apoptosis, and Potentiates Prostaglandin Production. Molecular and Cellular Biology *21*, 4470-4481.

Sidoli, S., Bhanu, N.V., Karch, K.R., Wang, X., and Garcia, B.A. (2016). Complete Workflow for Analysis of Histone Post-translational Modifications Using Bottom-up Mass Spectrometry: From Histone Extraction to Data Analysis. J Vis Exp, e54112.

Simo-Riudalbas, L., Perez-Salvia, M., Setien, F., Villanueva, A., Moutinho, C., Martinez-Cardus, A., Moran, S., Berdasco, M., Gomez, A., Vidal, E., *et al.* (2015). KAT6B Is a Tumor Suppressor Histone H3 Lysine 23 Acetyltransferase Undergoing Genomic Loss in Small Cell Lung Cancer. Cancer Res *75*, 3936-3945.

Slupianek, A., Yerrum, S., Safadi, F.F., and Monroy, M.A. (2010). The chromatin remodeling factor SRCAP modulates expression of prostate specific antigen and cellular proliferation in prostate cancer cells. J Cell Physiol *224*, 369-375.

Smith, E.R., Pannuti, A., Gu, W., Steurnagel, A., Cook, R.G., Allis, C.D., and Lucchesi, J.C. (2000). The Drosophila MSL Complex Acetylates Histone H4 at Lysine 16, a Chromatin Modification Linked to Dosage Compensation. Molecular and Cellular Biology *20*, 312-318.

Smith, S., and Stillman, B. (1989). Purification and characterization of CAF-I, a human cell factor required for chromatin assembly during DNA replication in vitro. Cell *58*, 15-25.

Smith, S., and Stillman, B. (1991). Stepwise assembly of chromatin during DNA replication in vitro. EMBO J *10*, 971-980.

Smits, A.H., Ziebell, F., Joberty, G., Zinn, N., Mueller, W.F., Clauder-Munster, S., Eberhard, D., Falth Savitski, M., Grandi, P., Jakob, P., *et al.* (2019). Biological plasticity rescues target activity in CRISPR knock outs. Nat Methods *16*, 1087-1093.

Sogo, J.M., Stahl, H., Koller, T., and Knippers, R. (1986). Structure of replicating simian virus 40 minichromosomes. The replication fork, core histone segregation and terminal structures. J Mol Biol *189*, 189-204.

Song, J.S., Chun, S.-M., Lee, J.Y., Kim, D.K., Kim, Y.H., and Jang, S.J. (2011). The Histone Acetyltransferase hMOF is Overexpressed in Non-small Cell Lung Carcinoma. The Korean Journal of Pathology *45*, 386.

Stasevich, T.J., Hayashi-Takanaka, Y., Sato, Y., Maehara, K., Ohkawa, Y., Sakata-Sogawa, K., Tokunaga, M., Nagase, T., Nozaki, N., McNally, J.G., *et al.* (2014). Regulation of RNA polymerase II activation by histone acetylation in single living cells. Nature *516*, 272-275.

Strahl, B.D., and Allis, C.D. (2000). The language of covalent histone modifications. Nature *403*, 41-45.

Suka, N., Luo, K., and Grunstein, M. (2002). Sir2p and Sas2p opposingly regulate acetylation of yeast histone H4 lysine16 and spreading of heterochromatin. Nature Genetics *32*, 378-383.

Sullivan, B.A., and Karpen, G.H. (2004). Centromeric chromatin exhibits a histone modification pattern that is distinct from both euchromatin and heterochromatin. Nat Struct Mol Biol *11*, 1076-1083.

Sun, Y., Jiang, X., Chen, S., Fernandes, N., and Price, B.D. (2005). A role for the Tip60 histone acetyltransferase in the acetylation and activation of ATM. Proceedings of the National Academy of Sciences *102*, 13182-13187.

Sun, Y., Jiang, X., Xu, Y., Ayrapetov, M.K., Moreau, L.A., Whetstine, J.R., and Price, B.D. (2009). Histone H3 methylation links DNA damage detection to activation of the tumour suppressor Tip60. Nat Cell Biol *11*, 1376-1382.

Suto, R.K., Clarkson, M.J., Tremethick, D.J., and Luger, K. (2000). Crystal structure of a nucleosome core particle containing the variant histone H2A.Z. Nat Struct Biol *7*, 1121-1124.

Sykes, S.M., Mellert, H.S., Holbert, M.A., Li, K., Marmorstein, R., Lane, W.S., and McMahon, S.B. (2006). Acetylation of the p53 DNA-Binding Domain Regulates Apoptosis Induction. Molecular cell *24*, 841-851.

Taipale, M., Rea, S., Richter, K., Vilar, A., Lichter, P., Imhof, A., and Akhtar, A. (2005). hMOF histone acetyltransferase is required for histone H4 lysine 16 acetylation in mammalian cells. Mol Cell Biol *25*, 6798-6810.

Takami, Y., Ono, T., Fukagawa, T., Shibahara, K., and Nakayama, T. (2007). Essential role of chromatin assembly factor-1-mediated rapid nucleosome assembly for DNA replication and cell division in vertebrate cells. Molecular biology of the cell *18*, 129-141.

Tang, Y., Luo, J., Zhang, W., and Gu, W. (2006). Tip60-dependent acetylation of p53 modulates the decision between cell-cycle arrest and apoptosis. Molecular cell *24*, 827-839.

Tang, Y., Zhao, W., Chen, Y., Zhao, Y., and Gu, W. (2008). Acetylation is indispensable for p53 activation. Cell *133*, 612-626.

Tanner, K.G., Trievel, R.C., Kuo, M.H., Howard, R.M., Berger, S.L., Allis, C.D., Marmorstein, R., and Denu, J.M. (1999). Catalytic mechanism and function of invariant glutamic acid 173 from the histone acetyltransferase GCN5 transcriptional coactivator. J Biol Chem *274*, 18157-18160.

Taubert, S., Gorrini, C., Frank, S.R., Parisi, T., Fuchs, M., Chan, H.M., Livingston, D.M., and Amati, B. (2004). E2F-dependent histone acetylation and recruitment of the Tip60 acetyltransferase complex to chromatin in late G1. Mol Cell Biol *24*, 4546-4556.

Thatcher, T.H., and Gorovsky, M.A. (1994). Phylogenetic analysis of the core histones H2A, H2B, H3, and H4. Nucleic Acids Res *22*, 174-179.

Thiriet, C. (2005). Replication-independent core histone dynamics at transcriptionally active loci in vivo. Genes & Development *19*, 677-682.

Thomas, T., Dixon, M.P., Kueh, A.J., and Voss, A.K. (2008). Mof (MYST1 or KAT8) is essential for progression of embryonic development past the blastocyst stage and required for normal chromatin architecture. Mol Cell Biol *28*, 5093-5105.

Thomas, T., Loveland, K.L., and Voss, A.K. (2007). The genes coding for the MYST family histone acetyltransferases, Tip60 and Mof, are expressed at high levels during sperm development. Gene Expr Patterns *7*, 657-665.

Thorne, A.W., Kmiciek, D., Mitchelson, K., Sautiere, P., and Crane-Robinson, C. (1990). Patterns of histone acetylation. Eur J Biochem *193*, 701-713.

Tremethick, D.J. (2007). Higher-Order Structures of Chromatin: The Elusive 30 nm Fiber. Cell *128*, 651-654.

Tronche, F., Kellendonk, C., Kretz, O., Gass, P., Anlag, K., Orban, P.C., Bock, R., Klein, R., and Schütz, G. (1999). Disruption of the glucocorticoid receptor gene in the nervous system results in reduced anxiety. Nature Genetics *23*, 99-103.

Tropberger, P., and Schneider, R. (2010). Going global: novel histone modifications in the globular domain of H3. Epigenetics *5*, 112-117.

Tsunaka, Y., Fujiwara, Y., Oyama, T., Hirose, S., and Morikawa, K. (2016). Integrated molecular mechanism directing nucleosome reorganization by human FACT. Genes Dev *30*, 673-686.

Uziel, T., Lerenthal, Y., Moyal, L., Andegeko, Y., Mittelman, L., and Shiloh, Y. (2003). Requirement of the MRN complex for ATM activation by DNA damage. EMBO J *22*, 5612-5621.

Valdes-Mora, F., Gould, C.M., Colino-Sanguino, Y., Qu, W., Song, J.Z., Taylor, K.M., Buske, F.A., Statham, A.L., Nair, S.S., Armstrong, N.J., *et al.* (2017). Acetylated histone variant H2A.Z is involved in the activation of neo-enhancers in prostate cancer. Nat Commun *8*, 1346.

Valdes-Mora, F., Song, J.Z., Statham, A.L., Strbenac, D., Robinson, M.D., Nair, S.S., Patterson, K.I., Tremethick, D.J., Stirzaker, C., and Clark, S.J. (2012). Acetylation of H2A.Z is a key epigenetic modification associated with gene deregulation and epigenetic remodeling in cancer. Genome Res *22*, 307-321.

van Daal, A., White, E.M., Gorovsky, M.A., and Elgin, S.C. (1988). Drosophila has a single copy of the gene encoding a highly conserved histone H2A variant of the H2A.F/Z type. Nucleic Acids Res *16*, 7487-7497.

Van Holde, K.E. (1988). Histone Modifications. In Chromatin (Springer-Verlag, New York), pp. 111 - 148.

VanDemark, A.P., Blanksma, M., Ferris, E., Heroux, A., Hill, C.P., and Formosa, T. (2006). The structure of the yFACT Pob3-M domain, its interaction with the DNA replication factor RPA, and a potential role in nucleosome deposition. Molecular cell *22*, 363-374.

Vardabasso, C., Gaspar-Maia, A., Hasson, D., Punzeler, S., Valle-Garcia, D., Straub, T., Keilhauer, E.C., Strub, T., Dong, J., Panda, T., *et al.* (2015). Histone Variant H2A.Z.2 Mediates Proliferation and Drug Sensitivity of Malignant Melanoma. Molecular cell *59*, 75-88.

Venkatraman, A., Hu, Y.-S., Didonna, A., Cvetanovic, M., Krbanjevic, A., Bilesimo, P., and Opal, P. (2014). The histone deacetylase HDAC3 is essential for Purkinje cell function, potentially complicating the use of HDAC inhibitors in SCA1. Human molecular genetics *23*, 3733-3745.

Vermeulen, K., Van Bockstaele, D.R., and Berneman, Z.N. (2003). The cell cycle: a review of regulation, deregulation and therapeutic targets in cancer. Cell Prolif *36*, 131-149.

Voigt, P., Tee, W.W., and Reinberg, D. (2013). A double take on bivalent promoters. Genes Dev *27*, 1318-1338.

Voss, A.K., Collin, C., Dixon, M.P., and Thomas, T. (2009). Moz and Retinoic Acid Coordinately Regulate H3K9 Acetylation, Hox Gene Expression, and Segment Identity. Developmental Cell *17*, 674-686.

Voss, A.K., and Thomas, T. (2018). Histone Lysine and Genomic Targets of Histone Acetyltransferases in Mammals. Bioessays *40*, e1800078.

Voss, A.K., Vanyai, H.K., Collin, C., Dixon, M.P., McLennan, T.J., Sheikh, B.N., Scambler, P., and Thomas, T. (2012). MOZ regulates the Tbx1 locus, and Moz mutation partially phenocopies DiGeorge syndrome. Dev Cell *23*, 652-663.

Vousden, K.H. (2006). Outcomes of p53 activation--spoilt for choice. J Cell Sci *119*, 5015-5020.

Vousden, K.H., and Prives, C. (2009). Blinded by the Light: The Growing Complexity of p53. Cell *137*, 413-431.

Waddington, C.H. (1956). Genetic Assimilation of the Bithorax Phenotype. Evolution *10*, 1-13.

Waddington, C.H. (2014). The Strategy of the Genes (Taylor & Francis).
Wang, A.Y., Schulze, J.M., Skordalakes, E., Gin, J.W., Berger, J.M., Rine, J., and Kobor, M.S. (2009a). Asf1-like structure of the conserved Yaf9 YEATS domain and role in H2A.Z deposition and acetylation. Proceedings of the National Academy of Sciences *106*, 21573-21578.
Wang, L., Liu, L., and Berger, S.L. (1998). Critical residues for histone acetylation by Gcn5, functioning in Ada and SAGA complexes, are also required for transcriptional function in vivo. Genes Dev *12*, 640-653.
Wang, Q., Zhang, Y., Yang, C., Xiong, H., Lin, Y., Yao, J., Li, H., Xie, L., Zhao, W., Yao, Y., *et al.* (2010). Acetylation of Metabolic Enzymes Coordinates Carbon Source Utilization and Metabolic Flux. Science *327*, 1004-1007.
Wang, X., Ahmad, S., Zhang, Z., Cote, J., and Cai, G. (2018a). Architecture of the Saccharomyces cerevisiae NuA4/TIP60 complex. Nat Commun *9*, 1147.
Wang, Y., Jin, J., Chung, M.W.H., Feng, L., Sun, H., and Hao, Q. (2018b). Identification of the YEATS domain of GAS41 as a pH-dependent reader of histone succinylation. Proceedings of the National Academy of Sciences *115*, 2365-2370.
Wang, Z., Zang, C., Cui, K., Schones, D.E., Barski, A., Peng, W., and Zhao, K. (2009b). Genome-wide mapping of HATs and HDACs reveals distinct functions in active and inactive genes. Cell *138*, 1019-1031.
Wang, Z., Zang, C., Rosenfeld, J.A., Schones, D.E., Barski, A., Cuddapah, S., Cui, K., Roh, T.Y., Peng, W., Zhang, M.Q., *et al.* (2008). Combinatorial patterns of histone acetylations and methylations in the human genome. Nat Genet *40*, 897-903.
Watanabe, S., Radman-Livaja, M., Rando, O.J., and Peterson, C.L. (2013). A histone acetylation switch regulates H2A.Z deposition by the SWR-C remodeling enzyme. Science *340*, 195-199.
Weber, C.M., Ramachandran, S., and Henikoff, S. (2014). Nucleosomes are context-specific, H2A.Z-modulated barriers to RNA polymerase. Molecular cell *53*, 819-830.
Weber, M., Hellmann, I., Stadler, M.B., Ramos, L., Pääbo, S., Rebhan, M., and Schübeler, D. (2007). Distribution, silencing potential and evolutionary impact of promoter DNA methylation in the human genome. Nature Genetics *39*, 457-466.
Weinberg, R.A. (2014). The biology of cancer, Second edition. edn (Garland Science).
Weinert, B.T., Narita, T., Satpathy, S., Srinivasan, B., Hansen, B.K., Scholz, C., Hamilton, W.B., Zucconi, B.E., Wang, W.W., Liu, W.R., *et al.* (2018). Time-Resolved Analysis Reveals Rapid Dynamics and Broad Scope of the CBP/p300 Acetylome. Cell *174*, 231-244 e212.
West, M.H.P., and Bonner, W.M. (2002). Histone 2A, a heteromorphous family of eight protein species. Biochemistry *19*, 3238-3245.
Wilkins, M.H.F., Stokes, A.R., and Wilson, H.R. (1953). Molecular Structure of Nucleic Acids: Molecular Structure of Deoxypentose Nucleic Acids. Nature *171*, 738-740.
Wolf, E., Vassilev, A., Makino, Y., Sali, A., Nakatani, Y., and Burley, S.K. (1998). Crystal structure of a GCN5-related N-acetyltransferase: Serratia marcescens aminoglycoside 3-N-acetyltransferase. Cell *94*, 439-449.
Wu, C.t. (2001). Genes, Genetics, and Epigenetics: A Correspondence. Science *293*, 1103-1105.

Wu, D., Lim, E., Vaillant, F., Asselin-Labat, M.L., Visvader, J.E., and Smyth, G.K. (2010). ROAST: rotation gene set tests for complex microarray experiments. Bioinformatics *26*, 2176-2182.

Wu, H., Min, J., Dombrovski, L., Loppnau, P., Weigelt, J., Sundstrom, M., Arrowsmith, C.H., Edwards, A.M., Bochkarev, A., Plotnikov, A.N. The Crystal Structure of acetyltransferase domain of Human HIV-1 Tat interacting protein in complex with acetylcoenzyme A.

Wu, R.S., and Bonner, W.M. (1981). Separation of basal histone synthesis from S-phase histone synthesis in dividing cells. Cell *27*, 321-330.

Wu, W.H., Alami, S., Luk, E., Wu, C.H., Sen, S., Mizuguchi, G., Wei, D., and Wu, C. (2005). Swc2 is a widely conserved H2AZ-binding module essential for ATP-dependent histone exchange. Nat Struct Mol Biol *12*, 1064-1071.

Xiao, H., Chung, J., Kao, H.-Y., and Yang, Y.-C. (2003). Tip60 Is a Co-repressor for STAT3. Journal of Biological Chemistry *278*, 11197-11204.

Xiao, Y., Nagai, Y., Deng, G., Ohtani, T., Zhu, Z., Zhou, Z., Zhang, H., Ji, M.Q., Lough, J.W., Samanta, A., *et al.* (2014). Dynamic interactions between TIP60 and p300 regulate FOXP3 function through a structural switch defined by a single lysine on TIP60. Cell Rep *7*, 1471-1480.

Xu, S., Wilf, R., Menon, T., Panikker, P., Sarthi, J., and Elefant, F. (2014). Epigenetic Control of Learning and Memory inDrosophilaby Tip60 HAT Action. Genetics *198*, 1571-1586.

Xu, Y., Ayrapetov, M.K., Xu, C., Gursoy-Yuzugullu, O., Hu, Y., and Price, B.D. (2012). Histone H2A.Z controls a critical chromatin remodeling step required for DNA double-strand break repair. Molecular cell *48*, 723-733.

Xu, Y., Sun, Y., Jiang, X., Ayrapetov, M.K., Moskwa, P., Yang, S., Weinstock, D.M., and Price, B.D. (2010). The p400 ATPase regulates nucleosome stability and chromatin ubiquitination during DNA repair. J Cell Biol *191*, 31-43.

Yan, G., Eller, M.S., Elm, C., Larocca, C.A., Ryu, B., Panova, I.P., Dancy, B.M., Bowers, E.M., Meyers, D., Lareau, L., *et al.* (2013). Selective inhibition of p300 HAT blocks cell cycle progression, induces cellular senescence, and inhibits the DNA damage response in melanoma cells. J Invest Dermatol *133*, 2444-2452.

Yan, Y., Harper, S., Speicher, D.W., and Marmorstein, R. (2002). The catalytic mechanism of the ESA1 histone acetyltransferase involves a self-acetylated intermediate. Nat Struct Biol *9*, 862-869.

Yang, C., Wu, J., and Zheng, Y.G. (2012). Function of the active site lysine autoacetylation in Tip60 catalysis. PloS one *7*, e32886.

Yang, X.J., and Gregoire, S. (2005). Class II histone deacetylases: from sequence to function, regulation, and clinical implication. Mol Cell Biol *25*, 2873-2884.

Yi, J., Huang, X., Yang, Y., Zhu, W.G., Gu, W., and Luo, J. (2014). Regulation of histone acetyltransferase TIP60 function by histone deacetylase 3. J Biol Chem *289*, 33878-33886.

Yuan, G.C. (2005). Genome-Scale Identification of Nucleosome Positions in S. cerevisiae. Science *309*, 626-630.

Yun, M., Wu, J., Workman, J.L., and Li, B. (2011). Readers of histone modifications. Cell Res *21*, 564-578.

Zemach, A., McDaniel, I.E., Silva, P., and Zilberman, D. (2010). Genome-wide evolutionary analysis of eukaryotic DNA methylation. Science *328*, 916-919.

Zhang, H., Devoucoux, M., Song, X., Li, L., Ayaz, G., Cheng, H., Tempel, W., Dong, C., Loppnau, P., Côté, J., *et al.* (2020). Structural Basis for EPC1-Mediated

Recruitment of MBTD1 into the NuA4/TIP60 Acetyltransferase Complex. Cell Reports *30*, 3996-4002.e3994.

Zhang, H., Roberts, D.N., and Cairns, B.R. (2005). Genome-wide dynamics of Htz1, a histone H2A variant that poises repressed/basal promoters for activation through histone loss. Cell *123*, 219-231.

Zhang, P., Du, J., Sun, B., Dong, X., Xu, G., Zhou, J., Huang, Q., Liu, Q., Hao, Q., and Ding, J. (2006). Structure of human MRG15 chromo domain and its binding to Lys36-methylated histone H3. Nucleic Acids Research *34*, 6621-6628.

Zhao, H., Jin, S., and Gewirtz, A.M. (2012). The histone acetyltransferase TIP60 interacts with c-Myb and inactivates its transcriptional activity in human leukemia. J Biol Chem *287*, 925-934.

Zhao, K., Wang, W., Rando, O.J., Xue, Y., Swiderek, K., Kuo, A., and Crabtree, G.R. (1998). Rapid and phosphoinositol-dependent binding of the SWI/SNF-like BAF complex to chromatin after T lymphocyte receptor signaling. Cell *95*, 625-636.

Zhao, Y., and Garcia, B.A. (2015). Comprehensive Catalog of Currently Documented Histone Modifications. Cold Spring Harb Perspect Biol *7*, a025064.

Zilberman, D., Coleman-Derr, D., Ballinger, T., and Henikoff, S. (2008). Histone H2A.Z and DNA methylation are mutually antagonistic chromatin marks. Nature *456*, 125-129.

Zovkic, I.B., Paulukaitis, B.S., Day, J.J., Etikala, D.M., and Sweatt, J.D. (2014). Histone H2A.Z subunit exchange controls consolidation of recent and remote memory. Nature *515*, 582-586.